

COLLECTED PAPERS  
ON  
QUANTUM OPTICS AND TECHNOLOGY

Volume 9  
August 1993—July 1994

Professor  
Motoichi OHTSU

TOKYO INSTITUTE OF TECHNOLOGY

Interdisciplinary Graduate School of Science and Engineering

4259 Nagatsuta, Midori-ku, Yokohama,

Kanagawa 227, JAPAN

各位殿

拝啓 時下ますますご清祥のこととお慶び申し上げます。

さて、このたび、前回に引き続きまして、最近の私どもの発表論文をまとめましたので、ここにお送り致します。よろしくご査収下されば幸いです。いずれも未熟な論文ばかりでございますので、ご意見、ご批評を賜ればと、お待ちしております。

昨年より発足しました（財）神奈川科学技術アカデミー「フォトン制御」プロジェクトも順調に進展しており、フォトンSTMシステムとそのナノ・フォトニクスへの展開、高コヒーレントレーザシステムの開発、に関して研究を遂行しております。今後ともご指導ご鞭撻のほど、よろしくお願い申し上げます。

敬具

平成6年8月

東京工業大学総合理工学研究科

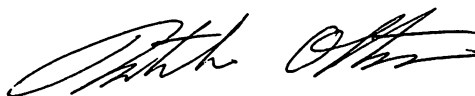


## PREFACE

In order to realize the ultimate status of light and matter, M. Ohtsu tries to control temporal and spatial properties of light. The former corresponds to developing laser frequency control technology. The latter corresponds to the research of photon scanning tunneling microscopy ( photon STM ) and its application. It should be pointed out that the photon STM is closely related to the quantum optics, atom manipulation, high density optical storage, biotechnology, and so on. And by this relationship with a variety of fields, photon STM and near-field photonics exhibit rapid progresses. Following these trends, Ohtsu's principal activities are shifting from controlling the temporal property of light to controlling the spatial property. Further research will be done to realize novel nanometric materials and devices by using nano-structural optical probes of photon STM.

A "PHOTON CONTROL" project of Kanagawa Academy of Science and Technology<sup>(\*)</sup>, directed by Ohtsu is also engaged in the research subjects described above. Twelve research staffs including three visiting scientists from industries and three visiting fellows from Sweden, Italy, and France have obtained several results on photon STM and laser frequency control. Their details will be reviewed in the forthcoming volume.

August 1994



Motoichi OHTSU

(\*) Address: Kanagawa Academy of Science and Technology  
3-2-1 Sakado, Takatsu-ku, Kawasaki-shi, Kanagawa  
213, Japan  
Phone: 044-819-2071, Fax: 044-819-2072

## MEMBERS

### Professor

Motoichi OHTSU ( Dr. Eng. )<sup>a)</sup>

### Research Associate

Ken'ichi NAKAGAWA ( Dr. Sci. )<sup>b)</sup>

Motonobu KOUROGI ( Dr. Eng. )<sup>c)</sup>

### Graduate Students ( Doctor Candidates )

Mituru MUSHA ( M. Eng. ) ( - 03/1994 )

Togar PANGARIBUAN ( M. Eng. ) ( - 03/1994 )<sup>d)</sup>

Weizhi WANG ( M. Eng. ) ( - 03/1994 )<sup>e)</sup>

Yoshinari AWAJI ( M. Eng. )

Yasunori TODA ( M. Eng. )

Mikio KOZUMA ( M. Eng. ) ( 04/1994 - )

Shuji SAYAMA ( M. Eng. ) ( 04/1994 - )

### Graduate Students ( Master Course )

Takeshi KATSUTA ( B. Sci. ) ( - 03/1994 )<sup>f)</sup>

Mikio KOZUMA ( B. Sci. ) ( - 03/1994 )

Shuji SAHAMA ( B. Eng. ) ( - 03/1994 )

Yutaka IMAI ( B. Sci. )

Takeshi ENAMI ( B. Eng. )

Bambang WIDIYATMOKO ( B. Eng. )

Kazuhiro IMAI ( B. Eng. ) ( 04/1994 - )

Takeshi NAKATA ( B. Sci. ) ( 04/1994 - )

Takuya MATSUMOTO ( B. Eng. ) ( 04/1994 - )

Keiji SAKAKI ( B. Eng. ) ( 04/1994 - )

### Undergraduate Students

Takeo UENO ( - 03/1994 )<sup>g)</sup>

Kazuhiro IMAI ( - 03/1994 )

Takeshi NAKATA ( - 03/1994 )  
Takuya MATSUMOTO ( - 03/1994 )

Research Students

Toru IMAI ( - 03/1994 )<sup>h)</sup>  
Mituru MUSA ( Dr. Eng. ) ( 04/1994 - )

Visiting Scientists

Shudong JIANG  
Michel DE LABACHELERIE<sup>i)</sup>  
Kyohya FUKUDA ( - 03/1994 )<sup>j)</sup>

Secretaries

Sanae OKAMOTO  
Kaoru OGURA

- a) Also with Kanagawa Academy of Science and Technology  
( Director, "Photon Control" Project )
- b) Also with Kanagawa Academy of Science and Technology  
( Research staff member, "Photon Control" Project )  
( - 06/1994 )
- c) Also with Kanagawa Academy of Science and Technology  
( Research staff member, "Photon Control" Project )
- d) Presently with University of Indonesia
- e) Presently with E.L. Ginzton Laboratory, Stanford University
- f) Presently with Toyota Mobil Co. Ltd.
- g) Presently with University of Tokyo
- h) Permanent affiliation : Tokyo Aircraft Instrument Co. Ltd.,  
Tokyo, Japan
- i) Permanent affiliation : Laboratoire de l'Horloge Atomique/CNRS  
Orsay, France
- j) Permanent affiliation : Communications Research Laboratory,  
Tokyo, Japan

## LIST OF PAPERS

### [I] CONTROL OF THE SPATIAL PROPERTY OF LIGHT ( PHOTON STM )

#### (a) Journal Papers

[1] M. Ohtsu, "Photon scanning tunneling microscopy and nanofabrication", Surface, Vol.31, No.9, September 1993, pp.693-697 ( Review paper, in Japanese )

[ pp.1 - 5 ]

[2] M. Ohtsu, "Future technology and advanced technology", J. Institute of Electrical Engineers, Vol.113, No.11, November 1993, pp.925-927 ( Review paper, in Japanese )

[ pp.6 - 8 ]

[3] T. Pangaribuan, S. Jiang and M. Ohtsu, "Two-step etching method for fabrication of fibre probe for photon scanning tunneling microscope", Electron. Lett., Vol.29, No.22, October 1993, pp.1978-1979

[ pp.9 - 10 ]

[4] M. Ohtsu, "A Photon Scanning Tunneling Microscope and Its Application", Biomedical Engineering, Vol.7, No.11, November 1993, pp.47-53 ( Review paper, in Japanese )

[ pp.11 - 17 ]

[5] S. Jiang, K. Nakagawa and M. Ohtsu, "Reflection-Resonance-Type Photon Scanning Tunneling Microscope", Jpn. J. Appl. Phys., Vol.33, No.1A, January 1994, pp.L55-L58

[ pp.18 - 21 ]

[6] M. Ohtsu, "A Photon Scanning Tunneling Microscope and Atom Manipulation", Optical and Electro-Optical Engineering Contact, Vol.32, No.1, January 1994, pp.45-48 ( Review paper, in Japanese )

[ pp.22 - 25 ]

[7] S. Jiang, J. Ichihashi, H. Monobe, M. Fujihira and M. Ohtsu,

"Highly localized photochemical processes in LB films of photochromic material by using a photon scanning tunneling microscope", Opt. Commun., Vol.106, numbers 4,5,6, March 1994, pp.173-177

[ pp.26 - 30 ]

(b) International Conferences

[1] S. Jiang, T. Pangaribuan, M. Kozuma, J. Ichihashi, T. Ueno, M. Ohtsu and H. Ohsawa, "Photon Scanning Tunneling Microscope using Diode Lasers", Proc. of the 16th Congress of the International Commission for Optics, pp. 193-194, ( SPIE Vol.1983 ), August 1993, Budapest, Hungary

[ pp.31 - 32 ]

[2] M. Kozuma, M. Ohtsu and H. Hori, "Experimental Confirmation of Enhanced Momentum of Localized Evanescent Field by using Doppler-Free Laser Spectroscopy in Rb<sup>85</sup>", Second International Conference on Near Field Optics, paper number F1-3, October 1993, Raleigh, NC, USA

[ p.33 ]

[3] S. Jiang, J. Ichihashi, H. Mononobe, M. Fujihira and M. Ohtsu, "Localized photochemical process in LB films of photochromic material by using a photon scanning tunneling microscope", Second International Conference on Near Field Optics, paper number WP5-2, October 1993, Raleigh, NC, USA

[ p.34 ]

[4] M. Ohtsu, "Photon Scanning Tunneling Microscopy and Its Application", Tech. Digest of Symp. on Optical Memory, pp. 13-14, July 1994, Waseda, Tokyo, Japan ( Invited )

[ pp.35 - 36 ]

[5] Y. Toda and M. Ohtsu, "High spatial resolution diagnostics technique for optical waveguides using a photon scanning tunneling microscope", Tech. Digest of the Fifth Optoelectronics Con-

ference, pp.322-323, July 1994, Makuhari, Chiba, Japan  
[ pp.37 - 38 ]

[II] CONTROL OF TEMPORAL PROPERTY OF LIGHT  
( LASER FREQUENCY CONTROL )

(a) Journal Papers

[1] Y. Toda, T. Enami and M. Ohtsu, "Frequency Stabilization of 1.5 um Diode Laser Using Nonlinear Optical Frequency Conversion in Organic Fiber", Jpn. J. Appl. Phys., Vol.32, No.9A, September 1993, pp.L1233-1235

[ pp.39 - 41 ]

[2] A. Akulshin, AS. Celicov, M. Ohtsu, K. Nakagawa and V. Velichansky, "Sub-MHz Doppler-Free Spectral Line of  $5^1S_0$ - $5^3P_1$  Intercombination Transition in Strontium", Jpn. J. Appl. Phys., Vol.32, No.9B, September 1993, pp.L1356-1358

[ pp.42 - 44 ]

[3] W. Wang and M. Ohtsu, "Frequency-tunable sum- and difference-frequency generation by using two diode lasers in a KTP crystal", Opt. Commun., Vol.102, Nos.3,4, October 1993, pp.304-308

[ pp.45 - 49 ]

[4] M. Kouroggi, K. Nakagawa and M. Ohtsu, "Wide-Span Optical Frequency Comb Generator for Accurate Optical Frequency Difference Measurement", IEEE J. Quantum Electron., Vol.29, No.10, October 1993, pp.2693-2701

[ pp.50 - 58 ]

[5] K. Nakagawa and M. Ohtsu, "Proposal of a Frequency-Synthesis Chain Between the Microwave and Optical Frequencies of the Ca Intercombination Line at 657 nm Using Diode Lasers", Appl. Phys., Vol.B57, No.6, December 1993, pp.452-430

[ pp.59 - 64 ]



[6] W. Wang, A. M. Akulshin and M. Ohtsu, "Pump-probe Spectroscopy in Potassium using an AlGaAs Laser and the Second-harmonic Generation of an InGaAsP Laser for Frequency Stabilization and Linking", IEEE Photonics Technol. Lett., Vol.6, No.1, January 1994, pp.95-97

[ pp.65 - 67 ]

[7] K. Tanaka, M. Kawasaki, K. Fumito, Y. Harada, M. Sano, K. Mizobuchi, Y. Higashino, H. Koinuma, M. Sekine and M. Ohtsu, "Optical Response of Single Crystal and Bicrystal  $\text{YBa}_2\text{Cu}_3\text{O}_{7-d}$  Thin Films", Physica B, Vo.194-196 (1994) pp.2323-2324

[ pp.68 - 69 ]

[8] M. Kouroggi, T. Enami and M. Ohtsu, "A Monolithic Optical Frequency Comb Generator", IEEE Photonics Technol. Lett., Vol.6, No.2, February 1994, pp.214-217

[ pp.70 - 73 ]

[9] M. Musha, A. Zvyagin, K. Nakagawa and M. Ohtsu, "Development of All-Semiconductor Laser Sources for Studies of  $^{88}\text{Sr}^+$  Ions Confined in RF Trap", Jpn. J. Appl. Phys., Vol.33, No.3B, March 1994, pp.1603-1607

[ pp.74 - 78 ]

[10] J. Kawakami, M. Kouroggi and M. Ohtsu, "Computer-Controlled Narrow-Linewidth and Frequency-Stabilized AlGaAs Laser System with Unmodulated Output", Jpn. J. Appl. Phys., Vol.33, No.3B, March 1994, pp.1623-1627

[ pp.79 - 83 ]

[11] W. Wang and M. Ohtsu, "Iodine Absorption-Line-Stabilized Frequency-Tunable Green Light Using Sum-Frequency Generation of Diode Lasers", Jpn. J. Appl. Phys., Vol.33, No.3B, March 1994, pp.1648-1651

[ pp.84 - 87 ]

[12] K. Nakagawa, T. Katsuta, A.S. Shelkovernikov, M. de Labachellerie and M. Ohtsu, "Highly sensitive detection of molecular absorption using a high finesse optical cavity", Opt. Commun.,

Vol.107, May 1994, pp.369-372

[ pp.88 - 91 ]

[13] K. Nakagawa, Y. Shimizu and M. Ohtsu, "High Power Diode-Laser-Pumped Twisted-Mode Nd:YAG Laser", IEEE Photonics Technol. Lett., Vol.6, No.4, April 1994, pp.499-501

[ pp.92 - 94 ]

[14] M. de Labachellerie, K. Nakagawa and M. Ohtsu, "Ultrannarrow  $^{13}\text{C}_2\text{H}_2$  saturated-absorption lines at 1.5  $\mu\text{m}$ ", Opt. Lett., Vol.19, No.11, June 1994, pp.840-842

[ pp.95 - 97 ]

(b) International Conferences

[1] M. Ohtsu, K. Nakagawa, M. Kourogi and W. Wang, "A Peta-Hertz Optical Frequency Sweep Generator", Proc. of 16th Congress of the International Commission for Optics, pp.52-56, ( SPIE Vol.1983 ), August 1993, Budapest, Hungary ( Invited )

[ pp.98 - 102 ]

[2] M. de Labachellerie, C. Latrasse, K. Nakagawa and M. Ohtsu, "Metrological Lasers around 1.5  $\mu\text{m}$ ", Tech. Digest of the Int. Symp. on Atomic Frequency Standards and Coherent Quantum Electronics, pp.5-8, August 1993, Nara, Japan ( Invited )

[ pp.103 - 106 ]

[3] W. Wang and M. Ohtsu, "Iodine absorption line stabilized frequency-tunable green light by sum-frequency generations of diode lasers", Tech. Digest of the Int. Symp. on Atomic Frequency Standards and Coherent Quantum Electronics, pp.29-30, August 1993, Nara, Japan

[ pp.107 - 1108 ]

[4] Y. Toda, T. Enami and M. Ohtsu, "Frequency Stabilization of a 1.5  $\mu\text{m}$  LD by using a Nonlinear Optical Frequency Conversion in an Organic Fiber", Tech. Digest of the Int. Symp. on Atomic Frequency Standards and Coherent Quantum Electronics, pp.29-30, August 1993, Nara, Japan

[ pp.109 - 110 ]

[5] J. Kawakami, M. Kouroggi and M. Ohtsu, "Computer-Controlled Narrow-Linewidth and Frequency-Stabilized AlGaAs Laser System with Unmodulated Output", Tech. Digest of the Int. Symp. on Atomic Frequency Standards and Coherent Quantum Electronics, pp.37-38, August 1993, Nara, Japan

[ pp.111 - 112 ]

[6] K. Nakagawa, A.S. Shelkovnikov, T. Katsuda and M. Ohtsu, "Frequency Stabilized Diode-Pumped Nd:YAG Lasers and Its Applications", Tech. Digest of the Int. Symp. on Atomic Frequency Standards and Coherent Quantum Electronics, pp.41-42, August 1993, Nara, Japan

[ pp.113 - 114 ]

[7] M. Kouroggi, T. Enami and M. Ohtsu, "Monolithic Optical Frequency Comb Generator for Optical Frequency Difference Measurement", Tech. Digest of the Int. Symp. on Atomic Frequency Standards and Coherent Quantum Electronics, pp.50-51, August 1993, Nara, Japan

[ pp.115 - 116 ]

[8] M. Musha, A. Zvyagin, K. Nakagawa and M. Ohtsu, "Development of LD Sources for Studies of Sr Ions Confined in R.F. Trap", Tech. Digest of the Int. Symp. on Atomic Frequency Standards and Coherent Quantum Electronics, pp.64-65, August 1993, Nara, Japan

[ pp.117 - 118 ]

[9] V. Barychev and M. Ohtsu, "A Laser Cooled Cesium Fountain Raman Clock: A Proposal", Tech. Digest of the Int. Symp. on Atomic Frequency Standards and Coherent Quantum Electronics, pp.74-75, August 1993, Nara, Japan

[ pp.119 - 120 ]

[10] M. Ohtsu, K. Nakagawa, M. Kouroggi, W. Wang, Y. Awaji and Y. Toda, "One Peta Hertz Coherent Optical Frequency Sweep Generator and Accurate Optical Frequency Counting", Abstracts of the XXIVth General Assembly of the International Union of Radio Science, p.3, August 1993, Kyoto, Japan

[ p.121 ]

[11] M. Kouroggi, T. Saito, T. Enami and M. Ohtsu, "Monolithic Optical Frequency Comb Generators at 1.5-um Wavelength Region", in Conference on Lasers and Electro-Optics, Vol.8, 1994 OSA Technical Digest Series ( Optical Society of America, Washington, D.C., 1994 ), pp.272-273, May 1994, Anaheim, CA, USA

[ pp.122 - 123 ]

[12] M. de Labachellerie, K. Nakagawa, M. Ohtsu and H. Sasada, "Compact Narrow Linewidth 1.5-um Frequency References for Laser Diode Frequency Stabilization", in International Quantum Electronics Conference, Vol.9, 1994 OSA Technical Digest Series ( Optical Society of America, Washington, D.C., 1994 ), pp.59-60, May 1994, Anaheim, CA, USA

[ pp.124 - 125 ]

[13] M. Ohtsu, "Ultra-Wide Band Optical Frequency Grids Generation", Tech. Digest of the Int. Symp. on Ultrafast and Ultra-Parallel Optoelectronics, pp.27-30, July 1994, Makuhari, Chiba, Japan

[ pp.126 - 129 ]

#### PUBLISHED BOOKS

[1] M. Ohtsu, Chapters 2 and 6 in *Ultimate Optical Technologies*, ed. by M. Ohtsu, H. Sakaki, H. Takuma, T. Kamiya and M. Morimura, Optronics Publishing, Tokyo, 1993 ( in Japanese )

#### PRESENTED PH.D. THESIS

[1] Weizhi Wang, "Study on a Diode Laser Based Wideband Coherent Optical Frequency Sweep Generator", January 1994

[2] Togar Harapan Pangaribuan, "An Etching-based Fabrication Method of Fiber Probe for Photon Scanning Tunneling Microscope",

January 1994

[3] M. Musha, "Analytical Study on the Motion of Cooled Sr Ions",  
January 1994 ( in Japanese )

#### AWARDS

[1] M. Kouroggi, Ph.D. Thesis Award from Teshima Foundation,  
Tokyo, May 1994

# フォトン走査トンネル顕微鏡と極微加工

大津 元一\*

## アブストラクト

先鋭化された光ファイバ・プローブを用いると光の波長よりはるかに小さい寸法をもつ試料を観測することのできる顕微鏡が実現する。すなわち、従来の光学顕微鏡の分解能をはるかにこえるフォトン走査トンネル顕微鏡である。これはさらに原子レベルの極微加工機としても使える。本稿ではこの装置の原理、性能加工機としての応用等について述べる。

### 1. はじめに

従来の光学顕微鏡の分解能は光の波長程度である。これは光をレンズの焦点面に結像させようとしても、光の波を波長より小さい領域には集光できないという性質により像がぼけることに起因する。このような分解能は「回折限界」と呼ばれ、光学の教科書などでは越えることが出来ない基本的な限界のように記述されている。

しかし、物質との相互作用によってその近傍の小さな領域に局在させられた光を使えば回折限界を越える分解能をもつ光学顕微鏡を実現することが可能である。このような光学顕微鏡はフォトン走査トンネル顕微鏡(フォトンSTMと略記)と呼ばれ、最近になって研究開発が急激に活発化している。本稿ではこの原理、実際について解説する。特にこの装置は単に微小物体形状の測定機としてのみではなく、極微加工機としても使用可能であるので、これについても触れる。

### 2. フォトン走査トンネル顕微鏡の原理

物体に光を照射すると、その散乱光には図1に示すように二つの成分が含まれる。すなわち、

- (1) 遠くまで伝搬する波としての光であり、この光は従来の光学顕微鏡、さらには一般に光計測や光通信

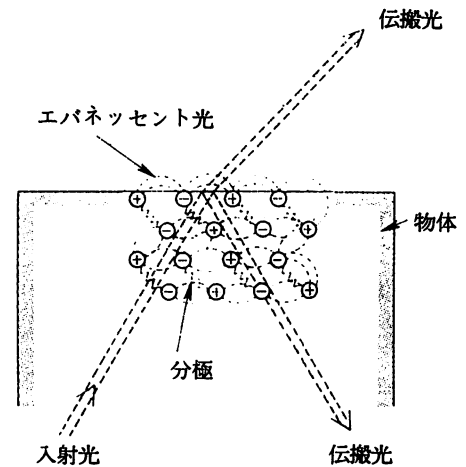


図1 伝搬光, エバネッセント光の説明。

にも使われている。

- (2) 第二は光照射によって物質に誘起された分極どうしの相互作用によって、その近傍のみに作られる電磁場、すなわち伝搬しない光である。

第二の光は光学の教科書にはエバネッセント光、または表面波として記述されている。フォトンSTMではこのエバネッセント光を用いる。すなわち図2に

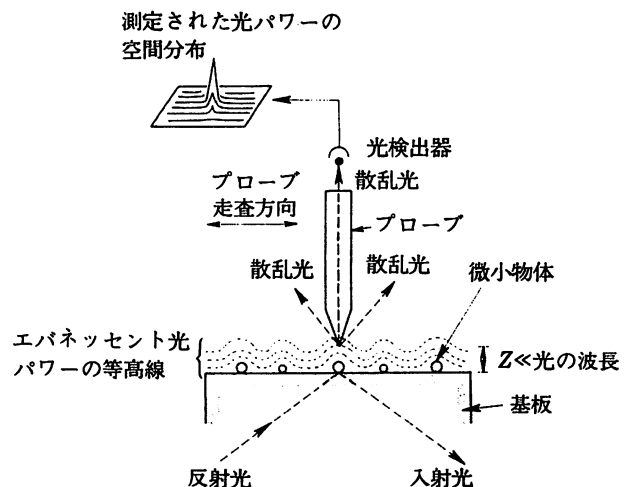


図2 フォトン走査トンネル顕微鏡の原理。

\* Motoichi OHTSU 東京工業大学総合理工学研究所 (〒227 横浜市緑区長津田 4259)

示すように、エバネッセント光パワーは物質表面から光の波長程度離れるとほぼ0となり、物質表面現状と同等の空間分布を持っている。そこで、先端の鋭いプローブの先でこの光を散乱させて上記の第一の光に変換し、このパワーを測定する。そのときプローブを物体のわずかに上空で物体表面に沿って走査し、プローブの位置の関数として測定パワー値を図示すれば物体の三次元形状が観測される。この場合、分解能はプローブ先端の曲率半径を原子の寸法まで尖らせれば、原子を見ることのできる分解能が実現する。

さて、上記の二種類の光を物質との相互作用の見地から調べてみよう。図1に示すように物質を構成する原子には光照射により分極が誘起される。各原子に誘起された分極は、その近傍の原子に誘起された分極とともに相互作用し、この結果光の散乱体としての物体の形状に依存した複雑な分極の分布が作られる。従ってこのような分極が作る第二波の波数ベクトルは完全には平行、同位相ではなく、物質の形状によって変化している。それらのうち平行、同位相の成分は干渉しあわず重ね合わさって遠くまで伝搬する光となる。これが第一の光である。一方、非平行、異位相成分は干渉しあうので、そのパワーは物質表面からの距離の増加とともに急激に減少する。これが第二の光、すなわちエバネッセント光である。

いいかえると光照射のもとでは近接する原子どうしは光を介して相互作用しており、その相互作用を媒介する光が第二の光である。すなわち、原子はエバネッセント光を交換しながら相互作用しているので、この波数ベクトルは第一の光の伝搬方向とは非平行であり、原子のまわりに局在している。この交換は、原子間のフォトン(光子)のトンネル効果に他ならない。類似の現象として、原子核中の陽子と中性子とを結び付ける中間子の交換など、多くの例がある。このようなトンネル効果を利用していることから、この顕微鏡はフォトンSTMと呼ばれている。

### 3. フォトン走査トンネル顕微鏡の実際

基本となる素子は先端の尖ったプローブである。加工の再現性の高さの点で、光ファイバを弗酸などによりエッチングして作るのが現在のところ最も優れている。また、散乱させたエバネッセント光を光検出器の位置まで効率よく導波するために光ファイバの使用が特に有利である。図3には光ファイバ・プローブの電子顕微鏡写真を示す<sup>1)</sup>。コア先端は先鋭角20度である。先端曲率半径は非常に小さく、高分解能の電子顕

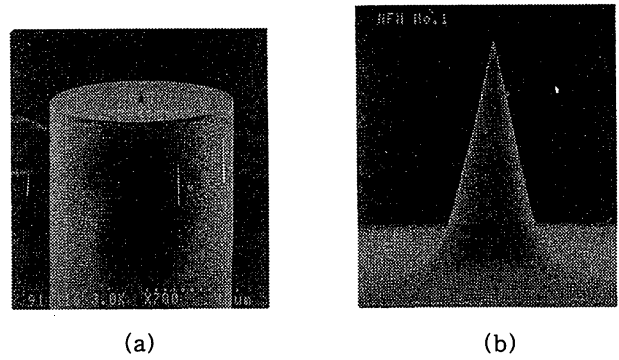


図3 光ファイバ・プローブの電子顕微鏡写真<sup>1)</sup>。(a) 光ファイバ外径は90 $\mu$ m。(b) 先端部の拡大写真。写真の横幅は5.6 $\mu$ mに相当。

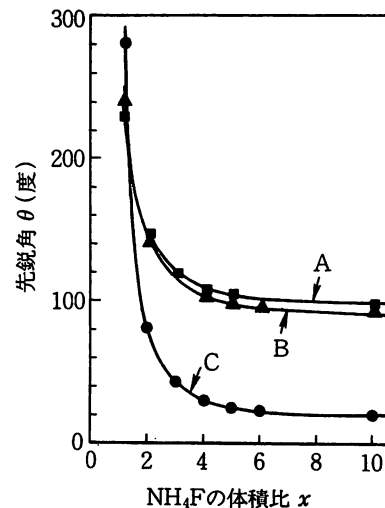


図4 光ファイバ・プローブの先鋭角 $\theta$ の $x$ 依存性<sup>1)</sup>。曲線A, B, Cは各々GeO<sub>2</sub>のドーピング比が3.6, 8.5, 23モル%の光ファイバを使った場合。

微鏡を用いても観測するのが容易ではないが、ほぼ5 nm以内と推定されている。最近では先鋭角15度、先端曲率半径約1nmのものも再現性よく作られている。

光伝送用単一モードファイバのコア部にはGeO<sub>2</sub>がドーピングされていることを利用し、緩衝弗酸により選択エッチングを行う。図4は緩衝弗酸溶液中のNH<sub>4</sub>Fの体積比 $x$ に対し、エッチングにより得られたコア先端の先鋭角 $\theta$ の値をプロットしたものである<sup>1)</sup>。GeO<sub>2</sub>ドーピング量が多いほど小さい $\theta$ の値が実現している。図中 $\theta > 180$ 度の領域はコア先端が尖るのではなく、クラッド中にへこむことを表している。すなわち、このエッチング法はクラッドに対し、コアを凸状にも凹状にもできる。ちなみに、複数本のファイバを同時に同じ条件でエッチングしたときに得られた $\theta$ の値の再現性を表す標準偏差値は0.5度であり、このことは本方法が高い再現性を有することを意味している。

このように選択エッチングにより先鋭化できる理

由として、ファイバ線引きの段階で生じたファイバ断面内の残留応力分布、などが考えられるが、現在のところ先鋭化の素過程は明らかにされておらず、今後、プローブの性能向上のためにはその解明が必要である。

なお筆者らは二段階エッチングにより、クラッド端部を切り欠くこと<sup>2)</sup>、また、マルチコアファイバ中の複数コアを同時先鋭化すること、などにも成功している。これらはフォトンSTMの機能を拡大するための素子作成技術として有用である。

実際の装置の構成例を図5に示す。光源には波長 $0.8\mu\text{m}$ の半導体レーザを用いることで測定ヘッドが小型化されている。プリズム面に試料を固定し、試料裏側から全反射されるのでプローブには到達しない。第二の光、すなわちエバネッセント光だけが試料表面に発生する。これを試料表面に接近させたプローブで測定する。プローブは piezoアクチュエータにより掃引する。光検出器で検出した信号をコンピュータ・ディスプレイ上に表示させる。なお、不透明物質を観測する場合、表面の斜め上から光を照射し、発生するエバネッセント光だけを検出してもよい。プローブ先端寸法が光の波長以下であれば第一の光は光ファイバ中に入っていない。

図6は周期 $1.5\mu\text{m}$ および $0.22\mu\text{m}$ の格子が網の目状に直交し、網の目の位置に直径 $300\text{nm}$ 、深さ $80\text{nm}$ のピットを有する蛾の目形光ディスクの表面を示す<sup>3,4)</sup>。この図中、(d)は視野の一边が $0.5\mu\text{m}$ 、すなわち光の波長の約半分であるので、従来の光学顕微鏡を使ったとするとこの大きさの視野内に像は見えない。しかしながら、フォトンSTMではこの図のようにピットの凹みの像が見えている。この他、図7にはガラス基板の上に凝集した直径 $80\text{nm}$ のラテックス球集団の像を示す<sup>3)</sup>。

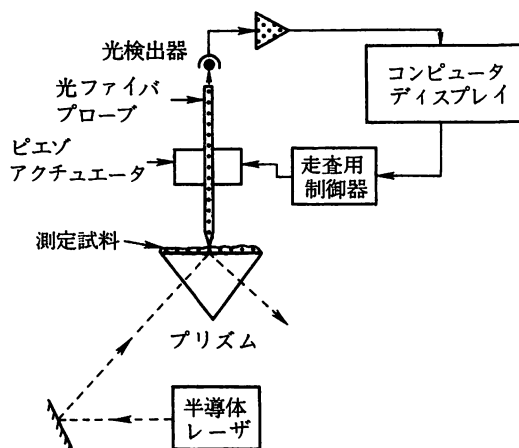


図5 フォトン走査トンネル顕微鏡の装置の例。

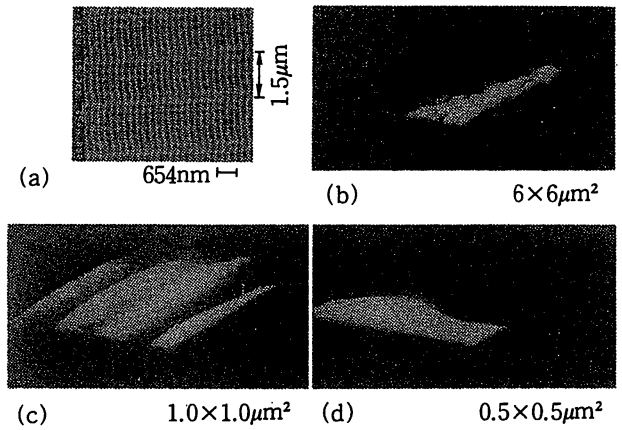


図6 蛾の目形光ディスク表面の像<sup>3,4)</sup>。(a)は電子顕微鏡写真。(b), (c), (d)はフォトンSTMによる像で、各々の視野は $6\times 6\mu\text{m}^2$ ,  $1.0\times 1.0\mu\text{m}^2$ ,  $0.5\times 0.5\mu\text{m}^2$ 。

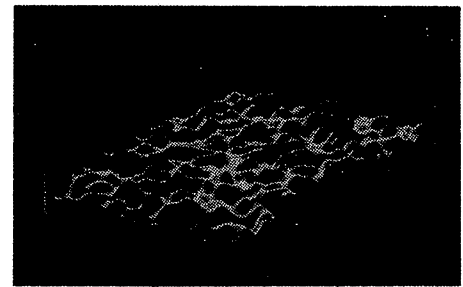


図7 ガラス基板の上に凝集した直径 $80\text{nm}$ のラテックス球集団の像<sup>3)</sup>。

フォトンSTMが電子顕微鏡などと異なるのは空气中で動作することである。そこで、図8に示すようにバクテリオファージT4などの生体微粒子の像がレプリカをとる必要なしに測定できる<sup>4)</sup>。

なお、この分解能は測定の際に混入する雑音(プローブの音響振動など)によって制限されている。これを除去し、光検出器のショット雑音レベルまで低雑音化すれば測定感度は現在より約 $30\text{dB}$ 向上する。このときの分解能は $0.1\text{nm}$ 以内、すなわち原子レベルの分解能が得られると予測されている。

#### 4. 極微加工機としての応用

エバネッセント光が原子間相互作用を媒介していることに注意すると、エバネッセント光によって原子間の相互作用を誘起し制御することが可能になる。すなわち、エバネッセント光のもつエネルギー、力(運動量)によって極微加工ができる。ここではそのような例を二つ示す。

第一の例は超高密度光記録である。フォトンSTMのプローブとして用いる光ファイバの後端からレーザ光を入射し、先端からしみ出したエバネッセン



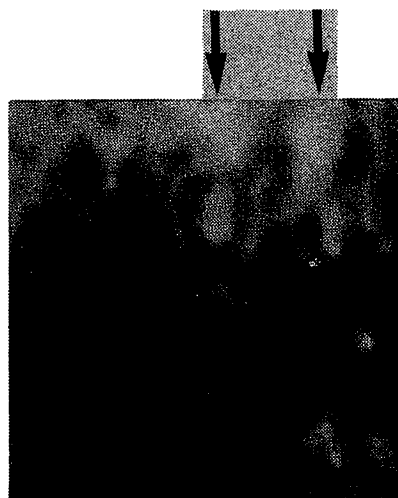
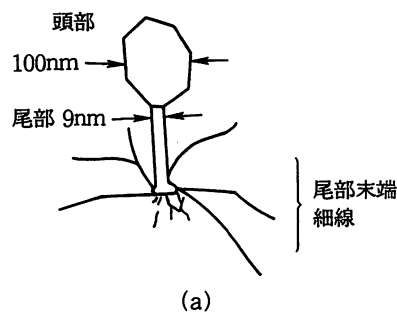


図8 バクテリオファージT4の測定結晶<sup>4)</sup>。(a) 形状説明図。  
(b) 測定結果。二本の矢印の先の位置に一つづつ像が見られる。写真の一边の幅は0.6μmに相当。

ト光により光記録材料に書き込みを行う。従来の光メモリではレーザー光をレンズで集光して記録していた。この場合、光学顕微鏡と同様、記録の最小寸法は光の回折限界により決まる。それに対し本方法ではプローブ先端寸法によって決まる微小な記録寸法が得られる。

米国のAT&Tベル研究所では磁気光学材料に直径100nmの記録を行い、従来の光メモリより数10倍高密度の光記録を実現した<sup>5)</sup>。これは光のエネルギーにより材料を局所的加熱することによる記録であり、サーマルモード記録と呼ばれる。一方、光により材料の構造を変化させる記録方法、すなわちフォトンモード記録もある。図9にその結果の例を示す。これはガラス板上に固定したジアゾベンゼン誘導体高分子からなる有機超薄膜(ラングミュア・プロジェクト膜)にエバネッセント光を照射したとき、高分子がトランス型からシス型へ遷移することにより膜の吸光度が変化することを利用する。このような光化学反応はフォトクロミック反応と呼ばれているが、この反応を起こさせることが記録に相当する。また、吸光度変化量を測定することにより読み出しができる。さらに、他の光を

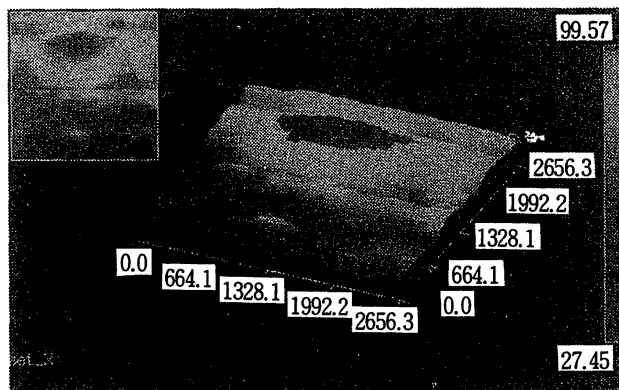


図9 有機薄膜への光記録の結果。視野の一边は約1.4μm。図中の赤い部分は吸光度が変化している。左上の内挿図は中央の鳥かん図を真上から見たもの。

照射したり、温度を変化させると消去も可能であるという特長をもつ。

図9の記録寸法は直径約140nmである。この値の下限は微弱なパワーのエバネッセント光による数分間にわたる記録中のプローブの位置変動(位置のドリフトは1分あたり1nmと推定されている)により制限されている。プローブ位置制御の精度を向上させれば、記録寸法をプローブ曲率半径によって決まる値まで小さくすることが可能である。

第二の例は単原子捕獲の可能性である<sup>6)</sup>。これは結晶成長技術の極限ともいえる。図10に示すように真空中に置いたプローブ先端からエバネッセント光をしみ出しておく。そこに真空中を浮遊する原子が飛び込むとプローブ先端とその原子との間でエバネッセント光を媒介として相互作用が発生し、ファンデルワールス分子のように二原子分子を形成する。すなわちこの単原子捕獲はファンデルワールス力による二原子分

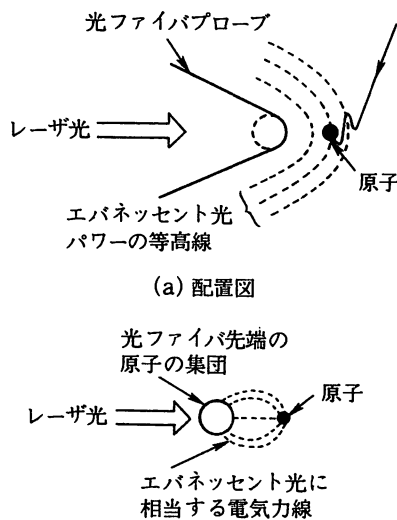


図10 単原子捕獲の原理<sup>6)</sup>。(a) 配置図。(b) ファンデルワールス分子としての説明図。

子の構成と同等である。

原子を捕獲する場合、エバネッセント光の空間的広がり小さいため二つ以上の原子が同時に飛び込むことはまれであり、このようなことが起きたとしても原子間の相互作用により単原子捕獲のみが安定に起こる。一方、原子が捕獲されれば、原子から発する蛍光を検出することにより捕獲原子の有無を知ることができる。また、捕獲位置はプローブ先端からプローブ先端曲率半径程度はなれた位置であるが、これは通常の原子間力であるファンデルワールス力のポテンシャルが最小となる位置にくらべて10倍以上はなれているので、このファンデルワールス力により原子がプローブ表面に吸着することはない。

なお、図10では原子がエバネッセント光によって捕獲される場合を説明しているが、これは原子の共鳴周波数に対して光の周波数が10MHz程度低周波側にあるときである。高周波側にあるときは原子はエバネッセント光によってプローブ先端から遠ざかる方向へ押し出されてしまう。このことを利用し、光周波数を調節して、まず真空中に浮遊する原子を捕獲し、その後押し出し、冷えた結晶基板に吹き付け吸着させることが可能である。これにより単一原子レベルでの結晶成長が期待される。

多種類の原子に対して、捕獲のためのパラメータが設計されている。図11は各種の原子に対する捕獲のための捕獲ポテンシャルの深さを表す等価温度  $T_{eq}$  とプローブ先端曲率半径の最適値  $a$  との関係の計算結果で

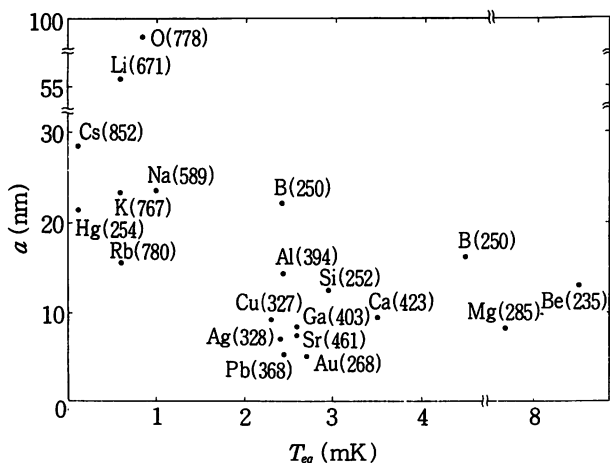


図11 各種原子の捕獲のためのポテンシャル深さを表す等価温度  $T_{eq}$  とプローブ先端曲率半径  $a$  の最適値の計算結果<sup>7)</sup>。かっこ内の数字は使用する光波長を単位 nm に表す。

ある<sup>6)</sup>。曲率半径の最適値は数 nm 以上なので、選択エッチング法で実現可能である。一方、等価温度は数 mK であり、これは小さい値であるが、現在までに確立している技術であるレーザ冷却法<sup>7,8)</sup>を用いれば真空中に浮遊する原子集団を等価温度数  $\mu$ K 以下まで予備冷却できる。そこでこの予備冷却された原子集団のうちの一つを捕獲すればよい。このような理論的考察からも単原子レベルの結晶成長の実現が期待される。真空中を浮遊する原子とエバネッセント光との相互作用についての子備実験がすでに行われている。

## 5. おわりに

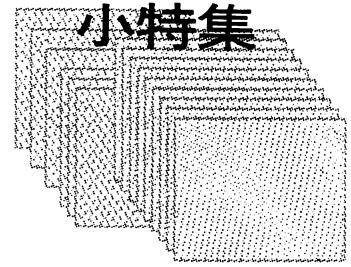
フォトンSTMの提案は60年前にさかのぼるといわれるが、良好なプローブが実現したのはここ数年である。しかし、諸物質の表面状態の観測、極微材料の評価、バイオエレクトロニクス、光記録、極微結晶成長などへの広い応用可能性のためにごく最近になって研究が急激に活発化し、昨年末にはフランスで国際集会在初めて開催され盛会であった。次回は今年10月、米国で開催される。しかし、この顕微鏡の動作原理についてはまだ解明されていない問題が多い。また、光を古典的に扱うべきか量子論的に扱うべきかの問題、などについても十分理解されていない。このような光の本質にせまる問題も含め、フォトンSTMの研究は新しく、重要で、かつ魅力に富むといえる。

## 文 献

- 1) T. Pangaribuan, K. Yamada, S. Jiang, H. Ohsawa and M. Ohtsu, Jpn. J. Appl. Phys., 31, L1302 (1992)
- 2) パンガリブアントガル, 蔣曙東, 大津元一, 第11回, 光波センシング技術研究会講演予講集, 論文番号 LST11-7, 1993年 6月
- 3) S. Jiang, N. Tomita, H. Ohsawa and M. Ohtsu, Jpn. J. Appl. Phys., 30, 2107 (1991)
- 4) S. Jiang, H. Ohsawa, K. Yamada, T. Pangaribuan, M. Ohtsu, K. Imai and A. Ikai, Jpn. J. Appl. Phys., 31, 2282 (1992)
- 5) E. Betzig, J. K. Trautman, R. Wolfe, E. M. Gyorgy and P. L. Finn, Appl. Phys. Lett., 61, 142 (1992)
- 6) H. Hori, S. Jiang, M. Ohtsu and H. Ohsawa, Tech. Digest of the 18th International Quantum Electronics Conference (June, 1992, Vienna) pp. 48-49
- 7) 清水富士夫, 応用物理, 60, 864 (1991)
- 8) 大津元一, 「コヒーレント光量子工学」, 133頁, 朝倉書店 (1990)

## VIII. 将来技術・先端技術

正員 大津元一

東京工業大学 大学院 総合理工学研究所  
神奈川科学技術アカデミー

キーワード：コヒーレント，光の局在，極微加工

## 1. はじめに

現在は基礎研究段階であるが、今後発展しそうなレーザ関連技術について著者の周辺を見まわすと次の3種類の試みがある。

- (1) レーザの発明当初のもくろみはずれ実現しなかったレーザの特性があるが、最近の周辺技術の進歩に助けられこれを実現しようとする試み。
- (2) レーザの光とは異なる特性の光を発生する試み。
- (3) 上記(1)の試みにより高性能のレーザが実現したとき、それを光源として用いて物質構造を制御する。すなわち新しい光により新しい物質を創造する試み。

これらの試みはいずれも基礎研究段階であるが、これらの半ば理学的研究対象を、自動制御、微細加工という工学の代表的手法を使って実行しているところが特徴である。以下ではこれらの試みについて紹介する。第2章，第3～5章，第6章ではそれぞれ上記の例のうち(1)，(2)，(3)を示す。

## 2. ハイパーコヒーレント光の発生と超広帯域周波数掃引光源

レーザ発明当初は装置の安定性が不十分であったために出力光の周波数がマイクロ波発振器ほど安定ではなかった。しかし半導体レーザのように注入電流の変調により周波数が容易に変調される光源に対して自動制御を施し、レーザ素子単体のもつ量子力学的な揺らぎよりさらに小さい周波数揺らぎを実現することができるようになった。これはハイパーコヒーレント光と呼ばれている<sup>(1)</sup>。周波数揺らぎを表わす尺度である発振スペクトル幅の値は、前者が約10～100 kHzであるのに対

し、後者の最小値として7 Hzが得られている<sup>(2)</sup>。

レーザ発明以来、現在まで実現し得なかったもう一つの性能として、周波数を高安定に保ったままでの広帯域掃引がある。しかし現在すでに市販の半導体レーザは可視～近赤外の範囲にわたって多くの波長範囲をカバーするようになってきているから、これらの複数の半導体レーザの周波数揺らぎを上記の自動制御で抑圧し、かつ最近進歩の速い非線形光学結晶により第二高調波、和周波数、差周波数などを発生させれば波長0.3～1.8 μmの範囲、すなわち周波数範囲600 THzにわたる掃引が可能になる<sup>(3)</sup>。つまり1 PHzに迫る掃引範囲が期待される。将来は通信、計測、分析化学、基礎物理学、医学など広い分野での応用が期待される。

## 3. スクイズド光

第2章では自動制御を施すことによりレーザ素子単体の量子力学的揺らぎより小さな周波数揺らぎを実現していたが、本章では非線形光学的な効果を利用して、光の特性を表わす二つの共役な物理量のうちの一方の揺らぎを従来知られていた量子力学的限界値よりも小さくする試みについて述べる。このような物理量として光の波のsine, cosine成分がある。このような光はスクイズド(Squeezed)光と呼ばれているが、これを実現するには光パラメトリック増幅などの非線形光学効果を用いて光のsine, cosine成分の揺らぎの間に相関を実現し、一方の成分の揺らぎを小さくする<sup>(4)</sup>。ただしその代償として他方の揺らぎは大きくなる。

現在のところ一方の成分の揺らぎは量子力学的限界より約10 dB小さくなっており、通信、分光分析化学などへの応用が試みられ始めている。

非線形光学素子の性能向上によりさらに揺らぎの小さな光が実現する可能性があり、これも広い応用が期待される。

#### 4. 共振器内量子電気力学

最近半導体デバイスの極微加工技術の進歩により  $1\ \mu\text{m}$  以下の寸法をもつ半導体共振器が実現している。このような微小共振器の寸法は光の半波長以下になり得るので、その共振モードの数は1または0である。したがってその中に発光物質を置いたとき、それが自然放出光を発生しようとしてもその発生確率は共振器長に依存するようになる。なぜなら、共振器長が光の半波長以下の場合には発生した自然放出光は共振器内に共振モードとして存在し得ないからである。つまり、微小共振器中ではその長さが光の半波長と異なるように調節すれば自然放出光の発生が抑圧される。一方、その長さを半波長に等しくすると、発生した総ての自然放出光は共振器中で共振するが、この場合一つの共振モードしかないので、自然放出光発生確率は大きくなる。

以上の現象は微小共振器の長さを調節することにより自然放出光発生確率を制御することが可能になることを意味し、この研究分野は共振器内量子電気力学と呼ばれている。従来は自然放出光はランダムに発生するのでその確率は制御できないと考えられていたが、微小共振器によりそれが可能となる。レーザ発振の種となる自然放出光の発生確率が制御できるようになると、このような微小共振器を使ったレーザでは発振のしきい値がほぼ0になるなど、いくつかの特異な性質を示す<sup>(5)</sup>。これは高効率の発光素子として今後の発展

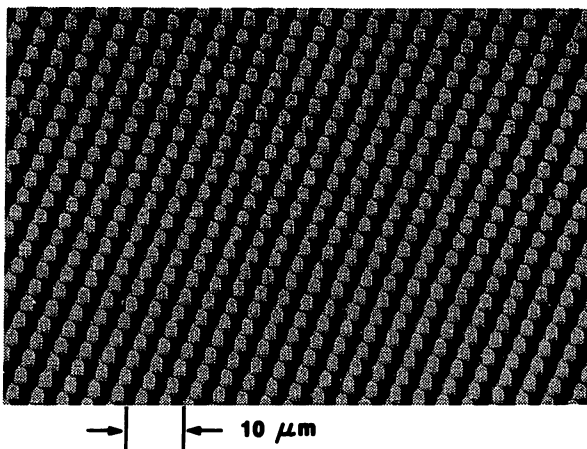


図1 半導体基板上に二次元アレー状に加工された半導体微小共振器の写真<sup>(6)</sup>

が期待されている。図1にはそのような微小共振器が半導体基板の上に二次元アレー状に加工された様子を示す<sup>(6)</sup>。

#### 5. 光のアンダーソン局在

結晶中の電子の運動状態には許容されるエネルギー帯と禁止されるエネルギーギャップがあるのはよく知られている。このようなエネルギーの範囲が形成されるのは電子の波動性に起因している。特にその波動の干渉に起因する現象として、電子の波動関数の空間的局在がある。すなわち、結晶に乱れがあるとそれは電子の伝導を阻害し、ある範囲のエネルギーに対しては電子の波動関数は空間的に局在する。この電子局在はアンダーソン局在と呼ばれている。

電子局在と同様の現象が光についても起こる。すなわち適当な誘電体の微細構造を用いれば光の散乱と干渉によって電子の波動と類似の光の局在が起こり得る。電子局在の場合と同様、光の局在も光の波長と同程度まで短い領域で多重散乱が起こる場合に実現する現象である。

この光の局在の結果、ある種の構造をもつ誘電媒質ではどの方向にも光が伝搬できないような周波数帯がある。光子のエネルギーは周波数に比例するので、このような周波数帯が存在することは光子のエネルギーギャップが形成されることに相当する。より詳しい研究によれば光子のエネルギーギャップを形成するには、結晶の単位胞の中に複数の散乱体をもつ結晶格子構造などを用いるのがよいとされている<sup>(7)</sup>。

原子のエネルギー準位間隔が光子のバンドギャップ中のエネルギーに対応する場合、その原子は光を放出することはできない。したがってこのような物質からの発光特性は従来の物質からの発光特性と異なっており、従来の発光ダイオードやレーザとは異なる発光素子の出現の可能性をもっている。

#### 6. 光による極微物質の観測と原子の運動制御

第2章の高性能レーザを光源として、その光の圧力で真空中に浮遊する原子を減速するレーザ冷却、さらには減速した原子を光ビーム中の直径数mmの領域内に閉じこめる光糖蜜法などの技術が近年発達している<sup>(8)</sup>。さらに、減速した原子の波動性を利用して原子波干渉の実験も可能となっ

た<sup>(9)</sup>。このように光によって原子の運動制御ができるようになると、結晶成長における分子ビームエピタキシー法、さらには荷電ビームによる描画、などの方法にこれらの原子運動制御の技術が利用できる可能性がある。ただしこれらの方法では単一原子の運動を制御するわけではないので、極微結晶成長への応用に関しては技術的な問題点が多い。この問題を解決する方法として、最近フォトン走査トンネル顕微鏡用の光ファイバプローブ先端に局在した光子を用いて真空中に浮遊する原子を一つずつ捕獲し、さらに冷却結晶基板上にこの原子を一つずつ固定していく方法、すなわち単原子結晶成長法が提案され、予備実験が行われている。これは空間的に局在した光によって極微物質を作り出していくための将来技術と考えられる<sup>(10)</sup>。

フォトン走査トンネル顕微鏡は物質表面に局在するエバネッセント光を用いて光の回折限界を越える分解能を実現する測定装置であり、近年その進歩が著しい<sup>(10)</sup>。これは極微加工技術により先端曲率半径が数 nm 以内に先鋭化された光ファイバプローブを作って用いることにより実現した装置である。この装置の極微加工への応用も試みられており、従来の光記録に比べて約 100 倍高密度の光記録の予備実験結果が報告されている<sup>(11)</sup>。

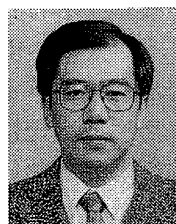
## 7. まとめ

本稿では自動制御や極微加工などの工学的手法に助けられた先端科学技術について紹介した。なお、より専門的な術語で説明すると、本稿で触れ

た内容はすべて光や物質の存在する場の真空揺らぎを制御することに対応しており、いわば「0 (ゼロ) を制御する工学」といえる。この詳細については文献 (12), (13)などを参照されたい。  
(平成 5 年 9 月 13 日)

## 文 献

- (1) 大津：日経サイエンス，1989年3月号，p.64
- (2) C.-H. Shin & M. Ohtsu: *Opt. Lett.*, **15**, 1455 (1990)
- (3) M. Ohtsu, et al.: *J. Appl. Phys.*, **73**, R1 (1993)
- (4) M. C. タイク & B. E. A. サラー，(久我訳)：パリティ，1990年11月号，p.2
- (5) S. ハロシ，J.-M. レイモンド，(川上・横山，訳)：日経サイエンス，1993年6月号，p.60
- (6) J. L. Jewell, et al.: *Appl. Phys. Lett.*, **54**, 1400 (1989)
- (7) S. ジョン，(家訳)：パリティ，1991年10月号，p.14
- (8) D. ワインランド & W. イタノ，(五神訳)：パリティ，1988年3月号，p.2
- (9) B. G. Levi: *Phys. Today*, p.17 (1991-7)
- (10) 大津：電学誌，**113**，381 (平5-5)
- (11) E. Betzig, et al.: *Appl. Phys. Lett.*, **61**，142 (1992)
- (12) 大津：信学誌，**75**，870 (平4)
- (13) 大津：真空，**36**，461 (平5)



大津 元一 (正員)

昭和 48 年東京工業大学電子工学科卒業。53 年同大学院博士課程修了。工学博士。同大学助手，助教授を経て平成 3 年同大学教授。平成 5 年より神奈川科学技術アカデミー・「フォトン制御」プロジェクトリーダーを兼任。量子操作工学，特に極限光子と極限物質の創造に関する研究に従事。

# Two-step etching method for fabrication of fibre probe for photon scanning tunnelling microscope

T. Pangaribuan, S. Jiang and M. Ohtsu

*Indexing terms: Scanning tunnelling microscope, Optical fibres, Etching techniques*

The authors propose a novel two-step etching method for fabricating a fibre probe, with good reproducibility, for a photon scanning tunnelling microscope. A fibre probe with a cladding diameter of 14µm and cone angle of 20° was fabricated by adjusting the first-step etching time and the composition of the second-step etching solution.

Recently remarkable progress in the application of the photon scanning tunnelling microscope (PSTM) has been achieved by using the capability of sharpened fibre to probe the exponential evanescent field spatially localised around a nanometric sample [1–3]. By etching a singlemode fibre in a buffered hydrofluoric acid solution, we have succeeded in fabricating a PSTM fibre probe with a cone angle,  $\theta$ , of 20° and a tip of diameter less than 10nm [4]. However, the cladding diameter of the fibre probe is more than 16 times the length of the tip. This large ratio means that the tip-sample separation (several tens of nanometres) which is applied during scanning cannot be maintained without contact between the edge of the cladding and the sample surface. To avoid this contact, we propose a two-step etching method as a novel and controllable technique for reducing the cladding diameter while retaining the sharpness, denoted by the cone angle of the fibre probe tip, and the nanometric tip diameter. As a result, a fibre probe with a cone angle of 20° and a cladding diameter of 14µm was fabricated.

In previous papers [1, 2, 4] the fibre probe was fabricated by etching the fibre in a solution composed of  $\text{NH}_4\text{F}$ , HF and  $\text{H}_2\text{O}$ . The volume ratio of  $\text{NH}_4\text{F}$ , denoted as  $X$ , was varied and the volume ratio of HF to  $\text{H}_2\text{O}$  was maintained at 1:1. Hereafter we will call this technique the one-step etching method because it uses only one kind of etching solution to sharpen the fibre. Using this technique, a fibre probe with a cladding diameter larger than 90µm ([4], Fig. 2) and tip length depending on the cone angle of ~2–6µm was fabricated. Certainly, the cladding diameter can be reduced by increasing the etching time. However, in comparison with the result obtained by the one-step etching method, where the sharpening process depends on the difference in etching rates between core and cladding, sharpening only the core at the end of this long etching process will degrade the sharpness of the tip. Degradation of the sharpness then increases the diameter of the tip.

To overcome this difficulty, two etching solutions are used. The solution in the first step is used to reduce the cladding diameter and the solution in the second step is used to sharpen the fibre. To avoid a negative cone angle (see [4], Fig. 3b) which occurred in the one-step etching method, and to obtain the minimum etching time for reducing the cladding diameter, an etching solution with a

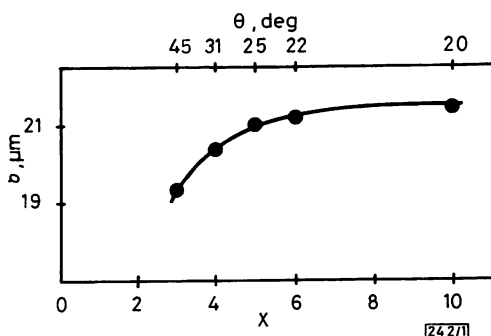


Fig. 1 Reduction of cladding diameter after second-step etching against volume ratio of  $\text{NH}_4\text{F}$  ( $X$ ) in etching solution

$\theta$  is cone angle associated with value of  $X$

composition of  $X = 1.7$  is used in the first step.

To control the etching time of the first step we investigated the relationship between etching time and the diameter of the cladding. Two singlemode fibres with pure silica claddings and  $\text{GeO}_2$ -doping core ratios of 3.6 mol% and 25 mol% were used. The core diameters are 3.4µm and 6µm, respectively, and the cladding diameters are 125µm. By varying the first-step etching time, we found that by using the etching solution with a composition of  $X = 1.7$ , the etching rate of the cladding diameter is linear and can be expressed by  $v = -0.95\mu\text{m}/\text{min}$ . Although the cladding diameter can be reduced until the end of the fibre probe consists only of a core, when the propagation loss of the fibre probe is considered, it is necessary to maintain a cladding diameter of twice the core diameter [5]

To obtain the desired cone angle  $\theta$  of the fibre probe, an etching solution with composition of  $X = 3$  or larger is used in the second step. It was found that the associated minimum etching time for each value of  $X$  used in the one-step method does not change when the temperature is constant. Keeping the second-step etching time equal to this minimum etching time, the reduced cladding diameter can be considered as a constant value. A relationship between the reduced cladding diameter ( $\delta$ ) and the value of  $X$  is shown in Fig. 1. The cone angle of the fibre probe associated with the value of  $X$  is expressed by  $\theta$ . From this result, we can see that the reduced cladding diameter  $\delta$  tends to be constant when  $X$  is greater than 4 and the maximum difference of  $\delta$  obtained when  $X = 3$  and  $X = 10$  is 2µm.

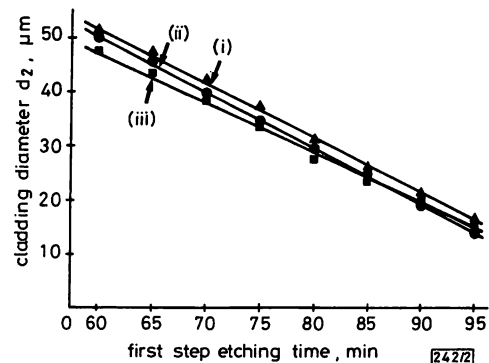


Fig. 2 Cladding diameter of fibre probe produced by two-step etching method

Lines (i), (ii) and (iii) are fitted to the experimental results for cone angles  $\theta = 45^\circ, 25^\circ$  and  $20^\circ$ , respectively

Combining the etching rate obtained from the first-step etching with the result of second-step etching shown by Fig. 1, the cladding diameter  $d_2$  obtained by the two-step etching method can be empirically expressed as

$$d_2 = d_0 - 0.95 t_1 - \delta_x \quad (1)$$

where  $d_0 = 125\mu\text{m}$  is the initial cladding diameter,  $t_1$  is the first-step etching time and  $\delta_x$  is the cladding diameter reduced during the second step. Varying the first-step etching time  $t_1$  and using etching solutions with values of  $X = 3$  ( $\theta = 45^\circ$ ),  $X = 5$  ( $\theta = 25^\circ$ ) and  $X = 10$  ( $\theta = 20^\circ$ ) for the second-step etching, experimental results for the two-step etching were obtained (Fig. 2). Lines (i), (ii) and (iii) are fitted to the results for  $X$  values of 3, 5 and 10, respectively. It is clear from this Figure that the cladding diameter of the fibre probe can be easily controlled by adjusting the first-step etching time. Numerous experiments demonstrated good reproducibility for this method and the standard deviation of the cladding diameter  $\Delta d_2$  was confirmed within 1.5µm. It was also confirmed that the relative variation of the cone angles defined by  $(\theta_1 - \theta_2)/\theta_1$ , were less than 4% (for  $\text{GeO}_2$  core-doping ratio of 3.6 mol%) and 2% (for  $\text{GeO}_2$  core-doping ratio of 25 mol%). Here,  $\theta_1$  and  $\theta_2$  are the cone angles of the fibre probes produced by one-step and two-step etching methods, respectively. The length of the tip was also unchanged at 2–6µm.

An example of the experimental result of this two-step etching method is shown by the SEM photograph in Fig. 3. An etching solution with a composition of  $X = 1.7$  was used for 95min during the first step and a composition of  $X = 10$  was used for 120min during the second step. A cladding diameter of  $14\mu\text{m}$  was achieved and the cone angle of this fibre probe was  $20^\circ$ . Comparison with the result shown in Fig. 2 [4] shows that the cladding diameter has

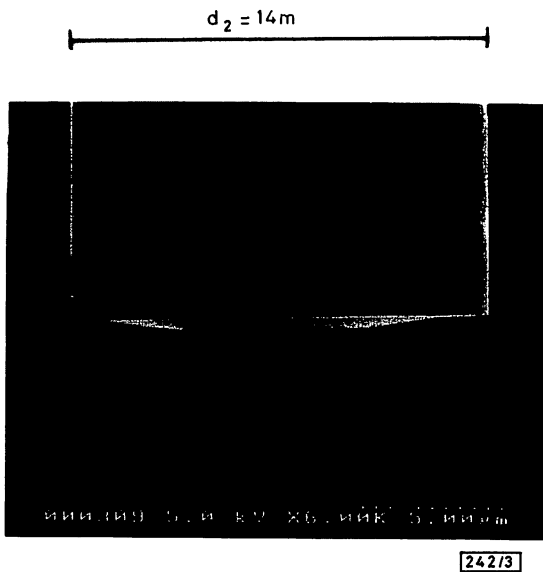


**Fig. 3** SEM image of fibre probe fabricated by two-step etching method  
Cladding diameter and cone angle are  $14\mu\text{m}$  and  $20^\circ$ , respectively

been reduced to  $1/6$  while the cone angle is the same. Also, the ratio between the cladding diameter and the tip length has been reduced to  $1/4$ .

In summary, a two-step etching method has been proposed and realised as a novel technique for fabricating fibre probes for a PSTM. The cladding diameter of the fibre probe was reduced to  $1/6$  of the value obtained by the one-step etching method and was

easily controlled by varying the first-step etching time. A fibre probe with cone angle of  $20^\circ$  and cladding diameter of  $14\mu\text{m}$  was obtained. A relative variation of cone angle smaller than 4% and a standard deviation of cladding diameter  $\Delta d_2$  within  $1.5\mu\text{m}$  were achieved.

*Acknowledgment:* The authors would like to thank S. Miyamoto (Fujikura) for discussions on the optical fibre.

© IEE 1993

23 August 1993

*Electronics Letters Online No:* 19931239

T. Pangribuan, S. Jiang and M. Ohtsu (*Interdisciplinary Graduate School of Science & Engineering, Tokyo Institute of Technology, 4259 Nagatsuta, Midori-ku, Yokohama, Kanagawa 227, Japan*)

M. Ohtsu is also with the Kanagawa Academy of Science & Technology, KSP East 408, 3-2-1 Sakado, Takatsu-ku, Kawasaki 213, Japan

### References

- 1 JIANG, S., TOMITA, N., OSHAWA, H., and OHTSU, M.: 'A photon scanning tunnelling microscope using an AlGaAs laser', *Jpn. J. Appl. Phys.*, 1991, **30**, (9A), pp. 2107-2111
- 2 JIANG, S., OSHAWA, H., YAMADA, K., PANGARIBUAN, T., OHTSU, M., IMAI, K., and IKAI, K.: 'Nanometric scale biosample observation using a photon scanning tunnelling microscope', *Jpn. J. Appl. Phys.*, 1992, **31**, (7), pp. 2282-2287
- 3 REDDICK, R.C., WARMACK, R.J., and FERREL, T.L.: 'New form of scanning optical microscopy', *Phys. Rev. B.*, 1989, **39**, (1), pp. 767-770
- 4 PANGARIBUAN, T., YAMADA, K., JIANG, S., OSHAWA, H., and OHTSU, M.: 'Reproducible fabrication technique of nanometric tip diameter fiber probe for photon scanning tunnelling microscope', *Jpn. J. Appl. Phys.*, 1992, **31**, (9A), pp. L1302-L1304
- 5 BARNARD, C.W., and LIT, J.W.Y.: 'Single-mode fiber microlens with controllable spot size', *Appl. Opt.*, 1991, **30**, (15), pp. 1958-1962

# フォトン走査トンネル顕微鏡とその応用

大津 元一\*

## 1. はじめに

顕微鏡は肉眼では見えない物体を可視化するための装置であり、現代の科学技術における必須装置である。光学顕微鏡や電子顕微鏡は医用電子工学、生体工学の分野でも日常的に使われていることはいうまでもないが、筆者が推測するに、このような生体試料を扱う分野では顕微鏡の性能に対する要求として

- (1) 大気中、または溶液中での動作が可能。
- (2) 試料に対して非接触、非破壊であること。
- (3) 形状のみでなく構造も分析できること。
- (4) 光の波長の値より小さいものが見える高い分解能を有すること。

などが上げられると思う。ところで上記(1)～(3)を満たす顕微鏡として光学顕微鏡がある。しかし、光学顕微鏡では(4)を満たさないことは周知のとおりである。光を波としてとらえると、これは自由空間をまっすぐ進むが、もし板に開けられた微小な穴(開口と呼ばれる)があると、それを通り抜けた光波は広がる性質をもつ。これは「回折」と呼ばれる現象である。この性質のために従来の光学顕微鏡では(4)を満たすことができない。

しかし、ごく最近上記の(1)～(4)をすべて満たす光学顕微鏡が出現した。特に(4)を満たすことは光学の教科書に古くから記されている回折限界を打破し、光の波長よりも小さい寸法をもつ物体を観測することを可能にしたことを意味する。

すなわち光学の常識をくつがえす顕微鏡であり、それがフォトン走査トンネル顕微鏡(フォトンSTM)である。フォトンSTMの原理にもとづくと、計測器としてのみでなく、光の波長以下の寸法をもつ物体を加工する新しい「光メス」として、さらにそのような物体の運動状態を制御し操作する新しい「光ピンセット」としても使用可能である。本稿ではこれらについて概説する。なお、著者自身による同様の解説記事があることを付記する<sup>1-3)</sup>。

## 2. 原理

図1にフォトンSTMの原理を示す。微小な被測定物体が平坦な基板の上に置かれている。基板裏面から全反射が生じるような角度で光を入射すると伝搬光はすべて反射するが、基板および被測定物体表面付近にはエバネッセント光と呼ばれる表面波が発生する。この表面波のパワーは物体表面のまわりの光の波長以内の寸法の領域に局在している。ここで先の鋭いプローブをエバネッセント光の場の中に差し込んでエバネッセント光を散乱させる。プローブを物体上空を走査しながら散乱光パワーを測定し、プローブの位置に対してプロットすると、それは物体の三次元的な形状を表す。このとき、エバネッセント光を散乱するプローブの先端が鋭いほど高い分解能が得られる。すなわち分解能はプローブの先端曲率半径によって決まる。

実際には必ずしも全反射が起こるような角度で入射させなくともよい。図2に示すように、任意

\* Ohtsu M 東京工業大学総合理工学研究科, 神奈川科学技術アカデミー



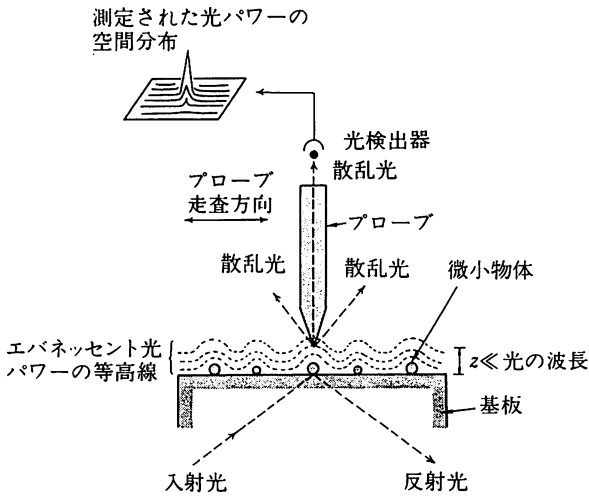


図1 フォトンSTMの原理

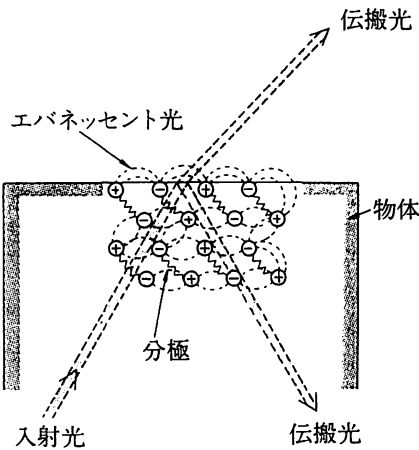


図2 伝搬光とエバネッセント光の説明

の方向から（、従って不透明な被測定物体の上方向からでもよい）被測定物体に光を照射すると、その散乱光には二つの成分が含まれる。第一は遠くまで伝搬する波としての光であり、これが従来の光学顕微鏡に使われている。第二はエバネッセント光であるが、これは見方を変えると光照射によって物質に誘起された分極どうしの相互作用を媒介するために分極近傍に作られた電磁場、すなわち伝搬しない光である。このように光を電磁相互作用を媒介する量子と考えると、光の波長以内の近距離での電磁相互作用はさらに光の量子（、すなわち光子）のトンネリングと考えることができる。フォトンSTMは微小な被測定物体とプローブ先端との間でこのようにエバネッセント光としての光子をトンネリングさせて交換することにより動作する顕微鏡である。従って、フ

ォトンSTMの動作原理は電子のトンネリングを使う従来の電子STM、クーロン力の交換を使う原子間力顕微鏡（AFM）、などと本質的に同じであり、この理由からこの装置には「フォトンSTM」なる名称が与えられている。

### 3. 装置の性能

#### 3.1 プローブ

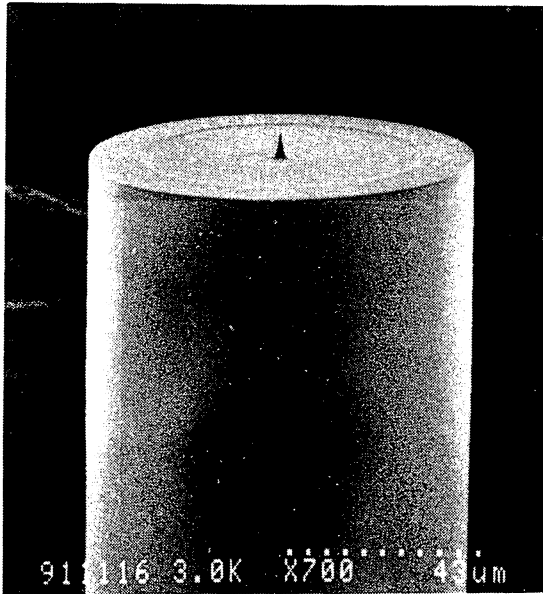
前節で述べたようにフォトンSTMの分解能を決める基本要素はプローブであり、フォトンSTMの開発はプローブ用デバイスの開発であるといっても過言ではない。従来はガラス製のマイクロピペットを加熱し引き延ばしたもの<sup>4)</sup>、光ファイバを加熱して引き延ばしたもの<sup>5)</sup>、などがある。これらの方法では作成の再現性が低いこと、量産性に欠けること、集光効率が低いこと、またプローブ先端曲率半径を10 nm以下にすることが難しいこと、などの問題がある。これらの問題を解決するために、われわれの開発した光ファイバの選択エッチング法について説明する。

単一モードファイバのコアにはGeO<sub>2</sub>がドーブされていることを利用し、緩衝フッ酸溶液により選択エッチングを行う。図3にはこのようにして先鋭化されたファイバ・プローブの電子顕微鏡写真を示す。現在までに先鋭角15度、先端曲率半径5 nmが実現しており、最も鋭いプローブとなっている。特に同一エッチング条件で作られたファイバ・プローブの先鋭角のばらつきは0.5度以内であり、作成の再現性が高いことが確認されている<sup>6)</sup>。

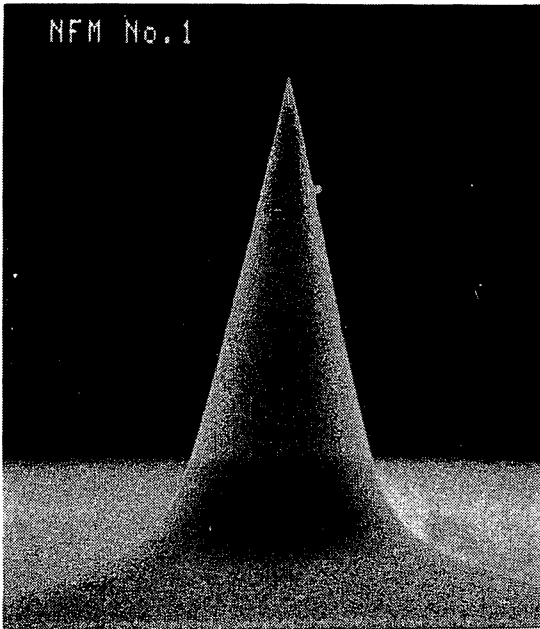
この他、原子間力顕微鏡用のカンチレバーをプローブとして用いてエバネッセント光を散乱させるもの<sup>7)</sup>、蛍光測定のためにマイクロピペットに蛍光微粒子を固定したものも提案されている<sup>8)</sup>。

#### 3.2 装置の構成と測定例

代表的なフォトンSTM装置の構成を図4に示す。光源とファイバ・プローブ以外は電子STM、AFMなど同様である。この図は微小物体を透過するエバネッセント光を測定するので透過形フォトンSTMといえるが、不透明物体測定用の反射



(a)



(b)

図3 ファイバ・プローブの電子顕微鏡写真<sup>6)</sup>  
 (a) 光ファイバ端全体像。外形は  $90\ \mu\text{m}$ 。(b) 先端部の拡大像。写真の横幅は  $5.6\ \mu\text{m}$  に相当。

形もある。図5、図6は各々ガラス面に凝集した直径  $80\ \text{nm}$  のラテックス球<sup>9)</sup>、ガラス基板に固定したバクテリオファージ T4 の測定例である<sup>10)</sup>。以上は図3のファイバ・プローブを用いて空気中で測定した結果であるが、分解能  $5\sim 10\ \text{nm}$  (すなわち可視光の波長の約  $1/100$ ) が得られている。

一方、マイクロピペット、加熱によるファイバ延伸によるプローブは未だ先端寸法が大きいので分解能は数十  $\text{nm}$  に留まっている。この場合、プロ

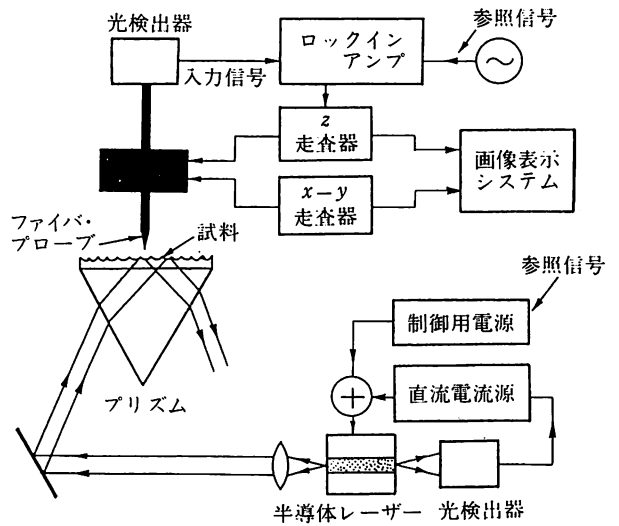


図4 フォトンSTMの装置

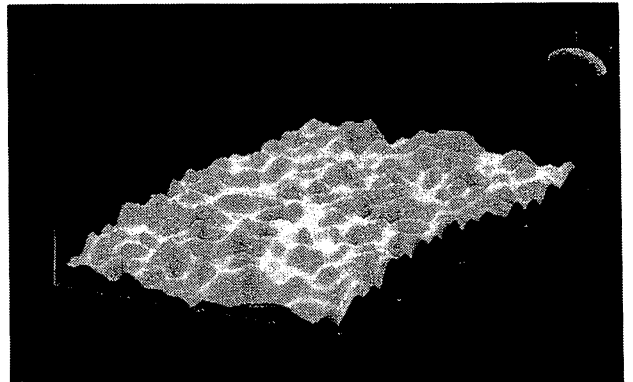


図5 直径  $80\ \mu\text{m}$  のラテックス球集団の像<sup>10)</sup>  
 視野の一辺は  $1.0\ \mu\text{m}$ 。

ーブの位置の機械的振動を抑えて少しでも高い分解能を得るためにプローブの位置制御精度を向上させる方法が採用されている。それはプローブに被測定物体から及ぼされるせん断応力をモニターしてその値が一定になるように位置制御するものである<sup>11)</sup>。これにより約  $20\ \text{nm}$  の分解能を実現している。その他、最近では生物、化学などへの応用のために液面上の微小物体を測定する試み、さらに蛍光を利用した単分子検出の試み、などがある。

本説の最後に分解能の限界について述べる。プローブ自身が原子の集合から形成されているので、プローブ先端の最小凹凸の寸法は原子の寸法によって決まる。従って分解能の限界はプローブ先端曲率半径の最小値、すなわち原子の寸法に相当する。ただし、原子の寸法と同程度の分解能を

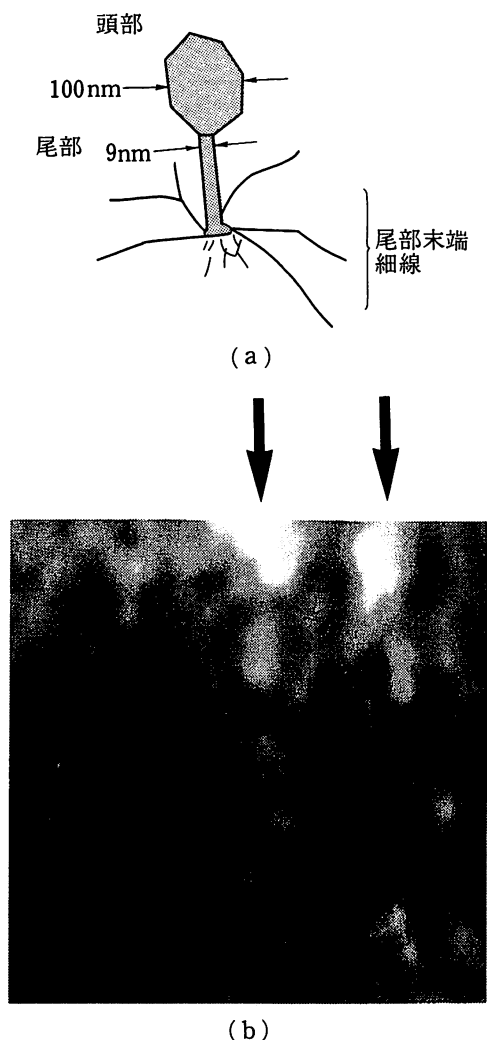


図6 バクテリオファージ T4 の像<sup>11)</sup>  
 (a) 形状説明図。(b) 測定結果。2本の矢印の先の位置に一つずつ像がみられる。視野の一边は0.6 μm。

得ようとする、被測定物体に対してプローブを原子の寸法と同程度まで近づけ、十分なフォントンのトンネリング効率を確保しなくてはならない。従って実際には被測定物体の厚み方向のプローブの位置制御の精度が決め手となる。ところで、微小物体に照射されるレーザー光パワーが数 mW であるとき、検出されるエバネッセント光パワーは 1 nW 程度の小さい値であるが、その検出感度はショット雑音限界に達している。この場合の信号対雑音比によって決まる厚み方向のプローブ位置制御の精度はフーリエ周波数 10 Hz 以上では  $3 \times 10^{-3} \text{ nm}$  に達している。しかし 10 Hz 以下のフーリエ周波数領域でのシステム雑音の主要因は機械振動によるものであり、この場合の厚み方向のプ

ローブ位置制御精度の限界は 0.1 nm である。従って、この値が現在の分解能の技術的限界を与えている。この値はすでに原子の寸法と同程度であるが、さらに注意深い除振を施すことにより今後原子寸法より小さな高分解能化が期待される。

#### 4. 可能な応用

フォトン STM の応用範囲はきわめて多岐にわたる。これらについて紹介するために、まず第 1 章で述べたフォトン STM の特徴のうち (2), (3) について補足する。

フォトン STM では非電気伝導体を大気中で測定することができるので、電子 STM や電子顕微鏡のように被測定物体に金属膜を蒸着する必要がなく、また AFM のように被測定物体に圧力を加えることもない。このようにフォトン STM は非接触、非破壊測定が可能である。これが第 1 章 (2) に対応するが、生体微粒子のように柔らかい微小物体を測定するにはこの特徴は有利である。

一方、光の波長を掃引することにより分光分析が可能になる。これにより被測定物体の構造が局所的に変わっている部分を測定することができる。これが第 1 章 (3) に対応する。特に生物分野では生体微粒子の局所的な化学種を同定するためにフォトン STM を用いた分光分析の研究が始まっている。

以上は顕微鏡としての優れた特徴といえる。ところでフォトン STM の逆過程を考えてみよう。すなわち、ファイバ・プローブの後端からレーザー光を入射したとき先鋭化された先端に発生する局在したエバネッセント光のエネルギー密度を利用すれば、ナノメータ領域の分解能をもつ加工機、操作機を実現することができる。これは微小物体の状態や構造を人工的に変化させるので、第 1 章 (2) の非破壊性に反するものではない。まず加工の例として超高密度光記録について示す。

光磁気記録材料に対して直径約 100 nm のピットを記録し、読み出す実験が報告されている<sup>12)</sup>。これらの寸法は従来の光メモリーの 100 倍の記録密度に相当する。これは材料に対する光の熱効果を

利用した記録方式であり、言い換えれば第1章で述べた「光メス」を用いた加工である。これに対し、メモリーの消去可能な記録方式がジアゾベンゼン誘導体のラングミュア・プロジェクト膜 (LB 膜) を記録材料として用いて試みられている<sup>13)</sup>。それはこの LB 膜にプローブ先端のエバネッセント光を照射し、図7に示すようにトランス形からシス形への構造変化を起こさせるものである。これがメモリーの記録に相当する。この結果、シス形に構造変化した部分は紫外光の吸収係数がトランス形の場合の半分になるので、紫外のエバネッセント光を再照射し、その光の吸収を測定することによりメモリーの読み出しができる。図8に示す

ように光磁気材料と同様の寸法の光メモリーが実現している。なおシス形からトランス形への構造変化は LB 膜を可視光を照射するなどすれば可能なので、消去可能メモリーとなっている。

この LB 膜に対する光記録の特徴は LB 膜の形状を変化させているわけではないことである。構造を変化させ、それを光の波長を掃引することにより吸収分光分析を行って読出しを行っている。いわば第1章(3)を利用しており、この読出し方法は生体試料の化学種同定などのための局所分光分析への応用可能性を示唆している。

以上の超高密度光記録の方式の実用化のためには記録時間などをはじめとする多くの解決すべき技術的問題が残されているものの、光メモリー産業の分野では画期的な方式として注目を集めている。

この他、操作機への応用の極限的な例として、ファイバ・プローブ先端にしみ出し局在したエバネッセント光の圧力を利用して真空中に浮遊した原子をエバネッセント光の場の中に一つずつ捕獲する試みがある<sup>14)</sup>。その理論的根拠の説明は本誌のカバーする分野とだいぶ異なるので他の解説にゆずるが<sup>3)</sup>、このように真空中で原子が一つずつ捕獲できれば、その後捕獲原子を冷却された結晶

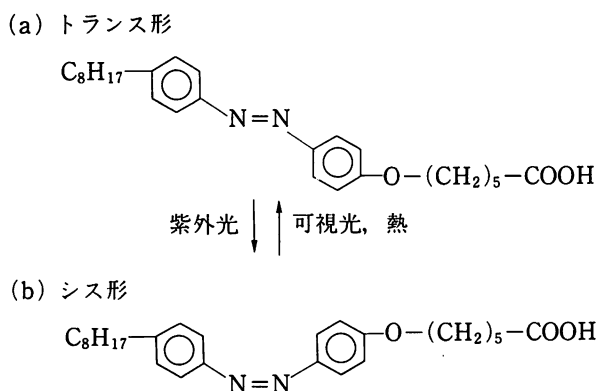


図7 ジアゾベンゼン誘導体の LB 膜の分子構造

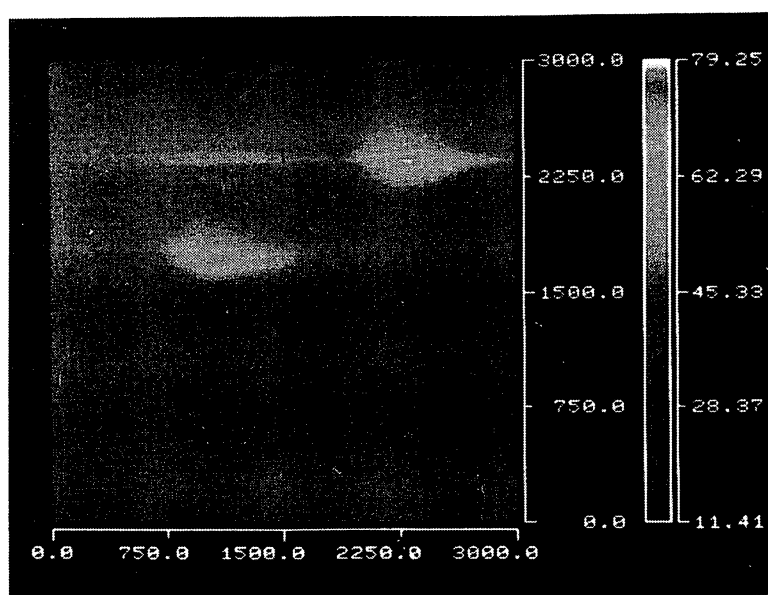


図8 光記録の読み出し結果<sup>13)</sup>  
視野の一边は3.0 μm。図中の二つの明るい楕円部分の吸収係数が変化している。

基板の上に落とし、単原子レベルでの極微結晶成長が可能となり、新奇な人口物質創製の可能性が開ける。現在までに予備実験によって原子とエバネッセント光との間の大きな運動量のやりとりが確認されている<sup>15)</sup>。

上記の単原子捕獲はファイバ・プローブ先端にしみ出し、局在したエバネッセント光を原子に対する「光ピンセット」として使う試みである。このように極限的に小さい対象としての原子以外にも、より大きい物体をつかむ「光ピンセット」としても使える可能性がある。従来の「光ピンセット」は通常のレーザ光をレンズで絞り、その焦点面に微粒子を捕獲するものであった<sup>16,17)</sup>。この場合は捕獲できる微粒子の寸法の下限は従来の光学顕微鏡と同じように回折限界によって決まり、光の波長程度である。これに対し、本方法では光の波長以下の微粒子を捕獲できる。従ってタンパク質のアクチンフィラメント、DNA など、生体微小試料の運動制御、操作には有望な方法と考えられる。

## 5. おわりに

フォトン STM の提案は古く、約 60 年前にさかのぼるが、その実験的発展は最近の約 5 年である。それはプローブの作成技術の進歩によるところが大きい。しかし、この 1, 2 年の研究開発の進歩および研究開発人口の増加はめざましく、特に米国では生物、化学への応用研究がきわめて活発化している。また、生物、医用分野で加工機、操作機としての応用は表だって行われていないが、近い将来、先進諸国で着手されると思われる。

フォトン STM を生物、医用分野で用いるとき、観測用微小試料を溶液中に用意したり、ガラス基板上に固定すること、など技術的なノウハウがまだ十分とはいえない。著者のような量子光学を専門とする分野の人間と生物、医用分野の研究者諸氏との間の学際的な協力が必要である。本稿が本誌読者諸氏にとって有用な情報となれば幸いであるが、著者にとっては本誌は専門外の機関誌であり、生物、医用分野からみてピントのはずれた論

法になっているかもしれない。ご批評いただければ幸いである。

なお、この研究分野の急速な立上りに対応し、“Near Field Optics” (近接場光学) と称する国際会議が過去 2 回開催され、盛会であった。第 1 回目 (1992 年 10 月) のプロシーディングはすでに出版されている<sup>18)</sup>。第 4 回目 (1997 年) は日本で開催される可能性が大きい。

## 文 献

- 1) 大津元一, 堀 裕和: フォトン STM の実験と理論. 光学 **21**: 780-788, 1992
- 2) 大津元一: フォトン走査トンネル顕微鏡: 光の回折限界を越えて. 日本物理学会誌 **48**: 25-28, 1993
- 3) 大津元一: 0 (ゼロ) を制御する工学—光による新しい「真空」の工学—. 真空 **36**: 461-470, 1993
- 4) Betzig E, Isaacson M, Barshatzky H, Lewis A, Lin K: Near-field scanning optical microscopy (NSOM). SPIE Vol. 897, Scanning Microscopy Technologies and Applications: 91-99, 1988
- 5) Durig U, Pohl D, Rohner F: Near-field optical scanning microscopy with tunneling distance regulation. IBM J Res Dev **30**: 478-483, 1986
- 6) Pangaribuan T, Yamada K, Jiang S, Ohsawa H, Ohtsu M: Reproducible fabrication technique of nanometric tip diameter fiber probe for photon scanning tunneling microscope. Jpn J Appl Phys **31**: L 1302-L 1304, 1992
- 7) Van Hulst NF, Moers MHP, Noordman OFJ, Tack RG, Segerink FB, Bogler B: Near-field optical microscope using a silicon-nitride probe. Appl Phys Lett **62**: 461-463, 1993
- 8) Dunn RC, Allen EV, Joyce SA, Xie SX: Towards the ultimate sensitivity of near-field fluorescence detection. Adv Program, The 2nd Int Conf on NFO Raleigh NC USA Oct 1993
- 9) Jiang S, Tomita N, Ohsawa H, Ohtsu M: A photon scanning tunneling microscope using an AlGaAs laser. Jpn J Appl Phys **30**: 2107-2111, 1991
- 10) Jiang S, Ohsawa H, Yamada K, Pangaribuan T, Ohtsu M, Imai K, Ikai A: Nanometric scale biosample observation using a photon scanning tunneling microscope. Jpn J Appl Phys **31**: 2282-2287, 1992
- 11) Betzig E, Finn PL, Weiner JS: Combined shear force and near-field scanning tunneling microscopy. Appl Phys Lett **60**: 2484-2486, 1992

- 12) Betzig E, Trautman JK, Wolfe R, Gyorgy EM, Finn PL : Near-field magnetooptics and high density data storage. *Appl Phys Lett* **61** : 142-144, 1992
- 13) Jiang S, Ichihashi J, Monobe H, Fujihira M, Ohtsu M : Localized photochemical processes in Langmuir-Blodgett films of photochromic material by using a photon scanning tunneling microscope. *Adv Program, The 2 nd Int Conf on NFO, Raleigh NC USA Oct 1993*
- 14) 大津元一：フォトン STM (V) 単原子レベル結晶成長。第 51 回応用物理学会学術講演会，講演番号 27 aL 79 1990 秋期
- 15) Kozuma M, Ohtsu M, Hori H : Experimental confirmation of enhanced momentum of localized evanescent field by using Doppler-free laser spectroscopy in Rb 85. *Adv Program, The 2 nd Int Conf on NFO, Raleigh NC USA Oct 1993*
- 16) Ashkin A : Acceleration and trapping of particles by radiation pressure. *Phys Rev Lett* **24** : 156-159, 1970
- 17) Sasaki K, Koshioka M, Misawa H, Kitamura N, Masuhara H : Laser-scanning micromanipulation and spatial patterning of fine particles. *Jpn J Appl Phys* **30** : L 907-L 909, 1991
- 18) Pohl EW, Courjon D : *Near Field Optics*, Kluwer Academic Publishers Dordrecht 1993

## Reflection-Resonance-Type Photon Scanning Tunneling Microscope

Shudong JIANG<sup>1</sup>, Ken'ichi NAKAGAWA<sup>1,2</sup> and Motoichi OHTSU<sup>1,2</sup>

<sup>1</sup>Interdisciplinary Graduate School of Science and Engineering, Tokyo Institute of Technology,  
 4259 Nagatsuta-cho, Midori-ku, Yokohama 227

<sup>2</sup>Kanagawa Academy of Science and Technology, KSP East, 3-2-1 Sakado, Takatsu-ku, Kawasaki 213

(Received September 14, 1993; accepted for publication November 20, 1993)

A novel reflection-resonance-type photon scanning tunneling microscope is proposed to measure the sub-wavelength sample profile by detecting the resonant frequency shifts of a probe cavity. Simulation experiments were carried out to confirm the effectiveness of the present proposal and the theoretical estimation shows that the shot-noise-limited lateral resolution as high as  $2.3 \times 10^{-3} \lambda$  can be expected.

**KEYWORDS:** optical microscope, reflection resonance, near field, photon tunneling, frequency shifts, cavity, sub-wavelength lateral resolution

### 1. Introduction

Photon scanning tunneling microscopy (PSTM) is a novel technique for realizing noncontact and nondestructive measurement with the ability to circumvent the diffraction limit.<sup>1-3</sup> For obtaining the information of an opaque sample surface, reflection-type PSTM has been demonstrated.<sup>4</sup> However, it is difficult to obtain high resolution because the information of the sample surface is obtained by detecting the very weak power which leaks out from and back to the aperture whose diameter is smaller than the wavelength of the light source used.

On the other hand, in the microwave region, schemes for achieving sub-wavelength resolution have been proposed by detecting the resonant frequency shift of a microwave cavity with a sub-wavelength aperture<sup>5</sup> or by detecting the phase and amplitude of the reflected signal from the probe generated by an open-ended transmission line.<sup>6</sup> In this letter, we propose for the first time in the optical wave-length region, a novel PSTM,<sup>7,8</sup> i.e., the reflection-resonance-type PSTM (RR-PSTM) using an optical phase-locked loop (OPLL) with high resolution of frequency tracking, and show the results of the preliminary experiment in optical region and simulation experiment by microwave. By using such a PSTM, high sensitivity and high resolution can be expected because the topographical information of the sample is given by tire shift of the resonant frequency which can be detected with high accuracy up to  $4 \times 10^{-4}$  Hz.<sup>9</sup>

### 2. Theoretical Analysis and Discussion

Figure 1 shows the scheme for the proposed RR-PSTM, in which a frequency-stabilized diode laser (LD1) and a fiber Fabry-Perot cavity are used as the light source and probe, respectively. Of course, other frequency-stabilized lasers, such as an LD-pumped YAG laser, can also be used as the light source to replace LD1. One of the probe-cavity facets has a sub-wavelength aperture out of which the evanescent light leaks. The laser beam from LD1 is injected into this cavity, and its frequency is optically locked to the resonant frequency of the probe cavity by optical feed-back from the cavity. When the probe is scanned along

the sample surface with a sample-aperture separation smaller than the wavelength, its resonant frequency will be shifted depending on the sample profile because the effective complex impedance of the probe cavity changes due to the tunneling effect of the evanescent light which leaks out through the aperture. Subsequently, this frequency shift is optically fed back to the laser, and detected by measuring the heterodyne signal between the frequencies of LD1 and a reference laser (LD2).

To theoretically analyze the resolution of the RR-PSTM, the relationship between the aperture diameter of the probe cavity and the induced resonant frequency shift was calculated. For simplicity, a model of the conventional Fabry-Perot cavity was used for the probe and a dielectric flat surface was used as the sample.

Since a monochromatic electric field  $E_0$  propagates along the  $z$  axis in the probe cavity, the electric field leaking out from the aperture including the evanescent field can be expressed in terms of its spatial plane-wave spectrum by using Fourier transform.<sup>10,11</sup> Considering that the leaked electric field would partly tunnel to the sample when the probe cavity to sample separation is smaller than the wavelength, we decomposed this tunneling effect into separate plane-wave components, and the reflected field from the aperture can be expressed as

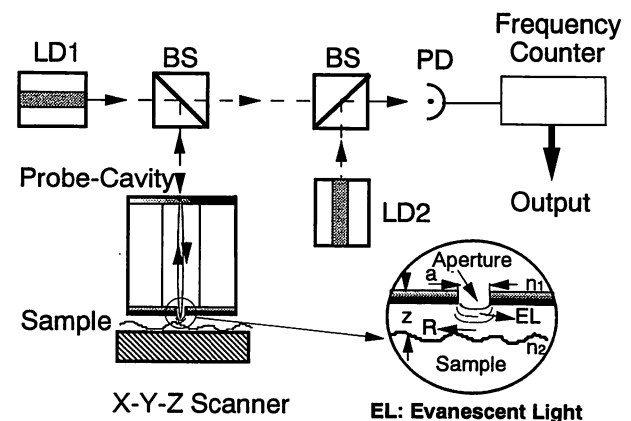


Fig. 1. The scheme of the proposed reflection-resonance-type PSTM.

$$E_r(R, z=0) = 4\pi^3 a \int_0^{1/\lambda} \int_0^{a/2} \int_{1/\lambda}^{\infty} K_T \rho r J_0(2\pi\rho R) J_0(2\pi\rho r) J_0(2\pi r \xi) J_1(\pi a \xi) d\rho dr d\xi, \quad (1)$$

where

$$K_T = \frac{(n_1^2 - 1)(\exp(-j2\pi(\lambda^2\xi^2 - 1)^{1/2}z/\lambda) - 1) - 4j(\lambda^2\xi^2 - 1)^{1/2}(n_1^2 - \lambda^2\xi^2)^{1/2}}{-2(n_1^2 - \lambda^2\xi^2)^{1/2}((n_2^2 - \lambda^2\xi^2)^{1/2} + j(\lambda^2\xi^2 - 1)^{1/2})} \quad (2)$$

is the coefficient of the tunneling effect,  $J_0(x)$  and  $J_1(x)$  are the Bessel functions of the 0-th and 1st order, respectively.  $a$  is the aperture diameter,  $z$  is the sample-aperture separation,  $R$  is the radius from the center of the aperture in the plane paralleled to the probe-cavity facet, and  $n_1$  and  $n_2$  are the refractive indices of the medium of the cavity and the sample, respectively.

As long as the aperture is much smaller than  $\lambda$ , only very little energy will leak out from the aperture and  $E_0$  will be nearly totally reflected. Therefore, the resonant frequency shift normalized by the free spectral range (FSR), depending on the aperture diameter and the sample profile can be written as

$$\frac{\Delta f}{\text{FSR}} = \frac{-\text{Im}\{E_r(R, 0)\}}{2\pi}. \quad (3)$$

The numerically calculated result of the relationship between the frequency shift and the aperture diameter obtained using eqs. (1)–(3) is shown in Fig. 2. Lines A–D are the shot-noise limit values for A:  $P=10$  mW,  $F=10^2$ ; B:  $P=1$  W,  $F=10^2$ ; C:  $P=10$  mW,  $F=10^5$ ; and D:  $P=1$  W,  $F=10^5$ , where  $F$ ,  $P$  are the finesse and the detected power respectively. In the case of  $F=100$ , and  $P=10$  mW (curve A), the shot-noise-limited lateral resolution, defined as the diameter of the aperture is evaluated as  $1 \times 10^{-2}\lambda$ , corresponding to a frequency shift of 14 Hz for the FSR of 100 GHz (assuming  $\lambda=800$  nm). The realization of the highly coherent semiconductor laser with the linewidth of 7 Hz<sup>12)</sup> and the

heterodyne optical phase-locked loop with the tracking accuracy of  $4 \times 10^{-4}$  Hz<sup>9)</sup> can guarantee the detection of such a frequency shift. On the other hand, since the super-cavity with finesse higher than  $10^5$  and the single-mode diode laser with an output power on the order of 1 watt is available, the shot-noise-limited lateral resolution higher than  $2.3 \times 10^{-3}\lambda$  (1.7 nm) (curve D) can be expected.

If a sub-wavelength aperture is fabricated on the facet of the laser diode chip, the probe-cavity can be removed because this laser serves as an active probe cavity.<sup>7)</sup>

### 3. Simulation Experiments

To confirm the effect that the resonant frequency of the cavity can be shifted by the sub-wavelength sample structure, we detected the resonant frequency shift of a high reflection coated (HR-coated) Fresnel-Rhomb prism by changing the separation between the prism and a sharpened fiber with the sub-wavelength tip diameter (fibercavity separation).

Figure 3(a) shows the setup of the experiment. An Al-GaAs diode laser with 830 nm wavelength whose linewidth was narrowed by the optical feedback, was used as a light source. A sharpened fiber with the cone angle of 100 degrees and tip diameter  $< 80$  nm, sharpened by our chemical etching technique,<sup>13)</sup> was used to shift the resonant frequency of a HR-coated Fresnel-Rhomb prism cavity with the FSR and  $F$  of 1.75 GHz and 10, respectively. To simplify the experiment, the phase-sensitive detection technique was used for detecting the resonant frequency shift induced by the tunneling effect.

Figure 3(b) shows the relationship between the resonant frequency shift  $\Delta f$  normalized to the FSR on the fiber-cavity separation normalized to  $\lambda$ . It can be seen that the resonant frequency shifted 16 MHz as the fiber-cavity separation was changed about  $1 \mu\text{m}$ . Considering that the resonant frequency changes exponentially as the fiber-cavity separation is changed linearly, and the experimental resolution of the phase sensitive detection was higher than  $(10^{-3} \sim 10^{-5} \times \text{FSR}/F)$ , the normal resolution as high as  $0.1 \sim 0.001$  nm can be obtained with the fiber-cavity separation smaller than 10 nm. Furthermore, since the frequency shift as small as  $4 \times 10^{-4}$  Hz can be detected by the OPLL, the normal resolution higher than  $10^{-3}$  nm can be expected by using the setup shown in Fig. 1.

Because it is difficult to fabricate the sub-wavelength aperture on the facet of the high finesse cavity and a reference sample with sub-wavelength structure, further demonstration, for confirming the operation of the present RR-PSTM and the results of calculation, was

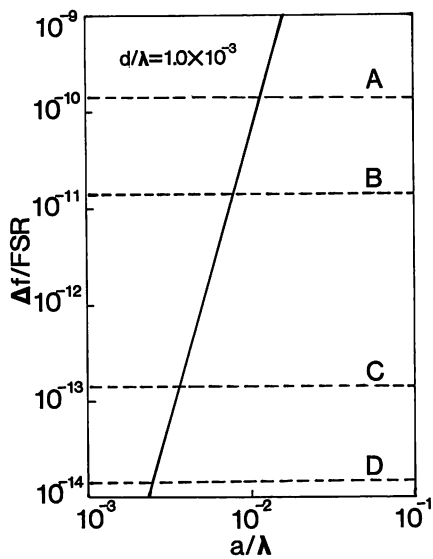


Fig. 2. Numerically estimated results of the relationship between the frequency shift and the aperture diameter. Lines A–D are the shot-noise limit values for A:  $P=10$  mW,  $F=10^2$ ; B:  $P=1$  W,  $F=10^2$ ; C:  $P=10$  mW,  $F=10^5$ ; and D:  $P=1$  W,  $F=10^5$ .



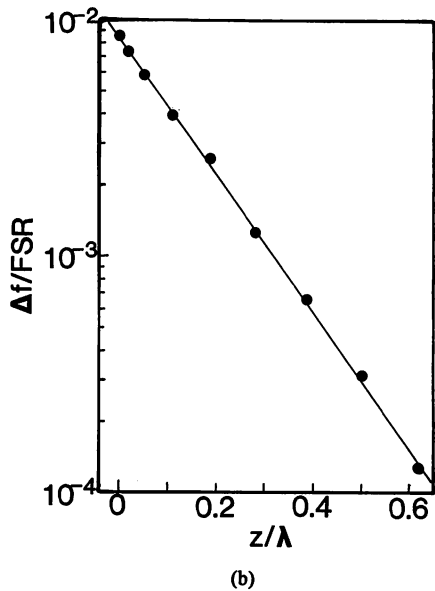
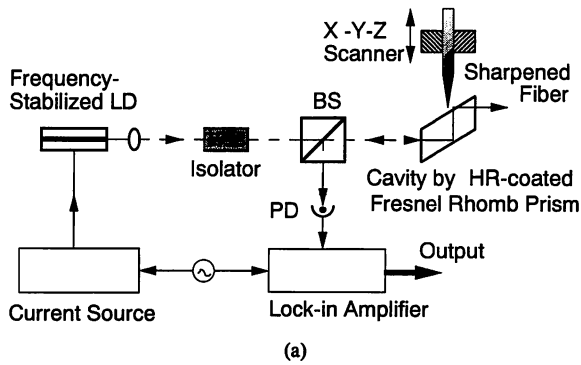


Fig. 3. Simulation experimental setup and result of the resonant frequency shift of the HR-coated Fresnel-Rhomb prism when the evanescent field disturbed by a sharpened fiber with the cone angle and tip diameter of 100 degrees and <80 nm, respectively. Wavelength, FSR and finesse of the prism used in this experiment were 830 nm, 1.75 GHz and 10, respectively. (a) Setup. (b) Dependence of the resonant frequency on the separation between the prism and the sharpened fiber.

carried out by using the microwave with  $\lambda = 4.4$  cm (frequency  $f_0 = 6.8$  GHz). In this experiment, a synthesizer with a frequency multiplier and a microwave cavity for  $TE_{111}$  mode were used as the source and probe, respectively. The resonant frequency shift of the cavity was measured by the phase-sensitive detection as was shown in Fig. 1 of ref. 5. Figure 4(a) shows the cross-sectional profile of an aluminum plate with the sub-wavelength structure which we used as the sample. Figure 4(b) shows the frequency shift when the probe was scanned along the  $x$  direction. The aperture diameter of the probe cavity, the height of the corrugations and the separation between the aperture and the highest point of the sample were  $a = 0.2\lambda$ ,  $\Delta z = 0.05\lambda$  and  $z_0 = 0.02\lambda$ , respectively. It can be seen that the separation,  $b = 0.13\lambda$ , of two corrugation elements, corresponding to the separation between two peaks of the resonant frequency shift, was resolved clearly and the value of the resonant frequency shift  $\Delta f/f_0$  was in the

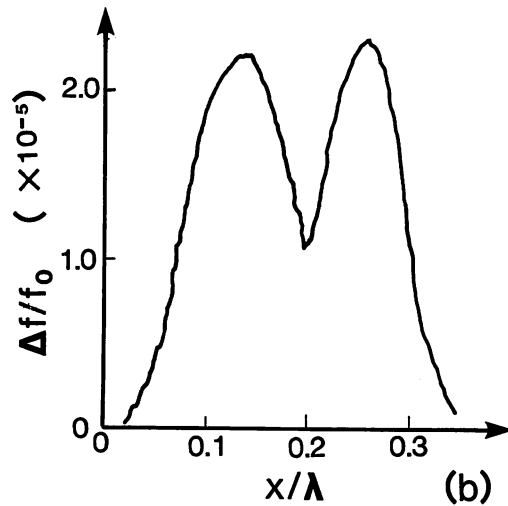
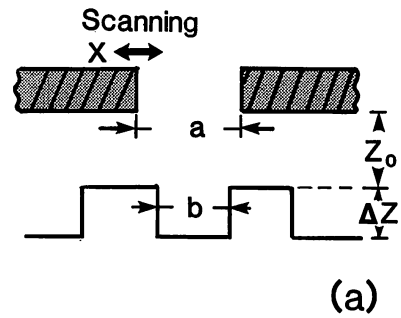


Fig. 4. Dependence of the resonant frequency shift on the profile of the sample surface.  $\lambda$  used in this experiment was 4.4 cm. The aperture diameter of the probe cavity, the separation between two corrugations, the height of the corrugations, and the separation between the aperture and the highest point of the sample were  $a = 0.2\lambda$ ,  $b = 0.13\lambda$ ,  $\Delta z = 0.05\lambda$ , and  $z_0 = 0.02\lambda$ , respectively. (a) Cross-section of the sample profile. (b) Resonant frequency shift when the probe-cavity was scanned above the cavity along the  $x$  direction.

order of  $10^{-5}$ . Considering the FSR of the microwave cavity which we used in the experiment is equal to the  $f_0$ , it can be seen that such a resonant frequency shift agreed with the result of the calculation as  $a = 0.2\lambda$  was used as the parameter. This result also confirmed that the RR-PSTM can resolve the structure ( $0.13\lambda$ ) which is even smaller than the aperture diameter ( $0.2\lambda$ ), because the intensity of the evanescent wave is concentrated on the center of the aperture.

#### 4. Conclusion

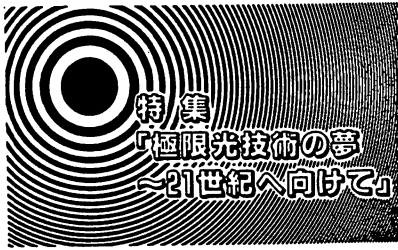
A reflection-resonance-type photon scanning microscope was proposed. Results of the simulation experiments by optical and microwave techniques confirmed that the resonant frequency of the probe cavity can be shifted by the sub-wavelength structure of the sample surface and such a structure can be resolved by detecting the resonant frequency shift. It was shown by the theoretical analysis that the shot-noise-limited lateral resolution can be improved to as high as  $2.3 \times 10^{-3}\lambda$  in

the case of probe-cavity finesse of  $F=10^5$  and the diode laser power  $P=1$  W.

### Acknowledgement

The authors wish to thank Mr. Yoshihiko Fujie for his help in the experiment.

- 1) U. Durig, D. W. Pohl and F. Rohner: J. Appl. Phys. **59** (1986) 3381.
- 2) E. Betzig and J. K. Trautman: Science **251** (1991) 1468.
- 3) S. Jiang, H. Ohsawa, K. Yamada, P. Togar, M. Ohtsu, K. Imai and A. Ikai: Jpn. J. Appl. Phys. **31** (1992) 2282.
- 4) D. Courjon and J. M. Vigouroux: Appl. Opt. **29** (1990) 3741.
- 5) E. A. Ash and G. Nicholls: Nature **237** (1972) 510.
- 6) M. Fee, S. Chu and T. W. Hansch: Opt. Comm. **69** (1989) 219.
- 7) S. Jiang, N. Tomita, K. Nakagawa and M. Ohtsu: OEC'90, Tech. Dig., Makuhari-Messe, 1990, Chiba, 12D1-3.
- 8) S. Jiang, N. Tomita, K. Nakagawa and M. Ohtsu: Proc. CLEO'91, Optical Society of America, Washington, D.C., 1991, p. 420.
- 9) C. H. Shin and M. Ohtsu: Photon. Technol. Lett. **2** (1990) 297.
- 10) O. Bryngdahl: *Progress in Optics*, ed. E. Wolf (Elsevier Scientific Publ., 1973) Vol. XI, p. 169.
- 11) J. W. Goodman: *Introduction to Fourier Optics* (McGraw-Hill, New York, 1968) 1st ed, Chap. 2.
- 12) C. H. Shin and M. Ohtsu: Opt. Lett. **15** (1990) 1455.
- 13) T. Pangaribuan, K. Yamada, S. Jiang and M. Ohtsu: Jpn. J. Appl. Phys. **31** (1992) L1304.



# フォトン走査トンネル 顕微鏡と原子操作

大 津 元 一

## 1. はじめに

フォトン走査トンネル顕微鏡（フォトンSTM）は近接場光学を利用した顕微鏡である。その分解能はプローブ形状によって決まり、光の波長にはよらない。すなわち、被測定物体に光を照射したときに物体表面に発生し、局在するエバネッセント光のパワー分布を測定する装置であるので、回折限界を越えた超解像顕微鏡となっている。この顕微鏡の提案は60年前にさかのぼるが、主要な実験が始まったのはここ数年の間である。この顕微鏡はバイオテクノロジー、化学、極微結晶工学などきわめて広範な分野へ適用可能であるために、特に欧米において応用研究が急激に活発化している。本稿ではフォトンSTMの概略、特に顕微鏡としてのみでなく極微加工機としての応用の可能性について述べる。そのような加工の極限的な対象が原子であるので、原子操作の可能性について解説する。

## 2. 原理とシステム性能

フォトンとは電磁相互作用を媒介する光の量子である。従来の光学やフォトニクスでは真空中や光ファイバなどの媒質中を伝搬しエネルギーや情報の伝達を担うフォトンがもっぱら興味の対象となった。しかし、近距離での電磁相

互作用（例えばイオン間のクーロン力や近接原子間の振動電気双極子相互作用など）もフォトンを通じて媒介されると考えられる。図1に示すようにフォトンSTMとはこのような極めて近距離での電磁相互作用をフォントンのトンネリングと考え、外部に伝搬するフォトンを経由して情報を担い手として用いてこの相互作用を観測する装置である。

物質の表面近傍での電磁相互作用を媒介し、外部に伝搬しないフォトン（局在光、エバネッセント光）と呼ばれているので、

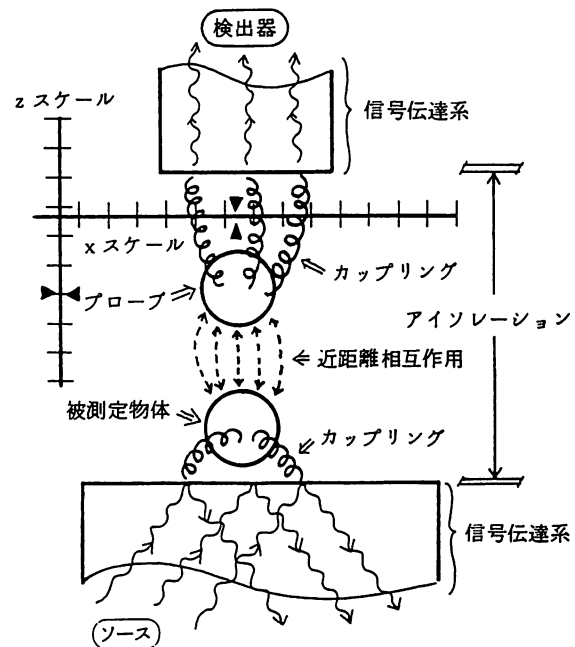


図1 フォトンSTMの動作原理

フォトンSTMとは外部からの光照射によって微小物体の近傍に誘起されたエバネッセント光をプローブを走査しながらピックアップし、その形状を測定する装置であると表現することもできる。

この顕微鏡の分解能を決めるものはプローブ先端形状であるが、光ファイバを化学エッチングにより先鋭化したプローブでは先端曲率半径5 nmに達しており、バクテリオファージT4の像などを分解能5 nm程度で観測するに至っている<sup>1, 2)</sup>。現在、先進諸国の主要研究機関では前節に示したような広範な応用分野に着手している。

### 3. 極微加工および原子操作

フォトンSTMの逆過程を考える。すなわち、光ファイバ・プローブにレーザー光を入射したときその先端に発生する局在したエバネッセント光の場を利用すれば、ナノメートル領域の分解能をもつ加工機、マニピュレータを実現することができる。

たとえば光磁気記録材料に対して直径約100 nmのピットを記録し、読み出す実験が報告されている<sup>3)</sup>。これは熱モードの記録方式であるが、消去可能なフォトンモードでの記録もなされている。それはジアゾベンゼン誘導体のLB膜にエバネッセント光を照射し、トランスミス遷移を誘起するものである。これにより図2

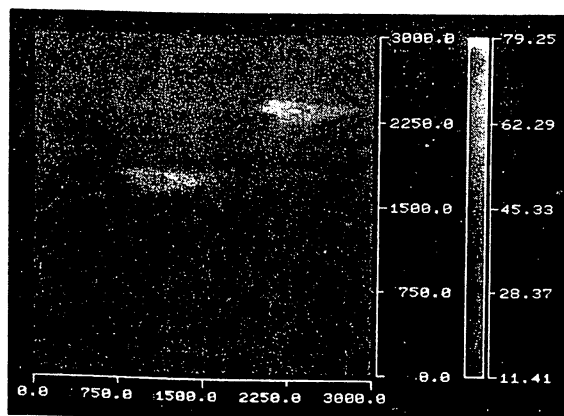


図2 フォトンモードでの光記録および読み出しの結果<sup>4)</sup>。図の一边は3  $\mu\text{m}$ 。色の薄い二つの楕円部がメモリに相当。楕円短辺の径は約100 nm。

に示すように上記と同様の寸法の記録が実現している<sup>4)</sup>。これらの寸法は従来の光メモリの100倍の記録密度に相当するが、実用化のためには記録時間などをはじめとする多くの解決すべき技術的問題が残されている

このような加工機としての他、生体微粒子の運動制御などの操作機としての興味深い応用が多数考えられる。特に極限的な可能性として単原子操作がある<sup>5)</sup>。光ファイバ・プローブ先端に局所的なエバネッセント光を発生させれば、原子との共鳴的近距離相互作用を起こすことができる。エバネッセント光は物質表面に誘起された分極の作る局所的電磁場であるので、外から来た原子からプローブを眺めた場合、あたかも励起されて振動双極子を持つ巨大原子のように見えるであろう。このような局所的エバネッセント光を通しての共鳴的相互作用は、プローブ先端と外来原子の間にファンデルワールス力に似た作用をもたらす。特に、外来原子が極低温状態にあって、波動関数の広がりがエバネッ

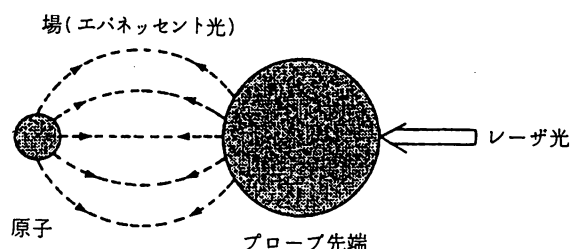


図3 光照射により形成される「疑似ファンデルワールス分子」の概念による単原子捕獲の説明。

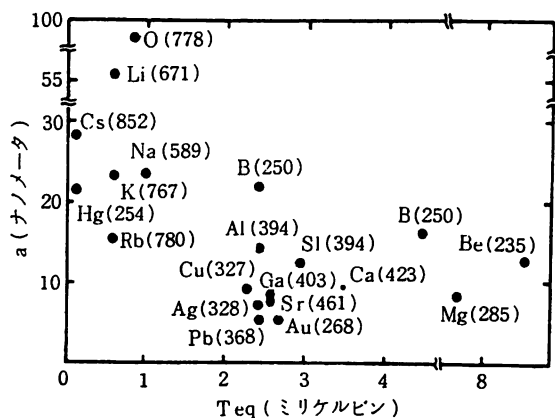


図4 いくつかの原子に対する捕獲ポテンシャル深さを表す等価温度  $T_{eq}$ 、プローブ先端曲率半径の最適値  $a$  の関係。各元素記号の隣の ( ) 内は原子共鳴波長<sup>6)</sup>。

セント光の広がりと同程度であるとき、このような共鳴的相互作用によって図3に示すような疑似的分子状態が生ずることが期待される。すなわち、真空中を浮遊する原子をプローブ先端のエバネッセント光の場の中に捕獲することが可能となる。

図4はいくつかの原子に対する捕獲ポテンシャル深さを表す等価温度 $T_{eq}$ 、プローブ先端曲率半径の最適値 $a$ との関係の計算結果である<sup>6)</sup>。ポテンシャル深さはわずか数mKであるが、レーザ冷却による光糖蜜法を利用して1mK以下の冷却原子を用意することができるので、このポテンシャルは十分深いと考えてよい。現在までに、予備実験によって原子とエバネッセント光との間の大きな運動量のやりとりが確認されている<sup>7)</sup>。

このように真空中で原子が捕獲できれば、その後、その原子を冷却結晶基板上に落とし、単原子レベルでの結晶成長が可能となる。

#### 4. あとがき

本稿では空間的に局在した光を用いた超高解像顕微鏡と原子レベルでの物質操作の可能性を記した。これらの話題は極限的な形態の光と物質を作ること念頭に置いている。これは学術的にも、また産業への応用にも重要で興味深い問題を提示している。本特集の「極限光技術の夢」に関する一つの話題として読者諸兄の興味を引くことができれば幸いである。なお、本稿の内容の詳細については筆者自身の解説などを参考にされたい<sup>8-10)</sup>。

#### 参考文献

- 1) T. Pangaribuan, K. Yamada, S. Jiang, H. Ohsawa and M. Ohtsu, "Reproducible Fabrication Technique of Nanometric Tip Diameter Fiber Probe for Photon Scanning Tunneling Microscope", Jpn. J. Appl. Phys., Vol.31, Part 2, No. 9A, (1992) pp.L1302-L1304
- 2) S. Jiang, H. Ohsawa, K. Yamada, T. Pangaribuan, M. Ohtsu, K. Imai and A. Ikai, "Nanometric Scale Biosample Observation Using a Photon Scanning Tunneling Microscope", Jpn. J. Appl. Phys., Vol.31, No.7, (1992) pp.2282-2287
- 3) E. Betzig, J.K. Trautman, R. Wolfe, E.M. Gyorgy and P.L. Finn, "Near-field magneto-optics and high density data storage", Appl. Phys. Lett., Vol.61, No.2, (1992), pp.142-144
- 4) S. Jiang, J. Ichihashi, H. Monobe, M. Fujihira and M. Ohtsu, "Localized Photochemical Processes in Langmuir-Blodgett Films on Photochromic Material by Using a Photon Scanning Tunneling Microscope", Adv. Program, The 2nd Int. Conf. on NFO, Oct. 1993, Raleigh, NC, USA
- 5) 大津元一, "フォトンSTM(V) -- 単原子レベル結晶成長" 第51回応用物理学会学術講演会, 1990年(平成2年)秋季, 講演番号 27aL79
- 6) M. Ohtsu, S. Jiang, T. Pangaribuan and M. Kozuma, "Nanometer Resolution Photon STM and Single Atom Manipulation", Near Field Optics, D.W. Pohl and D. Courjon (eds.), 1993 Kluwer Academic Publisher, Netherlands, pp.131-139
- 7) K. Kozuma, M. Ohtsu and H. Hori, Experimental Confirmation of Enhanced Momentum of Localized Evanescent Field by Using Doppler-Free Laser Spectroscopy in Rb85", Adv. Program, The 2nd Int. Conf. on NFO, Oct. 1993, Raleigh, NC, USA
- 8) 大津元一, 堀 裕和, "フォトンSTMの実験と理論", 光学, Vol.21, No.11,

- (1992) pp. 780-788
- 9) 大津元一, “フォトン走査トンネル顕微鏡 : 光の回折限界を超えて”, 日本物理学会誌, Vol. 48, No. 1, (1993), pp. 25-28
- 10) 大津元一, “0 (ゼロ) を制御する工学— 光による新しい「真空」の工学—”, 真空, Vol. 36, No. 5, (1993), pp. 461-470

## ◇第13回光波センシング技術研究会

### 論文募集

応用物理学会・光波センシング技術研究会主催

協 賛 : 日本オプトメカトロニクス協会ほか7学会

日 時 : 1994年6月1日(水), 2日(木)

場 所 : 川崎市産業振興会館ホール (川崎市)

### 論文募集内容

範 囲 : 光センサの基礎, 材料・デバイス, 光ファイバセンサ, 光計測機器および光センサ応用にわたる新しい手法, 新しい適用分野に関する発表

●特別セッション「エバネセント波利用」の研究と応用に関する発表

講演申込方法 : アブストラクト (A4判1~2枚) を2部, 下記事務局まで郵送。タイトル, 氏名(発表者に○印), 連絡先(住所☎FAX)を必ず記入。

申込締切 : 3月14日(月) 必着 (FAX可)

原稿締切 : 4月28日(木) 必着 カメラレディ原稿A4判8ページ以内

事務局 : 東京都世田谷区北沢4-16-27 桜ハイツ101 CFBC気付

☎&FAX 03-3466-1899 (福井)

# Highly localized photochemical processes in LB films of photochromic material by using a photon scanning tunneling microscope

Shudong Jiang<sup>1</sup>, Junichi Ichihashi<sup>1</sup>, Hirosato Monobe<sup>1</sup>, Masamichi Fujihira<sup>1</sup>  
and Motoichi Ohtsu<sup>1,2</sup>

<sup>1</sup> *Tokyo Institute of Technology, 4259, Nagatsuta-cho, Midori-ku, Yokohama 227, Japan*

<sup>2</sup> *Kanagawa Academy of Science and Technology, KSP East, 3-2-1 Sakado, Takatsu-ku, Kawasaki 213, Japan*

Received 28 September 1993

A highly localized evanescent light from a fiber probe with a 100 nm diameter aperture of a photon scanning tunneling microscope (PSTM) was used to realize localized photochemical processes in LB films of photochromic material. The localized photochemical processed region sized as small as 130 nm was obtained by using the transmission type PSTM.

## 1. Introduction

Recently, LB films of photochromic materials have been investigated for their possible use as high density information storage media and light switching devices [1]. A highly localized evanescent light from a fiber probe with a sub-wavelength aperture of a photon scanning tunneling microscope (PSTM) [2,3] provides a powerful tool to investigate the photochemical processes in an extremely small region which is limited only by the aperture diameter. It has been proven that the lateral resolution of the image breaks the diffraction limit and high density data storage with domains down to ~60 nm in magneto-optic materials [4] can be obtained by scanning a probe with a sub-wavelength-sized aperture as a light source or detector [5–7]. In this paper, we demonstrate the pure local photochemical processes, i.e. no thermal effect in the process, in the region sized as small as 130 nm. The fabrication of the sub-wavelength aperture in the fiber probe tip is also described. Such a technique can also be applied in the sub-wavelength cell surgery, gene transfection, and so on [8].

## 2. Experiment and discussion

It is well known that when an incident radiation is forced through a sub-wavelength aperture, the evanescent light, which localized around the aperture, can transmit radiative energy to the other object which locates closely to the aperture with a separation smaller than the wavelength of the incident light [6,7]. The basic principle of our local photochemical processing is to use such a transmitted radiative energy of a localized evanescent light to change the structure of a desired region of the sample.

A schematic of the system used for local photochemical processing and detection is shown in fig. 1a. An argon-ion laser with a 350 nm wavelength was employed as a light source. A fiber probe with a sub-wavelength aperture was used to generate the local evanescent light. The sample is a 1 mm thickness quartz substrate on which an amphiphilic azobenzene derivative in a Langmuir–Blodgett (LB) film was prepared as polyion complexes with ionic polymers. A photomultiplier and a lock-in amplifier were used for the phase sensitive detection of the transmission power passing through the sample.

The uv-visible absorption spectra of our sample is shown in fig. 1b [1]. The spectrum (a) corresponds to the trans-isomer and the spectrum (b) corresponds to the partial conversion of the trans-isomer

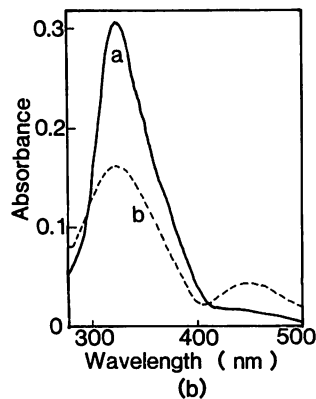
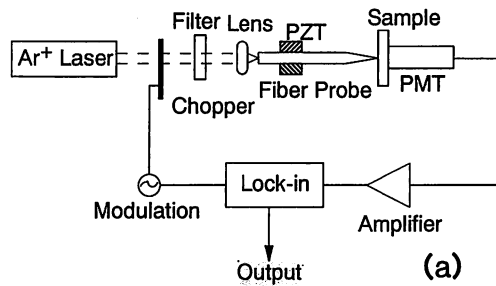


Fig. 1. Schematic of the system used for local photochemical processing and detection (a) and the uv-visible absorption spectra of the photochromic materials (b). Spectra a and b in (b) are the spectra before and after uv irradiation, respectively.

to the cis-isomer that was caused by irradiation of the LB film with uv light. It can be seen that the transmittance decreases to the saturation value of about 15% after the irradiation of a 350 nm wavelength light. In our experiment, the photochemical process was performed by irradiating the laser light with the wavelength of 350 nm to induce the local transition from trans-isomer to cis-isomer, and the detection was carried out by scanning the fiber probe which was coupled with the attenuated laser light with the same wavelength to observe the regions with different absorbance by measuring the transmission power pass through the sample. Because the thermal effect leads to the partial conversion of the cis-isomer to the trans-isomer which corresponds to the increase of absorbance, the decrease of absorbance after the irradiation can be considered only as the result of a pure photochemical process.

Based on the principle of our local photochemical processing, fabrication of a fiber probe with a sub-wavelength aperture to generate the evanescent light is indispensable. For this purpose, an optical fiber was sharpened to have a tip with a cone angle of 25

degrees and tip diameter smaller than 20 nm by using the selective chemical etching technique [5]. Then, the fiber tip was coated with a Au film with an average thickness of about 150 nm after predeposition of a Cr film with a thickness of about 5 nm. For obtaining a good uniformity of the thickness of the coated metal film, the fiber was installed inside the vacuum chamber with an angle of  $\sim 30$  degrees to the horizontal direction of the evaporation source and the fiber was rotated around its axis during evaporation. The power ratio before and after coating was measured to be  $10^{-6}$  when the same power was coupled to the fiber. At last, as shown in fig. 2a, an aperture less than 100 nm was made by control-

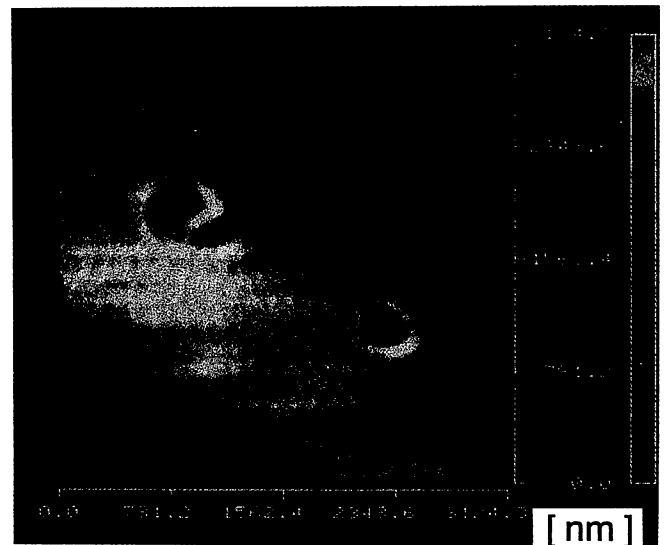
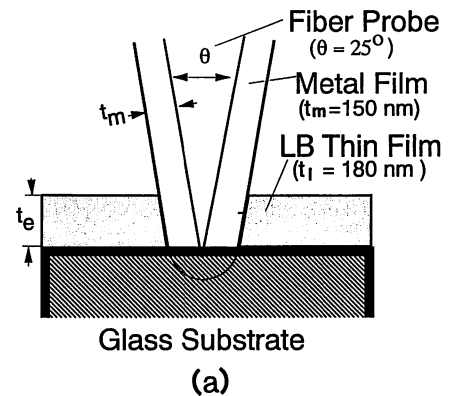


Fig. 2. Fabrication of a aperture with the sub-wavelength diameter in fiber probe tip. (a) The process of the aperture fabrication. (b) Image of the holes in LB thin film, which were obtained by pressing a coated fiber probe tip to the glass substrate.



ling the pressing force between the probe tip and a glass substrate covered with a LB film of  $\sim 180$  nm thickness while the leaked evanescent light was monitored.

Because the LB thin film prepared on the glass substrate is marked after being pressed by the coated fiber tip, the aperture diameter of the fabricated fiber probe can be estimated by measuring the holes diameter in LB thin film in the PSTM operation mode. It was found in the experiment that for fabricating perfectly the aperture with the sub-wavelength diameter, it is necessary to press the coated fiber probe tip to the glass substrate several times, while the pressing point changed slightly. Figure 2b shows the PSTM image of the LB thin film after the aperture fabrication by using the fabricated fiber probe itself. The scanning range was about  $3 \mu\text{m} \times 3 \mu\text{m}$  and the detected transmission power was 0.3 nW. From the result, the largest diameter of the holes was smaller than 400 nm, estimated from the scanning range, and the aperture diameter was measured to be smaller than 100 nm, considering the sharpness of the fiber probe tip and the thickness of the coated metal film and LB film of 150 nm and 180 nm, respectively (referring to fig. 2a). It was also found from a series of experiments that a good reproducibility of the aperture diameter whose variance was less than 30 nm was obtained. This result can be attributed to the fact that the pressing force was easy to be controlled because the cone angle and the cone angle variation of the fiber probe were 25 degrees and smaller than 0.5 degrees, respectively [3], and the coated metal film had a good uniformity.

The dependence of the transmission power on the sample-probe separation was measured for confirming the localization of the radiative energy from the fabricated fiber probe. Figure 3 shows the result. From this result, we concluded that the radiative energy from the fabricated fiber probe with the sub-wavelength diameter was localized with a good localization in normal direction because the power decays exponentially as the sample-probe separation is increased linearly.

Figure 4 shows the result of the localized photochemical process. Photochemical processing was carried out at two regions A and B with the separation of 500 nm in  $y$  direction and 1000 nm in  $x$  direction, respectively, by changing the voltage of the PZT

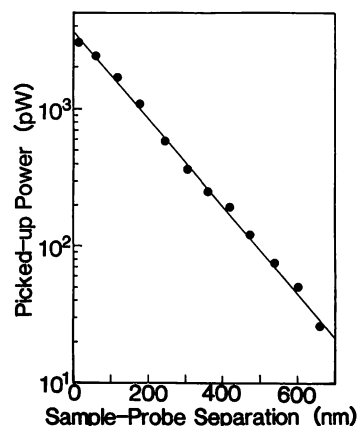


Fig. 3. Dependence between the transmission power and the separation between the glass substrate and the fiber probe.

scanner. The irradiating power for the processes was 30 nW and the processing time of A and B were 15 min and 30 min, respectively. Figure 4a is a PSTM image after such a process. The scanning range of the detection was about  $3 \mu\text{m} \times 3 \mu\text{m}$  with the number and speed of samplings of  $128 \times 128$  and 0.5 s/line, respectively, and the detected power for measuring the absorption difference was about 0.3 nW. The processed regions A and B look like ellipses in fig. 4a, because the time constant of 40 ms of the sensitive phase detection was too large, comparing with the line scanning speed, to have sufficient spatial resolution in the  $x$  direction. A part of the cross section along the a-a' and b-b' direction in fig. 4a is shown in fig. 4b. Peaks A and B were the transmission power difference corresponding to the absorbance difference of the processed regions A and B, respectively. The maximum value of the transmittance difference for both of A and B regions was about 8%, which implies that the change of transmittance was saturated in the case of our used power. The reason that the obtained maximum value of the transmittance difference was smaller than the value shown in fig. 1b can be considered as the amount of the conversion of the trans-isomer to the cis-isomer was changed as the irradiating power was changed. In our case, the size of the processed region is defined, for comparison, as the full width at half maximum of the transmission power difference. Thus, the sizes of A and B were 130 nm and 170 nm, respectively. It can also be found from the experiments that the size of the process region was expanded with the rate of about

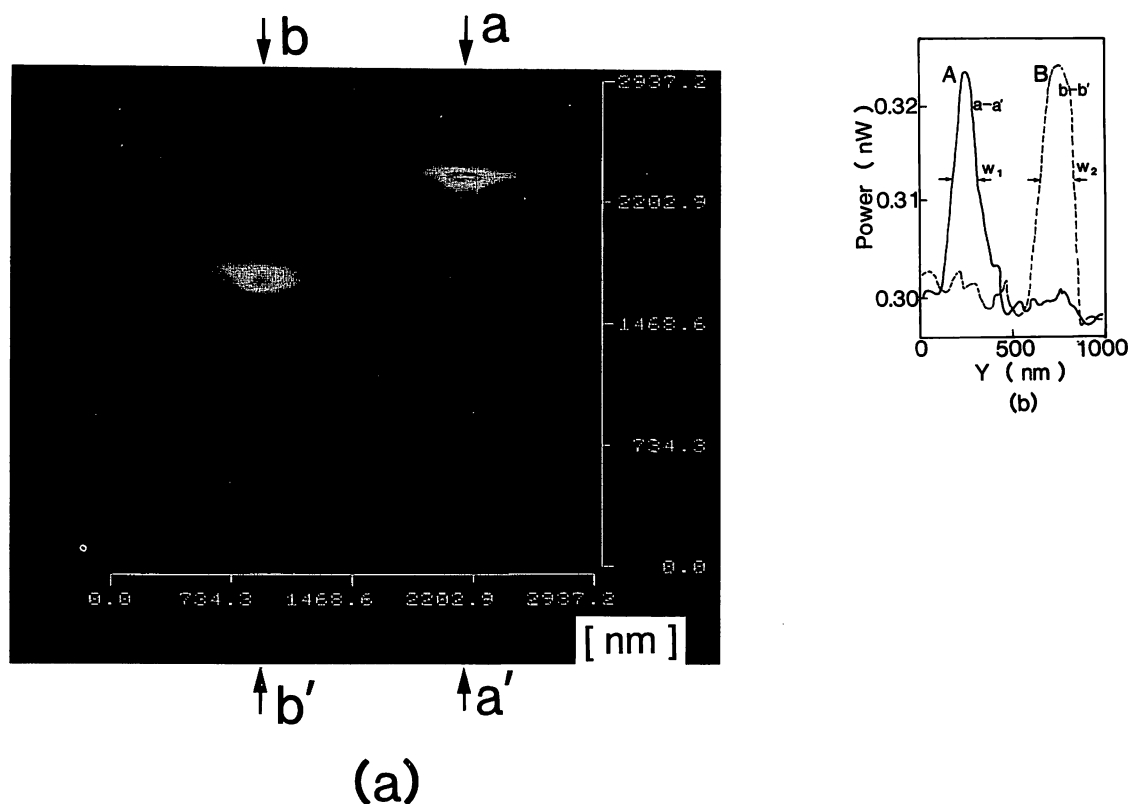


Fig. 4. Results of the localized photochemical process. (a) Image of the processed region observed by using PSTM. (b) Cross section along the a-a' and b-b' direction shown in (a).

2–3 nm/min as the irradiating time increased because the fiber probe drifted along  $x$ ,  $y$  and  $z$  direction due to thermal fluctuation. By improving the stability of the system and optimizing the irradiating time, photochemical process in a region of  $< 100$  nm can be expected.

### 3. Summary

A localized evanescent light from a fiber probe with a 100 nm less diameter aperture of a photon scanning tunneling microscope (PSTM) was used to realize a localized photochemical process in LB films of photochromic material. From the image of the PSTM, it was conformed that the size of localized photochemical-processed region, which was defined as the full width at half maximum of the transmission power difference, was as small as 130 nm. Because of the size, the process region was expanded by the fiber probe drift spatially with the rate of about 2–3 nm/min as the irradiating time increased. Local

photochemical process in a region of  $< 100$  nm can be expected by improving the stability of the system and optimizing the irradiating time. Such a result also demonstrated the possibility of ultra-high density optical storage.

### Acknowledgments

A part of this work was supported by a Grant-in-Aid for Scientific Research (Grant No. 03452089) of Ministry of Education, Science and Culture of Japan, The Kajima Foundation and International Communication Foundation.

### References

- [1] K. Nishiyama and M. Fujihira, *Chem. Lett.* (1988) 1257.
- [2] S. Jiang, N. Tomita, H. Ohsawa and M. Ohtsu, *Jpn. J. Appl. Phys.* 30 (1991) 2107.
- [3] T. Pangaribuan, K. Yamada, S. Jiang and M. Ohtsu, *Jpn. J. Appl. Phys.* 31 (1992) L1304.

- [4] E. Betzig, J.K. Trautman, R. Wolfe, E.M. Gyorgy and P.L. Finn, *Appl. Phys. Lett.* 61 (1992) 142.
- [5] S. Jiang, H. Ohsawa, K. Yamada, T. Pangaribuan, M. Ohtsu, K. Imai and A. Ikai, *Jpn. J. Appl. Phys.* 31 (1992) 2282.
- [6] U. Durig, D.W. Pohl and F. Rohner, *J. Appl. Phys.* 59 (1986) 3318.
- [7] E. Betzig, J.K. Trautman, T.D. Harris and J.S. Weiner, *Science* 251 (1991) 1468.
- [8] M. Tsukakoshi, S. Kurata, Y. Nomiya, Y. Ikawa and T. Kasuya, *Appl. Phys. B* 35 (1984) 135.

## PHOTON SCANNING TUNNELING MICROSCOPE USING DIODE LASERS

S. JIANG<sup>1)</sup>, P. TOGAR<sup>1)</sup>, M. KOZUMA<sup>1)</sup>, J. ICHIHASHI<sup>1)</sup>,  
T. UENO<sup>1)</sup>, M. OHTSU<sup>1,2)</sup> and H. OHSAWA<sup>3)</sup>

- 1) Graduate School, Tokyo Institute of Technology,  
4259 Nagatsuta, Midori-ku, Yokohama 227, Japan
- 2) Kanagawa Academy of science and Technology  
KSP West 614, Sakado, Takatsu-ku, kawasaki 213, Japan
- 3) Nikon Corporation,  
Nishi-Ohi 1-Chome, Shinagawa-ku, Tokyo 140 Japan

### ABSTRACT

A fiber probe with a cone angle and a curvature radius less than 15 degrees and 1nm, respectively, was fabricated. The validity of the quantum theoretical picture of the photon scanning tunneling microscope was confirmed by comparing the experimental and theoretical results of the picked-up efficiency. Sub-wavelength optical data storage with a pit diameter smaller than 270nm in a photochromic LB thin film was also achieved.

The photon scanning tunneling microscope (PSTM) is a powerful tool for observing and manipulating nanometric sample. We have fabricated fiber-probes with cone angles from 20 degrees to 145 degrees and the minimum curvature radius less than 5nm by a HF selective etching technique, and have observed dried T4 bacteriophages with heads (85nm by 115nm) and tails (9nm by 98nm) by using these fiber probes[1].

Based on the quantum theoretical picture of the PSTM[2], the curvature radius and the cone angle of the probe, which is used to disturb and detect the evanescent light localized around the sale surface, must be as small as possible to obtain a high resolution and to avoid picking up low spatial Fourier frequency components of the evanescent light generated from the substrate. For obtaining the fiber probe with smaller curvature radius and cone angle, we used fibers with a 22 mol% Ge doped core and a 2.1mol% F doped cladding to fabricated the fiber probes with the curvature radius and cone angle less than 1nm and 15 degrees, respectively. To demonstrate the high reproducibility of our fiber probe fabrication, a dual-tip fiber probe was fabricated by using a dual core fiber with 60 $\mu$ m core diameter and 40 $\mu$ m core

separation. As a result, the cone angle and height differences between two tips were smaller than 0.2 degrees and 20 nm, respectively.

For evaluating the theoretical resolution of the PSTM by the quantum theoretical picture[2], it is needed to check the validity of this quantum theoretical picture by referring to the experiment. The relationship between the picked up power and the fiber probe cone angle, when the probe-prism separation was at constant, was measured for comparing with the results estimated by the quantum optical picture. A good agreement between the experimental picked up power and the theoretically estimation was obtained.

To demonstrate high density optical data storage, a 200nm Au coated fiber probe with a cone angle of 45 degrees and a sub-wavelength aperture was used. Because the evanescent light emitted from this aperture is used for writing and reading, the diameter of the recorded pit is limited only by the diameter of the aperture. A LB film of azobenzene with the thickness of 180nm was used as the storage medium[3]. Writing was performed by irradiating the laser light with a wavelength of 350nm through the fiber probe to induce local transition from the trans-isomer to cis-isomer, while reading was performed by scanning the fiber probe to detect the absorption difference before and after transition. A pit with a diameter smaller than 270nm was read successfully after 8-min writing by using a 70mW Ar laser power.

Furthermore, as a preliminary experiment of the proposed single atom trapping[2], the Doppler-free spectrum of rubidium atoms was obtained by using evanescent light.

#### ACKNOWLEDGMENTS

The authors wish to thank Prof. M. Fujihira of Tokyo Institute of Technology for supplying the storage medium.

#### REFERENCES

- [1] S.Jiang, H.Ohsawa, K.Yamada, T. Pangaribuan, M. Ohtsu, K.Imai, and A.Ikai, "Nanometric Scale Biosample Observation Using a Photon Scanning Tunneling Microscope", Jpn. J. Appl. Phys., Vol.31, 2282-2287 1992.
- [2] H.Hori, S.Jiang, M. Ohtsu, and H.Ohsawa, "A Nanometer-Resolution Photon Scanning Tunneling Microscope and Proposal of Single Atom Manipulation", Tech. Digest of the 18th International Quantum Electronics Conference pp.48-49, June 1991.
- [3] K.Nishiyama, and M.Fujihira, " cis-trans Reversible photoisomerization of an amphiphic azobenzene derivative in its pure LB film prepared as polyion complexes with polyallylamine", Chem. Lett., pp.1257-1260 1988.

## Experimental Confirmation of Enhanced Momentum of Localized Evanescent Field by using Doppler-Free Laser Spectroscopy in $\text{Rb}^{85}$

M. Kozuma<sup>1)</sup>, M. Ohtsu<sup>1)2)</sup>, H.Hori<sup>3)</sup>

1)Interdisciplinary Graduate School of Science and Engineering,  
Tokyo Institute of Technology, 4259 Nagatsuta, Midori-ku, Yokohama 227, Japan

2)Kanagawa Academy and Science Technology,  
KSP East Rm408, 3-2-1 Sakado, Takatsu-ku, Kawasaki 213, Japan

3)Faculty of Engineering, Yamanashi University,

4 Takeda, Koufu-shi, Yamanashi 400, Japan

We have already proposed a novel physical model for analyzing the fundamental process in a photon scanning tunneling microscope by using Yukawa type function and the possibility of single atom trapping by using the evanescent field localized on the top of a nanometric probe-tip [1, 2]. Such a possibility is due to the high spatial locality and the enhanced momentum of evanescent photon.

If the momentum of an evanescent photon is enhanced compared with that of a free photon, such an enhancement can be considered to come from a dielectric surface directly.

As a preliminary experiment of single atom trapping, we employed the Doppler-free spectroscopic technique in the case of two evanescent fields which were generated by two co-propagating laser beams with different incident angles to confirm the enhanced momentum of evanescent photon. This momentum can be expressed as  $n \sin \theta P_0$ , where  $n$  is the refractive index of a dielectric surface,  $\theta$  is the incident angle of a laser beam and  $P_0$  is the free photon's momentum in a vacuum. When  $\theta$  is larger than the critical angle, the momentum of evanescent photon becomes larger than  $P_0$ . If the momentum is really enhanced, the atom will receive different recoil momenta from each evanescent photon due to the difference of the incident angles.

To demonstrate this phenomenon, the pump frequency was 270MHz blue-shifted from the transition of  $\text{Rb}^{85}$   $D_2$  line  $5S_{1/2} F = 3 - 5P_{3/2} F = 4$  and the probe beam saw a saturation dip due to this velocity-selective pumping. The incident angles of the pump

and probe beams were set to be equal to the critical angle and critical angle  $\pm 3$  degree respectively. The saturation dip shifted from the pump frequency as much as 30MHz was observed as shown in Fig.1. This value agreed with calculated result assuming the momentum of evanescent photon equal to  $n \sin \theta P_0$ .

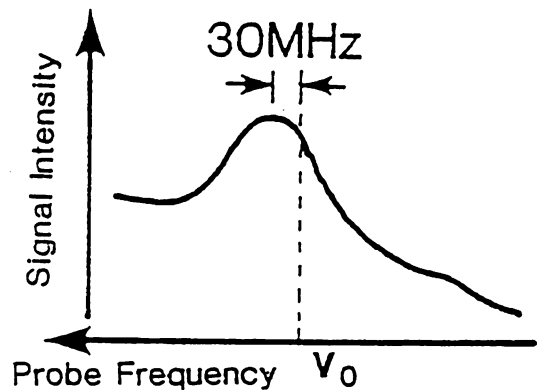


Fig.1 Doppler-Free spectral profile in  $\text{Rb}^{85}$  by using two evanescent fields.  $\nu_0$  represents the pump frequency.

### References

- [1] H. Hori, S.Jiang, M.Ohtsu, and H.Ohsawa. In *18th Int. Quantum Electronics Conf.*, Vienna, June 14-19 1992.
- [2] M. Kozuma, S.Jiang, T.Pangaribuan, M.Ohtsu, and H.Hori. In *Quantum Electronics and Laser Science Conf.*, Baltimore, May 3-7 1993.

Localized photochemical processes in LB films of photochromic material  
by using a photon scanning tunneling microscope

Shudong JIANG<sup>1</sup>, Junichi ICHIHASHI<sup>1</sup>, Hirosato MONOBE<sup>1</sup>,  
Masamichi FUJIHIRA<sup>1</sup> and Motoichi OHTSU<sup>1,2</sup>

<sup>1</sup>Tokyo Institute of Technology, 4259, Nagatsuta-cho, Midori-ku, Yokohama 227, Japan

<sup>2</sup>Kanagawa Academy of Science and Technology, KSP East, 3-2-1 Sakado, Takatsu-ku,  
Kawasaki 213, Japan

Recently, the LB films of photochromic materials have been paid attention for its possible use as high density information storage media and light switching devices[1]. A highly localized evanescent light from a fiber probe with a sub-wavelength aperture of a photon scanning tunneling microscope (PSTM)[2] provides a powerful tool to investigate the photochemical processes in an extremely small region which is limited only by the aperture diameter. A fiber probe with a cone angle of 25 degrees and a tip diameter less than 20nm was fabricated by using the selective chemical etching technique[2], and was coated with a 700nm-thick Cr-Au film. An aperture less than 100nm was made by controlling the pressing force between the probe tip and a glass plate while the leaked evanescent light was monitored. An Argon-ion laser with a 350 nm wavelength was used as a light source and the detector was a photomultiplier. The photochemical process was performed in a LB film of azobenzene with a thickness of 180nm by irradiating the laser light through the fiber probe to induce the local transition from trans-isomer to cis-isomer, and the detection was carried out by scanning the fiber probe to measure the absorption difference before and after the transition[1]. The localized photochemical process was realized in a region with a waist as small as 140nm while the irradiating power and time were 30nW and 30min respectively. The detected power for measuring the absorption difference was about 3nW, and the maximum absorption difference before and after the transition was about 8%, which is the saturation point of the LB thin film which we used in the process. It was also found in the experiments that the region of the process was expanded with the rate of about 10nm/min as the irradiating time increased because the fiber probe drifted along x,y and z direction due to thermal fluctuation. By improving the stability of the system and optimizing the irradiating time, photochemical process in a region of < 100nm can be expected. Such a result demonstrated the possibility of ultra-high density optical storage.

[1] K. Nishiyama and M. Fujihira, *Chem. Lett.*, 1257 (1988).

[2] S. Jiang, H. Ohsawa, K. Yamada, T. Pangaribuan, M. Ohtsu, K. Imai, and A. Ikai, *Jpn. J. Appl. Phys.*, 31, 2282(1992).

Photon Scanning Tunneling Microscopy and Its Application

Motoichi OHTSU

Interdisciplinary Graduate School,  
Tokyo Institute of Technology,  
4259 Nagatsuta, Midori-ku, Yokohama 227, Japan

Ohtsu"Photon Control Project",  
Kanagawa Academy of Science and Technology,  
3-2-1 Sakado, Takatsu-ku, Kawakaki 213, Japan

A photon scanning tunneling microscope (PSTM) is an optical microscope with super-resolution beyond the diffraction-limit based on the near field optics. This paper reviews the recent progress of our study on PSTM which can be used not only as a microscope but also as a nanometric fabrication tool and a manipulator of nanometric particles.

A probe tip for picking up evanescent light is the most essential part in the PSTM system in order to realize high resolution and high sensitivity. One of the reproducible way of fabricating a probe tip is to use an optical fiber. To sharpen the top of the fiber core, we have proposed a selective chemical etching technique which uses a buffered HF solution[1]. By such a process, the curvature radius of the top of the fabricated probe tip was reduced to less than 5 nm and the minimum of the cone angle was as small as  $15^\circ$ .

In order to avoid scratching the sample surface with the cladding edge of the fiber, a two-step etching method was developed to reduce the cladding diameter as small as twice of the core diameter (see Fig.1)[2]. Furthermore, by modifying the selective etching process, a pencil-shaped probe tip without the edge of the fiber cladding and a probe tip with a nanometric flat top suitable for metal evaporation coating have been fabricated.

We have obtained the images of latex spheres with 80 nm diameter, a bacteriophage T4 with the body of 9 nm diameter, and so on[3,4]. Furthermore, we have obtained a near field image of the guided mode of a dielectric optical waveguide and identified the positions and sizes of the scattering sources which would induce a transmission loss of the waveguide.

For obtaining higher resolution and sensitivity, it would be essential to improve the control accuracy of the probe tip position. For this purpose, a slender fiber probe tip fabricated by the two-step etching was installed to the PSTM system and the atomic force induced bending of such a fiber probe tip was detected. This detection of atomic force is effective for position control because of the critical dependence of the atomic force on the tip-sample separation.

One of the possible applications of the PSTM system to the nanometric fabrication could be the high density optical storage which utilizes the high density evanescent optical power leaked from an aperture on the top of the fiber probe tip[5]. The photon-mode optical storage which we have carried out offers the possibility of an erasable optical memory[6]. In our experiment, the memory material was the amphiphilic azobenzene derivative in a Langmuir-Blodgett (LB) film. For storage, the LB film was irradiated with the evanescent light of 350 nm wavelength on the top of the probe tip to induce the local photochemical transition from trans- to cis-isomer, by which the optical transmission of the LB film was increased. By detecting this local increase of optical transmission using the PSTM system, stored memories can be read. Figure 2 shows the result of reading the bits of stored memories. The diameter of each bit was about 130 nm which was blurred by thermal drift of the position of the probe tip. Smaller diameter could be ex-



pected by improving the sensitivity of writing and reading.

As an example of the ultimate fabrication and manipulation by using the PSTM system, we have proposed a method of trapping a freely flying atom in vacuum by utilizing momentum exchange between the atom and the evanescent photon around the probe tip[7]. This proposal aims at realizing the single atom optical memory and the single atom crystal growth. As a preliminary experiment, momentum exchange between the atom and the two-dimensional evanescent photon was observed by using the technique of Doppler-free pump-probe laser spectroscopy[8]. The cavity quantum electrodynamics effect to the atom should be analyzed for more quantitative estimation of experimental parameters.

Fabrication of a functional probe tip and a probe tip array, system operation in liquid, and more reliable preparation of samples, etc., will be required for the PSTM system as being used as a powerful tool in the fields of biotechnology and chemistry.

### References

- [1] T. Pangaribuan, K. Yamada, S. Jiang, H. Ohsawa and M. Ohtsu, Jpn. J. Appl. Phys., Vol.31 (1992) pp.L1302-L1304
- [2] T. Pangaribuan, S. Jiang and M. Ohtsu, Electron. Lett., Vol.29 (1993) pp.1978-1979
- [3] S. Jiang, N. Tomita, H. Ohsawa and M. Ohtsu, Jpn. J. Appl. Phys., Vol.30 (1991) pp.2107-2111
- [4] S. Jiang, H. Ohsawa, K. Yamada, T. Pangaribuan, M. Ohtsu, K. Imai and A. Ikai, Jpn. J. Appl. Phys., Vol.31 (1992) pp.2282-2287
- [5] E. Betzig, J.K. Trautman, R. Wolfe, E.M. Gyorgy and P.L. Finn, Appl. Phys. Lett., Vol.61 (1992) pp.142-144
- [6] S. Jiang, J. Ichihashi, H. Monobe, M. Fujihira and M. Ohtsu, Opt. Commun., Vol.106 (1994) pp.173-177
- [7] H. Hori, S. Jiang, M. Ohtsu and H. Ohsawa, Tech. Digest of the 18th Int. Quantum Electron. Conf. ( June, 1992, Vienna ) pp.48-49
- [8] M. Kozuma, Y. Imai, M. Ohtsu and H. Hori, Tech. Digest of the Int. Quantum Electron. Conf. ( May 1994, Ahaheim ) QFA7

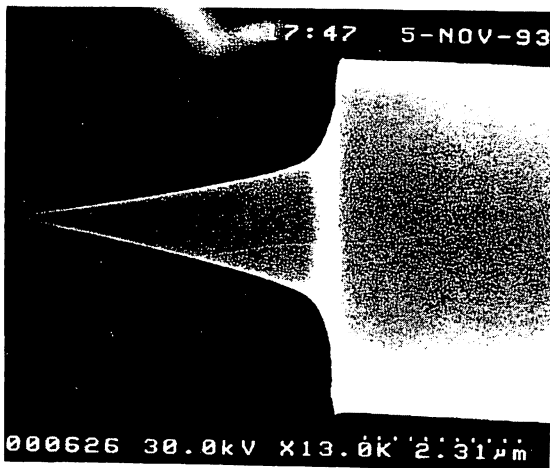


Fig.1 A SEM picture of a fiber probe tip prepared by the two-step selective etching.

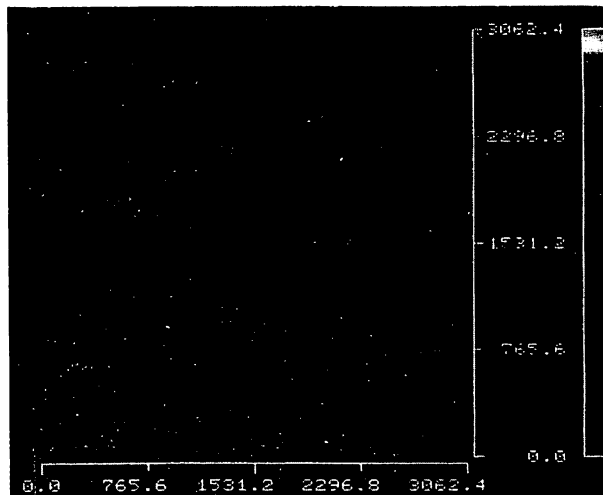


Fig.2 Image of the photon-mode recorded region of the LB film, which was observed by using PSTM.

## High spatial resolution diagnostics technique for optical waveguides using a photon scanning tunneling microscope

Yasunori Toda<sup>1)</sup> and Motoichi Ohtsu<sup>1),2)</sup>

<sup>1)</sup>Interdisciplinary Graduate School of Science and Engineering, Tokyo Institute of Technology, 4259 Nagatsuda, Midori-ku, Yokohama, Kanagawa 227, Japan.

<sup>2)</sup>Kanagawa Academy of Science and Technology, KSP East Rm 408, 3-2-1 Sakado, Takatsu-ku, Kawasaki, 213, Japan.

### abstract

We proposed a high spatial resolution diagnostics technique for the propagation losses and inhomogeneity of the refractive indices in an optical waveguide using a photon scanning tunneling microscope (P-STM). To evaluate the performances of this diagnostics technique, propagating mode profile of LiTaO<sub>3</sub> waveguide were measured.

### §1 Introduction

Propagation losses and refractive indices are important parameters for evaluating optical waveguides. In order to measure these parameters, several measurement methods has been reported so far[1]. However, it has been difficult to diagnose the mode profile in its propagation and uniformity of the waveguide nondestructively with a high spatial resolution.

On the other hand, a photon scanning tunneling microscope (P-STM), which has the advantage of high spatial resolution by scanning the evanescent field on the surface, enables us to diagnostics the propagating mode profile and the deformation of refractive indices of the optical waveguides directly and nondestructively with the subwavelength spatial resolution. Using the P-STM, we propose a high spatial resolution diagnostics technique for the optical waveguide. In order to evaluate this diagnostics technique, propagating mode profiles of LiTaO<sub>3</sub> waveguide were measured.

### §2 Principle and experimental setup

It is well known that an evanescent field is generated in the cladding when the laser light propagates along a waveguide. In the case of the waveguide whose upper cladding layer is air, it is possible to monitor this field by using a fiber probe, and then the propagating mode profile can be monitored through the interaction between waveguide and fiber tip by exchanging evanescent photons.

Because the size of the fiber tip is much smaller than that of the object, it can be regarded as a nondestructive measurement (fig 1.). We have already been succeeded in the fabrication of the fiber tip (fig 2.) of which the curvature radius is less than 10 nm by a chemical etching method[2], so the spatial resolution is expected to be sufficiently high to detect the deformation of the field due to imperfection of the waveguide design and fabrication process can be obtained in this technique by using the P-STM.

- [I] Deformation of structure and inhomogeneity of composition of the device.
  - [II] Propagating mode profile in an integrated optical device.
- They correspond to the characteristics of high spatial resolution and photon scanning of P-STM, respectively

This diagnostics system is constructed conveniently as shown in Fig 3. The light from a diode laser (LD) is incident to a waveguide (WG) coupled by a lens (L). The evanescent field in the layer can be picked up by the fiber tip as shown in Fig.2 and detected by a photomultiplier (PM). A piezo electric transducer (PZT) is used for scanning the fiber tip.

### §3 Evaluation of the system performance

The ferroelectric LiTaO<sub>3</sub> waveguides fabricated by the proton exchange method, which are single mode waveguides at the wavelength of 633nm, are used as samples for evaluating the performances of the present system.

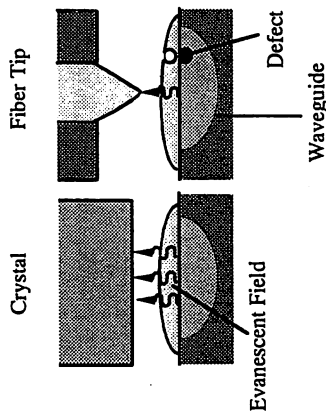


Fig.1 Principles of P-STM method

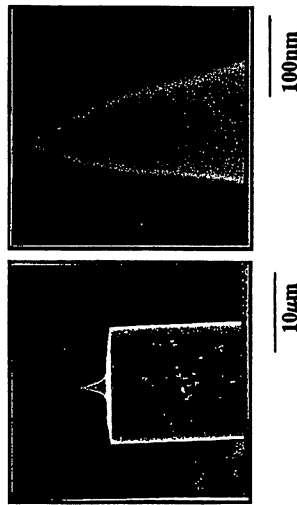


Fig.2 SEM image of fiber tip

For measuring [1], the spatial resolution is important. Fig 4(a) shows the image of the straight waveguide. The scanned area and scanning step of the probe are  $D=15 \times 15 \mu\text{m}^2$  and  $L=60\text{nm}$ , respectively. On the surface and inside of the waveguide, there are some defects which deform the mode profile. Figs 4(b) and (c) magnify one of these points, and the scan area is  $D=3 \times 3 \mu\text{m}^2$ ,  $1 \times 1 \mu\text{m}^2$  respectively. The full width at half maximum (FWHM) of the power distribution is about  $500\text{nm}$ . This results indicate that the spatial resolution of this system is higher than  $500\text{nm}$ , in other words, the resolution has been obtained beyond the diffraction limit. For measuring [II], the separation part of a Y-branch waveguide is measured. Image(a), power distribution(b) and contour plot(c) are shown in fig 5. The image(a) is  $D=5 \times 5 \mu\text{m}^2$ ,  $L=20\text{nm}$ . The present method makes it possible to investigate the separation of the propagating mode profile directly around this area. Combined with the calculation method so far[5], this technique can be employed for investigating the propagating mode in integrated optic devices with subwavelength resolution.

#### §4 Summary

We proposed a high spatial resolution measurement technique for the optical waveguide using photon scanning tunneling microscopy. To evaluate this diagnostics technique, propagating mode profiles were measured using LiTaO<sub>3</sub> waveguide. Some defects can be observed beyond the diffraction limit.

#### Acknowledgments

The authors would like to thank Y. Yokoo (HOYA. co., ltd.), and I.Tanaka (Nippon sheet glass. co., ltd.) for supplying the waveguide.

#### References

- [1] Y.Kokubun, T.Kuroiwa and A.Yamato: MOC/GRIN'93, Tokyo, C5 (1993).
- [2] T.Pangaribuan, K.Yamada, S.Jiang, H.Ohsawa, and M.Ohtsu: Jpn.J.Appl.Phys., vol 31 (1992) L1302.
- [3] S.Jiang, et.al.: Jpn.J.Appl.Phys., vol 30 (1991) 2107.
- [4] S.Jiang, et.al.: Jpn.J.Appl.Phys., vol 31 (1992) 2282.
- [5] T.B.Koch, J.B.Davies, and D.Wickramasinghe.: Electron.Lett., vol 25 (1989) 514.

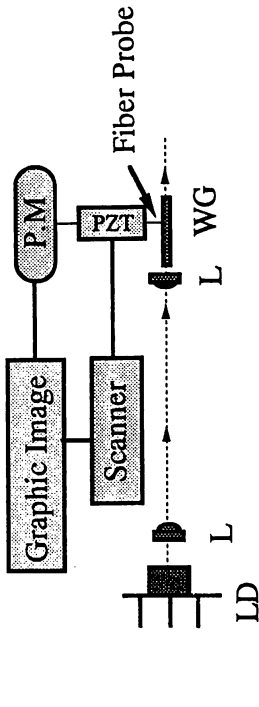


Fig 3. Experimental setup for P-STM method

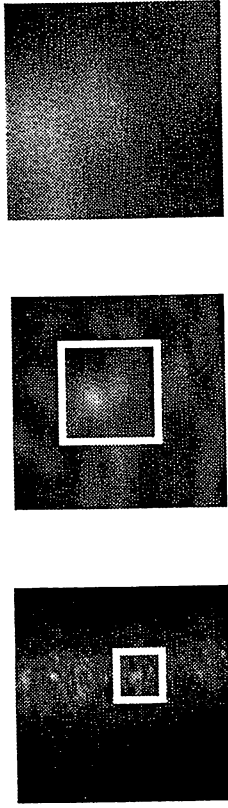


Fig 4. Image of LiTaO<sub>3</sub> straight waveguide  
(a)  $D=15 \times 15 \mu\text{m}^2$  (b)  $D=3 \times 3 \mu\text{m}^2$  (c)  $D=1 \times 1 \mu\text{m}^2$   $L=60\text{nm}$

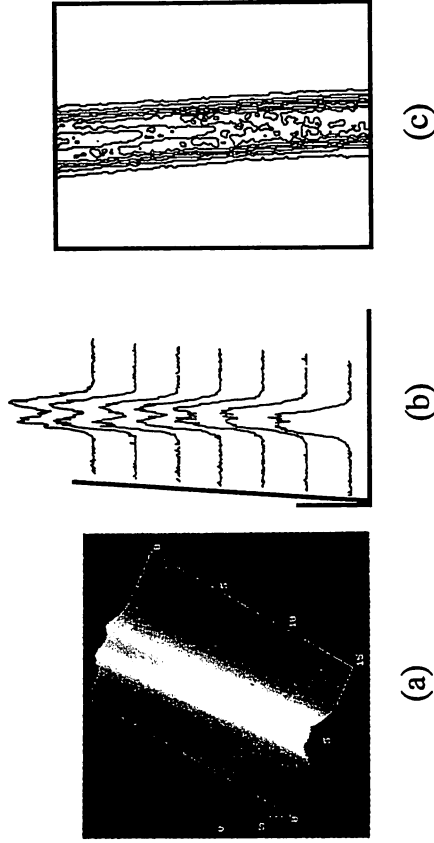


Fig 5. (a) Image (b) Power propagation (c) Contour plot in Y-branch LiTaO<sub>3</sub> waveguide

## Frequency Stabilization of 1.5 $\mu\text{m}$ Diode Laser Using Nonlinear Optical Frequency Conversion in Organic Fiber

Yasunori TODA<sup>1</sup>, Takashi ENAMI<sup>1</sup> and Motoichi OUTSU<sup>1,2</sup>

<sup>1</sup>Interdisciplinary Graduate School of Science and Engineering, Tokyo Institute of Technology, 4259 Nagatsuda, Midori-ku, Yokohama, Kanagawa 227

<sup>2</sup>Kanagawa Academy of Science and Technology, KSP East Rm 408, 3-2-1 Sakado, Takatsu-ku, Kawasaki 213

(Received June 30, 1993; accepted for publication July 17, 1993)

Second-harmonic generation using 1.5  $\mu\text{m}$  diode lasers in a nonlinear organic fiber with Cerenkov radiation phase matching is demonstrated for the first time. This second harmonic frequency was locked to the center of the rubidium spectral line to stabilize the fundamental frequency of the 1.56  $\mu\text{m}$  diode laser. The resultant frequency fluctuation, which was evaluated by the error signal from the lock-in amplifier, was maintained at less than 0.3 MHz for one hour.

**KEYWORDS:** second harmonic generation, nonlinear organic fiber, Cerenkov radiation phase matching, Rb spectral line, stabilization of the laser frequency

### 1. Introduction

There has been much interest in frequency-doubling devices using organic materials of which the second-order nonlinearity is larger than that of inorganic materials. In particular, organic waveguides which can be fabricated by conventional processes are attractive devices for use in optical systems.<sup>1-5</sup> In the case of second-harmonic (SH) generation using a waveguide, Cerenkov radiation phase matching (CRPM) has the advantage of intrinsic phase-matching capability and wide pass bandwidth of fundamental frequency.<sup>6,7</sup> A 3,5-dimethyl-1-(4-nitrophenyl)-pyrazole (DMNP) crystal is one of the developed materials and is suitable for use in a CRPM device because of its high nonlinear coefficient. The cutoff wavelength of this material is around 450 nm and its largest nonlinear optical coefficients  $d_{32}$  is measured to be as high as 90 pm/V.<sup>2</sup> The SH generations by both 0.8  $\mu\text{m}$  and 1.3  $\mu\text{m}$  diode lasers have been reported.<sup>3</sup>

On the other hand, 1.5  $\mu\text{m}$  diode lasers are widely used as the light sources for the coherent optical communication systems, and the frequency stabilization of these lasers is an important technique to be developed.<sup>8</sup> Using the SH generation, the 1.5  $\mu\text{m}$  diode laser frequency can be stabilized to be locked to the center of a rubidium (Rb) spectral line which can be used as a stable and accurate frequency reference at in the 0.78  $\mu\text{m}$  wavelength region.

In this letter, we report the SH generation of 1.5  $\mu\text{m}$  diode lasers in CRPM-DMNP-crystal-cored fiber, and the stabilization of the fundamental frequency by locking it to the Rb spectral line.

### 2. Experimental

The experimental setup for stabilizing laser frequency is shown in Fig. 1(a). In order to obtain higher power for frequency conversion, injection locking was used as the fundamental light source.<sup>9</sup> The master laser was a distributed feedback (DFB) laser with the maximum power of 3 mW and the side-mode suppression ratio of 50 dB. The slave laser was a high-power multimode laser (Oki OL503A-65) with the maximum

power of 65 mW. Under injection locking, the output power was 15 mW with a side-mode suppression ratio of 35 dB and a locking range of 8 GHz.

The schematic explanation of SH generation is shown in Fig. 1(b). The DMNP fiber was a single mode fiber with a cladding of superflint glass (SF15). The core diameter and the length were 1.25  $\mu\text{m}$  and 5 mm, respectively. The largest nonlinear coefficient  $d_{32}$  can be utilized for SH generation by adjusting the polarization direction of the fundamental light parallel to the Y axis of the fiber using a half-wave plate. In this case, the polarization direction of the SH wave was parallel to the Z axis. The fundamental beam of the diode laser was collimated and coupled into the fiber by the collimating lenses. Under the CRPM condition, the cross-sectional profile of SH beam power was conical, which can be collimated by an axicon lens to obtain high efficiency of collimation. After this collimation, the SH

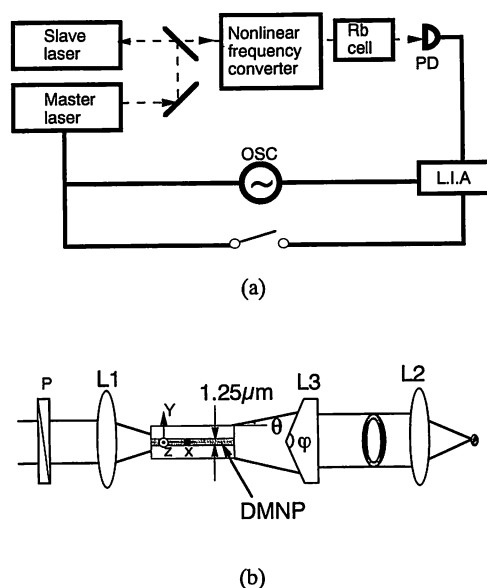


Fig. 1. (a) Experimental setup for stabilizing laser. L.I.A.: lock-in amplifier, O.S.C.: oscillator, PD: si photodetector. (b) The schematic explanation of SH generation. P: half wave plate, L1: collimating lens (N.A 0.5), L2: optical lens, L3: axicon lens.

wave was passed through a compact glass cell (35 mm long) of Rb atomic vapor, and detected by a Si photodiode.

The absorption spectral profile of Rb was measured by sweeping the injection current of the master laser. The frequency of the master laser was modulated by dithering the injection current in order to lock the SH frequency to the first derivative of the Rb absorption spectral line. This derivative signal, obtained via a lock-in amplifier, represents the magnitude of the free-running laser frequency fluctuation. This output signal was thus fed back to the current of the master laser to stabilize the laser frequency.

### 3. Results and discussion

The output power of the generated SH wave was measured to be  $P_{sh} = 1.4 \times 10^{-8} \times P_f^2$ , where  $P_f$  and  $P_{sh}$  represent the fundamental and the SH powers, respectively, in units of watts. The maximum power of the  $P_{sh}$  was 53 nW. Although the frequency doubling have been obtained in CRPM organic materials at the fundamental wavelength of 0.8, 1.06 and 1.3  $\mu\text{m}$ ,<sup>3)</sup> here SH generation in CRPM organic materials by using 1.5  $\mu\text{m}$  diode laser is reported, to our knowledge, for the first time. Because the CRPM condition is independent of the temperature, the temperature tolerance in our frequency conversion is much improved compared with inorganic nonlinear crystals having large nonlinear coefficients such as  $\text{KNbO}_3$ .<sup>10)</sup>

The beam divergence angle of the SH wave was observed using a charge coupled device (CCD) camera. The angle between the SH wave and core axis was

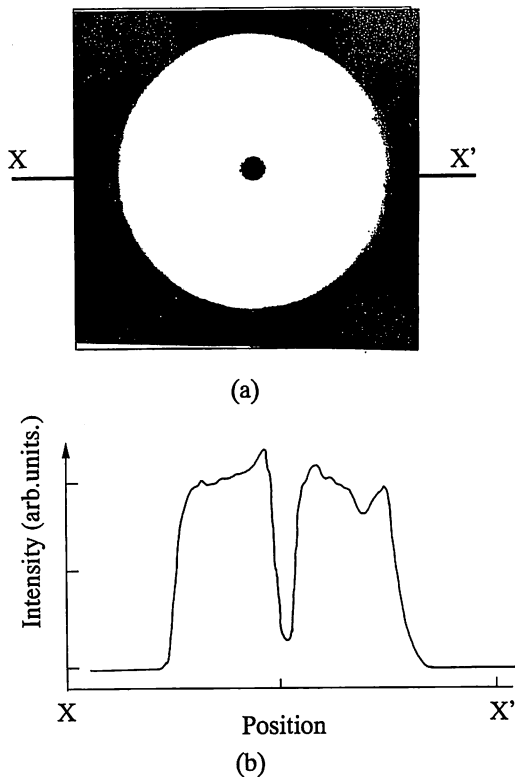


Fig. 2. (a) Pattern of focused SH wave. (b) Power distribution.

measured to be  $\theta = 13.0^\circ$ , as shown in Fig. 1(b). The cone angle  $\phi = 135.8^\circ$  of the axicon lens was determined by referring to the calculated value  $\phi = 136.2^\circ$  using Sellmeier equation<sup>11)</sup> at 0.78  $\mu\text{m}$  for the SF15 glass. After collimating the SH beam with this lens, the radiation angle was measured to be less than  $1^\circ$ . Figures 2(a) and 2(b) show the pattern of the focused SH wave and its cross-sectional power distribution, respectively, observed using the CCD camera.

Figures 3(a) and 3(b) show the absorption profile and the first derivative signal of the Rb- $D_2$  spectral line, respectively, monitored by the SH wave. The four spectral lines of this figure correspond to the transitions from the ground state  $5S_{1/2}$  to the excited states  $5P_{3/2}$  of  $\text{Rb}^{85}$  ( $F=2, F=3$ ) and  $\text{Rb}^{87}$  ( $F'=1, F'=2$ ). The frequency of the SH wave was locked to the transition from the  $F=3$  level of the  $\text{Rb}^{85}$  by closing the feedback

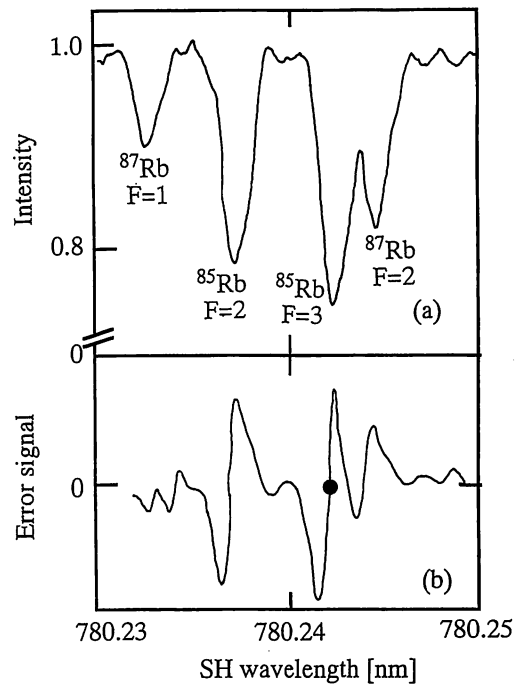


Fig. 3. (a) Linear absorption profile obtained using SH wave, and (b) first derivative signal of the Rb- $D_2$  spectral line.

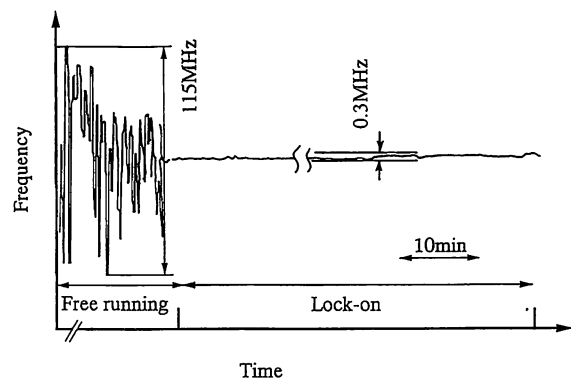


Fig. 4. Temporal variation of the error signal from the lock-in amplifier.

loop of Fig. 1(b). Figure 4 shows the temporal variation of error signal from the lock-in amplifier, which represents the fluctuation of the laser frequency. When the feedback loop was closed, the frequency fluctuation was reduced to less than 0.3 MHz over one hour, which was about 1/380 times that of the free-running laser. This confirms that SH generation in CRPM organic-cored fiber is one of the promising methods for the stabilization of the diode laser frequency at 1.5  $\mu\text{m}$ .

#### 4. Conclusions

Under the CRPM condition, SF generation of a diode laser at 1.5  $\mu\text{m}$  was obtained by using DMNP-cored fiber with the maximum output power of 53 nW. The Rb absorption spectral lines were observed using the SH wave. Frequency stabilization of the 1.5  $\mu\text{m}$  diode laser by locking to one of the spectral lines in Rb has been demonstrated for the first time using the organic device. The resultant frequency fluctuation, which was evaluated as the error signal from the lock-in amplifier, was maintained at less than 0.3 MHz for over one hour.

#### Acknowledgments

The authors would like to thank K. Kamiyama, N.

Nozaki and K. Kubo of Fuji Photo Film Co Ltd. for their useful discussions and comments on the organic-cored fiber.

- 1) J. L. Stevenson and R. B. Dyott: *Electron. Lett.* **10** (1974) 449.
- 2) A. Harada, Y. Okazaki, K. Kamiyama and S. Umegaki: *Tech. Dig. Ser. CLEO'90, Conf. Lasers & Electro-Optics 1992*, paper CFE3, p. 496.
- 3) C. Goto, A. Harada, K. Kamiyama and S. Umegaki: *Tech. Dig. Ser. CLEO'92, Conf. Lasers & Electro Optics 1992*, paper CThA4, p. 392.
- 4) A. Harada, Y. Okazaki, K. Kamiyama and S. Umegaki: *Appl. Phys. Lett.* **59** (1991) 1535.
- 5) O. Sugihara, S. Kunioka, Y. Nonaka, T. Aizawa, Y. Koike, T. Kinoshita and K. Sasaki: *J. Appl. Phys.* **70** (1991) 15.
- 6) P. K. Tien, R. Ulrich and R. J. Martin: *Appl. Phys. Lett.* **17** (1970) 447.
- 7) N. A. Sanford and J. M. Connors: *J. Appl. Phys.* **65** (1989) 1429.
- 8) M. Ohtsu and E. Ikegami: *Electron. Lett.* **25** (1989) 22.
- 9) K. Nakagawa, M. Teshima and M. Ohtsu: *Opt. Lett.* **16** (1991) 1590.
- 10) W. P. Risk, R. Pon and W. Lenth: *Appl. Phys. Lett.* **54** (1989) 1625.
- 11) *Optical Glass Technical Data* (HOYA Co Ltd. Tokyo, 1988) p. 188.

## Sub-MHz Doppler-Free Spectral Line of $5^1S_0-5^3P_1$ Intercombination Transition in Strontium

Alexander AKULSHIN, Alexander CELICOV, Motoichi OHTSU<sup>1,2</sup>,  
Ken'ichi NAKAGAWA<sup>1,2</sup> and Vladimir VELICHANSKY

*P. N. Lebedev Physical Institute, Leninsky pr. 53, Moscow 117924, Russia*

<sup>1</sup>*Interdisciplinary Graduate School of Science and Technology, Tokyo Institute of Technology, 4259 Nagatsuta-cho, Midori-ku, Yokohama 227*

<sup>2</sup>*Kanagawa Academy of Science and Technology, KSP East, Rm. 408, 3-2-1 Sakado, Takatsu-ku, Kawasaki 213*

(Received July 7, 1993; accepted for publication July 28, 1993)

The saturated absorption resonance of an intercombination transition of  $^{88}\text{Sr}$  ( $\lambda=689\text{ nm}$ ) has been observed using a carefully designed external cavity laser diode and gas cell without buffer gas. A minimum linewidth of  $0.7\pm 0.1\text{ MHz}$  has been obtained. The comparison between Sr and Ca reference lines was performed for laser frequency stabilization.

**KEYWORDS:** Sr intercombination transition, laser diode, nonlinear Doppler-free spectroscopy

The intercombination transitions of even isotopes of alkaline-earth metals are very promising for metrological applications due to the fact that they have narrow natural linewidths (Ca, 400 Hz; Sr, 6.9 kHz; and Ba, 250 kHz)<sup>1-3</sup> and both the S and P levels do not have hyperfine structure. Therefore, the transitions are convenient for optical frequency stabilization with high accuracy.<sup>2,3</sup> Also, the  $^1S_0-^3P_1$  transitions are attractive due to the possibility of trapping atoms using their intercombination lines as a second cooling transition. An ultracold gas sample can be obtained in this manner.<sup>4</sup>

Since highly coherent laser diodes (LDs) are now available in the spectral range of these transitions, it is possible to make a simple, inexpensive and compact source of stable optical frequency using LDs and the intercombination transitions of alkaline-earth metals. Based on this trend, nonlinear absorption lines in Ba have been observed using an external-cavity LD.<sup>5</sup> Since the first observation of Doppler-free resonance in a Ca intercombination line using LD,<sup>6</sup> further investigations have been carried out.

In the case of the Sr intercombination line, high-resolution spectroscopy was recently demonstrated by recording the sub-Doppler signal using LD. The observed minimum spectral linewidth was as wide as 6 MHz although the natural width is much smaller.<sup>7</sup> We report here the results of Doppler-free spectroscopy of the Sr  $5^1S_0-5^3P_1$  intercombination line at 689 nm wavelength with improved spectral resolution, using a narrow-linewidth external-cavity LD as a coherent light source and a carefully designed gas cell.

The experimental setup is shown in Fig. 1. We used a 20-cm-long stainless steel cell with hot sapphire windows without buffer gas, similar to that described in ref. 5. Such a cell can be used without windows degradation and without inducing collisional broadening due to buffer gases. In the case of Sr, the cell was heated up to 650°C and continuously pumped during the experiment. The cell pressure did not exceed 0.1 mTorr.

An external cavity LD was used as a light source. The InGaAlP LD device for this light source was Toshiba TOLD 9140 with a 20 mW maximum available output power and a 60 MHz spectral linewidth. An

anti-reflection (AR) film was carefully coated on the LD output facet to achieve stable optical feedback by improving the optical coupling efficiency of the external cavity. The solitary laser threshold currents before and after AR coating were 36 mA and 45 mA, respectively. Fluctuations of the LD heat sink temperature were within 1 mK. The dispersive 30-cm-long external cavity contained a 0.65 NA coupling lens, a piezo-electric transducer (PZT) driven mirror, and a holographic diffraction grating.<sup>8</sup> The external cavity LD was operated in a single longitudinal mode of the external cavity up to 67 mA whereas the threshold current was 39 mA with optical feedback. The maximum single-mode output power of the grating zero order diffracted beam was 6.5 mW. A small part of this power was used to monitor the laser spectrum using a confocal Fabry-Perot cavity and a monochromator. Coarse tuning was achieved by rotating the grating. A continuous fine tuning range as wide as 3.5 GHz was achieved by sweeping the injection current and the cavity length synchronously. The spectral linewidth of the external cavity LD did not exceed 100 kHz even when it was operated in a free-running condition.

The output beam was split into two beams. The lower intensity beam probed the saturation in Sr caused by the higher intensity counter propagating pump beam. The angle between the pump and probe beams was maintained at 0.5 mrad to avoid a parasitic optical feedback to the laser. A weak transverse magnetic field parallel to laser polarization was applied to the Sr cell to allow only  $\Delta m=0$  transitions. The magnitude of linear absorption was about 15%.

Figure 2 shows the saturated absorption spectral dip at the top of the Doppler-broadened profile. The intensities of the pump and probe beams used for this observation were 0.4 mW/cm<sup>2</sup> and 0.1 mW/cm<sup>2</sup>, respectively. The contrast of nonlinear to linear absorption was several percent. The minimum width of the observed Doppler-free resonance was  $0.7\pm 0.1\text{ MHz}$ , which is almost ten times smaller than that previously reported.<sup>7</sup> The improvement of spectral resolution was due to the carefully fabricated stable light source and gas cell without buffer gas. The residual Doppler

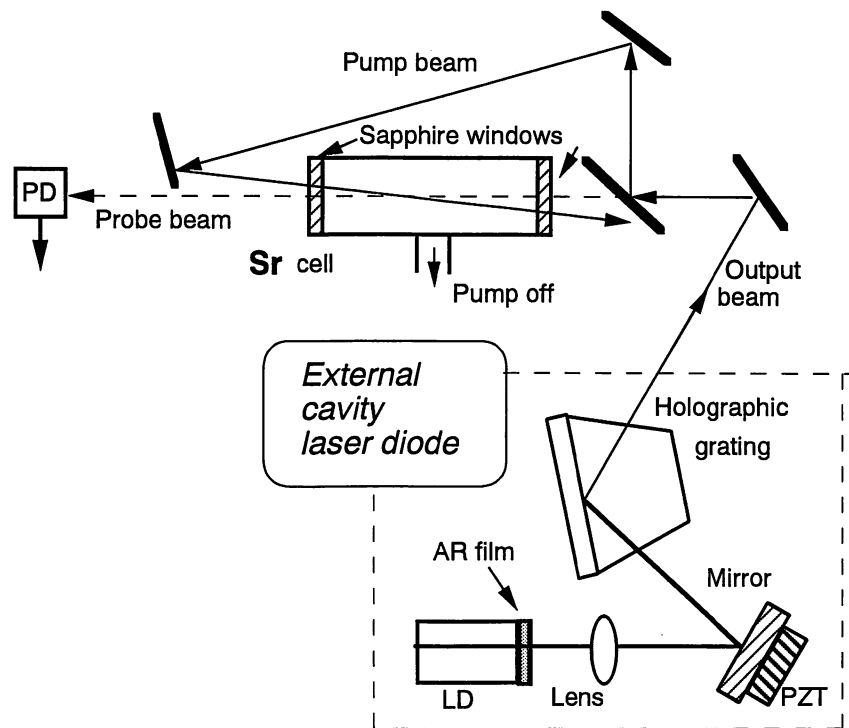


Fig. 1. Optical part of experimental set up. ECLD—external-cavity laser diode; LD—laser diode; HG—holographic grating; PD—photodiode; PZT—piezoceramic; L—microscope objective lens.

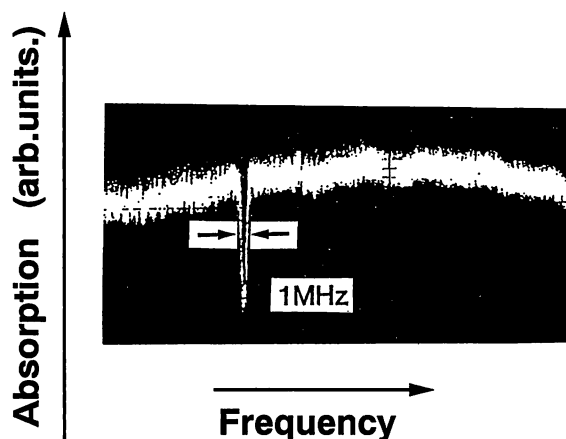


Fig. 2. Nonlinear resonance of saturated absorption on top of Doppler profile on intercombination transition of  $^{88}\text{Sr}$  at 689 nm.

broadening caused by the angle between the pump and probe beams was 0.5 MHz which was the main contribution to the observed spectral broadening. The transit-time broadening and the laser frequency fluctuations due to acoustic noise contributed to the spectral width as well.

For some metrological applications, it is interesting to note that the present intercombination line of  $^{88}\text{Sr}$  at 689 nm has several advantages over the well-known 657 nm intercombination transition in Ca.

1) Sr atoms are heavier, therefore the linear Doppler broadening ( $\Delta\nu_D \approx 1.0$  GHz) is narrower than that in Ca ( $\Delta\nu_D \approx 1.7$  GHz) and the temperature shift of the non-

linear resonance due to the second-order Doppler effect is 0.46 Hz/deg,<sup>1)</sup> which is two times smaller than that for Ca.

2) Since the intercombination transitions in Sr are about 16 times stronger (oscillator strength  $f = 8.6 \times 10^{-4}$ ),<sup>1)</sup> the same magnitude of optical absorption can be obtained for lower atom density using lower vapor temperature.

3) The intercombination transitions in Sr fall within the oscillation spectral range of the visible LD where commercial LD devices have higher power than those for Ca.

It appears reasonable to take into account old suggestions of the self-stabilization of a tunable laser frequency by using a nonlinear absorption cell with alkaline-earth atoms<sup>1)</sup> and a coherent LD. Recently, preliminary results on LD linewidth narrowing have been obtained through the use of the self-stabilization regime on the Rb D<sub>2</sub>-line.<sup>9)</sup> From this point of view, the  $^{88}\text{Sr}$  line is very attractive because the self-stabilization factor is exceptionally high ( $10^4$ – $10^5$ ) and LD linewidth can be reduced to  $10$ – $10^3$  Hz without the use of a servo control system.<sup>1)</sup>

Based on these advantages, it is expected that a narrow Doppler-free resonance in  $^{88}\text{Sr}$  will provide an excellent frequency reference for LD frequency stabilization.

In summary, a  $0.7 \pm 0.1$ -MHz-linewidth Doppler-free saturated absorption spectral profile in Sr was obtained by using a carefully fabricated coherent external-cavity LD and a gas cell.



- 1) V. L. Letokhov and B. D. Pavlik: *Sov. J. Quantum. Electron.* **6** (1976) 32.
- 2) R. L. Barger, J. C. Bergquist and D. J. Glaze: *J. Opt. Soc. Am.* **68** (1978) 1634.
- 3) J. Helmcke, A. Morinaga, J. Ishikawa and F. Riehle: *IEEE Trans. Instrum. & Meas.* **38** (1989) 524.
- 4) J. L. Hall, M. Zhu and P. Buch: *J. Opt. Soc. Am.* **6** (1989) 2196.
- 5) A. Akulshin, A. Celikov and V. Velichansky: *Opt. Commun.* **93** (1992) 54.
- 6) L. Hollberg, R. Fox, N. Mackie, A. S. Zibrov, V. L. Velichansky, R. Ellingsen and H. G. Robinson: in *Laser Spectroscopy X*, ed. G. Camy (World Scientific, Singapore, 1992) p. 347.
- 7) G. M. Tino, M. Barsanti, M. de Angelis, L. Giafranti and M. Inguscio: *Appl. Phys. B* **55** (1992) 397.
- 8) M. S. Soskin and V. B. Taranenko: *Sov. J. Quantum. Electron.* **7** (1977) 298.
- 9) A. Akulshin and M. Ohtsu: under preparation for publication.

## Frequency-tunable sum- and difference-frequency generation by using two diode lasers in a KTP crystal

Weizhi Wang and Motoichi Ohtsu

*Interdisciplinary Graduate School of Science and Engineering, Tokyo Institute of Technology,  
4259, Nagatsuta-cho, Midori-ku, Yokohama 227, Japan*

Received 11 May 1993

Reported are the frequency-tunable sum-frequency generation at 0.52  $\mu\text{m}$  and the difference-frequency generation at 1.6  $\mu\text{m}$  by using two diode lasers at 0.78  $\mu\text{m}$  and 1.54  $\mu\text{m}$ . The influence of the walk-off effect associated with the elliptical gaussian beam of the diode laser was calculated and compared with the experimental results.

A wideband highly coherent tunable light source is required urgently in rapidly developed fields, such as quantum optics and high resolution spectroscopy, in which manipulation of atoms or ions, optical frequency and fundamental physical constant measurements have been paid much attention. To realize a diode-laser-based optical frequency sweep generator covering the wavelengths from ultraviolet to near infrared, nonlinear frequency conversions are performed by employing diode laser and nonlinear crystals [1,2]. By using a KTP crystal, which has large nonlinear coefficients, larger angular and temperature acceptance widths, frequency-tunable coherent light in the green region can be obtained in the sum-frequency generation of diode lasers, while in the near infrared region, frequency down-conversion such as parametric amplification which uses a diode laser and a solid-state laser has been also demonstrated [3]. In this paper, we show our recent experiment results on the sum-frequency generation, in which a 0.52  $\mu\text{m}$  coherent tunable light was obtained by using high-power single mode diode lasers at 0.78  $\mu\text{m}$  and 1.5  $\mu\text{m}$ , and compare the theoretical calculation with the experimental result of the influence of the walk-off in the used KTP crystal on the nonlinear conversion efficiency associated with the elliptical gaussian beam of the diode laser. Furthermore, we also demonstrate the difference-frequency generation, for the first time

to the author's knowledge, by using these two diode lasers.

To extend the sum-frequency generation at a wavelength shorter than the previously reported 0.54  $\mu\text{m}$  green light for which a multimode high-power 1.5  $\mu\text{m}$  diode laser was used [2], we used here a high-power 1.54  $\mu\text{m}$  multi-electrode corrugation-pitch-modulated MQW-DFB laser [4] with a maximum power of 50 mW, and a 50 mW, 0.78  $\mu\text{m}$  diode laser. The experimental setup was the same as our previous one [2] in which a 10 mm length KTP was put in the  $\theta$  plane, i.e.,  $\phi=0^\circ$ , the polarization of the 1.5  $\mu\text{m}$  laser was perpendicular to the  $\theta$  plane and the polarization of the 0.78  $\mu\text{m}$  laser was in the  $\theta$  plane for satisfying the type-II phase matching. A maximum 0.34  $\mu\text{W}$  output at 0.52  $\mu\text{m}$  was obtained. To investigate the angle tuning characteristics of the used KTP crystal in the case of sum-frequency generation, the relation between the output power at the sum-frequency and the detuning of the matching angle of the KTP crystal was measured and is shown in fig. 1. The acceptance angle defined by the fwhm of the curve of the output power versus phase mismatch was measured to be about  $0.5^\circ$ . We also carried out the sum-frequency generation by replacing the 0.78  $\mu\text{m}$  laser with the high-power single mode diode lasers in the 0.8  $\mu\text{m}$  region. The combination of these results has provided us the highly coherent tunable output from 0.51  $\mu\text{m}$  to 0.56  $\mu\text{m}$  corresponding to a span of

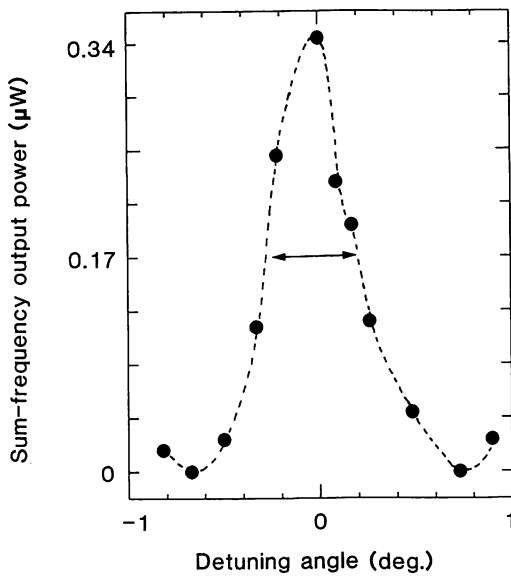


Fig. 1. Measured relation between the output power of the sum-frequency generation and the detuning angle. The phase-matching angle is  $61^\circ$ .

50 THz in the green region by using only diode lasers.

A series of our experiments show that the KTP crystal in the angle matching manner is insensitive to both slight deviation from the matching angle and the temperature fluctuation so as to offer an excellent stability. However, the walk-off effect in KTP, which is due to the double refraction when non-critical phase matching is unavailable, degrades the conversion efficiency. As the walk-off effect becomes more serious when the beams participating in the frequency mixing are focused to make the diameters as small as several tens of  $\mu\text{m}$ , that is the case when the relatively low power single mode diode lasers are employed for the highly coherent light generation, we should pay more attention to optimizing the nonlinear conversion efficiency. Although the theoretical analysis of the nonlinear conversion involving the walk-off effect and the circular gaussian beams has been carried out by several authors [5-7], the influence of the walk-off effect associated with the elliptical gaussian beams as in the case of using diode lasers has not been documented. We present here an extension of the heuristic theory mentioned-above to the case of the type-II frequency mixing in a KTP crystal with the near field approximation and compare the calculation with the experimental results.

In the case that the depletion of the fundamental

waves is insignificant compared with their inputs and the phase matching condition is satisfied, the fundamental waves are assumed to be plane waves and take forms as

$$E_1 = E_{10} \exp[-(x^2/w_{1x}^2 + y^2/w_{1y}^2)] \exp(-i\omega_1 t),$$

and

$$E_2 = E_{20} \exp[-(x'^2/w_{2x}^2 + y'^2/w_{2y}^2)] \exp(-i\omega_2 t),$$

where  $E_{10}$  and  $E_{20}$  represent the field amplitudes at the beam center of the fundamental waves,  $w_{ix}$  and  $w_{iy}$  represent beam waists along the short- and long-axis of the elliptical gaussian beam cross-section, respectively, coordinates  $x'$  and  $y'$  represent so called extra-ordinary waves which deviate from the ordinary waves (coordinates  $x$  and  $y$ ) in propagation [8]. Then we can express the generated wave in the process of frequency mixing (sum or difference) as follows:

$$E_3 = -i \frac{\omega_3 d_{\text{eff}}}{2n_3 c} E_{10} E_{20}$$

$$\times \int_0^L \exp\left[-\left(\frac{x^2}{w_{1x}^2} + \frac{y^2}{w_{1y}^2} + \frac{x'^2}{w_{2x}^2} + \frac{y'^2}{w_{2y}^2}\right)\right] dz,$$

where the subscript  $i$  ( $i=1, 2, 3$ ) denotes the light-wave at the frequency  $\omega_i$ , and  $\omega_i$  satisfies  $\omega_3 = \omega_1 \pm \omega_2$ , i.e., the energy conservation in the frequency conversion, and the temporal terms were neglected for simplicity.  $n$  is the refractive index,  $c$  is the speed of light in vacuum,  $L$  is the length of the crystal, and  $d_{\text{eff}}$  is the effective nonlinear coefficient.

We discuss here only the case of  $\theta$ -phase-matching in which  $\phi=0^\circ$ , so we have  $x' = x - \rho z$ , and  $y' = y$  by referring to fig. 2a, where  $\rho$  represents the double refraction or the walk-off angle. The generated power at  $\omega_3$  can be calculated by

$$P_3 = \frac{1}{2} n_3 c \epsilon_0 \iint_{\text{c.s.}} E_3 E_3^* dx dy,$$

where c.s. implies that the integral is carried out over the crystal cross-section,  $E_3^*$  denotes the complex conjugation of  $E_3$ . As the plane waves have been assumed, better approximation is expected to the case of loose beam focusing, while in the case of tight beam focusing, variation of beam diameters along the propagation inside the crystal should be taken into

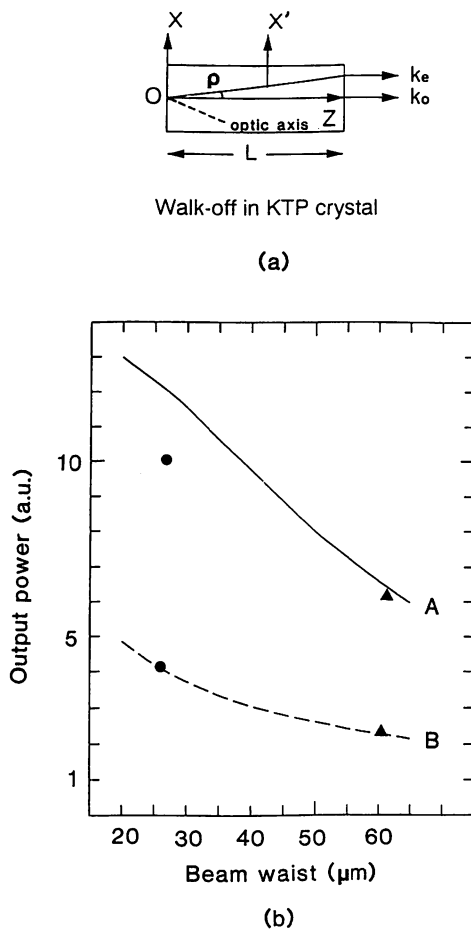


Fig. 2. (a) Coordinates in the crystal.  $k_o$  and  $k_e$  represent ordinary and extra-ordinary waves in the case of  $\phi=0$ ,  $\rho$  represents the walk-off angle. (b) Relative output powers versus beam diameters. Curve A and curve B correspond to the cases that the walk-off occurs along the long- and the short-axis of the elliptical gaussian beam, respectively. One of the participating beams is circular and its diameter is equal to the short-axis diameter of the elliptical beam.

account for evaluating the total output power. However, in comparison of the difference of the walk-off effect between the case that the walk-off takes place along the short-axis of the elliptical beam cross-section and the case of the long-axis, such a calculation offered a good approximation. Figure 2b show the calculation results. Curves A and B correspond to the above-mentioned two cases. For the purpose of comparing the calculation with the experiment, a circular gaussian beam which corresponds to the  $1.5 \mu\text{m}$  diode laser and an elliptical gaussian beam which corresponds to the  $0.78 \mu\text{m}$  diode laser were used in calculation, while the ratio of long-axis short-axis of the elliptical gaussian beam was 3:1 and the walk-off an-

gle was  $\rho=3 \times 10^{-2}$  rad for the used KTP crystal. It is shown that when the walk-off occurs along the long-axis of the elliptical beam, the output power can be more than doubled with respect to the case that the walk-off occurs along the short-axis of the elliptical beam. To confirm our theoretical estimation of the walk-off influence associated with the elliptical gaussian beam shape of the diode laser, we measured the power differences through changing the relative orientation between the crystal and the elliptical beam cross-section. The measurement was carried out by using half-wave plates to change the polarizations of the laser beams and rotating the  $\theta$  plane of the KTP crystal. Two sets of the measured values in fig. 2b are normalized to the smaller one for comparison, corresponding to the experimental condition that lenses with focal lengths of 80 mm and 200 mm were used to focus the two collimated fundamental beams. Enhancement factors by arranging the walk-off along the long-axis of the elliptical beam were 2.13 and 2.26, respectively, and were in fair accordance with the calculated values of 2.9 and 2.3, respectively.

For optimizing the beam parameters in frequency conversion of diode lasers, we also calculated the relation between the output power and the long- to short-axis ratio  $r=w_{1x}/w_{1y}$  ( $w_{2x}/w_{2y}=1$ ), using the beam diameter as a parameter. Figure 3 shows the calculation result. Curves A, B and C correspond to the cases when the beam diameter of the circular one, which is assumed to be equal to the short-axis diameter of the elliptical one, is 30, 60 and 100  $\mu\text{m}$ , respectively. It is noted that the maximum output does not happen at  $r=1$ , which means that the elliptical beam is preferable to the circular one, such an effect was also confirmed in other work [9]. With the increase of the beam diameter, the maximum trends to  $r=1$ , implying that the circular beams can offer good conversion efficiency in the case of large beam diameters. Because the influence of the walk-off effect also depends on the beam diameters, the optimum value of  $r$  for the conversion efficiency varies as the focusing condition is different.

In order to demonstrate the feasibility of the difference-frequency generation using two diode lasers for our intended continuous-wave highly coherent frequency sweep generator [3], we used the same laser in the above experiment to generate the coherent light at  $1.6 \mu\text{m}$ . The experiment setup is shown

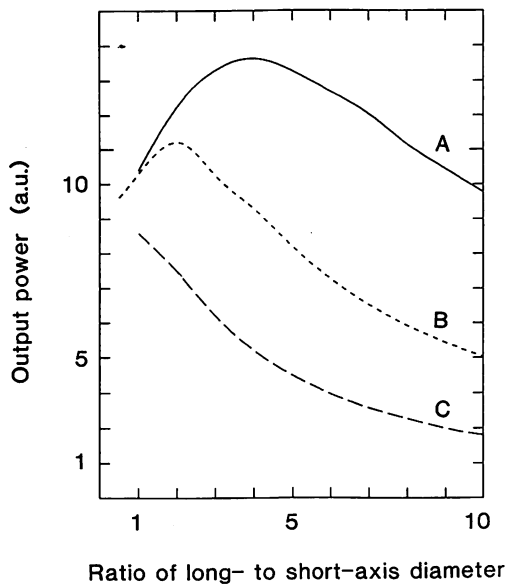
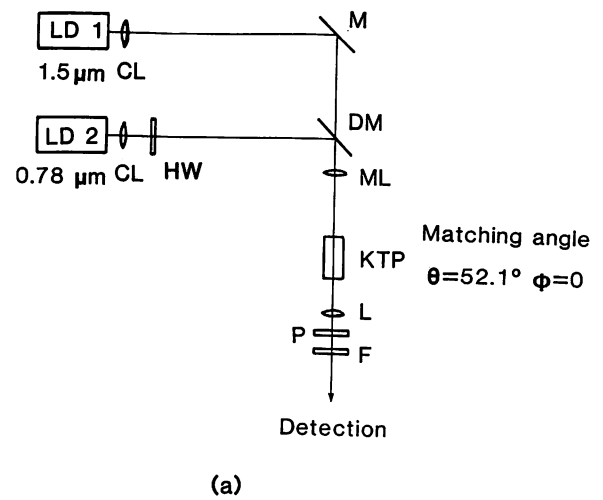


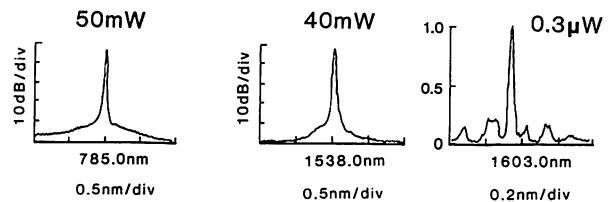
Fig. 3. Calculated relation between relative output power and the long- to short-axis ratio  $r = w_{1x}/w_{1y}$ . The walk-off occurs along the long-axis of the elliptical gaussian beam. Curves A, B and C correspond to  $w_{2x} = w_{2y} = w_{1y} = 30 \mu\text{m}$ ,  $60 \mu\text{m}$  and  $100 \mu\text{m}$ , respectively.

in fig. 4a. The polarization of the  $0.78 \mu\text{m}$  laser was perpendicular to the  $\theta$  plane and the polarization of the  $1.5 \mu\text{m}$  laser was in the  $\theta$  plane. The phase matching angle was  $52.1^\circ$  which was in agreement with the calculated value. The beams were arranged to obtain the higher efficiency based on the above theoretical calculation. Figure 4b shows the measured spectral profiles of the three participating light waves by using an optical spectrum analyzer (Anritsu MS9702B). A  $0.3 \mu\text{W}$  output was obtained. It is the first report of the different-frequency generation by using only diode lasers. The tunable range can be larger than 5 THz ( $1.58\text{--}1.62 \mu\text{m}$ ) by controlling the operation temperatures and currents of the lasers. Since the coherence of diode lasers is conveniently improved by optical and/or electrical feedback techniques [10], the difference-frequency generation by diode lasers can provide us the highly coherent cw tunable light in the near infrared region.

In summary, we reported our experimental progress in realization of the diode-laser-based wideband highly coherent light source. The sum-frequency generation in KTP was extended to  $0.52 \mu\text{m}$  with a  $0.34 \mu\text{W}$  output power by using a  $0.78 \mu\text{m}$  and a  $1.54 \mu\text{m}$  high power single mode laser. For optimizing the nonlinear frequency conversion efficiency in the case



(a)



(b)

Fig. 4. (a) Experimental setup for the difference-frequency generation. HW: half-wave plate; F: filter; P: polarizer; DM: dichroic mirror; L: lens; CL: collimating lens. (b) Spectral profiles of the fundamental waves at  $0.78 \mu\text{m}$  and  $1.54 \mu\text{m}$  and the generated wave at  $1.6 \mu\text{m}$  measured by an optical spectrum analyzer.

of using diode lasers, the influence of the walk-off effect was calculated and compared with the experimental results. Difference-frequency generation at  $1.6 \mu\text{m}$  with a frequency tunable range larger than 5 THz in the same KTP was also achieved by using the above two lasers. Although the output power in our engaged tunable light source system is still low, it can be ready for some primary experiments on spectroscopy and even on the advanced quantum optics. For example, observation of iodine molecule absorption lines by using the sum-frequency generation is under investigation for stabilizing the diode laser frequency and providing a frequency link to the absolute frequency reference in our wideband frequency sweep generator.

The authors would like to thank Dr. M. Okai of

Hitachi Corp. for discussion on the high-power 1.5  $\mu\text{m}$  multi-electrode DFB laser.

### References

- [1] M. Ohtsu, K. Nakagawa, C-H Shin, H. Kusuzawa, M. Kouroggi and H. Suzuki, CLEO'90 (Optical Society of America, Washington, DC, 1990) paper CME5.
- [2] W. Wang, K. Nakagawa, Y. Toda and M. Ohtsu, Appl. Phys. Lett. 61 (1992) 1886; in this paper there is a mistake in the phase matching angle of the sum-frequency generation; it should be  $59^\circ$ .
- [3] W. Wang and M. Ohtsu, Optics Lett., in press.
- [4] M. Okai, T. Tsuchiya, K. Oumi, N. Chinone and T. Harada, IEEE Photon. Technol. Lett. 2 (1990) 529.
- [5] G.D. Boyd and D.A. Kleinman, J. Appl. Phys. 39 (1968) 3597.
- [6] J.-J. Zondy, Optics Comm. 81 (1991) 427.
- [7] K. Asaumi, Appl. Phys. B 54 (1992) 265.
- [8] V.G. Dmitriev and D.N. Nikogosyan, Optics Comm. 95 (1993) 173.
- [9] T. Taira, Jpn. J. Appl. Phys. 31 (1992) L 682.
- [10] M. Ohtsu, K. Nakagawa, M. Kouroggi and W. Wang, J. Appl. Phys., in press.

# Wide-Span Optical Frequency Comb Generator for Accurate Optical Frequency Difference Measurement

Motonobu Kouroggi, Ken'ichi Nakagawa and Motoichi Ohtsu, *Senior Member, IEEE*

**Abstract**—An optical frequency comb (OFC) generator was realized for accurate optical frequency difference measurement of 1.5  $\mu\text{m}$  wavelength semiconductor lasers by using a high frequency LiNbO<sub>3</sub> electrooptic phase modulator which was installed in a Fabry-Perot cavity. It was confirmed that the span of the OFC was wider than 4 THz. By using semiconductor lasers whose spectrum linewidths were narrowed to 1 kHz and a sensitive optical balanced-mixer-receiver for measuring beat signal between the sideband of the comb and the laser, we demonstrated a frequency difference measurement up to 0.5 THz with a signal-to-noise ratio higher than 61 dB, and a heterodyne optical phase locking with a heterodyne frequency of 0.5 THz in which the residual phase error variance was less than 0.01 rad<sup>2</sup>. The maximum measurable frequency difference, which was defined as the sideband frequency with the signal-to-noise ratio of 0 dB, was estimated to be 4 THz.

## I. INTRODUCTION

HIGHLY accurate laser frequency measurement [1]–[5] is an essential technique for industrial applications such as coherent optical communication systems, and for precision physical measurements, such as standard of length and Rydberg constant measurements [1], [2]. However, highly accurate laser frequency measurement systems, which directly measure the absolute optical frequency, need many big gas lasers and short-lifetime point contact diodes such as metal-insulator-metal diodes [6]. Furthermore, coherent optical communication systems require frequency difference measurements to determine the arbitrary frequencies of lasers which are spaced in a span as wide as several terahertz (THz). However it is difficult to measure such a high frequency difference. Though a metal-insulator-metal diode is known as a device which can measure frequency differences up to 2.5 THz [6], it is inconvenient because the device cannot be stable for long time, and a far infrared laser is required. Although a system using frequency dividing method [7] has been proposed, the system requires about ten tunable lasers to measure a frequency difference as high as 1 THz.

Hänsch *et al.* developed an electrooptic (EO) modula-

tor [8] which was modulated by a 72 GHz modulation frequency, and they used it for a frequency difference measurement. Wong *et al.* proposed an optical frequency measurement system which uses optical parametric oscillators and an optical frequency comb (OFC) generated by an EO modulator [9]. The reason why the optical frequency measurement method using a modulator is paid attention to is that the method is highly accurate and simple. Kobayashi *et al.* successfully achieved generating an OFC with a span of 0.68 THz by using a high frequency EO modulator at 0.5  $\mu\text{m}$  wavelength [10] even though the purpose of their device was not for optical frequency measurements. It is known that it is possible to increase the span of the sidebands by installing a modulator in an optical cavity [11]. It is expected that, when both the methods reported in [10], [11] are used for generation of an OFC, a frequency difference as high as several THz can be measured.

Recently, we have proposed a compact, highly accurate, and wide span optical frequency measurement system at 1.5  $\mu\text{m}$  wavelength [12] using an OFC generator. This system covers wide window region of optical fiber around 1.5  $\mu\text{m}$  wavelength for optical fiber communication systems, such as a channel selector for frequency division multiplexed communication systems over 1000 channels. We have also reported preliminary experimental results [13] of the proposed frequency difference measurement system using a modulator installed in an optical cavity as an OFC generator, and have shown that a 0.85 THz frequency difference can be measured.

In this paper, we show the principle of the proposed high accurate laser frequency measurement system at 1.5  $\mu\text{m}$  wavelength, and report the experimental results of an OFC generator which was developed by using an improved EO phase modulator installed in a Fabry-Perot cavity. By using semiconductor lasers whose spectral linewidths were narrowed to 1 kHz and a sensitive optical balanced-mixer-receiver for measuring the beat signal between the OFC and the laser, we demonstrate a frequency difference measurement up to 0.5 THz, and a heterodyne optical phase locking with a heterodyne frequency of 0.5 THz. We show that the maximum measurable frequency difference using the OFC generator was 4 THz, which was defined as a sideband frequency with a signal-to-noise

The authors are with the Interdisciplinary Graduate School of Science and Engineering, Tokyo Institute of Technology, 4259 Nagatsuta, Midori-ku, Yokohama Kanagawa 227, Japan.

IEEE Log Number 9211558.

ratio of 0 dB, and we discuss the necessary conditions in order to increase the maximum measurable frequency difference to 10 THz.

## II. EXPERIMENT OF OPTICAL-FREQUENCY-COMB-GENERATOR AND OPTICAL PHASE LOCKING

At the beginning, we propose an optical frequency measurement system at 1.5  $\mu\text{m}$  wavelength and explain the principle of optical frequency difference measurement using an OFC generator.

Fig. 1(a) shows the proposed highly accurate optical frequency measurement system at 1.5  $\mu\text{m}$  wavelength. This system consists of two parts. One is a highly accurate frequency reference laser ( $\text{LD}_R$ ) system at 1.55  $\mu\text{m}$ . The other one is an OFC generator for the measurement of the frequency difference between the  $\text{LD}_R$  and lasers under test ( $\text{LD}_X$ ), and the frequency difference can be as large as several THz.

The frequency  $\nu_R$  of the  $\text{LD}_R$  is fixed to  $(\nu_1 - \nu_2)/2$  by generating the lightwave of the sum and difference frequencies of  $\text{LD}_R$  and a solid-state laser at 1.06  $\mu\text{m}$  ( $\nu_s$ ), and by locking the sum and difference frequencies to the frequencies ( $\nu_1$  and  $\nu_2$ ) of two stabilized He-Ne lasers, where  $\nu_1$  and  $\nu_2$  are the absolute frequencies of two stabilized He-Ne lasers locked to  $^{127}\text{I}_2$  (0.633  $\mu\text{m}$ ), and  $\text{CH}_4$  (3.39  $\mu\text{m}$ ), respectively.  $\text{LiNbO}_3$  can be used for sum and difference frequency generations. Since the heterodyne measurement is very high sensitive, high powers of the sum and difference frequency signals are not required for the present system. For example, by a preliminary experiment, we have already obtained a heterodyne signal between the sum frequency signal of 0.7  $\mu\text{W}$  power and stabilized 0.633  $\mu\text{m}$  He-Ne laser. The accuracy of  $\nu_R$  is determined by those of the two stabilized He-Ne lasers. From the values of the uncertainty for  $\text{I}_2$ - and  $\text{CH}_4$ -stabilized He-Ne lasers which are documented in [3], i.e., 74 and 9 kHz, respectively, the uncertainty of  $\nu_R$  is estimated to be 37 kHz ( $:\sqrt{(74 \text{ kHz}/2)^2 + (9 \text{ kHz}/2)^2}$ ), or 1.9 part in  $10^{10}$ . From the results of more recent measurements of He-Ne laser frequencies [4], [5], the uncertainty of  $\nu_R$  is estimated to be one part in  $10^{11}$ .

The OFC generator generates modulation sidebands from an incident laser beam, and the generated sidebands are used as local oscillators to measure the frequency difference between the  $\text{LD}_X(\nu_X)$  and  $\text{LD}_R$  whose frequency difference is higher than the responsible frequency ( $\cong 10$  GHz) of photo diodes. As shown in Fig. 1(b), the value of the frequency  $\nu_X$  of laser under test  $\text{LD}_X$  is determined by measuring the frequency difference  $f_H$  between  $k$ th generated sideband of  $\text{LD}_R$  and  $\text{LD}_X$ , i.e.,  $\nu_X = \nu_R + f_H + kf_m$ , where  $f_m$  is the modulation frequency of the OFC generator. The accuracy of the frequency difference measurement can be equal to that of the modulation frequency. From this, we can say that it is important to realize a wide-span OFC generator for the proposed accurate optical frequency measurement system. Next we show the experimental study of the wide-span OFC generator.

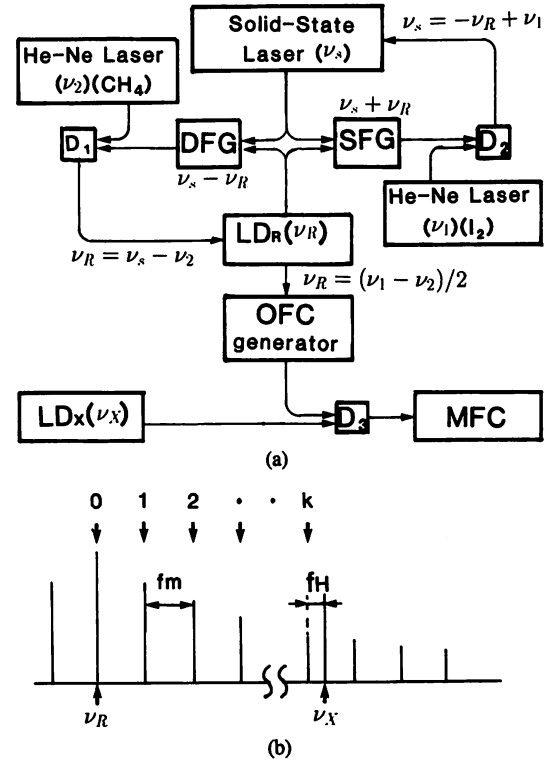


Fig. 1. (a) Proposed optical frequency measurement system for 1.5  $\mu\text{m}$  wavelength semiconductor lasers. SFG, sum frequency generator; DFG, difference frequency generator; MFC, microwave frequency counter; D's, photodiodes. (b) Schematic explanation of the relative frequency locations of the lasers.

Fig. 2 shows the improved OFC generator which consists of an improved bulk-type EO phase modulator, which is similar to the scheme proposed by Lee *et al.* [10] installed in a Fabry-Perot cavity. The EO phase modulator was composed of an antireflection coated  $\text{LiNbO}_3$  crystal ( $1.25 \times 1.0 \times 20.0 \text{ mm}^3$ ) inserted in a microwave guide. In order to realize a highly efficient EO phase modulator which is operated at a high frequency, the width of the microwave guide was designed to be microwave-resonant in order to concentrate the microwave power in the crystal and to match the optical group velocity and microwave phase velocity in the crystal. By installing the modulator in the Fabry-Perot cavity, it is possible to increase the span of the OFC when the modulation frequency is nearly equal to  $n \times \text{FSR}$ , where  $n$  is an integer and FSR is the free spectral range of the Fabry-Perot cavity.

Specifications of the OFC generator were:

Modulation frequency:  $f_m \cong f_{m0} \cong 3 \text{ FSR} = 5.8 \text{ GHz}$  ( $\text{TE}_{102}$  mode.)

Microwave power:  $P_\mu = 10 \text{ W}$ ,

Modulation index:  $m = 0.2 \pi \text{ rad}$ ,

Crystal-loaded finesse of the Fabry-Perot cavity:  $F = 200$ ,

Efficiency of the Fabry-Perot cavity:  $\eta_{\text{FP}} = 5\%$ .

Fig. 3 shows the experimental set up.  $\text{LD}_R$  and  $\text{LD}_X$  were both multi-quantum-well distributed feedback lasers at 1.5  $\mu\text{m}$  wavelength. In order to achieve high resolution



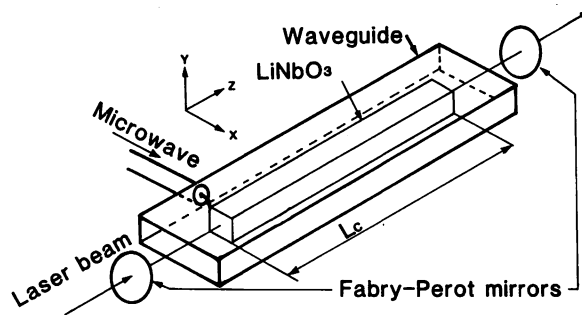
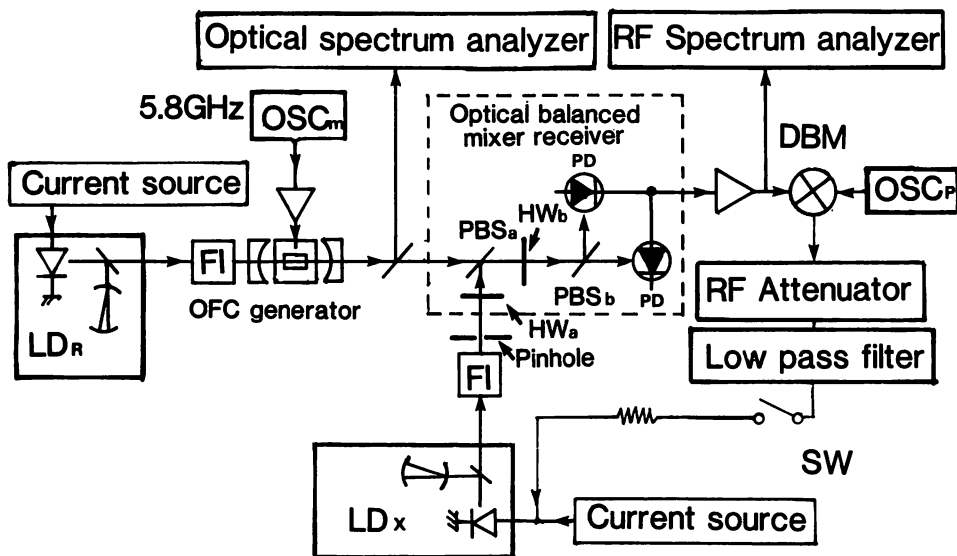


Fig. 2. The construction of the present optical frequency comb generator.


 Fig. 3. Experimental setup. LD's, optically fed-back multi-quantum-well distributed feedback lasers at  $1.5 \mu\text{m}$  wavelength; FI, Faraday isolator; PD's, photodiodes; PBS's, polarized beam splitters; HW's, half wave plates; DBM, RF double balanced mixer; OSC's, RF oscillators.

measurement of the beat signal between one sideband of  $\text{LD}_R$  generated by the OFC generator and  $\text{LD}_X$ , we used an optical feedback method [14] to reduce their spectral linewidths. Their 3 dB-linewidths  $\Delta\nu_X$  and  $\Delta\nu_R$  were estimated to be about 1 kHz from the experimental results of optical phase locking which are shown later in this section. The laser power  $P_i$  of the  $\text{LD}_R$  incident into the OFC generator was about 7 mW. The value of  $\nu_R - \nu_X$  was controlled within 0.5 THz by controlling the temperatures and the injection currents of the lasers. An optical balanced-mixer-receiver is known as a reliable photo-detector for heterodyne signal detection because it conserves local oscillator power and cancels excess intensity noise [15]–[17]. Thus, we used a balanced-mixer-receiver. The optical balanced-mixer-receiver consisted of two photodiodes with the quantum efficiency  $\eta_{\text{PD}}$  of 0.8, two polarization beam splitters (PBS's) and two half wave plates (HW's). The laser powers detected by the two photodiodes of the optical balanced-mixer-receiver are adjusted by the half wave plate ( $\text{HW}_b$ ). A pin hole was used in order to achieve matching of the beam spot size of  $\text{LD}_X$  and  $\text{LD}_R$ . As a result, laser power  $P_X$  from  $\text{LD}_X$  to the

optical-balanced-mixer-receiver was reduced to 3 mW, but this value was high enough to obtain shot-noise limited signal. Additional circuits, composed of a radio frequency (RF) double balanced mixer, a low pass filter, an RF attenuator, and an RF oscillator ( $\text{OSC}_P$ ), inserted between the optical balanced-mixer-receiver and  $\text{LD}_X$ , were for the optical phase locking.

In Fig. 4, curves *A* and *B* show the noise level of the beat signal detection without and with the optical balanced-mixer-receiver, respectively. The broken line shows the shot noise level. By an auxiliary experiment, it was confirmed that the principal contribution to the noise of the curve *A* was the intensity fluctuation of the  $\text{LD}_X$ . It is seen that the noise level of the curve *B* was reduced to the shot noise level in a wide range of Fourier frequency. When the beat frequency  $f_H$  is in such a range, it is possible to realize the shot-noise-limited detection of the beat signal between  $\text{LD}_X$  and a sideband of  $\text{LD}_R$ . In the following discussion, the noise level is assumed to be the shot noise level.

Fig. 5 shows a typical spectral profile of the beat signal between the  $\text{LD}_X$  and the 84th sideband of the  $\text{LD}_R$ . The

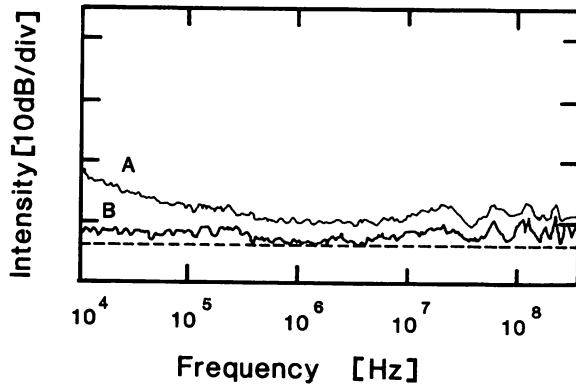


Fig. 4. The noise level in the measurement of the beat signal. Curves A and B are the noise levels without and with balanced mixer receiver, respectively. Broken line is the shot noise level.

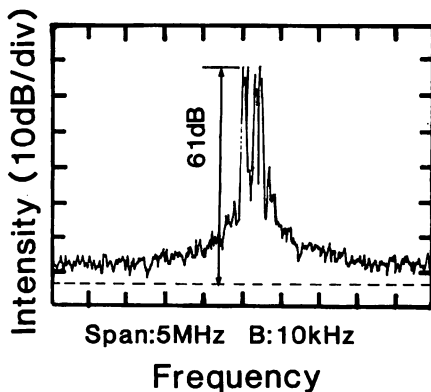


Fig. 5. Spectral profile of a beat signal. Broken line is the shot noise level.

resolution bandwidth  $B$  of the RF spectrum analyzer was 10 kHz. The broken line was the shot noise level. In this measurement, the detuning of the modulation frequency  $\Delta f_m (\equiv f_m - f_{m0})$  and phase of the Fabry-Perot cavity  $\varphi (\equiv \pi(\nu_R - \nu_{FP})/FSR)$ , where  $\nu_{FP}$  is the closest resonant frequency of the Fabry-Perot cavity) were set to 0 Hz and 0 rad by adjusting the modulation frequency and voltage of a PZT attached to the Fabry-Perot cavity mirror. In order to know the order of sideband,  $k$ , we measured the frequency shift of  $f_H$  by changing slightly the modulation frequency. The shift of the  $f_H$  must be equal to the value of  $k$  times the shift of modulation frequency. As a result,  $k$  of the Fig. 5 was measured to be 84, i.e.,  $\nu_R - \nu_X \cong 0.487$  THz. The uncertainty of the measured frequency difference depends on the accuracy of  $f_m$  and the RF spectrum analyzer. If  $f_m$  is calibrated by an atomic clock, such as a rubidium clock (6.8 GHz) or a Cesium clock (9.2 GHz), the value of frequency difference can be measured with an uncertainty of 1 part in  $10^{12} \sim 10^{14}$ . It is seen that the signal-to-noise ratio was 61 dB in Fig. 5. This value was increased by 43 dB in comparison with the previous experiment [13], because of using of the balanced-mixer-receiver and increasing of the modulation frequency.

Fig. 6 shows the relation between the signal-to-noise ratio and  $kf_m$  (frequency difference between the carrier fre-

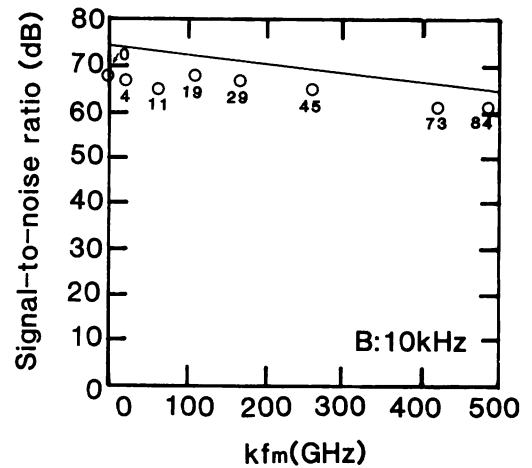


Fig. 6. Signal to noise ratio of the beat signals. Solid line is the calculated result. Open circles are experimental results.

quency and the  $k$ th sideband frequency of  $LD_R$ ). Open circles are the experimental results. The resolution bandwidth  $B$  was 10 kHz. The numbers attached to the open circles indicate the orders of sidebands. The solid line shows the value calculated by (1) and (4) in Section IV. It can be seen from this figure that the experimental results were in good agreement with the calculated results, and that the slope of the signal-to-noise ratio as a function of  $kf_m$  is 19 dB/THz. The maximum measurable frequency difference is roughly estimated from this result to be 4 THz, which is defined as  $kf_m$  at a signal-to-noise ratio of 0 dB. In Section IV, we calculate it by taking account of a crystal dispersion.

Fig. 7(a)-(c) show the envelope of the OFC spectrum observed with an optical spectrum analyzer, where (a)  $\varphi = 0$ ,  $\Delta f_m = 0$ , (b)  $\varphi = 0$ ,  $\Delta f_m = 5.5$  MHz, and (c)  $\varphi = 0.15\pi$ ,  $\Delta f_m = 5.5$  MHz. The broken lines in these figures show the sensitivity limit of the optical spectrum analyzer. The center wavelength in these figures is the wavelength of  $LD_R$ . From these figures, the shape of the envelope of the OFC was controlled by changing the values of  $\varphi$  and  $\Delta f_m$ . In Section IV, we will discuss about the optimization of  $\varphi$  and  $\Delta f_m$  to increase a maximum measurable frequency difference. It is seen from Fig. 7(a) that the envelope extends to a width as wide as 32 nm (or 4 THz). To our knowledge, this value is the widest span of an OFC generated by EO modulation. Because the measurement of the optical beat signal is more sensitive than the measurement using an optical spectrum analyzer, it is possible to use higher order sidebands which have not been observed with the optical spectrum analyzer. Compared to the result in Fig. 6, it is expected that the signal-to-noise ratio of the beat signal detection between sideband of  $kf_m \cong 2$  THz and  $LD_X$  will be higher than 30 dB.

An optical phase locking loop [14] is an essential technique for synthesizing and measuring the optical frequency. If we phase-lock a laser to a high order sideband of the OFC, this laser can be used for generating another new OFC. By repeating this process, the span of the entire OFC can be expanded. We tried to phase-lock  $LD_X$

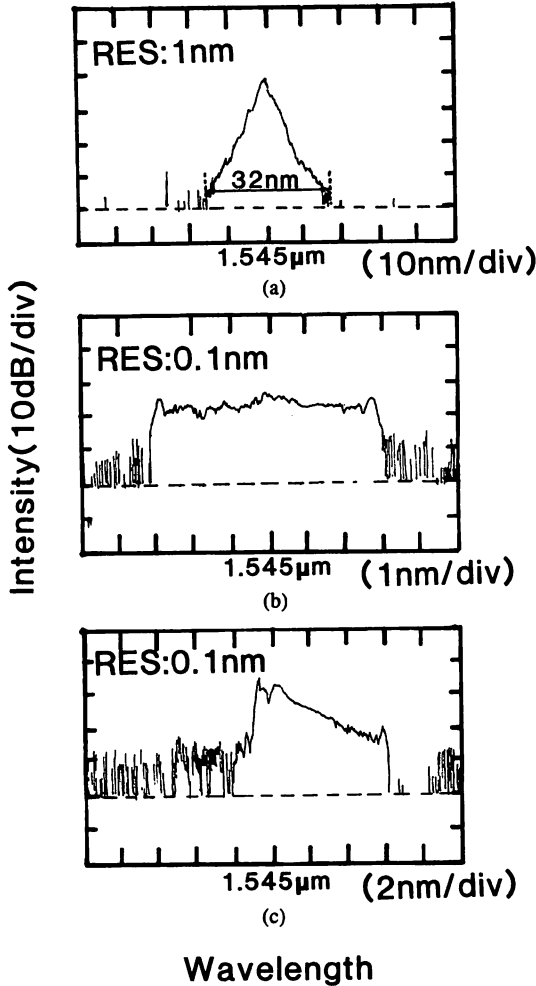


Fig. 7. Experimental results of the spectral envelope of the OFC. Broken lines are the limits of the sensitivity of the optical spectrum analyzer. (a)  $\varphi = 0$ ,  $\Delta f_m = 0$ . (b)  $\varphi = 0$ ,  $\Delta f_m = 5.5$  MHz. (c)  $\varphi = 0.15\pi$ ,  $\Delta f_m = 5.5$  MHz.

to one sideband of  $LD_R$  generated by the OFC generator for demonstration. The experimental setup is shown in Fig. 3 (in which the switch (SW) is on). Fig. 8(a) and (b) show the spectral profile of the beat signal under phase locked condition for which  $LD_X$  was locked to 84th sideband of the OFC, i.e.,  $\nu_R - \nu_X = 0.487$  THz. The resolution bandwidths of Fig. 8(a) and (b) were 1 kHz and 30 Hz, respectively. This is the first report of an optical phase locking with a frequency difference as high as 0.5 THz. From the wing of the residual phase noise seen in these figures, short-term residual phase error variance was estimated to be less than  $0.01 \text{ rad}^2$ . From Fig. 8(b), the linewidth of the beat signal was estimated to be narrower than 30 Hz since the resolution bandwidth is 30 Hz. Therefore, the present phase locking does not limit the accuracy of the frequency measurement, and the measurable range can be increased by applying optical phase locking to higher order sidebands. Residual phase noise in low Fourier frequency shown in Fig. 8(b) resulted from the low gain of the feedback circuit. If an active loop filter is used, further reduction of the residual phase noise can be expected.

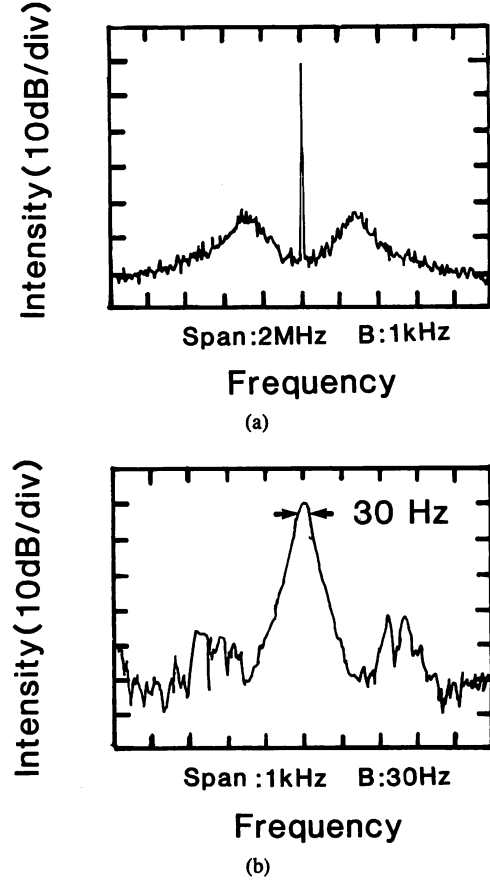


Fig. 8. Spectral profile of a beat signal under optical phase-locked condition.

### III. THEORETICAL ANALYSIS OF AN OFC GENERATOR

From the experimental results, the maximum measurable frequency difference has been roughly estimated to be 4 THz. In this section, we calculate the spectrum of OFC by taking into account the crystal dispersion, and then derive the maximum measurable frequency difference.

Fig. 9 shows an analytical model of the OFC generator used for our calculations. The EO crystal in the Fabry-Perot cavity is assumed to be composed of two parts. One part is a phase modulator without the crystal dispersion. The other part gives the dispersion effect to the laser beam. By using a linear approximation of the refraction index  $n_e$  of the extraordinary ray in a  $\text{LiNbO}_3$  crystal, the optical power  $P_{ok}$  of the  $k$ th order of the sideband generated by OFC generator is

$$P_{ok} = \eta_{FP} \left| \frac{E_{ok}}{E_i} \right|^2 P_i \quad (1a)$$

where

$$E_{ok} = t \times E_i \delta(k) + r \exp \left( -\frac{j4\pi L_c (kf_m)^2}{c} \frac{dn_e}{dv} - \frac{j2\pi k \Delta f_m}{FSR} - j2\varphi \right) \sum_{q=-\infty}^{\infty} J_{k-q}(2m) E_{oq} \quad (1b)$$

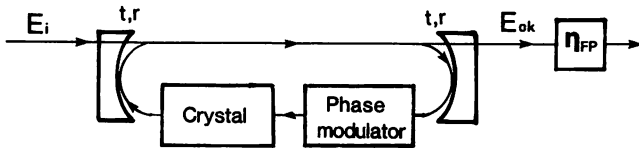


Fig. 9. A model for analyzing the OFC generator.

where  $E_i$  and  $E_{ok}$  are amplitudes of the electric fields of the incident laser beam and the  $k$ th sideband of output beam of OFC generator, respectively.  $J_{k-q}(\cdot)$  is the  $(k-q)$ -th Bessel function,  $\delta(\cdot)$  is the delta function,  $r$  and  $t$  are reflectivity and transmittance, i.e.,  $r \cong 1 - \pi/F$ ,  $t = 1 - r$ , respectively.  $c$  is the speed of light in vacuum. The value of  $dn_e/d\nu$  is  $2.3 \times 10^{-16} \text{ Hz}^{-1}$  ( $1.5 \mu\text{m}$ ) and  $L_c$  is the crystal length. The wavelength sensitive reflectivity of the Fabry-Perot mirror is ignored because it is very small in comparison with the effect of the crystal dispersion within the range of 10 THz.

The calculated results of the envelope of the OFC spectrum from (1), are shown by solid lines in Fig. 10(a)–(c), where (a)  $\varphi = 0$ ,  $\Delta f_m = 0$ , (b)  $\varphi = 0$ ,  $\Delta f_m = 5.5 \text{ MHz}$ , and (c)  $\varphi = 0.15\pi$ ,  $\Delta f_m = 5.5 \text{ MHz}$ . In order to compare them with the experimental results in Fig. 7(a)–(c), we replace  $k$  by the wavelength of the  $k$ th sideband  $\lambda_k$  in the relation between  $P_{ok}$  and  $k$ , considering that  $\lambda_k \cong \lambda_R - (c/\nu_R^2)kf_m$  (where  $\lambda_R \cong c/\nu_R$  is the wavelength of  $\text{LD}_R$ ), it is found that they are in good agreement with each other.

Although (1) can represent the results which are in good agreement with experimental results, this calculation is too complicated to estimate the maximum measurable frequency difference. Then we derived the approximated expression of (1). That is

$$P_{ok} = \begin{cases} \eta_{FP} \left( \frac{\pi}{2mF} \right)^2 \exp \left( -\frac{|k|\pi}{mF} \right) P_i, & \text{for } g(k') \leq m; \\ 0, & \text{otherwise} \end{cases} \quad (2a)$$

$$g(k') = \left| \frac{2\pi L_c (k'f_m)^2}{c} \frac{dn_e}{d\nu} + \frac{\pi k' \Delta f_m}{\text{FSR}} + \varphi + M\pi \right| \quad (2b)$$

where  $M$  is an integer which satisfies  $|\varphi + M\pi| \leq m$ , and the condition should be valid when  $k'$  involves all integers from 0 to  $k$ . The relation  $P_{ok} = \eta_{FP} (\pi/2mF)^2 \exp(-(|k|\pi/mF)) P_i$  in (2a) represents an analytical equation calculated from (1) under the condition in which the crystal dispersion is ignored and  $mF \gg 1$ . The value of  $g(k')$  is proportional to the frequency difference between the  $k'$ th sideband and the closest resonant frequency of the Fabry-Perot cavity. When a value of  $k$  does not satisfy the relation  $g(k) \leq m$ , the order of the sideband is higher than the value of  $k$  and such a sideband cannot exist. We show examples of the calculation using (2) by broken lines in Fig. 10(a)–(c) to compare the solid lines exactly calculated result by using (1). By comparing the calculations, it is seen that they are in good agreement with each other. We use (2) in the following discussion.

The signal-to-noise ratio  $S/N_k$  of the beat signal detec-

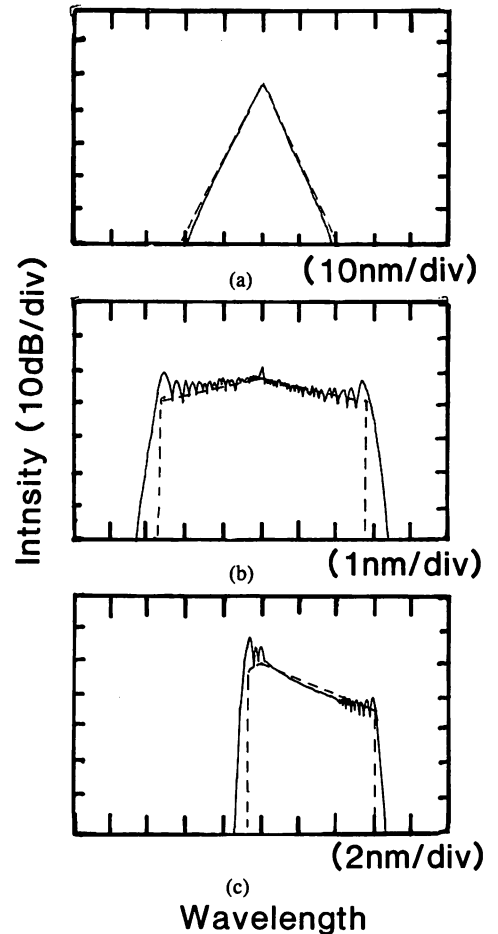


Fig. 10. Calculated results of the spectral envelope of the OFC. Solid and broken lines are calculated results by (1) and (5), respectively. (a)  $\varphi = 0$ ,  $\Delta f_m = 0$ . (b)  $\varphi = 0$ ,  $\Delta f_m = 5.5 \text{ MHz}$ . (c)  $\varphi = 0.15\pi$ ,  $\Delta f_m = 5.5 \text{ MHz}$ . The center wavelength is  $\lambda_R$ .

tion between the  $k$ th sideband of  $\text{LD}_R$  and  $\text{LD}_X$  is

$$S/N_k = \frac{\eta_{PD} P_{ok} P_X}{\left( \sum_{k=-\infty}^{\infty} P_{ok} + P_X \right) (B + \Delta\nu_X + \Delta\nu_R) h\nu_X} \quad (3)$$

where  $h$  is the Planck's constant. By using the relation  $\sum_{k=-\infty}^{\infty} P_{ok} \cong (\eta_{FP} \pi / mF) P_i \ll P_X$ ,  $\Delta\nu_X, \Delta\nu_R \ll B$ , (3) can be reduced to

$$S/N_k \cong \frac{\eta_{PD} P_k}{h\nu_X B}. \quad (4)$$

One should remember that the experimental results are in good agreement with the calculated result of (4) in Fig. 6.

The maximum measurable frequency difference  $f_{d-\max}$ , which is defined as  $kf_m$  at a signal-to-noise of 0 dB, esti-

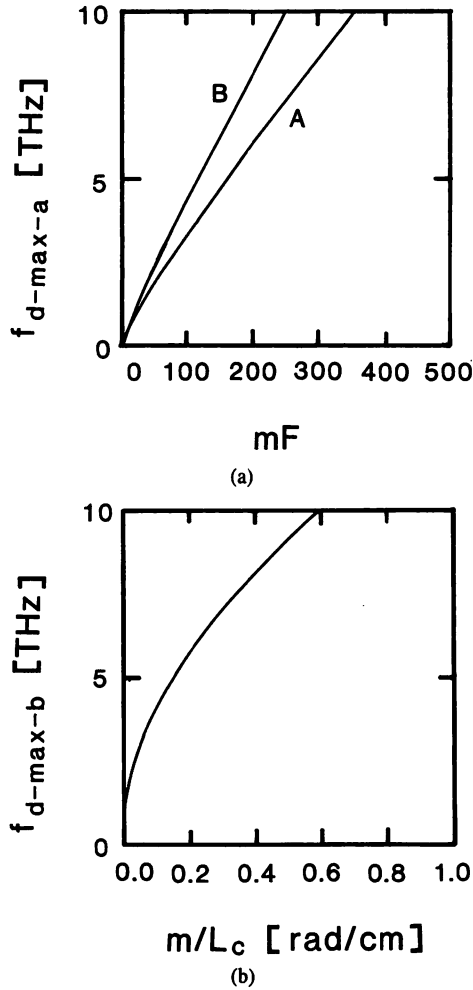


Fig. 11. The maximum measurable frequency difference. (a)  $f_{d-\max-a}$ . (b)  $f_{d-\max-b}$ . In (a), curves A and B shows a result calculated by using the value of  $Z = 2 \times 10^{11}$  and  $Z = 6 \times 10^{13}$ , respectively.

mated from (2a), (2b), and (4), is the smaller one between  $f_{d-\max-a}$  and  $f_{d-\max-b}$ .

$$f_{d-\max-a} = f_m \frac{\ln\left(\frac{\pi}{2mF}\right) + 0.5 \ln(Z)}{\frac{\pi}{2mF}} \quad (5a)$$

$$f_{d-\max-b} = 2 \sqrt{\frac{mc}{\pi L_c \frac{dn_e}{dv}}} \quad (5b)$$

where  $Z = \eta_{FP} \eta_{PD} P_i / h\nu_X B$ , is the signal-to-noise ratio of the beat signal detection between  $LD_R$  through the Fabry-Perot cavity and  $LD_X$ .  $f_{d-\max-a}$  is calculated by assuming  $dn_e/dv = 0$ .  $f_{d-\max-b}$  is calculated by assuming  $Z = \infty$  and optimizing the values of  $\varphi$  and  $\Delta f_m$ .

In Fig. 11(a) and (b),  $f_{d-\max-a}$  and  $f_{d-\max-b}$  are shown as functions of  $mF$  and  $m/L_c$ , respectively. Curve A in Fig. 11(a) is calculated by using values of experimental condition such as  $Z = 2 \times 10^{11}$  ( $\eta_{FP} = 0.05$ ,  $\eta_{PD} = 0.9$ ,  $P_i = 7$  mW, and  $B = 10$  kHz). Curve B in Fig. 11(a) is calculated by using values of  $Z = 6 \times 10^{13}$ . Curve B will

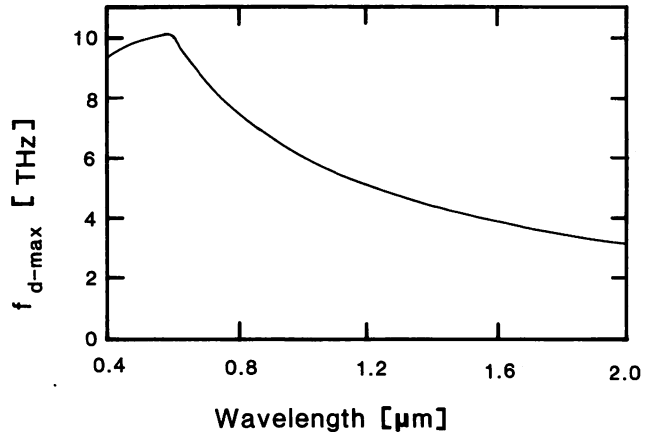


Fig. 12. The maximum measurable frequency difference as a function of wavelength.

be referred to in Section V. From curve A in Fig. 11(a), and Fig. 11(b), the value of  $f_{d-\max}$  can be estimated to be 4 THz by the experimental conditions  $mF \approx 125$ , and  $m/L_c = 0.31$  rad/cm.

It is interesting and important to consider how the OFC generator works in other wavelength region. By assuming that all incident microwave power is feeded to the crystal, the modulation index  $m$  is expressed as

$$m \approx \frac{1}{\sqrt{2}} \frac{n_e^3 \gamma_{33}}{\lambda_R} \sqrt{\frac{P_\mu L_c \pi}{A f_m \epsilon \tan \delta}} \quad (6)$$

where  $A$ ,  $\gamma_{33}$ , and  $\epsilon$  are the cross-sectional area of the crystal, EO coefficient, and dielectric constant, respectively. By substituting the experimental values into (6), dielectric loss tangent  $\tan \delta$  is estimated to be 0.0017. The value of  $dn_e/dv$  is calculated from a Sellmeier equation given in [18]. In Fig. 12,  $f_{d-\max}$  is shown as a function of  $\lambda_R$ , in which it can be seen that  $f_{d-\max}$  reaches to 10 THz at  $\lambda_R \approx 0.6$   $\mu\text{m}$ . This wavelength is important for precision spectroscopy, such as for  $I_2$  and Ca. In the range of wavelength shorter than 0.6  $\mu\text{m}$ , a decrease of  $f_{d-\max}$  can be seen owing to the increase of dispersion effect of the  $\text{LiNbO}_3$  crystal near the absorption.

#### IV. DISCUSSIONS

We discuss here how to increase the maximum measurable frequency difference to 10 THz by improving the performance of the present OFC generator at 1.5  $\mu\text{m}$  wavelength. In order to achieve a 10 THz frequency difference measurement, there are two problems to be solved.

One is to realize

$$f_{d-\max-a} \geq 10 \text{ THz} \quad (7a)$$

and the other one is

$$f_{d-\max-b} \geq 10 \text{ THz} \quad (7b)$$

First, we consider (7b). From (5b) and (7b), it is easily calculated that  $m/L_c$  must be larger than 0.6 rad/cm (in the case of  $\text{LiNbO}_3$ ). This condition can be realized easily

when the modulation frequency is low, but it is preferable to realize it using a modulation frequency as high as possible. Lee *et al.* realized a very large phase modulation of  $0.5 \mu\text{m}$  laser [10] by using a high microwave power. The value of the modulation index was  $10.5 \text{ rad/cm}$  at a modulation frequency of  $16.2 \text{ GHz}$ . If this modulator is used for a  $1.5 \mu\text{m}$  wavelength laser, the modulation index is estimated to be  $m/L_c = 3.5 \text{ rad/cm}$ . This value is large enough, but such a high power modulation is practically inconvenient. In the present system, we operated the modulator continuously by using  $10 \text{ W}$  microwave, and the realized value of the  $m/L_c$  is  $0.31 \text{ rad/cm}$ . In order to increase this value to  $0.6 \text{ rad/cm}$ , we must increase the microwave power concentration ratio ( $P_\mu/L_c A$ ) or we must use low loss crystal. If the cross-sectional area of the crystal is decreased to the diffraction limit (the crystal area can be decreased to  $0.5 \times 0.5 \text{ mm}^2$  for  $L_c = 2 \text{ cm}$ ), the power concentration is then increased by five times, and the value of the  $m/L_c$  is increased to  $0.71 \text{ rad/cm}$ . This is enough to satisfy (7b). The advantage of our modulator is that the phase velocity of the microwave can be controlled by waveguide width, and the width of the crystal can be decreased to a size smaller than the crystal width of Lee's modulator which use a micro-strip-line resonator on an EO crystal. If we use a crystal with low  $\tan \delta$ , the value of  $m/L_c$  can be increased easily, but the value of  $\tan \delta$  of  $\text{LiNbO}_3$  in the microwave range is not clear because it depends on the crystal quality.

Next, we consider (7a) by assuming that the value of the  $m/L_c$  is  $0.6 \text{ rad/cm}$ . Under the condition of  $F = 200$  ( $mF = 250$ ),  $f_{d-\max-a}$  is estimated to be  $7.4 \text{ THz}$  from the curve *A* in Fig. 11(a). There can be three ways to increase this value to  $10 \text{ THz}$ . They are: 1) Increasing of  $f_m$ , 2) increasing of  $Z$ , 3) increasing of  $F$ . Although the maximum modulation frequency is not clearly known which keeps the relation of (7b), we point out that relation of (7a) is realized when the modulation frequency is higher than  $8 \text{ GHz}$ . The way to realize (2) and (3) is to increase the signal-to-noise ratio of the beat detection. The value of  $\eta_{FP} P_i$  is increased by using low loss optics and/or a high power laser. When the linewidth of the lasers are decreased, the resolution band width  $B$  can be decreased and then the signal-to-noise ratio is increased. The spectral linewidth of the  $1.5 \mu\text{m}$  wavelength laser has been narrowed to  $80 \text{ Hz}$  [19], and if the value of  $Z$  is increased by 300 times which can be realized by increasing the  $\eta_{FP} P_i$  and using such lasers, it is possible [from curve *B* in Fig. 11(a)] to increase the value of  $f_{d-\max-a}$  to  $10 \text{ THz}$  at  $mF = 250$ . The way of realizing (3) is most hopeful to satisfy (7a) because optical loss of the  $\text{LiNbO}_3$  is very low and the value of  $F$  can be increased by employing a monolithic Fabry-Perot cavity made of  $\text{LiNbO}_3$ . Recently, a monolithic  $\text{LiNbO}_3$  optical cavity, of which the value of  $F$  is 960, has been reported [18]. In order to realize (7a), a finesse of 300 is enough. A monolithic type  $\text{LiNbO}_3$  Fabry-Perot cavity for the OFC generator will be easily realized by coating with high reflection films the crystal facets of the EO modulator.

In order to measure a frequency difference higher than  $10 \text{ THz}$ , it can be easier to use the optical phase locking technique with many OFC's than to improve a single OFC generator because the dispersion in reflectivity of the Fabry-Perot mirror cannot be ignored in a range higher than  $10 \text{ THz}$ .

## V. SUMMARY

A wide-span optical frequency comb (OFC) generator was realized for accurate optical frequency difference measurement of  $1.5 \mu\text{m}$  wavelength semiconductor lasers by using a high frequency electrooptic phase modulator ( $\text{LiNbO}_3$ ) which is installed in a Fabry-Perot cavity. It was confirmed that the span of the OFC is wider than  $4 \text{ THz}$ . By using such an OFC generator, semiconductor lasers whose spectrum linewidths are narrowed to  $1 \text{ kHz}$ , and a sensitive optical balanced-mixer-receiver, we demonstrated the frequency difference measurement up to  $0.5 \text{ THz}$  with signal-to-noise ratio higher than  $61 \text{ dB}$ . We also demonstrated the heterodyne optical phase locking with the heterodyne frequency of  $0.5 \text{ THz}$  and achieved the residual phase error variance less than  $0.01 \text{ rad}^2$ . The maximum measurable frequency difference, which is defined by a signal-to-noise ratio of  $0 \text{ dB}$ , was estimated to be  $4 \text{ THz}$ . It is expected that the maximum measurable frequency difference is increased to  $10 \text{ THz}$  if the modulation index normalized to the crystal length become higher than  $0.6 \text{ rad/cm}$ .

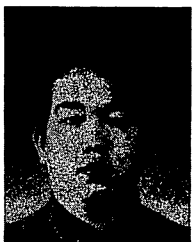
## ACKNOWLEDGMENT

The authors would like to thank Prof. Kobayashi and Dr. Morimoto of the Osaka University for helpful comments on an electrooptic modulator. They also thank Drs. Okai and Kuboki of the Hitachi corporation for discussions on the semiconductor lasers.

## REFERENCES

- [1] T. Andreae, W. König, R. Wynands, D. Leibfried, F. Schmidt-Kaler, C. Zimmermann, D. Meschede, and T. W. Hänsch, "Absolute frequency measurement of the hydrogen  $1S-2S$  transition and a new value of the Rydberg constant," *Phys. Rev. Lett.*, vol. 69, pp. 1923-1926, 1992.
- [2] F. Nez, M. D. Plimmer, S. Bourzeix, L. Julien, and F. Biraben, "Precise frequency measurement of the  $2S-8S/8D$  transitions in atomic hydrogen: new determination of the Rydberg constant," *Phys. Rev. Lett.*, vol. 69, pp. 2326-2329, 1992.
- [3] D. A. Jennings, C. R. Pollock, F. R. Petersen, R. E. Drullinger, K. M. Evenson, and J. S. Wells, "Direct frequency measurement of the  $I_2$ -stabilized He-Ne  $473\text{-THz}$  ( $633\text{-nm}$ ) laser," *Opt. Lett.*, vol. 8, pp. 136-138, 1983.
- [4] O. Acef, J. J. Zondy, M. Abed, D. G. Rovera, A. H. Gérard, and A. Clairon, "A  $\text{CO}_2$  to visible optical frequency synthesis chain: accurate measurement of the  $473 \text{ THz He-He}/I_2$  A highly accurate frequency counting system for  $1.5 \mu\text{m}$  wavelength semiconductor lasers," *Opt. Commun.*, to be submitted.
- [5] V. A. Alekseev, M. A. Gubin, and E. D. Protsenko, "High-precision optical frequency standards," *Laser Physics*, vol. 1, pp. 221-260, 1991.
- [6] R. E. Drullinger, K. M. Evenson, D. A. Jennings, F. R. Petersen, J. C. Bergquist, and L. Burkins, "2.5-THz frequency difference measurement in the visible using metal insulator-metal diodes," *Appl. Phys. Lett.*, vol. 42, pp. 137-138, 1983.

- [7] H. R. Telle, D. Meschede, and T. W. Hänsch, "Realization of a new concept for visible frequency division: Phase locking of harmonic and sum frequencies," *Opt. Lett.*, vol. 15, pp. 532-534, 1990.
- [8] R. Kallendach, B. Scheumann, C. Zimmermann, D. Meschede, and T. W. Hänsch, "Electro-optic sideband generation at 72 GHz," *Appl. Phys. Lett.*, vol. 54, pp. 1622-1624, 1989.
- [9] N. C. Wong, "Optical frequency counting from UV to the near IR," *Opt. Lett.*, vol. 17, pp. 1155-1157, 1992.
- [10] B. Y. Lee, T. Kobayashi, A. Morimoto, and T. Sueta, "Picosecond electro-optic modulator/deflector with velocity matching," in *Proc. Conf. Lasers Electro-Opt.*, Baltimore, MD, May 1991, paper number CTuR4.
- [11] T. Kobayashi, T. Sueta, Y. Cho, and Y. Matsuo, "High-repetition-rate optical pulse generator using a Fabry-Perot electro-optic modulator," *Appl. Phys. Lett.*, vol. 21, pp. 341-343, 1972.
- [12] M. Kourogi, K. Nakagawa, C. H. Shin, M. Teshima, and M. Ohtsu, "Accurate frequency measurement system for 1.5- $\mu\text{m}$  wavelength laser diodes," in *Proc. Conf. Lasers Electro-Opt.*, Baltimore, MD, May 1991, paper number CThR57.
- [13] M. Kourogi, K. Nakagawa, and M. Ohtsu, "A wideband optical frequency comb generator for a highly accurate laser frequency measurement," in *Proc. Internat. Quantum Electron. Conf.*, Vienna, June 1992, paper number TuM5.
- [14] C. H. Shin and M. Ohtsu, "Optical phase-locking of resonant cavity coupled semiconductor lasers," *IEEE J. Quantum Electron.*, to be published.
- [15] S. B. Alexander, "Design of wide-band optical heterodyne balanced mixer receivers," *J. Lightwave Technol.*, vol. LT-5, pp. 523-537, 1987.
- [16] J. M. Kahn, B. L. Kasper, and K. J. Pollock, "Optical phase receiver with multigigahertz signal bandwidth," *Electron Lett.*, vol. 25, pp. 626-628, 1989.
- [17] P. P. Smyth, A. A. Sayles, N. R. Back, A. P. McDonna, and M. J. Creaner, "High performance balanced dual-detector GaAs IC receiver for 565 Mbit/s optical heterodyne detection," *Electron. Lett.*, vol. 25, pp. 1414-1416, 1989.
- [18] R. C. Eckardt, C. D. Nabors, W. J. Kozlovsky, and R. L. Byer, "Optical parametric oscillator frequency tuning and control," *J. Opt. Soc. Amer. B*, vol. 8, pp. 646-667, 1991.
- [19] K. Nakagawa, M. Kourogi, and M. Ohtsu, "Frequency noise reduction of a diode laser by using the FM sideband technique," *Opt. Lett.*, vol. 17, pp. 934-936, 1992.



**Motonobu Kourogi** was born in Shiga, Japan, 1966. He received the B.S. degree from Shizuoka University, Shizuoka, Japan, in 1988, and the M.S. and Ph.D. degrees from the Tokyo Institute of Technology, Tokyo, Japan, in 1990 and 1993, respectively.

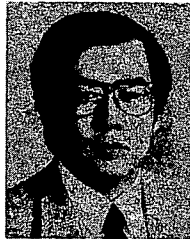
Since April 1993 he has been with Tokyo Institute of Technology as a Research Associate. His current research interests are the frequency synthesis of semiconductor lasers.

Dr. Kourogi is a member of the Japan Society

of Applied Physics.



**Ken'ichi Nakagawa** was born in Kanagawa, Japan, in 1961. He received the B.S., M.S., and Ph.D. degrees in physics from Tokyo University, Tokyo, Japan, in 1984, 1986, 1989, respectively. He has been with the Tokyo Institute of Technology since 1989. His current research interests are the frequency control of diode lasers and solid lasers, and its applications to spectroscopy and frequency synthesis chain.



**Motoichi Ohtsu (M'88-SM'90)** was born in Kanagawa, Japan, on October 5, 1950. He received the B.S., M.S., and Ph.D. degrees in electronics engineering from the Tokyo Institute of Technology, Tokyo, Japan, in 1973, 1975, and 1978, respectively.

In 1978 he was appointed as a Research Associate, and in 1982 he became Associate Professor at the Tokyo Institute of Technology. From September 1986 to July 1987, while on leave from the Tokyo Institute of Technology, he joined the

Crawford Hill Laboratory, AT&T Bell Laboratories, Holmdel, NJ. In 1991, he became a Professor at the Tokyo Institute of Technology. From April 1993, he has been concurrently the project leader of the "PHOTON CONTROL" project of Kanagawa Academy of Science and Technology, Kanagawa, Japan. His main fields of interest are the frequency control of lasers, photon scanning tunneling microscopy and its application to atom manipulation. He has written over 100 papers, received two patents, with 20 pending patents. He is the author and coauthor of eleven books including two in English, entitled *Highly Coherent Semiconductor Lasers* (Boston, MA: Artech House, 1991) and *Coherent Quantum Optics and Technology* (Dordrecht: Kluwer Academic, 1993). He has been a tutorial lecturer of the SPIE. He has been awarded eight prizes from academic institutions including the Issac Koga Gold Medal of URSI in 1984, Japan IBM Science Award in 1988, and the awards of the Japanese Society of Applied Physics in 1987 and 1990. He is a member of the Institute of Electronics, Information and Communication Engineering of Japan, the Institute of Electrical Engineering of Japan, the Japan Society of Applied Physics, and the Optical Society of America.

# Proposal of a Frequency-Synthesis Chain Between the Microwave and Optical Frequencies of the Ca Intercombination Line at 657 nm Using Diode Lasers

K. Nakagawa, M. Kourogi, M. Ohtsu

Graduate School at Nagatsuta, Tokyo Institute of Technology, 4259, Nagatsuta-cho, Midori-ku, Yokohama 227, Japan (Tel.: +81-45/922-1111 ext. 2526, Fax: +81-45/921-1204, e-mail: nakagawa@turing.ip.titech.ac.jp)

Received 11 May 1993/Accepted 3 August 1993

**Abstract.** We propose a frequency synthesis chain which can directly connect a microwave atomic clock with a visible laser. We design this chain for the frequency measurement of a visible laser locked on the intercombination transition of Ca at 657 nm. The proposed chain is based on both an optical difference frequency divider and an optical frequency comb generator, and it is designed to use nine visible and near-infrared diode lasers. We discuss the technical requirements to realize the frequency measurement accuracy level of  $10^{-14}$ .

PACS: 07.60. – j, 42.60. By

In recent years there has been renewed interest in optical frequency synthesis which connects the optical laser frequency to infrared frequency standards or microwave atomic clocks. It has been needed in metrology to measure the optical frequency in the visible region with high accuracy. The frequency measurement of  $I_2$  stabilized red He–Ne laser (633 nm) has been realized by using a frequency chain between the visible and the reference infrared lasers with an accuracy of  $10^{-10}$ – $10^{-11}$  [1, 2]. The Ca intercombination line at 657 nm is one of the promising candidates for an optical frequency standard [3]. For the frequency measurement of this line it is necessary to realize a measurement accuracy of better than  $10^{-12}$ .

Such an accurate optical frequency measurement is also needed in the field of high-resolution spectroscopy or fundamental physics. To determine the Rydberg constant, the optical frequency of the two-photon hydrogen transition at 243 nm has been measured with an accuracy of  $2 \times 10^{-11}$  by using a frequency chain based on the reference infrared He–Ne laser (3.392  $\mu\text{m}$ ) [4].

Optical frequency syntheses based on new concepts have been proposed and studied in recent years [5–8]. The basic concept is an optical difference frequency divider which can divide the frequency difference between lasers by using phase locking via a beat signal of their harmonics and sum frequency [5]. A similar method has also been proposed using optical parametric oscillators as an optical

frequency divider [7, 8]. Using these new methods, the frequency chain between the optical frequency and a microwave atomic clock can be realized only with visible or near-infrared lasers [6]. However, more than sixteen lasers are needed in a wide wavelength range. Diode lasers are attractive candidates for this purpose.

Here we propose new frequency synthesis chain which can directly connect the microwave frequency to the optical frequency in the visible using only nine lasers. This chain is designed for the frequency measurement of the Ca stabilized optical frequency standards at 657 nm [3]. Our chain relies on two new methods. One is, already mentioned, the optical difference frequency divider using sum frequency and second-harmonic generation [5]. The other is the optical frequency comb generator using an electro-optic (E/O) modulator in a high finesse optical cavity [9, 10]. This optical frequency comb generator can efficiently generate high-order sidebands in the frequency range higher than 1 THz. Another feature is that we can use commercially available visible and near-infrared diode lasers for all nine lasers and also highly efficient nonlinear crystals.

First, we briefly show the principles of the optical difference frequency divider and optical frequency comb generator. Next, we describe the design of our proposed frequency chain and discuss technical requirements for optical phase-locked loops to realize a phase coherent chain.

## 1 Optical Difference Frequency Divider

The optical difference frequency divider using sum frequency mixing (SFM) and second-harmonic generation (SHG) has been proposed and demonstrated experimentally [5, 11]. The schematic diagram of this method is shown in Fig. 1. Using the beat between the sum frequency (SF) of laser 1 ( $\nu_1$ ) and laser 2 ( $\nu_2$ ) and the second harmonic (SH) of laser 3 ( $\nu_3$ ), the phase locking between three lasers can be realized with the frequency relation

$$\nu_1 + \nu_2 + \delta = 2\nu_3 \quad \text{or} \quad \nu_1 - \nu_2 + \delta = 2(\nu_3 - \nu_2), \quad (1)$$



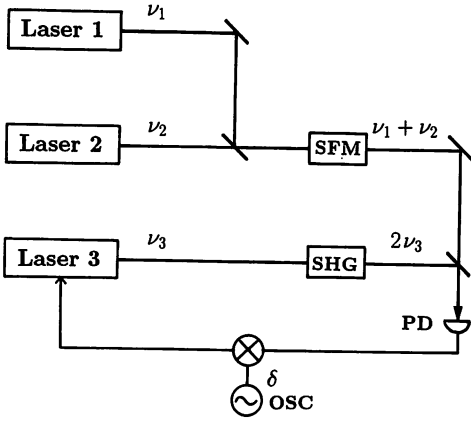


Fig. 1. Schematic diagram of the optical difference frequency divider

where  $\delta$  is the heterodyne beat frequency between SF and SH. For the optical frequency of about  $5 \times 10^{14}$  Hz ( $\lambda = 600$  nm), the optical frequency difference can be reduced to within 10 GHz after sixteen stages of this divider.

It is important to know the phase error of the optical phase-locked loop (OPLL) used in this method. Using a balanced homodyne detector [12], the signal to noise ratio of the beat between two lasers is given by

$$S/N = \frac{4\kappa^2 I_1 I_2}{[2e(I_1 + I_2) + i_N^2] BW}, \quad (2)$$

where  $\kappa$  is a coupling coefficient between two laser beams,  $I_1$  and  $I_2$  are dc photo currents of lasers 1 and 2,  $e$  is the electron charge,  $i_N$  is the current noise density of a preamplifier, and  $BW$  is the detection bandwidth. The dc photo currents  $I_i$  ( $i = 1, 2$ ) are given by  $e\eta P_i/h\nu_i$  ( $i = 1, 2$ ), where  $\eta$  is the photo diode quantum efficiency, and  $P_i$  and  $\nu_i$  are optical power and frequency of the two lasers, and  $h$  is the Planck constant. The first and second terms of the denominator of (2) represent the terms of shot noise and thermal noise, respectively. For an optical power  $P_1 (= P_2)$  of  $1 \mu\text{W}$  at  $\lambda = 440$  nm,  $BW = 100$  kHz,  $\eta = 0.5$ ,  $\kappa = 0.5$ , the shot noise limited  $S/N$  ratio is calculated to be about 59 dB, whereas the thermal noise limited one is about 42 dB at the preamplifier current noise density  $i_N$  of  $4.5 \text{ pA}/\sqrt{\text{Hz}}$ , as an example.

Here, we assume, for simplicity, that the laser frequency noise is white noise and we use a homodyne OPLL with a first-order loop filter. The laser linewidth  $\Delta\nu_L$  is given by  $\Delta\nu_L = \pi S$ , where  $S$  is the power spectrum density of white frequency noise. Under phase locking, the relative phase-error variance between two lasers is given by [13]

$$\sigma_\phi^2 = \frac{\pi S_B}{2f_L} + \frac{\pi S_{\phi_N} f_L}{2} \quad (3)$$

where  $S_B$  is the power spectral density of frequency noise of the lasers at the beat signal,  $f_L$  is the locking bandwidth of the phase-locked loop,  $S_{\phi_N}$  is the power spectral density of phase noise due to the finite  $S/N$  ratio of the beat signal and is given by  $1/(S/N)_{BW=1 \text{ Hz}}$ . The minimum phase error is given by  $\sigma_\phi^2 = \pi \sqrt{S_B S_{\phi_N}}$ , when the bandwidth is chosen to be  $f_L = (S_B/S_{\phi_N})^{1/2}$ . The power spectrum density  $S_B$  of

the beat signal between SF (lasers 1, 2) and SH (laser 3) is given by  $S_B = S_1 + S_2 + 4S_3$  when the three lasers are not correlated and the power spectral densities of the three lasers are  $S_i$  ( $i = 1 - 3$ ). When the linewidths  $\Delta\nu_L$  of the three lasers are 10 kHz and the  $S/N$  ratio of the beat signal is 42 dB ( $BW = 100$  kHz),  $S_B$  and  $S_{\phi_N}$  are about  $2 \times 10^4 \text{ Hz}^2/\text{Hz}$ , and  $6 \times 10^{-10} \text{ rad}^2/\text{Hz}$ , respectively. The optimum locking bandwidth  $f_L$  is about 6 MHz and the minimum phase error variance is  $\sigma_\phi^2 \sim 0.01 \text{ rad}^2$ . This phase error ( $\sim 0.1$  rad) is sufficiently small to get a precise frequency relation between the two lasers. In case of a heterodyne OPLL, the  $S/N$  ratio of the beat signal is 3 dB lower compared with the homodyne OPLL. If the laser linewidth is determined by  $1/f$  noise at low frequencies rather than white noise, the optimum feedback bandwidth is lower than the above-mentioned [13].

## 2 Optical Frequency Comb Generator

Wide frequency span optical frequency comb generator using an electro-optic modulator in a high finesse optical cavity has been proposed and demonstrated [7, 9, 10]. A schematic diagram of this comb generator is shown in Fig. 2. The laser beam is phase modulated by an electro-optic modulator in an optical cavity (finesse:  $F$ , free spectral range:  $\text{FSR} = c/2L$ ) at the modulation frequency  $f_m$ . When  $f_m \simeq n \times \text{FSR}$  ( $n = 1, 2, \dots$ ), the phase modulation can be effectively enhanced in the cavity by the order of the cavity finesse, and the higher order sidebands can be efficiently generated.

In our recent experiment [10], using a  $\text{LiNbO}_3$  E/O modulator with a modulation frequency of 5.8 GHz and a Fabry-Perot (FP) cavity (finesse  $\sim 200$ ), we have obtained more than 700 sidebands spread to about 4 THz. We could observe the heterodyne beat signal between the 58-th sideband and the other laser with a frequency difference of about 0.5 THz. We also demonstrated the optical phase locking using this heterodyne beat signal.

We now roughly estimate the higher-order sideband power generated by this optical frequency comb generator. When the laser frequency  $\nu_L$  is nearly equal to the optical cavity resonance frequency  $\nu_c = N \times \text{FSR}$  ( $N$ : integers)

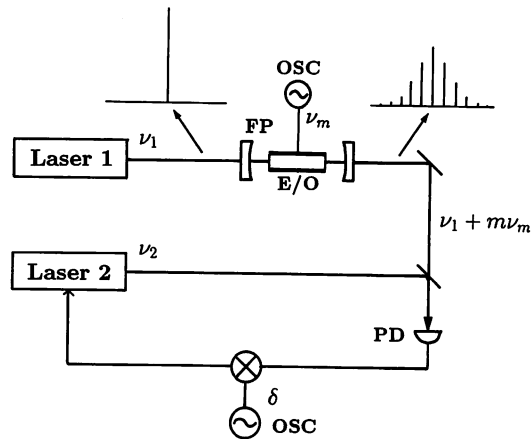


Fig. 2. Schematic diagram of the optical frequency comb generator

and the modulation  $f_m$  is also nearly equal to  $k \times \text{FSR}$  ( $k = 1, 2, 3, \dots$ ), the  $m$ -th order sideband power  $P_m$  of the transmitted light from the cavity exponentially decays against a sideband order  $m$  [10],

$$P_m \sim \eta_T \left( \frac{\pi}{2MF} \right)^2 \exp\left(-\frac{m\pi}{MF}\right) P_i, \quad (4)$$

where  $\eta_T$  is transmission efficiency of the FP cavity,  $M$  is modulation index,  $F$  is cavity finesse, and  $P_i$  is the optical power incident on the cavity. As an example, when  $\eta_T$  is  $\sim 20\%$ ,  $M \sim 1$ ,  $F = 200$ ,  $P_i = 10$  mW,  $\nu_m = 6$  GHz, the optical power of the 300-th order ( $300 \nu_m = 1.8$  THz) is about 1 nW.

We now estimate the required sideband power for OPLL. Here, we assume that the optical phase locking between a higher-order sideband of optical power  $P_1$  and the other laser of  $P_2$  ( $\gg P_1$ ). In this case, the  $S/N$  ratio of the beat signal is mainly determined by the shot noise (2) and is given by  $2\kappa^2\eta P_1/(h\nu \text{BW})$ .

For typical conditions  $\text{BW} = 100$  kHz,  $\kappa = 0.5$ ,  $P_1 = 1$  nW,  $P_2 = 3$  mW ( $\lambda = 875$  nm,  $\eta = 80\%$ ), the  $S/N$  ratio is about 42 dB. According to (3), the relative phase variance is calculated to be  $0.006 \text{ rad}^2$  when the laser linewidth  $\Delta\nu_L$  is 10 kHz, and the locking bandwidth  $f_L$  is 3 MHz.

It is important to know the magnitudes of phase or frequency noise of the higher-order sidebands due to the cavity-length fluctuation. The phase noise of the  $m$ -th order sideband is  $\delta\phi_m = m \times 2\pi\delta L/\lambda$ , where  $\delta L$  is the cavity length fluctuation. The frequency noise is given by  $\delta\nu_m(f) = f\delta\phi_m(f)$  at the Fourier frequency  $f$ . For example,  $\delta L$  of 1 nm at  $f = 1$  Hz induces a frequency noise of 2 Hz at the 300-th order sideband ( $\lambda = 875$  nm).

### 3 Design of the Frequency Chain

We design the frequency chain to measure the optical frequency of a frequency-standard laser locked on the Ca intercombination line at 657 nm. Using high resolution Ramsey spectroscopy of this Ca transition, the frequency accuracy and reproducibility of this standard laser is expected to be within  $10^{-12}$  [3]. The schematic diagram of this frequency chain is shown in Fig. 3. In this frequency chain, we use nine lasers at the wavelength of 1315 nm, 657 nm, 877 nm, 751 nm, 809 nm, 842 nm, 859 nm, 868 nm, and 872 nm, respectively. The optical frequency ( $\sim 456$  THz) of the standard laser (657 nm) is down converted to a microwave frequency by using another eight lasers.

At the first stage, the second harmonic (SH) of laser 1 (1315 nm) is generated in a KTP crystal, and laser 1 is phase-locked on the laser 2 (657 nm) by using the SH. The frequency relation between the laser 1 ( $\nu_1$ ) and laser 2 ( $\nu_2$ ) is given by  $\nu_2 = 2 \times \nu_1 + \Delta_1$ , where  $\Delta_1$  is the heterodyne beat frequency.

At the next stage, the frequency difference between laser 1 and laser 2 is divided by two using the optical difference frequency divider. The SF between laser 1 and laser 2 is generated in a KTP crystal, and the SH of the laser 3 (877 nm) is generated in a KNbO<sub>3</sub> crystal. Laser 3 ( $\nu_3$ ) is phase-locked by using the beat between the SF and SH, and the laser frequency  $\nu_3$  is given by  $\nu_3 = (\nu_1 + \nu_2 + \Delta_2)/2$ , where  $\Delta_2$  is the heterodyne beat frequency.

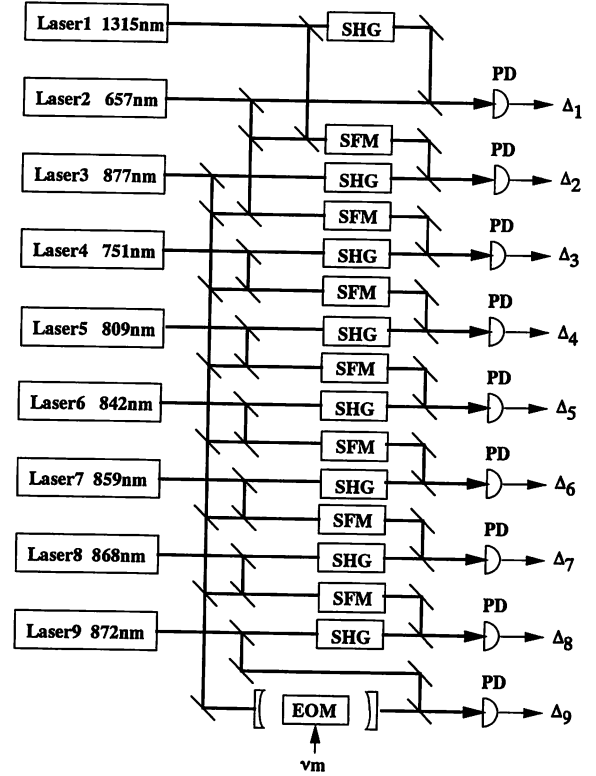


Fig. 3. Schematic diagram of the proposed frequency chain system

In the following six stages, the difference frequency between laser 2 (657 nm) and the laser 3 (877 nm) is divided by  $2^6 = 64$  using the same frequency dividers. The nonlinear frequency mixing (SFM and SHG) between laser 2, laser 3, laser 4, and laser 5 are obtained with LiIO<sub>3</sub> crystals. The SF and SH between laser 3, laser 5, laser 6, laser 7, laser 8, and laser 9 are obtained with KNbO<sub>3</sub> crystals.

Thus, the frequency difference between laser 3 (876 nm) and laser 9 (872 nm) is reduced to about 1.8 THz and is given by

$$\nu_9 - \nu_3 = \frac{1}{256} \nu_2 + \frac{\Delta_1}{256} - \frac{\Delta_2}{128} + \frac{\Delta_3}{64} + \dots + \frac{\Delta_8}{2}, \quad (5)$$

where  $\Delta_i$  ( $i = 1-9$ ) are the heterodyne beat frequencies at the frequency divider stages.

This frequency difference of 1.8 THz can be measured by using the optical comb generator. The output of laser 3 is phase-modulated at the modulation frequency  $\nu_m$  of about 6 GHz by a LiNbO<sub>3</sub> crystal in a Fabry-Perot cavity (FSR = 2 GHz, finesse  $\sim 200$ ) with a modulation index of about  $\pi/2$ . The heterodyne beat signal between the higher-order ( $m \sim 300$ ) sideband and the laser 9 is detected by a fast Si-PIN photodiode. The frequency relation between laser 9 and laser 3 is given by  $\nu_9 = \nu_3 + m \times \nu_m + \Delta_9$ , where  $\Delta_9$  is the heterodyne beat frequency.

Finally, the frequency  $\nu_2$  is given by the modulation frequency  $\nu_m$  and nine heterodyne beat frequencies  $\Delta_n$  ( $n = 1-9$ ),

$$\nu_2 = 256 \times m \times \nu_m + \Delta_1 - 2\Delta_2 + 4\Delta_3 + 8\Delta_4 + \dots + 256\Delta_9. \quad (6)$$

If all the heterodyne frequencies ( $\Delta_n$ ) and the modulation frequency ( $\nu_m$ ) are synthesized from a microwave Cs atomic clock, the optical frequency  $\nu_2$  can be determined with an accuracy of this atomic clock.

#### 4 Phase Coherence of the Frequency Chain

To realize a highly accurate measurement of the optical frequency using this frequency chain, it is important to evaluate the phase coherence or phase fidelity of all processes in this chain.

The accuracy of the optical frequency measurement is expected to be of the order of  $10^{-14}$  for an integration time of  $\tau = 100$  s, which is determined by the stability and accuracy of the reference microwave Cs atomic clock. According to this frequency measurement accuracy we assume, for simplicity, that the linewidth of the standard laser at 657 nm is 10 kHz, which is mainly determined by the white frequency noise of power spectrum density  $S$ . In this case, the square root of the Allan variance of this standard-laser frequency is given by  $\sigma_y(\tau) = (\Delta\nu_L/2\pi\tau)^{1/2} \sim 0.9 \times 10^{-13} \tau^{-1/2}$ , which is nearly of the same order as that of the reference Cs atomic clock.

The phase coherence of the 657 nm standard laser (laser 2) is transferred to the other eight lasers via optical phase-locking loops (OPLL). In the first stage of the OPLL between laser 1 and laser 2, the phase noise of laser 1 under phase locking ( $\delta\phi'_1$ ) is given by [13]

$$\delta\phi'_1 = H_1(f)(\delta\phi_2 - \delta\phi_{N1})/2 + [1 - H_1(f)]\delta\phi_1, \quad (7)$$

where  $H_1(f)$  is the transfer function of the phase-locked loop,  $\delta\phi_{N1}$  is the phase noise due to the beat  $S/N$  ratio,  $\delta\phi_1$  and  $\delta\phi_2$  is the phase noise of laser 1 and laser 2 under free running conditions, respectively.

In the following seven stages of the OPLL, the phase noise of seven lasers are given by

$$\begin{aligned} \delta\phi'_3 &= H_2(f)(\delta\phi'_1 + \delta\phi_2 - \delta\phi_{N2})/2 + [1 - H_2(f)]\delta\phi_3, \\ \delta\phi'_4 &= H_3(f)(\delta\phi'_2 + \delta\phi'_3 - \delta\phi_{N3})/2 + [1 - H_3(f)]\delta\phi_4, \\ \delta\phi'_5 &= H_4(f)(\delta\phi'_4 + \delta\phi'_5 - \delta\phi_{N4})/2 + [1 - H_4(f)]\delta\phi_5, \\ \delta\phi'_6 &= H_5(f)(\delta\phi'_5 + \delta\phi'_6 - \delta\phi_{N5})/2 + [1 - H_5(f)]\delta\phi_6, \\ &\vdots \\ \delta\phi'_9 &= H_8(f)(\delta\phi'_8 + \delta\phi'_9 - \delta\phi_{N8})/2 + [1 - H_8(f)]\delta\phi_9, \end{aligned} \quad (8)$$

where  $H_i$ ,  $\delta\phi_i$ ,  $\delta\phi_{Ni}$  are the same as in (7).

For simplicity, all nine loop filters are assumed to be the same first-order loop filters. The transfer functions are given by  $H_n(f) = f_L/(f_L + if)$  ( $n = 1-8$ ), where  $f_L$  is the phase locking bandwidth. The laser phase noise  $\delta\phi_i$  ( $i = 1, 3-8$ ) is assumed to be same as that of the reference laser 2  $\delta\phi_2$ . The phase noises  $\delta\phi_{Ni}$  ( $i = 1-8$ ) are also assumed to have the same magnitude. The bandwidth  $f_L$  is assumed to be 6 MHz to minimize the phase-error variance as described in the Sect. 1.

The power spectral density of the relative phase noise between laser 3 and laser 9 is calculated and shown in Fig. 4. The relation between the power spectral density  $S_\phi$  and the phase noise  $\delta\phi$  is  $S_\phi = |\delta\phi|^2$ . There are mainly three noise sources. The first is the sum of the additive phase

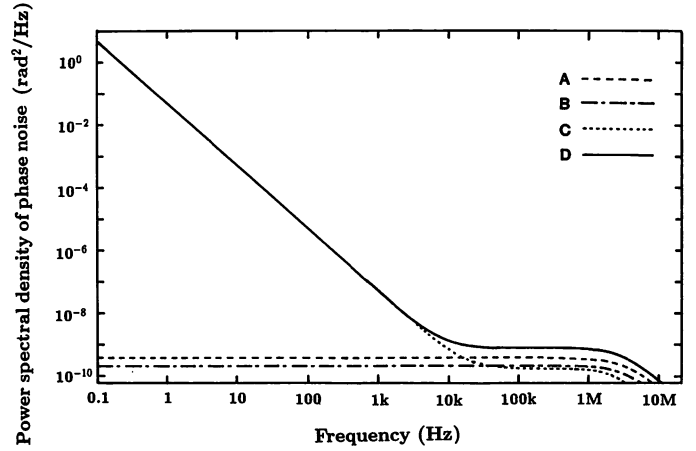


Fig. 4. Power spectral density of relative phase noise between laser 3 and laser 9. Curve A: the sum of  $S_{\phi_n}$ ; curve B: the sum of phase diffusion noise  $S_{\phi_i}$  ( $i = 1, 3-8$ ), curve C: the phase noise of laser 2; curve D: the sum of phase noise

noise  $S_{\phi_n}$  due to the finite  $S/N$  ratio of the beat signal in the OPLL (Fig. 4, curve A). The second is the sum of the phase-diffusion noise of eight lasers  $S_{\phi_i}$  ( $i = 1, 3-8$ ) (curve B). The third is the phase diffusion noise of laser 2  $S_{\phi_2}$  (curve C). The sum of three noise contributions is given by curve D. The total phase noise is approximately given by

$$S_{\phi_9-\phi_3} \sim \frac{1}{256^2} S_{\phi_2} + \left(\frac{206}{256}\right)^2 S_{\phi_n}. \quad (9)$$

When the  $S/N$  ratio of the beat at each OPLL is about 42 dB (BW = 100 kHz),  $S_{\phi_n}$  is  $6 \times 10^{-10}$  rad<sup>2</sup>/Hz. The phase noise of laser 2 (standard laser) is given by  $S_{\phi_2} = \Delta\nu_2/\pi f^2 \sim 3200/f^2$  rad<sup>2</sup>/Hz.

At  $f < 10$  kHz, the relative phase noise between laser 3 and laser 9 is mainly determined by the phase noise of laser 2  $S_{\phi_2}$ ; thus the phase coherence of laser 2 can be well preserved in the frequency difference between laser 3 and laser 9.

At the final stage, this frequency difference ( $\nu_9 - \nu_3 \sim 1.8$  THz) is further reduced to less than 6 GHz ( $\Delta_9$ ) by using the optical frequency comb generator. The higher-order sideband power of about 1 nW enables one to obtain a  $S/N$  ratio of about 42 dB (BW = 100 kHz) in the beat signal between the 300-th order sideband of laser 3 and laser 9. The additive phase noise  $S_{\phi_n}$  at the final stage is about  $6 \times 10^{-10}$  rad<sup>2</sup>/Hz. The phase noise of the heterodyne beat frequency  $\Delta_9$  is given by  $S_\phi = S_{\phi_9-\phi_3} + S_{\phi_n}$ . The phase noise of laser 2  $S_{\phi_2}$  appears in this beat frequency at  $f < 5$  kHz. Thus the phase coherence of laser 2 can be transferred to the beat frequency  $\Delta_9$ , which can be compared with the reference Cs atomic clock with an accuracy of  $10^{-14}$  at  $\tau = 100$  s.

We neglected the cycle slipping in the OPLL in the above discussion [13]. For a first-order loop filter, the mean time between cycle slipping is given by

$$t_s \simeq \pi \exp(2/\sigma_\phi^2)/4f_L, \quad (10)$$

where  $\sigma_\phi^2$  is the phase error variance and  $f_L$  is the locking bandwidth [13]. The mean frequency of cycle slipping is given by  $f_s = 1/t_s$ , which is the frequency error induced by

the cycle slipping. For the above condition ( $\sigma_\phi^2 = 0.01 \text{ rad}^2$ ,  $f_L = 6 \text{ MHz}$ ), this  $f_s$  is negligibly small. If the phase-error variance  $\sigma_\phi^2$  exceeds  $0.1 \text{ rad}^2$ , however, the cycle slipping is no longer negligible and  $f_s$  is calculated to be about  $0.016 \text{ Hz}$ . At the final stage of the OPLL, this frequency error  $f_s (= 0.016 \text{ Hz})$  corresponds to a relative frequency error of about  $10^{-14}$  on the optical frequency of about  $456 \text{ THz}$  ( $657 \text{ nm}$ ).

## 5 Nonlinear Frequency Conversions

Efficient nonlinear frequency conversion is important to realize this frequency chain using all diode lasers. As discussed in the previous section, sum-frequency (SF) and second-harmonic (SH) powers of about  $1 \mu\text{W}$  are sufficient to obtain a phase-error variance of  $0.01 \text{ rad}^2$  in the OPLL. Here we estimate the efficiency of nonlinear crystals and also show the preliminary experimental results.

The SHG of  $1315 \text{ nm}$  can be obtained using an angle-tuned KTP crystal. We have obtained a SH power of about  $10 \text{ nW}$  using a single-pass KTP crystal ( $l = 5 \text{ mm}$ ) with a fundamental power of  $50 \text{ mW}$ . Due to the large walk-off angle ( $\sim 2.7^\circ$ ), the conversion efficiency is rather low. We have also obtained the beat between this SH and the  $657 \text{ nm}$  laser with a  $S/N$  ratio of about  $30 \text{ dB}$  ( $\text{BW} = 30 \text{ kHz}$ ). If we use a noncritical phase-matched  $\text{LiNbO}_3$  crystal, we can expect a rather high conversion efficiency, however, the phase matching temperature is rather high ( $\sim 360^\circ\text{C}$ ).

The SFM between  $1315 \text{ nm}$  and  $657 \text{ nm}$  can be also obtained using an angle-tuned KTP crystal ( $\theta = 88^\circ$ ,  $\phi = 0^\circ$ ) at room temperature. Recently, noncritical phase matching of SFM between  $1319 \text{ nm}$  and  $660 \text{ nm}$  lasers has been reported at near room temperature ( $\sim 50^\circ\text{C}$ ) [14]. It is possible to get noncritical phase matching of SFM, between  $1315 \text{ nm}$  and  $657 \text{ nm}$  at temperature around  $-60^\circ\text{C}$  to  $-20^\circ\text{C}$ . In this case, a sum-frequency power of about  $3 \mu\text{W}$ , is expected using a single-pass crystal ( $l = 7 \text{ mm}$ ) with fundamental powers of  $30 \text{ mW}$  ( $1315 \text{ nm}$ ) and  $3 \text{ mW}$  ( $657 \text{ nm}$ ).

The SHG of  $751 \text{ nm}$  and  $809 \text{ nm}$ , and the SFM of  $657 \text{ nm}$ ,  $751 \text{ nm}$  and  $876 \text{ nm}$ , can be obtained using angle-tuned  $\text{LiIO}_3$  crystals. The conversion efficiency is not so

high due to large walk-off angle of about  $4.5^\circ$  ( $809 \text{ nm}$ ) [15]. In our recent experiment, we have obtained about  $40 \mu\text{W}$  of SH power at  $750 \text{ nm}$  and  $810 \text{ nm}$  with a fundamental power of about  $900 \text{ mW}$  in a single-pass crystal ( $l = 10 \text{ mm}$ ). A SH power of about  $0.6 \mu\text{W}$  is expected using a fundamental power of  $100 \text{ mW}$ .

For the SFM and SHG of wavelength around  $840\text{--}880 \text{ nm}$ , high conversion efficiencies are expected using a non-critically phase-matched A-cut  $\text{KNbO}_3$  crystal at the temperature around  $-30\text{--}70^\circ\text{C}$ . A SH power of  $50 \mu\text{W}$  can be generated in a single-pass crystal of  $l = 5 \text{ mm}$  with a fundamental power of  $50 \text{ mW}$  ( $875 \text{ nm}$ ). We have obtained about  $10 \mu\text{W}$  power of the sum frequency mixing between the  $875 \text{ nm}$  laser and  $825\text{--}842 \text{ nm}$  laser with each fundamental powers of about  $50 \text{ mW}$ . In Table 1, we summarize all nonlinear frequency conversions used in the present frequency chain.

## 6 Discussion

Technical requirements for the lasers to realize the present frequency chain are as follows

- (i) single-frequency high output power ( $50\text{--}100 \text{ mW}$ ),
- (ii) wide wavelength range ( $1.3\text{--}0.66 \mu\text{m}$ ),
- (iii) narrow linewidth ( $\sim 10 \text{ kHz}$ ),
- (iv) wide frequency control bandwidth ( $500 \text{ kHz}\text{--}10 \text{ MHz}$ ).

In the wavelength range of  $810\text{--}880 \text{ nm}$ , high power ( $\sim 100 \text{ mW}$ ) single-frequency AlGaAs diode lasers are available. Using an optical feedback from a confocal cavity, it is easy to obtain a narrow linewidth of about  $10 \text{ kHz}$  [16]. At  $1.3 \mu\text{m}$ , we have recently obtained a single-frequency output power of  $50 \text{ mW}$  from a high power ( $\sim 130 \text{ mW}$ ) InGaAsP diode laser using an external grating feedback [17]. We can also use an injection-locking technique to obtain high-power single-frequency operation of high-power diode lasers [18].

The output power of AlGaAs diode lasers at  $750 \text{ nm}$  is still low ( $\sim 10 \text{ mW}$ ) compared with longer wavelength lasers. A high power ( $50 \text{ mW}$ ) multi-quantum-well (MQW) AlGaAs lasers at  $780 \text{ nm}$  can be used at low temperature ( $\sim -80^\circ\text{C}$ ). A red AlInGaP diode laser at  $657 \text{ nm}$  can be used at room temperature. Using an anti-reflection coated laser with external grating feedback, it is easy to obtain single-frequency operation with narrow linewidth [19]. The output power of this laser is also still low ( $\sim 3 \text{ mW}$ ). High-power red diode lasers are now under development and the maximum output power is about  $35 \text{ mW}$  at rather longer wavelengths ( $675\text{--}680 \text{ nm}$ ). Until high-power diode lasers at  $750 \text{ nm}$  and  $657 \text{ nm}$  will be developed, we can use powerful dye and  $\text{Ti:Al}_2\text{O}_3$  lasers pumped by an  $\text{Ar}^+$  laser instead of diode lasers.

The bandwidth of the optical phase locking loop is required to be several MHz for minimizing the phase error. Using current modulation of the diode laser, it is easy to obtain a frequency-control bandwidth of more than  $1 \text{ MHz}$  [20–22]. Heterodyne and homodyne optical phase locking loops have been realized with a low phase-error variance of about  $0.01 \text{ rad}^2$  [23, 24].

Among the nonlinear crystals, the conversion efficiency of  $\text{LiIO}_3$  crystals is lower than that of other crystals and

**Table 1.** Nonlinear frequency conversions

Process	$\lambda$ [nm]	Crystal	T [ $^\circ\text{C}$ ]	Cut
$\nu_1 \times 2$	1315	KTP		$60^\circ$
$\nu_1 + \nu_2$	1315, 657	KTP		$88^\circ$
$\nu_3 \times 2$	877	$\text{KNbO}_3$	67	
$\nu_2 + \nu_3$	657, 877	$\text{LiIO}_3$		$29^\circ$
$\nu_4 \times 2$	751	$\text{LiIO}_3$		$47^\circ$
$\nu_3 + \nu_4$	877, 751	$\text{LiIO}_3$		$64^\circ$
$\nu_5 \times 2$	809	$\text{LiIO}_3$		44
$\nu_3 + \nu_5$	877, 809	$\text{KNbO}_3$	$-20$	
$\nu_6 \times 2$	842	$\text{KNbO}_3$	$-28$	
$\nu_3 + \nu_6$	877, 842	$\text{KNbO}_3$	22	
$\nu_7 \times 2$	859	$\text{KNbO}_3$	15	
$\nu_3 + \nu_7$	877, 859	$\text{KNbO}_3$	35	
$\nu_8 \times 2$	868	$\text{KNbO}_3$	41	
$\nu_3 + \nu_8$	877, 872	$\text{KNbO}_3$	50	
$\nu_9 \times 2$	872	$\text{KNbO}_3$	58	

not high enough for low-power diode lasers. Using an external resonant buildup cavity, the conversion efficiency can be easily enhanced [15, 25]. Recently, quasi-phase matching (QPM) waveguides have been developed and efficient SHG and SFM has been demonstrated using a LiTaO<sub>3</sub> or KTP waveguide [26, 27]. More than 2 mW, of blue SFM light has been generated with a fundamental laser power of 100 mW [27]. We can expect more than 10  $\mu$ W of SHG and SFG by using this QFM waveguide with a fundamental power of only 5 mW.

The present system requires nine lasers and 15 nonlinear crystals. There is still room to improve the frequency span of the optical frequency comb generator. If we obtain an overall cavity finesse of more than 500 and a modulation index of about  $\pi/2$  in the comb generator the frequency span is expected to be more than 7 THz, and we can reduce the number of lasers and nonlinear crystals to seven and 11, respectively.

The present frequency chain can provide many useful frequency markers in the near infrared and visible region. The S–D transition of a trapped Sr<sup>+</sup> ion at 674 nm is also a promising candidate for the optical frequency standard [28]. Its natural linewidth is estimated to be within 1 Hz. With two additional frequency divider stages between the 1315 nm laser and the 1348 nm laser, which is half the frequency of the 674 nm laser, the frequency difference can be reduced to about 1.4 THz.

Dividing 751 nm and 809 nm lasers, this middle laser at 779 nm is close to the Rb D<sub>2</sub> lines at 780 nm within 0.5 THz. The sum frequency between the 1315 nm and this 779 nm lasers is close to one quarter of the frequency (486 nm) of the 1S–2S transition of atomic hydrogen at 122 nm within 3.7 THz [4].

## 7 Summary

We have proposed a frequency chain between the microwave and the optical frequency for frequency measurement of a Ca stabilized laser at 657 nm. This chain can be realized with currently available diode lasers, nonlinear crystals and E/O phase modulators. We have shown the necessary conditions for the optical phase-locked loops to achieve the frequency measurement accuracy level of 10<sup>-14</sup>. The present chain will give us many useful landmarks of optical frequency for future optical frequency standards.

*Acknowledgements.* This work was supported by the Grant-in-Aid for Scientific Research (No. 03555006) from the Ministry of Education, Science, and Culture of Japan.

## References

1. D.A. Jennings, C.R. Pollock, F.R. Petersen, R.E. Drullinger, K.M. Evenson, J.S. Wells, J.L. Hall, H.P. Layer: *Opt. Lett.* **8**, 136 (1983)
2. O. Acef, J.J. Zondy, M. Abed, D.G. Rovera, A.H. Gerard, A. Clairon, Ph. Laurent, Y. Millieroux, P. Juncar: *Opt. Commun.* **97**, 29 (1993)
3. J. Helmcke, A. Morinaga, J. Ishikawa, F. Riehle: *IEEE Trans. IM-38*, 524 (1989)
4. T. Andreae, W. König, R. Wynands, D. Leibfried, F. Schidtkaler, C. Zimmermann, D. Meschede, T.W. Hänsch: *Phys. Rev. Lett.* **69**, 1923 (1992)
5. H.R. Telle, D. Meschede, T.W. Hänsch: *Opt. Lett.* **15**, (532) 1990
6. T. Sato, S. Singh, S. Swartz, J.L. Hall: *IQEC'90 Technical Digest, Paper QThD3* (1990)
7. N.C. Wong: *Opt. Lett.* **15**, 1129 (1990)
8. N.C. Wong: *Opt. Lett.* **17**, 1155 (1992)
9. M. Kourogi, K. Nakagawa, C.H. Shin, M. Teshima, M. Ohtsu: *CLEO'91 Technical Digest, paper CThR57* (1991)
10. M. Kourogi, K. Nakagawa, M. Ohtsu: *IEEE J. Quantum Electron*, to be published
11. R. Wynands, T. Mukai, T.W. Hänsch: *Opt. Lett.* **17**, 1749 (1992)
12. Horace P. Yuen, Vincent W.S. Chan: *Opt. Lett.* **8**, 177 (1983)
13. A. Blanchard: *Phase-Locked Loops. Application to Coherent Receiver Design* (Wiley, New York 1976)
14. R.A. Stolzenberger, Chia-Chen Hsu, N. Peyghambarian, J.J.E. Reid, R.A. Morgan: *IEEE Photon. Technol. Lett.* **1**, 446 (1989)
15. C.S. Adams, A.I. Ferguson: *Opt. Commun.* **79**, 219 (1990)
16. B. Dahmani, L. Hollberg, R. Drullinger: *Opt. Lett.* **12**, 876 (1987)
17. K. Nakagawa, M. Ohtsu, C.H. Shin, M. Kourogi, Y. Kikunaga: *Tenth International Conference on Laser Spectroscopy*, M. Ducloy, E. Giacobino, G. Camay, eds. (World Scientific, Singapore, 1992) p. 353
18. K. Nakagawa, M. Teshima, M. Ohtsu: *Opt. Lett.* **16**, 1590 (1991)
19. M.G. Boshier, D. Berkeland, E.A. Hinds, V. Sandoghdar: *Opt. Commun.* **85**, 355 (1991)
20. M. Kourogi, C-H. Shin, M. Ohtsu: *IEEE Photon. Technol. Lett.* **3**, 496 (1991)
21. C-H. Shin, M. Ohtsu: *Opt. Lett.* **15**, 1455 (1990)
22. K. Nakagawa, M. Kourogi, M. Ohtsu: *Opt. Lett.* **17**, 934 (1992)
23. C-H. Shin, M. Ohtsu: *IEEE Photon. Technol. Lett.* **2**, 297 (1990)
24. C-H. Shin, M. Ohtsu: *IEEE J. QE-29*, 374 (1993)
25. A. Hemmerich, D.H. McIntyre, C. Zimmermann, T.W. Hänsch: *Opt. Lett.* **15**, 372 (1990)
26. K. Mizuuchi, K. Yamamoto: *Appl Phys. Lett.* **60**, 1283 (1992)
27. F. Laurell, J.B. Brown, J.D. Bierlein: *Appl. Phys. Lett.* **60**, 1064 (1992)
28. A.A. Madej, J.D. Sankey: *Opt. Lett.* **15**, 634 (1990)

# Pump-probe Spectroscopy in Potassium using an AlGaAs Laser and the Second-harmonic Generation of an InGaAsP Laser for Frequency Stabilization and Linking

W. Wang, A. M. Akulshin, and M. Ohtsu, *Member, IEEE*

**Abstract**—Pump-probe spectroscopy in  $^{41}\text{K}$  by using a grating-feedback  $0.77\text{-}\mu\text{m}$  AlGaAs laser and the second-harmonic wave of a  $1.54\text{-}\mu\text{m}$  InGaAsP laser for providing a frequency reference in the  $1.5\text{ }\mu\text{m}$  region was performed. The pump laser frequency was locked to the Doppler-free resonance with frequency fluctuations less than  $50\text{ kHz}$  estimated from the error signal. The Doppler-free absorption spectra in both co- and counter-propagating schemes were obtained, and the feasibility of simultaneous frequency stabilization and linking for two diode lasers with a frequency difference as large as  $200\text{ THz}$  was demonstrated.

## I. INTRODUCTION

THE  $1.5\text{ }\mu\text{m}$  region is of great interest for the present optical communication systems. Considerable attention has been given to the search for a suitable absolute frequency reference at this wavelength, which is indispensable for near-future coherent multi-channel optical communications. Linear absorption lines of molecules, such as ammonia ( $\text{NH}_3$ ) and acetylene ( $\text{C}_2\text{H}_2$ ), and saturated absorptions of noble gases have been investigated for this purpose [1], [2], [3]. Rubidium atoms have been used to provide a frequency reference at this wavelength using the internal second-harmonic generation [4] or through a two-step excitation scheme, [5], [6]. On the other hand, the pump-probe spectroscopy scheme also provides a possibility for circumventing the requirement of high power for obtaining the Doppler-free saturation resonances for both molecules and atoms through nonlinear frequency conversion. Furthermore, when two independent lasers with a large frequency difference are used in this scheme, a frequency link can be established simultaneously, which is one of essential tasks in a wideband tunable light source system, e.g., for our engaged wideband highly-coherent optical-frequency sweep-generator [7]. In this letter, we report for the first time the observation of the Doppler-free absorption spectrum of the potassium  $D_1$  line in both co-propagating and counter-propagating pump-probe schemes by using an AlGaAs laser

as a pump and the second harmonic wave of an InGaAsP laser as a probe.

Potassium was chosen for our experiment since a high-power and highly coherent distributed feedback (DFB) laser is available at  $1.54\text{ }\mu\text{m}$  [8], the second harmonic of which just coincides with the potassium  $D_1$  line. It is also interesting to observe, by using two independent lasers, the characterized absorption profile due to the fact that the hyperfine splitting of the ground state is smaller than the Doppler broadening, especially for  $^{41}\text{K}$  which was rarely documented [9], [10], although the absorption spectrum of  $^{39}\text{K}$ - $D_1$  line has been observed through fluorescence [11]. The atomic cell containing  $^{41}\text{K}$  (2-cm long) used in our experiment was installed inside an oven to maintain the temperature close to  $60^\circ\text{C}$ . At this temperature, total absorption was measured to be  $40\sim 50\%$ , and the Doppler width is  $\sim 800\text{ MHz}$ . The wavelength of the  $D_1$  line  $770.109\text{ nm}$  (in vacuum).

To prepare two lasers for the pump-probe scheme, the second-harmonic wave of a  $1.54\text{ }\mu\text{m}$  in GaAsP multi-electrode DFB laser was generated in a 10-mm length KTP crystal. Type-II, angle-tuning phase matching at room temperature was employed as the crystal was installed along the  $\theta$  plane ( $\phi = 0, \theta = 54^\circ$ ). The fundamental power was  $40\text{ mW}$ , and the detected power after the spectroscopic system was measured to be  $20\text{ nW}$ . Although such a power is insufficient for saturating, it is enough for use a probe beam. The pump laser is a grating-feedback AlGaAs laser, and the laser facet was coated with an anti-reflection (AR) film to extend the tunability which is accomplished using an external grating ( $1200\text{ lines/mm}$ ). The operating injection current was  $100\text{ mA}$  while the threshold was  $\sim 85\text{ mA}$  due to the AR coating, and the output power was measured to be  $1.4\text{ mW}$ .

In order to provide a frequency reference for  $1.5\text{ }\mu\text{m}$  through the pump-probe spectroscopy scheme, the frequency of the pump laser must be locked to the absorption resonance. A conventional saturation-spectroscopy scheme, as shown in Fig. 1, was arranged for this purpose. The laser beam was divided into two parts, one for the pump and the other one for the probe in counter-propagating directions. The Doppler-free absorption resonances were observed to verify that the pump laser was on the potassium  $D_1$  resonance line and in a real single-mode regime. Fig. 2 shows the Doppler-free absorption

Manuscript received September 8, 1993.

W. Wang is with the Interdisciplinary Graduate School of Science and Engineering, Tokyo Institute of Technology, 4259, Nagatsuta-cho, Midori-ku, Yokohama 227, Japan.

M. Ohtsu is also with the Kanagawa Academy of Science and Technology, KSP East, Room 408, 3-2-1 Sakado, Takatsu-ku, Kawasaki 213, Japan.

M. Akulshin's permanent address is the P. N. Lebedev Physics Institute, Moscow, Russia.

IEEE Log Number 9214735.

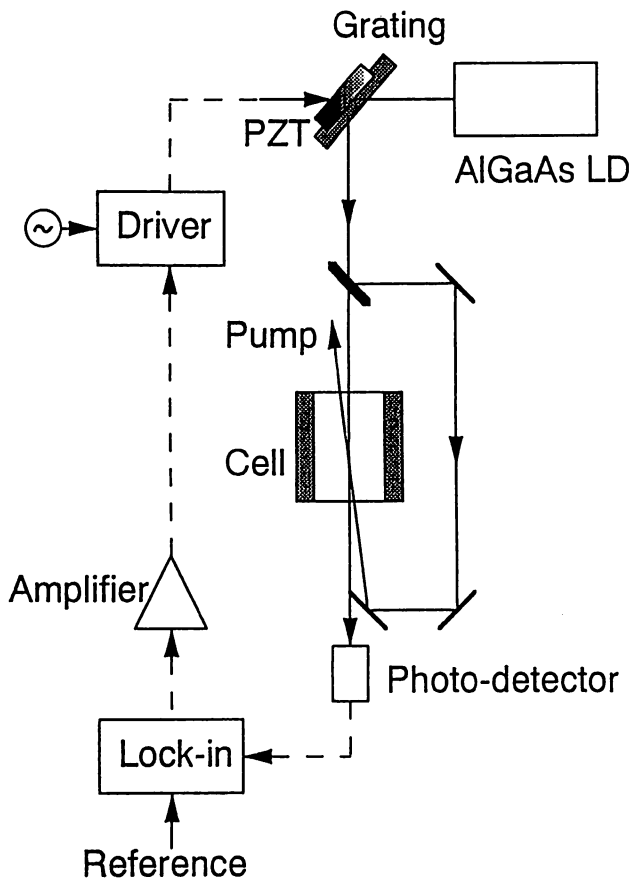


Fig. 1. Experiment setup for observing Doppler-free resonances and frequency stabilization. All parts were fixed on an invar plate to improve the thermal stability.

profile when the laser frequency was tuned to the top of the Doppler profile. The laser beam intensity used was  $\sim 4 \text{ mW/cm}^2$ . The very sharp absorption peak with some structure (in Fig. 2(b)) was the cross-over resonance which appeared when the laser frequency was tuned midway between the two sub-levels of the  $4S$  (ground) state corresponding to  $F=1$  and  $2$  respectively. It can be explained as the compensation of populating and de-populating due to the velocity-selective saturation and optical pumping in the sub-levels of the ground state [11]. The structure inside the absorption peak (Fig. 2(c)) shows the hyperfine structure of the excited state. Although the value of the hyperfine splitting for the  $4P_{1/2}$  state in  $^{41}\text{K}$  was not found in the literature, we measured this value as  $\sim 29 \text{ MHz}$  from our result based on the ground-state hyperfine splitting of  $254 \text{ MHz}$  [9]. It is very clear from this profile that the resolution was up to the natural linewidth limit ( $\sim 10 \text{ MHz}$ ). The small peaks appearing in Fig. 2(b) correspond to the cross-over resonances of the isotope  $^{39}\text{K}$ , with a shift (measured to be  $\sim 220 \text{ MHz}$ ) which agreed well with the estimated isotope shift for potassium ( $250 \text{ MHz}$ ).

Frequency stabilization of the pump laser was carried out by locking the laser frequency to the cross-over absorption peak. Fig. 3(a) shows the first derivative of the absorption profile obtained by the conventional phase-sensitive technique through a lock-in amplifier. The modulation frequency applied to the PZT was  $3 \text{ kHz}$  and the time constant was  $30 \text{ ms}$ .

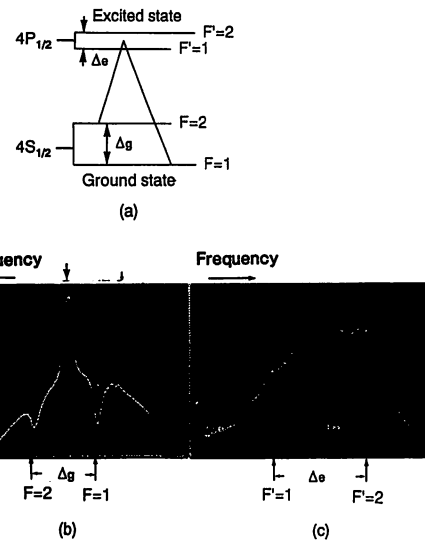


Fig. 2. (a) The energy level diagram of potassium.  $\Delta g$  and  $\Delta e$  represent the hyperfine splittings in ground and excited states, respectively. (b) The Doppler-free resonances of the  $D_1$  line in  $^{41}\text{K}$ . Two dips correspond to the two hyperfine sub-levels in the ground state ( $4S_{1/2}$ ). The high peak is the crossover resonance. The small peaks correspond to the isotope  $^{39}\text{K}$ . (c) The resonances observed inside the crossover peak in (b), these peaks correspond to two hyperfine sub-levels in the excited state ( $4P_{1/2}$ ) and a crossover resonance.

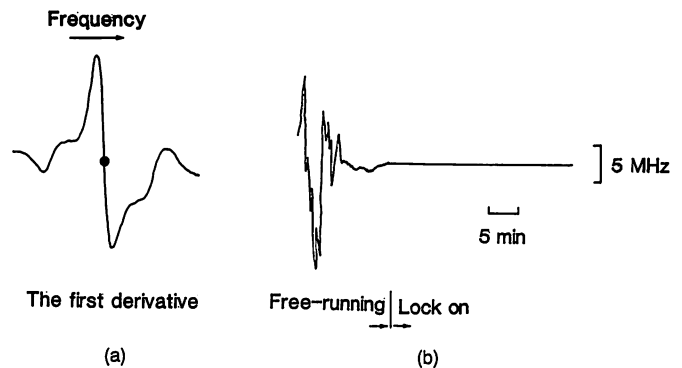


Fig. 3. (a) The first derivative of the Doppler-free resonances. (b) The error signal in frequency stabilization. The locking point corresponds to the top of the cross-over resonance.

The residual frequency fluctuations were estimated to be less than  $50 \text{ kHz}$  from the error signal shown in Fig. 3(b). This result demonstrates that the Doppler-free potassium absorption line also provides an absolute frequency reference for AlGaAs lasers, in addition to the well-utilized rubidium line.

For observing the pump-probe spectra by using two independent lasers, the second harmonic wave of the  $1.54 \mu\text{m}$  laser was used as a probe co- and counter propagating to the pump beam from the grating-feedback laser. To improve the signal-to-noise ratio, the probe beam was intensity-modulated by a chopper with a frequency of  $1 \text{ kHz}$ , and the output absorption profile was obtained from a lock-in amplifier while the probe frequency was swept slowly ( $0.01 \text{ Hz}$ ). In the counter-propagating scheme, the pump-probe angle was about  $5 \text{ mrad}$ , while in the co-propagating scheme, two crossed polarizers were used to block the direct incidence of the pump beam to the detector so as to maintain the angle between

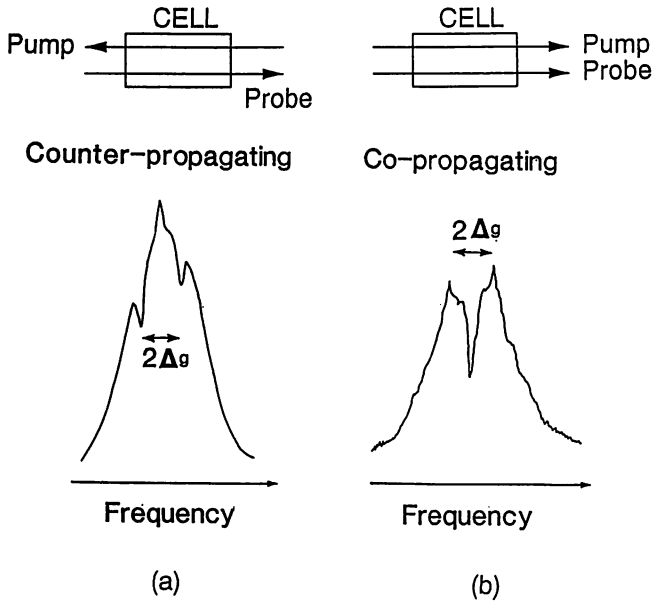


Fig. 4. The Doppler-free resonances using two independent lasers. The frequency intervals between two dips in the counter-propagating case (a), and between two peaks in the co-propagating case (b), are two times that of the hyperfine splitting of the ground state.

pump and probe beams to be less than 1 mrad. Figures 4(a) and (b) show the absorption profiles in both co- and counter-propagating schemes, respectively. The shapes of the absorption spectra can be explained by the basic principle of the pump-probe spectroscopy in the case of two independent lasers and including the effect of the optical pumping. Due to the optical pumping effect, populating and depopulating processes occur to redistribute the populations in both sub-levels of the ground state. Therefore, as shown in Fig. 4, two dips and one peak in a counter-propagating geometry, and two peaks and one dip in a co-propagating geometry were observed. Each dip or peak had fine structure corresponding to the hyperfine splitting in the excited state, which was not well resolved because such a splitting is comparable with the natural linewidth of  $^{41}\text{K}$ , and the signal-to-noise ratio in detection was limited. Comparing these two schemes, one feature in the absorption spectra is that the co-propagating scheme offers a nonlinear absorption resonance with a very large contrast (higher than 60%), and it is preferable for stabilization of the 1.5  $\mu\text{m}$  laser used as a frequency link and absolute frequency reference.

It should be noted that there are several alternative schemes for potassium which are also reasonable for frequency stabilization and linking. For example, use of the Doppler-free resonances of  $^{39}\text{K}$  is easier because of its larger hyperfine splittings; use of optical phase locking between the 0.77  $\mu\text{m}$  and

1.54  $\mu\text{m}$  lasers can improve the frequency tracking accuracy; moreover the two lasers can be locked simultaneously to  $D_1$  and  $D_2$  lines, respectively, to offer more transition options; and narrower resonance by using the coherent population-trapping [12] method is also possible if second-harmonic generation is enhanced by a buildup cavity.

## II. CONCLUSIONS

In summary, we have performed pump-probe spectroscopy in  $^{41}\text{K}$  by using a 0.77  $\mu\text{m}$  grating-feedback AlGaAs laser and the second harmonic of a 1.54  $\mu\text{m}$  InGaAsP multielectrode DFB laser to provide a frequency reference in the 1.5  $\mu\text{m}$  region. The AlGaAs laser frequency was locked to the Doppler-free resonance with residual frequency fluctuations less than 50 kHz estimated from the error signal. Both co- and counter-propagating schemes were employed to observe the Doppler-free absorption spectra in which the second harmonic wave of the InGaAsP laser was used as a probe. The feasibility of simultaneous frequency linking between frequencies as far apart as 200 THz has been demonstrated in a simple way. Because 1.54  $\mu\text{m}$  is closer to the lowest-loss region in optical fiber than 1.529  $\mu\text{m}$  [6], it is preferable for optical communications. The experimental result also showed that potassium is a candidate for frequency stabilization and linking 0.77  $\mu\text{m}$  and 1.54  $\mu\text{m}$  diode lasers by Doppler-free resonances, which is important for our engaged diode-laser-based highly coherent optical frequency sweep generator.

## ACKNOWLEDGMENT

The authors would like to thank M. Okai of Hitachi Corp. for helpful discussion on the DFB lasers.

## REFERENCES

- [1] Sakai, S. Sudo, and T. Ikegami, *IEEE J. Quantum Electron.* QE-28, 75 (1992).
- [2] M. Ohtsu, H. Kotani, and H. Tagawa, *Jpn. J. Appl. Phys.* 22, 1553 (1983).
- [3] A. J. Lucero, Y. C. Chung, S. Reilly, and R. W. Tkach, *Opt. Lett.* 16, 849 (1991).
- [4] M. Ohtsu, E. Ikegami, *Elect. Lett.* 25, 22 (1989).
- [5] Sarah Gilbert, in *QELS 93, paper QThE6*, Technical Digest p. 212, 1993.
- [6] H. Sasada, *IEEE Photon Technol. Lett.* 4, 1307 (1992).
- [7] W. Wang and M. Ohtsu, *Opt. Lett.* 18, 876 (1993).
- [8] M. Okai, T. Tsuchiya, K. Uomi, N. Chinone, and T. Harada, *IEEE Photon. Technol. Lett.* 2, 529 (1990).
- [9] E. Armondo, M. Inguscio, and P. Violino, *Rev. Mod. Phys.* 49, 31 (1977).
- [10] Sune Svanberg, *Atomic and molecular spectroscopy, Springer Series on Atoms and Plasmas; Springer-Verlag, Berlin, 1992*, vol. 6, 2nd ed. ch. 1, ch. 7, ch. 9.
- [11] V. L. Velichanskii, A. S. Zibrov, V. S. Kargopol'tsev, O. R. Kachurin, V. V. Nikitin, V. A. Sautenkov, G. G. Kharisov, and D. A. Tyurikov, *Sov. J. Quantum Electron.* 10, 1244 (1980).
- [12] A. M. Akulshin, A. A. Celikov, and V. L. Velichansky, *Opt. Commun.* 84, 139 (1991).



## OPTICAL RESPONSE OF SINGLE CRYSTAL AND BICRYSTAL YBa<sub>2</sub>Cu<sub>3</sub>O<sub>7- $\delta$</sub> THIN FILMS

K.Tanaka<sup>1)</sup>, M.Kawasaki<sup>2),3)</sup>, K.Fujito<sup>2)</sup>, Y.Harada<sup>1)</sup>, M.Sano<sup>1)</sup>, K.Mizobuchi<sup>4)</sup>, Y.Higashino<sup>4)</sup>,  
H.Koinuma<sup>2)</sup>, M.Sekine<sup>1)</sup>, and M.Ohtsu<sup>1)</sup>

<sup>1)</sup>Department of Applied Electronics, Tokyo Institute of Technology,

<sup>2)</sup>Research Laboratory of Engineering Materials, Tokyo Institute of Technology,

<sup>3)</sup>PRESTO-JRDC

4259 Nagatsuta, Midori-ku, Yokohama 227, Japan

<sup>4)</sup>Teratec Corporation, 2-11-13 Nakacho, Musashino, Tokyo 180, Japan

We have investigated the optical response of YBa<sub>2</sub>Cu<sub>3</sub>O<sub>7- $\delta$</sub>  grain boundary junctions as well as single crystal strip lines. For both devices, bolometric signal was detected between  $T_c(\text{zero})$  and  $T_c(\text{onset})$ , whereas nonbolometric signal was observed only in a temperature range just above  $T_c(\text{zero})$  where the current-voltage characteristic showed nonlinear behavior. The content of nonbolometric signal in the total response signal was remarkably increased with decreasing the film thickness. The effect of a single grain boundary on the nonbolometric response was described.

### 1 INTRODUCTION

So far, many High- $T_c$  superconducting devices have been proposed, in which Josephson effects or nonequilibrium phenomena are utilized. One of the nonequilibrium phenomena is based on the effect that energy injection, such as laser radiation, into a superconductor from an external source destroys the thermal equilibrium. From a rough estimate of superconducting energy gap ( $2\Delta \approx 40$  meV), it should be possible to detect infrared photons by using High- $T_c$  superconductors. We reported the evident nonbolometric response in YBa<sub>2</sub>Cu<sub>3</sub>O<sub>7- $\delta$</sub>  (YBCO) under the irradiation of infrared laser beam at a modulation frequency up to 300MHz[1]. Here we investigate possible photodetectors based on nonequilibrium phenomena in YBCO single crystal lines (SCLs) and single grain boundary junctions (GBJs).

### 2 EXPERIMENTS

Thin films were fabricated on SrTiO<sub>3</sub> substrates by using the laser ablation method. The configuration of the devices were summarized in Table 1. Fast optical response was measured by using beat-down technique with double balanced mixer[1]. A semiconductor laser diode was used as a radiation source ( $\lambda=830\text{nm}$ ). Since nonlinear behavior

Table 1: Device size and  $T_c$ .

Crystal	Single			Bi
$T_c(\text{zero})$	62K	81K	75K	78K
Thickness	200Å	1700Å	3000Å	1000Å
Length	2.5mm	400 $\mu\text{m}$	400 $\mu\text{m}$	400 $\mu\text{m}$
Width	1mm	25 $\mu\text{m}$	25 $\mu\text{m}$	50 $\mu\text{m}$

was observed in the current-voltage characteristics just above  $T_c(\text{zero})$ , the nonlinearity was defined as eq.(1) and was measured by using lock-in amplifier.

$$\text{Nonlinearity}(I = I_b) = \left. \frac{dV}{dI} \right|_{I_b} - \frac{V(I_b)}{I_b}. \quad (1)$$

### 3 RESULTS AND DISCUSSION

Figure 1(a) depicts the optical response of a 200Å thick SCL. The temperature dependence of optical response deviates from that of  $dV/dT$  to which the bolometric effect should be proportional. By subtracting the bolometric component from the

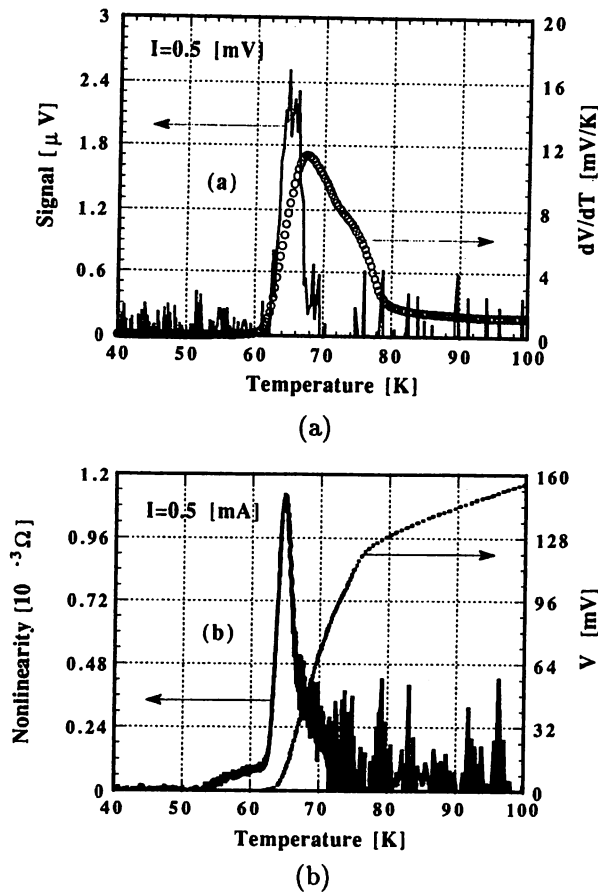


Figure 1: Temperature dependence of (a) signal and  $dV/dT$  and (b) nonlinearity (Thickness  $200\text{\AA}$ , Modulation frequency=5MHz).

total optical response signal, the nonbolometric component was calculated[1]. Figure 1(b) shows the nonlinearity measured for the same device. The temperature dependence of the nonlinearity well coincides with the nonbolometric signal, indicating the fluctuation of superconductivity, such as flux motion and pair breaking, should be responsible for nonbolometric signal. For thicker devices, similar experiments were carried out. The ratio of nonbolometric signal to bolometric signal was summarized in Figure 2. The nonbolometric component was more pronounced in the devices with using thinner films, suggesting the device should be thinner than the penetration depth ( $\sim 500\text{\AA}$ ) of laser light. In GBJs, the nonbolometric signal was also observed just above  $T_c$  (zero), and was related

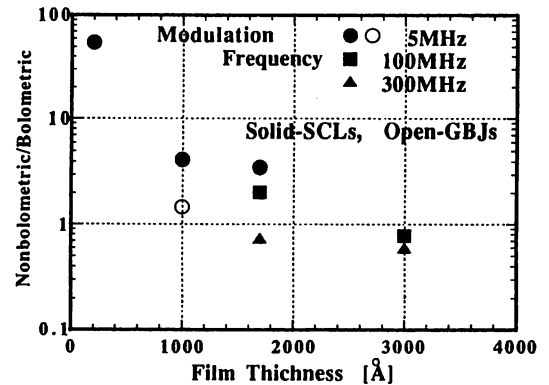


Figure 2: Thickness dependence of nonbolometric signal to bolometric signal ratio. (Laser Power  $\approx 3\text{mW}$ )

to the nonlinear current-voltage characteristics.

By scanning the laser beam (nominally  $25\mu\text{m} \sim 1\text{mm}\phi$ ) along strip line of GBJ, we found that optical response was observed only when the laser beam was adjusted on the grain boundary. Whereas, in case of SCLs, the position was unpredictable and we had to look for it. If one had expected homogeneous superconductivity in entire SCLs, one would observe optical response regardless of the laser beam position in SCLs. Low temperature SEM for a current biased SCL indicated that the weak spot in SCL was responsible for voltage generation responding to pulsed e-beam injection[2]. By taking the GBJ results into account, we conclude the optical response was observed when laser beam was impinged on the position with lower  $T_c$  and lower  $J_c$  among the entire device area. GBJs have an advantage in specifying the active region in devices.

## REFERENCES

- [1] K. Tanaka, et al.: *Proceedings of the Fourth International Symposium on Superconductivity, (ISS'92), Kobe., to be published.*
- [2] R. Gross, et al.: *Appl. Phys. Lett.*, **55**, pp.2132-2134, (1989).

# A Monolithic Optical Frequency Comb Generator

M. Kourogi, T. Enami and M. Ohtsu, *Senior Member, IEEE*

**Abstract**—A monolithic optical frequency comb (OFC) generator was realized by coating high reflection films on the facets of a LiNbO<sub>3</sub> crystal used for an electro-optic (EO) phase modulator. The optical round-trip loss in the monolithic OFC generator was reduced to extend the span of an OFC. It is confirmed that the envelope of the OFC extended to a span as wide as 48 nm (or 6.1 THz) around 1.5 μm. The maximum measurable frequency difference, which was defined as the sideband frequency with the signal-to-noise ratio of 0 dB, was estimated to be also 6.1 THz.

## I. INTRODUCTION

MEASUREMENT of frequency difference among lasers which are spaced in a span as wide as several THz is required for industrial applications such as optical frequency-division multiplexing in coherent optical communication systems and for precision physical measurements such as highly accurate absolute laser frequency measurement using a frequency-multiplication chain. However it has been difficult to measure such a high frequency difference because of the lack of reliable ultra-high speed optical heterodyne receiver. In order to overcome this difficulty, we have proposed a highly accurate, and wide span optical frequency difference measurement system [1] using an optical frequency comb (OFC) generator which generates a precisely spaced comb of frequencies through large-index phase modulation. We have demonstrated the OFC generation with a span of 4 THz [2], [3] by using an OFC generator which is composed of an electro-optic (EO) phase modulator installed within a Fabry-Perot cavity [4] so that the efficiency of the modulation is increased by multiple passes of light through the modulator. We have estimated that 4 THz frequency difference can be measured by using the OFC generator [2], [3]. We have also demonstrated a heterodyne optical phase locking with a heterodyne frequency of 0.5 THz [2], [3]–[5] by using the OFC generator. Recently, similar configurations for frequency synthesizing of lasers have been begun to be studied by many scientist, e. g., a similar experiment using an OFC generator and an optical parametric oscillator has been reported [6], and OFC generators using an acoustic modulator and optical amplifier have been proposed [7]–[8]. Our OFC generator could be intrinsically very compact and can generate very wide OFC because it does not include any complicated element such as an optical amplifier which limits the OFC bandwidth.

Manuscript received October 14, 1993; revised November 17, 1993.

The authors are with the Interdisciplinary Graduate School of Science and Engineering of Tokyo Institute of Technology, 4259 Nagatuta, Midori-ku, Yokohama, Kanagawa 227 Japan.

M. Kourogi and M. Ohtsu are also with the Kanagawa Academy of Science & Technology, KSP East Building, Room 408, 3-2-1 Sakado, Takatsu-ku, Kawasaki, Kanagawa 213 Japan.

IEEE Log Number 9215884.

In this letter, we report a novel OFC generator which was realized by coating high reflection films on the facets of a LiNbO<sub>3</sub> crystal used for an electro-optic (EO) phase modulator, i.e., a monolithic OFC generator. The monolithic OFC generator was compact, and the optical round-trip loss in the monolithic OFC generator was reduced so that the span of an OFC could be extended.

## II. DESIGN OF THE MONOLITHIC OPTICAL FREQUENCY COMB GENERATOR

An OFC generator is composed of an electro-optic phase modulator installed within a Fabry-Perot cavity, and a comb is generated by large-index phase modulation from multiple passes of light through the modulator. Therefore, it is required a low round-trip loss optical cavity (i.e., high finesse optical cavity) for OFC generator to increase the power of the high order sidebands of OFC so as to extend the observable span of an OFC. The power of the  $n$ -th sideband  $P_n$  of the OFC is approximately expressed as following. [3]

$$P_n = \eta_{FP} \left( \frac{\pi}{2mF} \right)^2 \exp \left( - \frac{|n|\pi}{mF} \right) P_{in}$$

where  $\eta_{FP}$ ,  $m$ ,  $F$  and  $P_{in}$  are the efficiency of the Fabry-Perot cavity, the single pass modulation index, the finesse of the optical cavity and input laser power, respectively. If the optical loss inside the cavity is reduced, both values of  $F$  and  $\eta_{FP}$  increase, and then the value of  $P_n$  increase. As shown in Fig. 1, the monolithic OFC generator is composed of an EO crystal (for transverse modulation) with high reflection coatings on the both ends, i.e., the EO crystal becomes an monolithic optical Fabry-Perot cavity so that the OFC generator can be made to be lower optical round-trip loss than previous OFC generator which was composed of separated parts such as an anti-reflection coated EO phase modulator and high reflection coated mirrors. The EO crystal is installed in the microwave waveguide resonator to increase the microwave electric field intensity in the EO crystal for highly efficient EO modulation. Two conditions must be satisfied to realize the maximum efficient OFC generation.

- (I) The microwave phase velocity in the direction of  $z$ -axis must be equal to the optical group velocity in the EO crystal [2]–[3], [9], i.e.,

$$v_m = c/n_g, \quad (1)$$

where  $v_m$  is the microwave phase velocity in the direction of  $z$ -axis,  $c$  is the speed of light in vacuum and  $n_g$  is the group index of refraction for laser light.

- (II) The resonant frequency of the microwave resonator  $f_m$  which will be a modulation frequency must be an integral

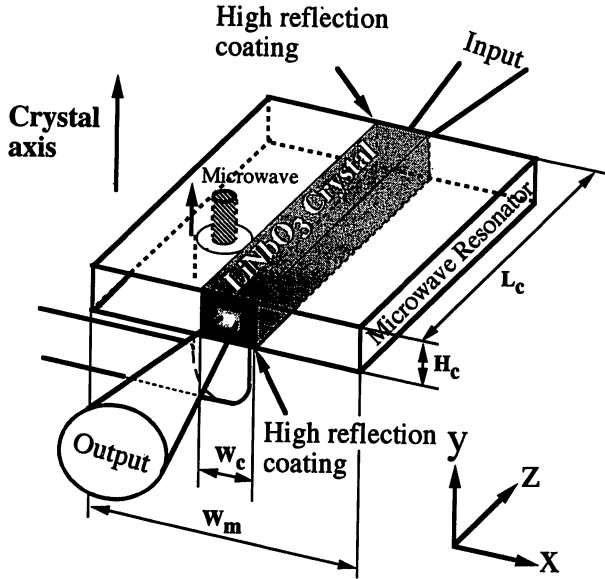


Fig. 1. Schematic illustration of monolithic OFC generator.

harmonic of the free-spectral-length FSR ( $\equiv c/2L_c n_g$ ) of the Fabry-Perot cavity [2]–[4], i. e.,

$$f_m = N \times \text{FSR} \equiv \frac{Nc}{2L_c n_g} \quad (2)$$

where  $N$  is an integer.

In order to satisfy the first condition, the values of the crystal width  $W_c$  and waveguide width  $W_m$  are determined in the following way. From the boundary condition of the microwave electric field between the inside and the outside of the crystal, the following equations are derived by assuming that the TE<sub>10</sub> mode of the microwave waveguide propagates.

$$\frac{k'_x}{k_x} = \tan\left(k_x \frac{W_c}{2}\right) \tanh\left(k'_x \frac{W_m - W_c}{2}\right) \quad (3)$$

$$\frac{(k_x, 0, k_z) \cdot (k_x, 0, k_z)}{\epsilon} = (jk'_x, 0, k_z) \cdot (jk'_x, 0, k_z) = k_o^2 \quad (4)$$

where  $(jk'_x, 0, k_z)$  and  $(k_x, 0, k_z)$  are the wave vectors of the microwave outside and inside the crystal respectively.  $\epsilon$  is the relative dielectric constant of the crystal axis around the frequency of the microwave.

$$k_o \equiv \frac{2\pi N \times \text{FSR}}{c} \quad (5)$$

is the wave number of the microwave in vacuum when the microwave frequency is assumed to be  $N \times \text{FSR}$ . From eqs. (3) and (4), the value of  $k_z$  can be derived to express the value of the microwave phase velocity as follows.

$$v_m = \frac{k_o}{k_z} c \quad (6)$$

Fig. 2 shows the calculated result of the equivalent index of refraction for the microwave (i.e.,  $k_z/k_o$ ), which depends on  $W_m/W_c$  and  $k_o W_c$ . For this calculation the crystal was assumed to be LiNbO<sub>3</sub>, i.e.,  $\epsilon = 28$ . By using this figure, the values of the crystal width  $W_c$  and waveguide width  $W_m$  can

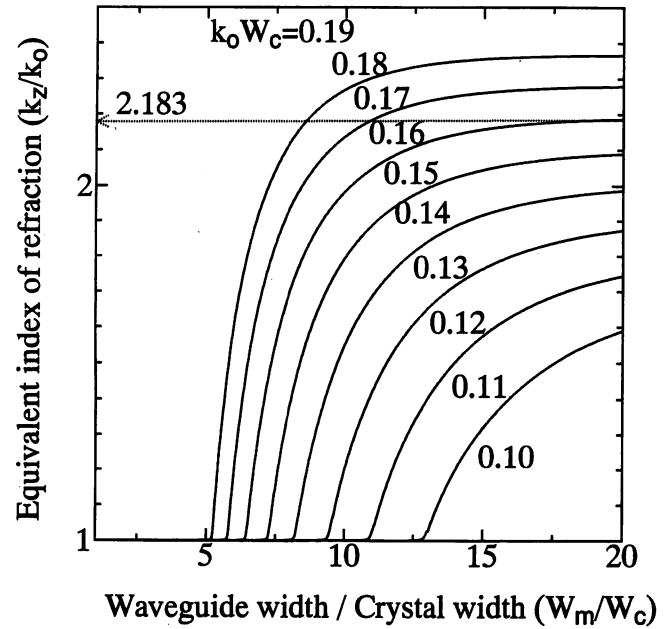


Fig. 2. Equivalent index of refraction of microwave (i.e.,  $k_z/k_o$ ) which is shown as a function of  $W_m/W_c$  and  $k_o W_c$ . The crystal was assumed to be LiNbO<sub>3</sub>. The value of 2.183 corresponding to the group index of refraction for extraordinary ray at 1.54  $\mu\text{m}$ .

be determined to match the microwave phase velocity  $v_m$  to the optical group velocity  $c/n_g$  through matching the value of the microwave equivalent index of the refraction to the value of the crystal group index of refraction.

In order to satisfy the second condition, the waveguide length and the structure of the both ends of the waveguide must be designed to satisfy the following equation for the resonant condition.

$$k_z = \pi N / L_c,$$

where the equation is derived by substituting eqs. (1), (2) and (5) to (6). This condition can be easily realized when the waveguide length is equal to the crystal length  $L_c$  and when the structure of the both ends of the waveguide are short-circuit or open-circuit. However, the ends of the waveguide must be open-circuit for phase matching between two counter-propagating running microwaves which are components of standing microwave in the crystal. Since each wave of two counter-propagating running microwaves effects the modulation of the laser beam which propagates in the same direction, if the phase matching between two counter-propagating running microwaves are not perfect, the modulation efficiency of the round-trip light inside the crystal is decreased. If the ends of the waveguide are short-circuit, the modulation induced by one of the two counter-propagating running microwaves is canceled by the modulation induced by another, because the phase difference between two counter-propagating running microwaves is  $\pi$ .

Fig. 3 shows the calculated  $y$ -component of the microwave electric field  $E_y$  inside the monolithic OFC generator which was obtained by using the experimental parameters. For this calculation, the running waves of the microwave leaked from the end of the crystal was ignored, because the dielectric

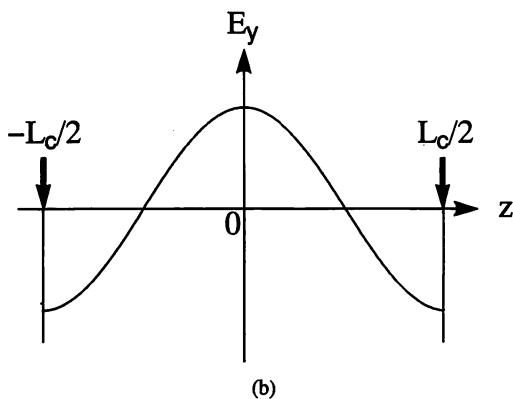
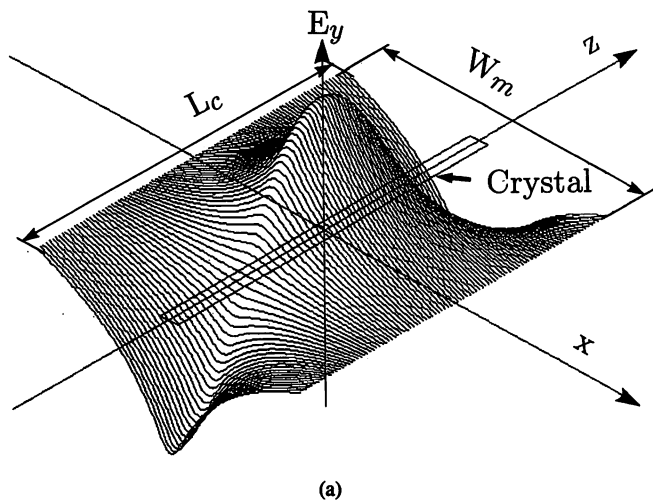


Fig. 3. Calculated amplitude of microwave electric field on  $y$  axis in the monolithic OFC generator, where  $L_c = 23.4$  mm,  $W_c = 1.25$  mm,  $W_m = 20$  mm, and  $N = 2$ . The crystal was assumed to be  $\text{LiNbO}_3$ . (a) Two dimensional distribution of  $E_y$  in  $x$ - $z$  plane. (b) The distribution of  $E_y$  on  $z$ -axis.

constant of the crystal is high. As shown in this figure, it is easy to see that, in the case of that the ends of the waveguide is opened, the antinodes appear at the ends of the crystal. In this case, the phase matching between two counter-propagating running wave of the microwave are perfect, and then the modulation efficiency of the round-trip light inside the crystal is maximum.

### III. EXPERIMENT

A  $\text{LiNbO}_3$  crystal was used for the experiment. The crystal group index of refraction  $n_g$  for extraordinary ray at  $1.54$   $\mu\text{m}$  is 2.183. The experimental parameters are fixed to be  $L_c = 23.4$  mm (FSR = 2.937 GHz, at  $1.54$   $\mu\text{m}$ ),  $W_c = 1.25$  mm,  $H_c = 1.0$  mm,  $W_m = 20.0$  mm,  $N = 2$  (i. e.,  $f_m = 5.874$  GHz). The crystal width was determined to satisfy  $k_o W_c = 0.16$  for obtaining the minimum value of  $W_c$ .  $W_c$  and  $H_c$  should be as small as possible in order to concentrate the microwave power to the optical axis in the crystal. However, they should be sufficiently large to reduce the diffraction loss. The present value of the  $W_c$  was determined to satisfy

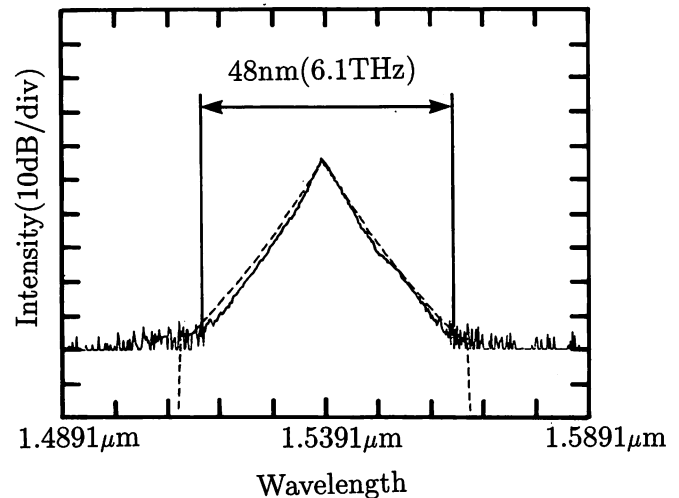


Fig. 4. Spectrum of the OFC envelope observed by an optical spectrum analyzer, with the resolution of 0.2 nm. The solid curve is experimental result. The broken line is theoretical result.

these two conditions. For introducing the microwave to the waveguide resonator which was made of brass, the coaxial cable connector ( $50 \Omega$ ) was fixed at the point of the central antinode in the waveguide resonator. The best impedance matching of the microwave to the waveguide resonator was obtained when the distance between the center of the crystal and that of the coaxial cable was 3 mm. The measured single pass modulation index was  $0.22\pi$  radian when the microwave power was  $\sim 10$  W. For obtaining a high finesse of the optical resonance, two ends of the crystal were polished to be flat and curved with the radius of curvature of 50 mm, respectively. The reflectivity of the coated mirror (dielectric multi-layers coating) on both ends was 99.0% at  $1.55$   $\mu\text{m}$  wavelength. The values of  $\eta_{\text{FP}}$  and  $F$  were  $\sim 60\%$  and 250, respectively. The value of  $F$  implies a round-trip optical loss of 2.5%. This value includes mirror losses of 2% (output coupling loss) and a residual loss of 0.5%. This residual loss is attributed to the bulk crystal loss.

A  $1.5391$   $\mu\text{m}$  DFB laser with the spectral linewidth of 1 MHz was modulated by using this OFC generator and the generated OFC spectrum was observed by an optical spectrum analyzer. The temperature of the OFC generator was stabilized for maintaining the optical resonator to be resonant to the laser frequency. The input power of the laser to the OFC generator was 7 mW. Fig. 4 shows the generated OFC spectrum. Although each sideband component of the OFC was not observed separately because the resolution bandwidth was larger than  $f_m$ , the envelope of the OFC was observed. It is confirmed from this figure that the envelope of the OFC extended to a span as wide as 48 nm (or 6.1 THz). This value is 1.5 times the value reported in [2], [3]. To our knowledge, this value is the widest span of an OFC generated by EO modulation. The number of the sidebands in this envelope is estimated to be larger than 1000. The calculated results of the envelope of the OFC spectrum from eq. (1) in [3], which expresses  $P_n$  without approximation, are shown by broken line in Fig. 4, it is found that they are in good agreement with each other. Because the measurement of the optical beat signal

(heterodyne detection) is more sensitive than the measurement by using an optical spectrum analyzer, it is possible to detect and use higher order sidebands which have not been observed with the optical spectrum analyzer. If lasers whose linewidth is less than 10 kHz are used for optical frequency difference measurement using the present OFC generator, the maximum measurable frequency difference, which was defined as the sideband frequency with the signal-to-noise ratio of 0 dB, can be estimated to be 6.1 THz from the eq. (5) shown in [3]. This value is happened to be equal to the span of the observed envelope of the OFC. Furthermore, if dielectric multi-layer coating with higher reflectivity is employed, the value of the maximum measurable frequency difference of the present monolithic optical frequency comb generator will be further increased.

#### IV. SUMMARY

A monolithic optical frequency comb (OFC) generator was realized by coating high reflection films on the facets of a LiNbO<sub>3</sub> crystal used for an electro-optic (EO) phase modulator. The optical round-trip loss in the monolithic OFC generator was reduced so that the span of an OFC envelope can be increased. It is confirmed that the envelope of the OFC extended to a span as wide as 48 nm (or 6.1 THz) around 1.5  $\mu\text{m}$ . The maximum measurable frequency difference, which

was defined as the sideband frequency with the signal-to-noise ratio of 0 dB, was estimated to be also 6.1 THz.

#### REFERENCES

- [1] M. Kourogi, N. Nakagawa, C. H. Shin, M. Teshima and M. Ohtsu, "Accurate frequency measurement system for 1.5- $\mu\text{m}$  wavelength laser diodes," in *Proc. Conf. on Lasers and Electro-Opt.*, Baltimore, paper number CThR57, May 1991.
- [2] M. Kourogi and M. Ohtsu, "A highly accurate frequency counting system for 1.5  $\mu\text{m}$  wavelength semiconductor lasers," in *Proc. SPIE Frequency-Stabilized Lasers and Their Applications*, Boston, vol. 1837, pp. 205-215, November 1992.
- [3] M. Kourogi, K. Nakagawa and M. Ohtsu, "Wide-span optical frequency comb generator for accurate optical frequency difference measurement," *IEEE J. Quantum Electron.*, vol. 29, pp. 2693-2701, October 1993.
- [4] T. Kobayashi, T. Sueta, Y. Cho and Y. Matsuo, "High-repetition-rate optical pulse generator using a fabry-perot electro-optic modulator," *Appl. Phys. Lett.*, vol. 21, pp. 341-343, 1972.
- [5] M. Kourogi, K. Nakagawa and M. Ohtsu, "A wide-span optical frequency comb generator for a highly accurate laser frequency measurement," in *Proc. International Quantum Electronics Conf.*, Vienna, papernumber TuM5, June 1992.
- [6] N. C. Wong, D. Lee and L. R. Brothers, "Optical frequency counting based on parametric oscillation," in *Technical Digest of the International Symposium on Atomic Frequency Standards and Coherent Quantum Electronics*, Nara, pp. 14-17, August 1993.
- [7] P. I. Richter and T. W. Hänsch, "Diode lasers in external cavities with frequency-shifted feedback," *Opt. Commun.*, vol. 85, pp. 414-418, 1991.
- [8] Ho. Keang-Po and J. M. Kahn, "Optical frequency comb generator using phase modulation in amplified circulating loop," *IEEE Photon. Technol. Lett.*, vol. 5, pp. 721-725, 1993.
- [9] B. Y. Lee, T. Kobayashi, A. Morimoto and T. Sueta, "Picosecond electro-optic modulator/deflector with velocity matching," in *Proc. Conf. on Lasers and Electro-Opt.*, Baltimore, paper number CTuR4, May 1991.

## Development of All-Semiconductor Laser Sources for Studies of $^{88}\text{Sr}^+$ Ions Confined in RF Trap

Mitsuru MUSA<sup>1</sup>, Andrei ZVYAGIN<sup>1,3</sup>, Ken-ichi NAKAGAWA<sup>1,2</sup> and Motoichi OHTSU<sup>1,2</sup>

<sup>1</sup>Interdisciplinary Graduate School of Science and Engineering,

Tokyo Institute of Technology, 4259 Nagatsuda, Midori-ku, Yokohama, Kanagawa 227

<sup>2</sup>Kanagawa Academy of Science and Technology, KSP East Room 408, 3-2-1 Sakado, Takatsu-ku, Kawasaki 213

<sup>3</sup>Institute of Metrology for Time and Space, VNIIFTRI Mendeleev, 141570 Moscow, Russia

(Received August 18, 1993; accepted for publication January 22, 1994)

Semiconductor-laser-based light sources have been developed for cooling and depopulating  $\text{Sr}^+$  ions confined in an rf trap. Single-mode laser oscillation at 422 nm and 21  $\mu\text{W}$  power was obtained, which corresponds to transition  $5s\ ^2S_{1/2}$ - $5p\ ^2P_{1/2}$  of  $\text{Sr}^+$ . An external-cavity-stabilized semiconductor laser with 1.8 mW power has been developed for pumping ions back from the  $4d\ ^2D_{3/2}$  metastable state to the cooling cycle. In this paper we present the reference spectrum for both lasers, which confirms the laser oscillation at appropriate transition of  $\text{Sr}^+$ .

**KEYWORDS:**  $\text{Sr}^+$  ion trap, laser cooling, grating feedback, 1.1  $\mu\text{m}$  semiconductor laser, optogalvanic signal,  $1/f$  investigation, Rb absorption,  $\text{Sr}^+$  absorption

### 1. Introduction

Recently, techniques for confining low-temperature ions in a small volume are attracting the interest of researchers in related fields, because these ions are nominally affected by collisional perturbations, and the second-order Doppler effect is small. This technique can realize a stationary isolated ion system which is free from external perturbations. These trapped ions have been applied to high-resolution spectroscopy,<sup>1)</sup> studies of single atom quantum phenomena<sup>2,3)</sup> and frequency standards which are advanced at a long interaction time.<sup>4)</sup>

Musha *et al.*<sup>5)</sup> found, by means of a Brillouin scattering experiment, that the energy partition among phonon modes in a quartz specimen is subject to  $1/f$  fluctuations. This finding suggests the impossibility of establishing thermal equilibrium within a laboratory time scale. More direct evidence supporting to Musha *et al.*'s idea can be obtained by observing collective motion of an ionic array confined in a linear rf trap. It is expected that a linear trap and a laser cooling technique are very useful for this purpose.<sup>6-8)</sup> Obtaining experimental evidence of slow energy partition among collection modes is another target of the present work.

In the present experiment  $^{88}\text{Sr}^+$  ions are used, and the energy diagram of  $^{88}\text{Sr}^+$  is shown in Fig. 1. The strong electric dipole associated with the allowed transition  $5s\ ^2S_{1/2}$ - $5p\ ^2P_{1/2}$  is used for laser cooling and detection. The transition wavelength and the natural linewidth are 422 nm and 43 MHz, respectively. However, ions in the  $5p\ ^2P_{1/2}$  state decay not only to the  $5s\ ^2S_{1/2}$  state but also to the  $4d\ ^2D_{3/2}$  metastable state with branching ratio of 13:1.<sup>9)</sup> Once the ion decays to this state, it hardly returns back to the cooling cycle: the lifetime of this metastable state is about 395 ms.<sup>10)</sup> If ions are concentrated in the metastable state, the cooling effect is quenched. Therefore, optical pumping back from the  $4d\ ^2D_{3/2}$  state to the  $5p\ ^2P_{1/2}$  state at 1092 nm is required for depopulation of the  $4d\ ^2D_{3/2}$  metastable state. To cool  $\text{Sr}^+$  ions, both 422 nm and 1092 nm

light sources are necessary. The 422 nm light can be provided by a dye laser<sup>11)</sup> or frequency doubling of 843 nm light with the aid of a high-power semiconductor laser.<sup>2)</sup> The 1092 nm light has been provided by a tunable  $\text{Nd}^{3+}$ -doped fiber laser which is pumped by a gas laser (such as an  $\text{Ar}^+$  or  $\text{Kr}^+$  laser),<sup>12)</sup> dye laser,<sup>13)</sup> or semiconductor laser ( $\lambda=826\text{ nm}$ ).<sup>2)</sup> However, the  $\text{Nd}^{3+}$ -doped fiber laser generates multiple modes with a wide spectral width. Another disadvantage is that narrowing the spectrum requires a set of intracavity elements which requires a complicated experimental setup. In the present experiment, a semiconductor laser was used for generating 1092 nm coherent light by a first report of generating 1092 nm coherent light by a semiconductor laser and applying it to a  $\text{Sr}^+$  ion trap experiment. The 422 nm light was obtained by frequency doubling of high-power output from the semiconductor laser in a  $\text{KNbO}_3$  crystal. We present in this paper the complete semiconductor laser system for cooling  $\text{Sr}^+$  ions. In §2 the detailed construction and performance of these light sources are described and the reference spectra for those light sources are mentioned in §3.

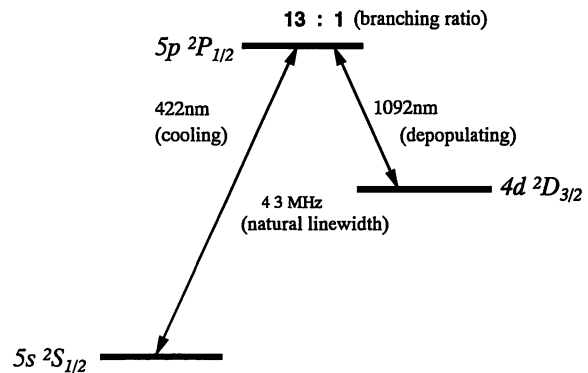


Fig. 1. Energy-level diagram of  $^{88}\text{Sr}^+$  ion showing the strongly allowed electric dipole S-P transition at 422 nm used for cooling and detection together with the P-D transition at 1092 nm used for pump back from the metastable D state. The natural linewidth of S-P transition is 43 MHz.

## 2. Experimental

### 2.1 Operation at 422 nm

Figure 2 shows a diagram of 422 nm light generation. The fundamental light at 843 nm was provided by a single-mode index-guided GaAlAs high-power semiconductor laser (Spectra Diode Lab. SDL5311) with a maximum output power of 91 mW at an injection current of 110 mA at room temperature. A glass plate 100  $\mu\text{m}$  thick mounted on a PZT disk was placed about 150  $\mu\text{m}$  from the laser facet. Optical feedback from this glass plate to the semiconductor laser allowed selection of the desired longitudinal mode by adjusting the position of the glass plate with respect to the laser. After collimation with a Corning spherical lens ( $f=2$  mm,  $NA=0.5$ ) and passage through an optical isolator whose isolation was  $-30$  dB, the 843 nm light was focused by a lens with focal length of 25 mm into a  $\text{KNbO}_3$  crystal. This  $a$ -cut  $\text{KNbO}_3$  crystal of  $3 \times 3 \times 5$  mm was contained in a vacuum chamber to avoid the creation of frost on the crystal. Both the crystal surface and the window of a vacuum chamber were antireflection-coated for 843 nm light to reduce backward reflections of the focused fundamental light onto the semiconductor laser. To realize a noncritical phase-matching condition for the second-harmonic generation, the  $\text{KNbO}_3$  crystal was cooled down to  $-17^\circ \pm 0.01^\circ\text{C}$  by means of a Peltier element. The beam crosssection at the center of this crystal was not circular but elliptical, and longer and shorter radii were 40  $\mu\text{m}$  and 20  $\mu\text{m}$ , respectively. The second-harmonic power of the focused Gaussian beam is expressed as<sup>14)</sup>

$$P_{2\omega} = \frac{8\pi d^2 l^2}{\lambda^2 n^3 c \epsilon_0 \omega_x \omega_y} P_\omega^2.$$

Here,  $c$ ,  $\epsilon_0$ ,  $P_\omega$ ,  $\omega_x$  and  $\omega_y$  indicate the speed of light, electric permittivity of free space, power of the fundamental light, the long and short radii of the beam waist, respectively. In the present case, the  $\text{KNbO}_3$  crystal has nonlinear coefficient  $d=20.5$  pm/V, refractive index  $n$  of 2.23<sup>14)</sup> and the length  $l$  of 5 mm, and the wavelength of the fundamental light  $\lambda$  is 843 nm. Therefore, when the input power of the fundamental component is 90 mW, the maximum power of the second-harmonics is calculated as  $P_{2\omega}=123$   $\mu\text{W}$ . The measured spectral linewidth of this 843 nm laser light was 2

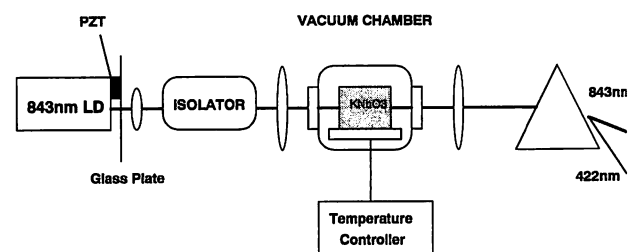


Fig. 2. Generation of 422 nm light. Frequency doubling of 843 nm semiconductor laser light in  $\text{KNbO}_3$  at  $-17^\circ\text{C}$ . The longitudinal mode of semiconductor laser is selected by moving a glass plate placed directly in front of the laser facet.

MHz.<sup>15)</sup> Therefore, the linewidth of the second-harmonic light at 422 nm was estimated to be less than the natural linewidth, 43 MHz, of the  $5s^2S_{1/2}-5p^2P_{1/2}$  transition.<sup>16)</sup> For cooling ions, the linewidth of a cooling laser should be narrower than that of the cooling transition; therefore, the linewidth of 422 nm laser light was sufficiently narrow for cooling  $\text{Sr}^+$  ions.

Power as large as 21  $\mu\text{W}$  was obtained at the 422 nm second-harmonic component generated from the fundamental input power of 89 mW. This power is smaller than the calculated value because the thermal distribution in the crystal was not uniform. The second-harmonic light (422 nm) was spatially separated from the fundamental light with a fused silica prism and introduced into a hollow cathode lamp (Hamamatsu L2783) which was followed by a photodetector. The wavelength of the fundamental light was monitored by an optical spectrum analyzer (Anritsu MS9702B) or a wave meter (Advantest TQ8325). The fundamental light spectrum was monitored with a confocal Fabry-Perot interferometer whose free spectral range and finesse were 1.5 GHz and 80, respectively. Modulation of the electric current which was injected into the semiconductor laser provided output frequency modulation over a 10 GHz frequency range without mode hopping.

### 2.2 Operation at 1.09 $\mu\text{m}$

The 1092 nm light for depopulating the  $4d^2D_{3/2}$  metastable state was generated with a polygonal channel buried heterostructure (PC-BH) InGaAsP multimode diode laser. This semiconductor laser generated optical power up to 7 mW at injection current of 300 mA, and the center wavelength observed at room temperature was 1098 nm. Figure 3 shows the experimental arrangement of the 1092 nm light source.

The resonance center wavelength of this laser at room temperature (1098 nm) was longer than the resonance wavelength corresponding to transition  $5p^2P_{1/2}-4d^2D_{3/2}$  (1092 nm). The grating feedback was applied to select the appropriate mode and to realize sin-

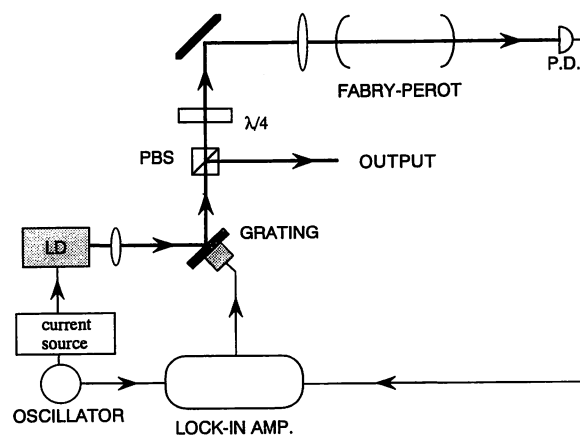


Fig. 3. Generation of 1092 nm light. The grating-feedback method was applied to the multimode laser to select the appropriate mode and to realize single-mode oscillation. By using electrical feedback with a Fabry-Perot interferometer, the frequency of the semiconductor laser was stabilized.



gle-mode oscillation. The length of the external cavity (distance between the semiconductor laser and the grating) was 20 mm, because a shorter external cavity would result in a wider continuous frequency sweeping range. This grating feedback system, whose groove distance  $d$  of this grating was  $8.3 \times 10^{-5}$  m, caused single-mode oscillation which was tunable over a range of 1090–1105 nm with a maximum power of 0.2 mW at an injection current of 180 mA. The side-mode suppression ratio was better than  $-20$  dB. Eventually, single-mode laser light was obtained with the exact wavelength of 1091.787 nm for depopulating the  $4d \ ^2D_{3/2}$  state. By tuning the injection current and the external cavity length, the laser frequency was swept over 30 MHz without mode hopping. However, the frequency was swept over a sufficiently large frequency range (1 GHz) only when the injection current was slightly above the threshold ( $I_{th}=100$  mA), in which the output power was insufficient for saturating the  $5p \ ^2P_{1/2}$ - $4d \ ^2D_{3/2}$  transition. Figure 4 shows the continuous sweeping range as a function of injection current. As can be seen in this figure, increase of the injection current resulted in decrease of the sweeping range.

The main problems of our uncoated laser at 1092 nm with grating feedback are mentioned below. The first is the narrow continuous sweeping range. It is not sufficiently wide to perform the Doppler-broadened  $Sr^+$  line profile ( $5p \ ^2P_{1/2}$ - $4d \ ^2D_{3/2}$ ) measurement, because the Doppler width was expected to be about 0.5 GHz. The second is comparatively low output power. It did not allow detection of such a reference signal as an optogalvanic signal in a  $Sr^+$  hollow cathode lamp. The third is frequency instability of the laser. It is due to the grating external cavity mode hoppings. The frequency difference between these modes is 2.5 GHz. Therefore we applied the antireflection coating to the laser to solve these problems. After the antireflection coating was applied the laser did not oscillate at all without grating feedback. Only the grating external cavity causes the laser to oscillate in the external cavity mode. The anti-

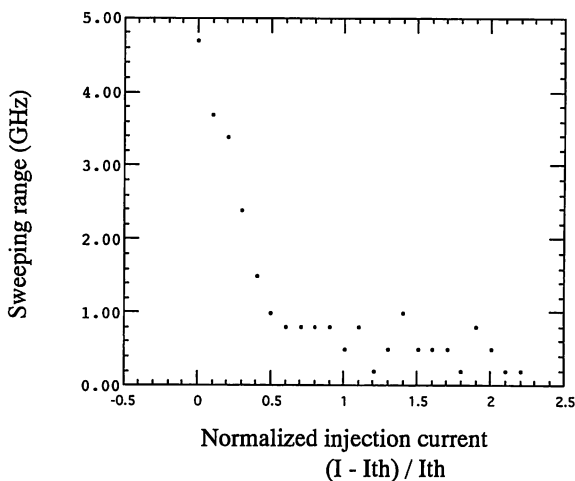


Fig. 4. Continuous sweeping range of uncoated laser with grating feedback as a function of injection current. As the injection current increases, the sweeping range decreases.

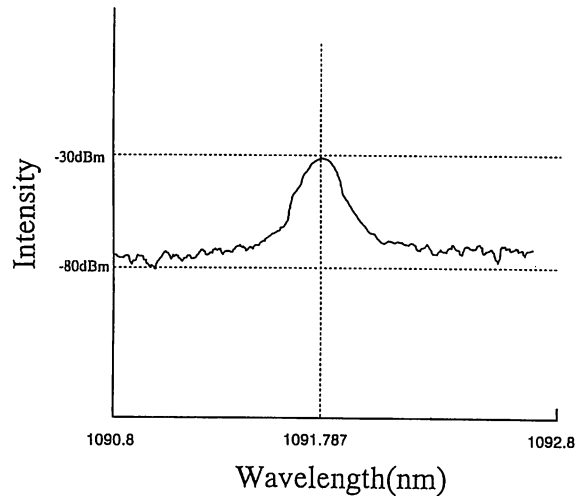


Fig. 5. Spectral line profile of 1092 nm antireflection-coated laser with grating feedback. The injection current is 150 mA.

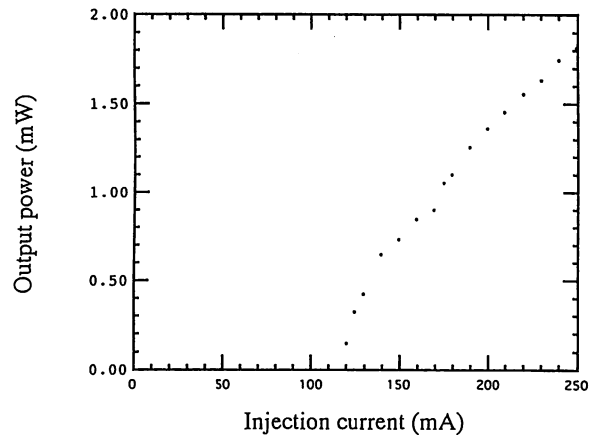


Fig. 6. Observed output power of 1092 nm antireflection-coated semiconductor laser with grating feedback as a function of injection current.

reflection-coated laser was applied to the grating feedback system, and single-mode oscillation was achieved. Figure 5 shows the spectral line shape of this laser at an injection current of 150 mA. The side-mode suppression ratio is better than  $-30$  dB. Figure 6 shows the observed output power of the antireflection-coated laser with grating external cavity as a function of the injection current. It is shown that the laser light with both comparatively high power and wide sweeping range was obtained.

At the maximum injection current of 250 mA, the antireflection coating enable single-mode oscillation with output power of 1.8 mW; with an uncoated laser, single-mode oscillation was hardly realized at a high injection current. It easily generated multi-mode oscillation as the injection current was increased.

### 3. Results and Discussion

The cooling transition should be saturated for effec-

tive cooling of ions. Saturation intensity is calculated from the following equations:

$$I_{31} = \frac{2hc}{\lambda_1^3}, \quad I_{32} = \frac{24hc}{5\lambda_2^3}.$$

Subscripts 1, 2, and 3 of  $I$  refer to states  $5s\ ^2S_{1/2}$ ,  $4d\ ^2D_{3/2}$ , and  $5p\ ^2P_{1/2}$ , respectively. The saturation power of the  $5s\ ^2S_{1/2}$ - $5p\ ^2P_{1/2}$  transition (422 nm) is estimated to be  $14\ \mu\text{W}$  under reasonable assumptions as regards temperature of the buffer gas, which cools ion clouds, at 2000 K and the beam waist diameter of about  $100\ \mu\text{m}$  at the center of the ion cloud. The required power of 1092 nm light is estimated to be about  $20\ \mu\text{W}$ . The linewidth of a cooling laser must be narrower than the natural linewidth of this transition (43 MHz), and the continuous sweeping range must be over 1 GHz for cooling ions from more than 500 K. As mentioned above, the 422 nm light had a linewidth of less than 43 MHz with an output power of  $21\ \mu\text{W}$  and a sweeping range of over 10 GHz. This is sufficient for a cooling light source. The output power of 1092 nm light was 1.8 mW and the tuning range of the light was set at 20 nm by changing the angle of the grating. The linewidth of this light was less than 34 MHz which was measured with a Fabry-Perot interferometer. The external cavity length (changing the distance between semiconductor laser and grating) continuously controlled the frequency over 1 GHz without mode hopping. Therefore, this light source has a sufficiently large spectral brightness to saturate the  $\text{Sr}^+\ 4d\ ^2D_{3/2}$ - $5p\ ^2P_{1/2}$  transition, and is used for depopulation of the D metastable state.

As can be seen in Fig. 3, the electric feedback was applied with a Fabry-Perot interferometer (FSR=2.7 GHz, *finesse*=80). With this configuration, the frequency was stabilized within 2 MHz for over 1 hour.

To verify that this 1092 nm laser can be used for exciting  $\text{Sr}^+$  ions on the  $5p\ ^2P_{1/2}$ - $4d\ ^2D_{3/2}$  transition, the optogalvanic signal was detected. The light coming from the 1092 nm component modulated at 500 Hz by means of a mechanical chopper was introduced into a Sr hollow-cathode lamp. This laser light changed the distribution of the energy levels of the  $\text{Sr}^+$  ion and resulted in a change of the electric conductivity of the discharge plasma. This effect changed the discharge current, and this optogalvanic signal was detected by means of phase-sensitive detection. The discharge voltage and injection current to this hollow cathode lamp were 1.5 kV and 18 mA, respectively. The power of 1092 nm laser light was 1.8 mW, and the wavelength of this light was swept continuously over 1.2 GHz around the resonance wavelength of the  $5p\ ^2P_{1/2}$ - $4d\ ^2D_{3/2}$  transition at 1091.787 nm by modulating the position of the grating. The results of this experiment are shown in Fig. 7. The upper and lower traces indicate an electric current of the charged cell without and with laser light, respectively. The optogalvanic signal is shown as the lower trace and the full width at half maxima (FWHM) of this line profile is about 460 MHz. It is comparable to the Doppler linewidth of 300 MHz at the Sr effective temperature of 103 K. The resonance frequency of iso-

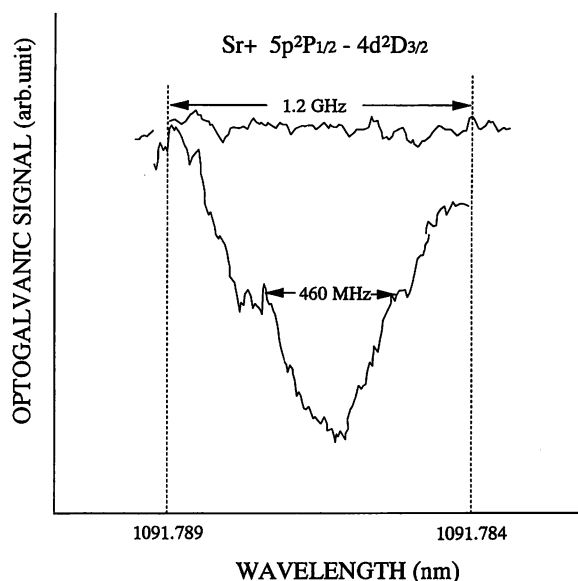


Fig. 7. Observed optogalvanic signal of  $\text{Sr}^+$  on P-D transition at 1092 nm. The power of the laser introduced into the hollow cathode tube is 1.8 mW and the injection current to the hollow cathode tube is 18 mA. Scanning speed is 10 s and the time constant of phase-sensitive detection is 1 s.

tope  $^{87}\text{Sr}^+$  corresponding to  $^2S_{1/2}$ - $5p\ ^2P_{1/2}$  ( $F=5$ ) is 1 GHz below that of  $^{88}\text{Sr}^+$ . However the isotope  $^{87}\text{Sr}$  exists 1/10 of  $^{88}\text{Sr}$ , and  $^{87}\text{Sr}$  ion gives little influence on the Doppler linewidth of  $^{88}\text{Sr}$ .<sup>17)</sup>

It is necessary to monitor the reference signal corresponding to the  $\text{Sr}^+\ 5s\ ^2S_{1/2}$ - $5p\ ^2P_{1/2}$  transition. A linear absorption spectrum was observed by detection with a photodetector, the frequency scanned second-harmonic output after passing through the Sr hollow cathode lamp. The upper trace in Figure 8 shows that 6% of the violet light was absorbed in the hollow cathode lamp at 20 mA discharge current. The linewidth of the Doppler profile is less than 1.2 GHz. In addition, we detected the linear absorption spectrum of the  $^{85}\text{Rb}\ 5S_{1/2}$  ( $F=2, 3$ )- $6P_{1/2}$  transition by introducing this light into a heated  $^{85}\text{Rb}$  cell, which is shown in the lower trace of Fig. 8. The length and temperature of the Rb cell are 20 mm and  $90^\circ\text{C}$ , respectively. In this figure both traces overlapped as shown by using the frequency marker from the Fabry-Perot interferometer. The first dip from the left corresponds to the absorption of isotope  $^{87}\text{Rb}$  which was contained in this cell as a residual. The second and the third dips from the left correspond to the transitions  $5S_{1/2}$  ( $F=2$ )- $6P_{1/2}$  and  $5S_{1/2}$  ( $F=3$ )- $6P_{1/2}$  of  $^{85}\text{Rb}$ , respectively. As can be seen in Fig. 8, the absorption of the transition  $5S_{1/2}$  ( $F=2$ )- $6P_{1/2}$  of  $^{85}\text{Rb}$  is about 40%, and the frequency of it coincides with that of  $^{88}\text{Sr}^+$  corresponding to the transition  $5s\ ^2S_{1/2}$ - $5p\ ^2P_{1/2}$  within 1 GHz. It is found that the heated  $^{85}\text{Rb}$  cell is more useful for obtaining the transition reference than the Sr hollow cathode lamp. This is because the light from the Sr hollow cathode lamp reflected back into the ion trap and illuminated the trap volume. Therefore, that scattered light caused an increase of background noise at

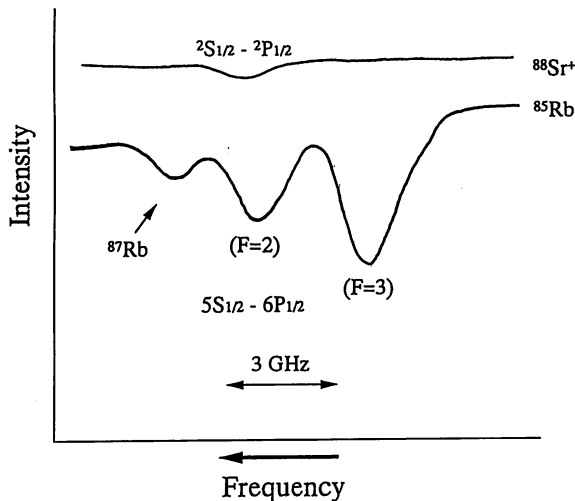


Fig. 8. The upper trace shows the absorption spectrum of  $5s\ ^2S_{1/2}-5p\ ^2P_{1/2}$  of  $^{88}\text{Sr}^+$ . The lower trace shows the absorption spectrum of Rb: the left dip in the lower trace is the absorption of  $^{87}\text{Rb}$ , and center and right dips show the absorptions corresponding to  $F=3$  and  $F=2$  of the  $^{85}\text{Rb}\ 5S_{1/2}-6P_{1/2}$  transition, respectively. Input laser power is  $21\ \mu\text{W}$ . Scanning time is 10 s.

the detection system which was designed to detect fluorescence from  $\text{Sr}^+$  ions confined in the trap, and on the other hand, the  $^{85}\text{Rb}$  cell exerted no influence on it.

#### 4. Conclusions

We have obtained all-semiconductor laser based light sources for cooling  $\text{Sr}^+$  ions upon the S-P transition at 422 nm as well as for optical depopulating upon the P-D transition at 1092 nm. The power and linewidth of 422 nm light were  $21\ \mu\text{W}$  and less than 43 MHz, respectively. The 1092 nm light source showed a maximum power of 1.8 mW, linewidth of 34 MHz, tunable range of over 1090–1105 nm and continuous sweeping range of over 1 GHz. The wavelength of 1092 nm light was stabilized within 2 MHz for over 1 h by electric feedback with a Fabry-Perot interferometer. The laser excitation at the P-D transition

was observed by means of the opto-galvanic signal with a Sr hollow cathode lamp. The absorption signal in the  $\text{Sr}^+$  S-P transition was detected and the absorption of  $^{85}\text{Rb}$  was observed within 1 GHz of this transition. The trapping, cooling, and detection of the fluorescence of  $\text{Sr}^+$  ions in a Paul trap is now under way.

#### Acknowledgments

The authors are grateful to Dr. Y. Saburi, Dr. H. Nagai and Anritsu Company for providing us with 1.1  $\mu\text{m}$  semiconductor laser chips. We also thank Dr. M. Labachellerie for fruitful discussions and suggestions. This research was partly supported by a NEDO grant.

- 1) J. C. Bergquist, W. M. Itano and D. J. Wineland: *Phys. Rev. A* **36** (1987) 428.
- 2) G. P. Barwood, C. S. Edwards, P. Gill, H. A. Klein and W. R. C. Rowley: *Opt. Lett.* **18** (1993) 732.
- 3) W. Nagourney, J. Sandberg and H. Dehmelt: *Phys. Rev. Lett.* **56** (1986) 2797.
- 4) H. G. Dehmelt: *IEEE Trans. Instrum. & Meas.* **IM-31** (1982) 83.
- 5) T. Musha, B. Gabor and M. Shoji: *Phys. Rev. Lett.* **64** (1990) 2394.
- 6) M. G. Reizen, J. M. Gilligan, J. C. Bergquist, W. M. Itano and D. J. Wineland: *J. Mod. Opt.* **39** (1992) 223.
- 7) R. K. Melbourne, J. D. Prestage and L. Maleki: *J. Appl. Phys.* **69** (1991) 276.
- 8) M. Tachikawa, M. Kajita and T. Shimizu: *IEEE Trans. Instrum. & Meas.* **42** (1993) 281.
- 9) A. Gallagher: *Phys. Rev.* **157** (1967) 24.
- 10) Ch. Gerz, Th. Hilberath and G. Werth: *Z. Phys. D* **5** (1987) 97.
- 11) A. A. Madej and J. D. Sankey: *Opt. Lett.* **15** (1990) 634.
- 12) A. A. Madej, W. E. Berger and G. R. Hanes: *Opt. Commun.* **73** (1989) 147.
- 13) I. P. Alcock, A. I. Ferguson, D. C. Hanna and A. C. Tropper: *Opt. Lett.* **11** (1986) 956.
- 14) J. C. Baumert, J. Hoffnagle and P. Günter: *Proc. SPIE* **492** (1984).
- 15) W. Wang, K. Nakagawa, S. Sayama and M. Ohtsu: *Opt. Lett.* **17** (1991) 1593.
- 16) H. R. Tell, D. Meschede and T. Hansche: *Opt. Lett.* **15** (1990) 532.
- 17) M. Wada, H. Sunaoshi, Y. Fukushima and S. Hayashibe: *Nucl. Instrum. & Methods B* **70** (1992) 500.

## Computer-Controlled Narrow-Linewidth and Frequency-Stabilized AlGaAs Laser System with Unmodulated Output

Jun KAWAKAMI, Motonobu KOUROGI<sup>1,2</sup> and Motoichi OHTSU<sup>1,2</sup>

Main Research Laboratory, Nikon Corporation, 1-6-3 Nishi-ohi, Shinagawa, Tokyo 140

<sup>1</sup>Interdisciplinary Graduate School of Science and Technology, Tokyo Institute of Technology, 4259 Nagatsuta, Midori-ku, Yokohama 227

<sup>2</sup>Kanagawa Academy of Science and Technology, KSP East, Rm 408, 3-2-1 Sakado, Takatsu-ku, Kawasaki 213

(Received August 18, 1993; accepted for publication October 16, 1993)

A narrow-linewidth semiconductor laser system at 780 nm wavelength was developed, with frequency locked to the saturation absorption resonance frequency of rubidium (<sup>87</sup>Rb). Optical feedback from an external Fabry-Perot cavity was employed to reduce the linewidth of the laser. The third derivative of the saturated absorption spectrum in <sup>87</sup>Rb was used as a frequency demodulator for frequency locking, for which the Zeeman modulation was employed to keep the output power and frequency unmodulated. The minimum of the square root of the Allan variance was  $2.1 \times 10^{-12}$  at the integration time of 300 s. The full linewidth at half maximum of the field spectrum was measured to be narrower than 170 kHz. A computer-control program was developed for automatic frequency locking to the <sup>87</sup>Rb line.

KEYWORDS: semiconductor laser, frequency stabilization, optical feedback, saturated absorption, linewidth

### 1. Introduction

Semiconductor lasers have been used for a variety of commercial optical systems because of their small size, low power consumption, high output power, wideband direct frequency modulation capabilities, and other advantageous properties. If their frequency fluctuations (FM noise) can be reduced to a sufficiently low level, further applications are expected, *e.g.*, analytical spectroscopy, coherent optical transmission, optical sensing, and optical pumping of microwave atomic clocks. Although research and development have been intensively carried out for this purpose,<sup>1,2</sup> their present status is still at the laboratory level, and it is not always easy to find an easily operated practical system with accurate optical carrier frequency and low FM noise.

This paper reports the development of a low-FM-noise practical light source by controlling a semiconductor laser. In order to realize an easily operated coherent light source, we have carried out computer-controlled automatic frequency locking to an absolute frequency reference and reduction of field spectral linewidth without amplitude and frequency modulations.

AlGaAs lasers at 780 nm wavelength were used for the present system because the resonance spectral line of the rubidium (Rb) atomic vapor can be used as an absolute frequency reference,<sup>3</sup> and they have been commercially available due to mass production for pick-ups of optical disk systems.

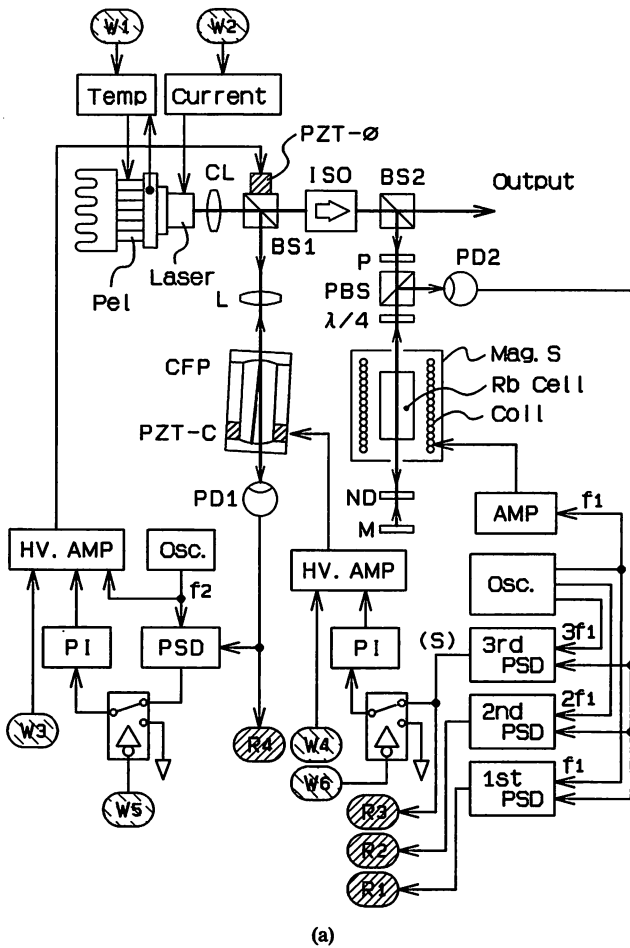
### 2. Principle and Setup of the System

For reproducible frequency locking, the saturated spectral frequency of the Rb-D<sub>2</sub> line was used as a frequency reference. For reducing the field spectral linewidth, resonant optical feedback from an external Fabry-Perot cavity was used.<sup>4</sup> This feedback system can also be used conveniently to sweep the laser frequency because the frequency locked to the cavity resonance frequency can be swept by sweeping the cavity length. In order to realize the unmodulated fre-

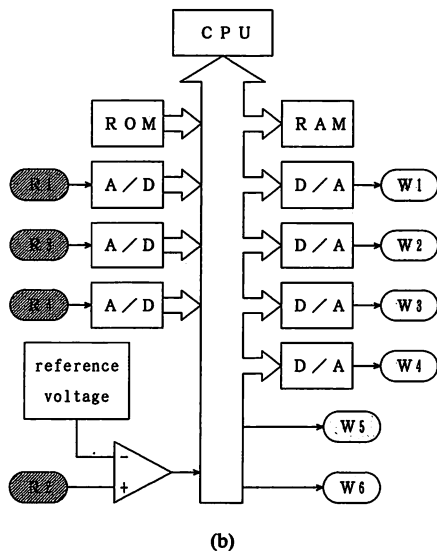
quency locking to Rb, the resonance frequency of Rb was Zeeman-modulated by modulating the applied magnetic field for the phase-sensitive detection. For computer-controlled automatic frequency locking, injection current and temperature of the semiconductor laser were controlled by a central processing unit (CPU) via D/A converters.

The setup of the system is shown in Fig. 1(a). Fluctuations of heat sink temperature and injection current of the free-running laser (Hitachi, HL7838G; 20 mW output power) were maintained within 0.01 K and 0.01 mA, respectively. A 25-mm-long confocal Fabry-Perot cavity with 3 GHz free spectral range was used for optical feedback. Its finesse was about 20. The light transmitted through the cavity was monitored by photodetector #1. The output beam of the optically fed-back laser was incident into the Rb cell after being converted from linear to circular polarization by a quarter-wave plate. An optical isolator of 60 dB isolation was used to avoid undesired parasitic optical feedback. The incident pump beam power density was  $50 \mu\text{W}/\text{mm}^2$ , and its 1% reflected beam was monitored by photodetector #2. The Rb cell was a cylindrical glass container of 10 mm diameter and 20 mm length filled with a natural Rb vapor without any buffer gases. It was used at room temperature. The solenoid for Zeeman modulation generated the axial dc magnetic field of  $4.7 \times 10^{-3}$  T/A, while the ac magnetic field was  $4.3 \times 10^{-3}$  T/A at 2.5 kHz. Variation of the axial magnetic field strength was maintained to be within 1% over the total length of the Rb cell. Magnetic field shielding was supplied around the solenoid.

A piezoelectric transducer (PZT-C) was used to control the length of the external cavity so that the optically fed-back laser frequency was swept and locked to the center frequency of the saturated absorption line in Rb. The Rb resonance frequency was Zeeman-modulated by applying an ac current at a frequency of 2.5 kHz to the solenoid. The third derivative of the saturated absorption spectral profile was detected by a phase-sensi-



(a)



(b)

Fig. 1. (a) Experimental setup. Pel: Peltier electric cooler. ISO: Optical isolator. CFP: Confocal Fabry-Perot cavity. Coil: Solenoid for Zeeman modulation. Mag. S: Magnetic shield. PSD: Phase-sensitive detector. (S): The error signal used to evaluate the magnitude of residual frequency fluctuations of the laser as a preliminary experiment. (b) Signal flows from/to analog part of the experimental setup via a digital signal processing. Inputs  $R_1$ - $R_4$  and outputs  $W_1$ - $W_6$  of this digital system correspond to the outputs  $R_1$ - $R_4$  and inputs  $W_1$ - $W_6$  of the analog part of (a), respectively.

tive detector, and its output signal was fed back to the PZT-C via a PI controller.

The light transmitted through the external cavity was maintained at its maximum value by controlling another piezoelectric transducer (PZT- $\phi$ ) attached to the beam splitter (BS1) to control the phase of the light reflected from the external cavity so as to stabilize the optical feedback. An ac voltage at a frequency of 2.1 kHz was applied to the PZT- $\phi$  for modulating the optical path length, and the first derivative of the spectral profile of the light transmitted through the external cavity was obtained by the phase-sensitive detector. The output signal was fed back to the PZT- $\phi$  via a PI controller.

Electric signals  $R_1$ - $R_4$  were connected to the digital signal processing system of Fig. 1(b) for automatic frequency locking. After processing, the output signals  $W_1$ - $W_6$  from the system of Fig. 1(b) were fed back to the analog part of the experimental setup shown in Fig. 1(a). The details of digital signal processing are presented in §4.

### 3. Experimental Results

Figure 2 shows an energy level diagram of the  $^{87}\text{Rb}$  atoms. The  $j$  and  $i$ - $j$  components of the  $D_2$  line were used as frequency references because their spectral strengths are large, where  $i$ - $j$  represents a cross-over resonance line between the  $i$  component (the transitions  $5S_{1/2}, F=2$ - $5P_{3/2}, F=2$ ) and the  $j$  component (the transition  $5S_{1/2}, F=2$ - $5P_{3/2}, F=3$ ). Calculated Zeeman coefficients of the frequency shifts of the  $j$  and  $i$ - $j$  components were 14.0 GHz/T and 12.8 GHz/T, respectively.

Curve A of Fig. 3 represents the third derivative profile of the  $i$ - $j$  component, where the modulation frequency and the maximum frequency modulation depth

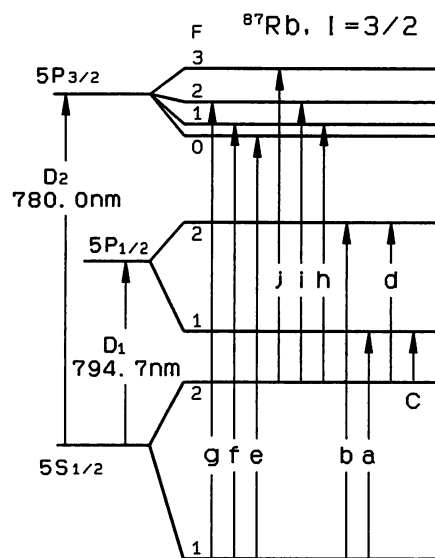


Fig. 2. Energy level diagram of the  $^{87}\text{Rb}$  atoms relevant to the  $D_1$  and  $D_2$  lines. The notations a-j identify the transitions between the hyperfine components of the ground and excited levels.

were 2.5 kHz and 30 MHz, respectively. The peak-to-peak linewidth of this derivative shape was 11 MHz. Curve B is the spectral profile of the light transmitted through the external Fabry-Perot cavity. The flat and broad profile indicates that stable optical feedback was realized and the locking range of the optical feedback was larger than the free spectral range of the external cavity. After the frequency of this optically fed-back laser was locked to the center frequency of curve A in Fig. 3, the Allan variance of the residual frequency fluctuations was evaluated by using two independent laser systems. As a preliminary experiment, the frequency fluctuations were evaluated by using the error signals (i.e., the signal (S) from the phase-sensitive detector of Fig. 1) from the feedback loops of two independent lasers. The results are shown in Fig. 4. The number of

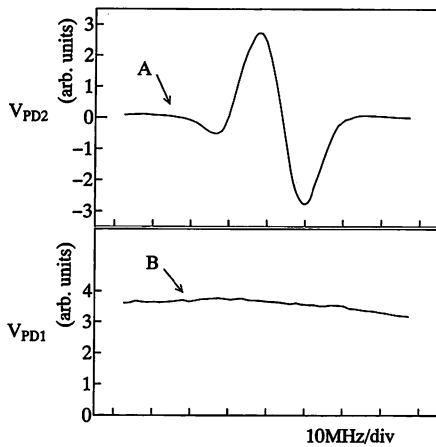


Fig. 3. Curve A: The third derivative profile of the i-j component of the D<sub>2</sub> line in <sup>87</sup>Rb. The vertical axis represents the output signal from photodetector #2 of Fig. 1(a). Curve B: The spectral profile of the light transmitted through the external Fabry-Perot cavity when the laser is optically fed back. The vertical axis represents the output signal from photo-detector #1.

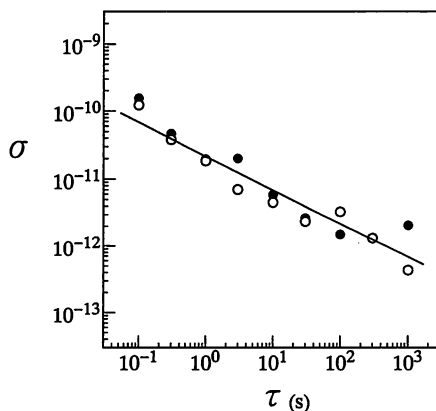


Fig. 4. Square root of the Allan variance  $\sigma$  of the residual frequency fluctuations, which were estimated by using the error signal at port (S) of Fig. 1(a). The open and closed circles represent the results for the independently stabilized lasers #1 and #2, respectively. The number of samplings at each integration time  $\tau$  was 20.

samplings at each integration time  $\tau$  was 20. The two curves in this figure take almost the same values, from which it can be confirmed that the two laser systems have almost equal feedback gains and short-term frequency stabilities. The frequency stabilities of the two lasers estimated from this figure were  $2 \times 10^{-11}$  at  $\tau = 1$  s. For more accurate evaluation, the beat frequency fluctuations between these two lasers were measured by a time interval counter (HP5345A). The frequencies of lasers #1 and #2 were locked to the j and i-j components, respectively, by which the beat frequency was fixed to 135 MHz. The number of samplings at each  $\tau$  was fixed also to 20. The results are shown in Fig. 5, where the square root of the Allan variance at  $\tau = 1$  s is  $1.9 \times 10^{-11}$  and its minimum is  $2.1 \times 10^{-12}$  at  $\tau = 300$  s. The feedback loops were operated in a stable manner for at least four days, or as long as they remained closed.

Linewidth of the laser field spectrum was measured to determine the effect of optical feedback. Figure 6 is the beat spectral profile between the two stabilized lasers measured by a microwave spectrum analyzer (HP8590A). The center frequency of the beat spectrum was 135 MHz, and the full linewidth at half maxi-

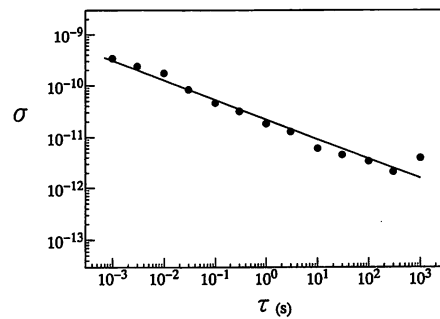


Fig. 5. Square root of the Allan variance of the beat frequency fluctuations between the independently stabilized lasers #1 and #2. The number of samplings at each integration time  $\tau$  was 20. The frequencies of the lasers #1 and #2 were locked to the j and i-j components, respectively, by which the beat frequency was fixed to 135 MHz.

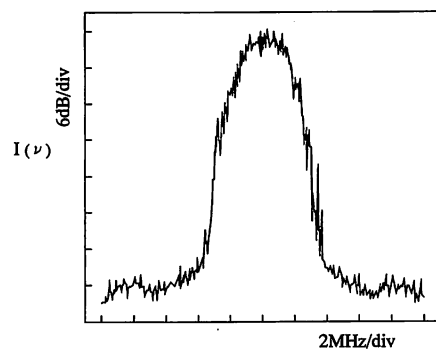


Fig. 6. Beat spectral profile between the two stabilized lasers measured by a microwave spectrum analyzer with the sweep time of 75 s.

imum was 1.36 MHz, which represents the magnitude of the frequency fluctuations of the two lasers for the 75 s sweep time of the spectrum analyzer. The short-term spectral linewidth was measured by a delayed self-homodyne technique using a 2-km-long optical

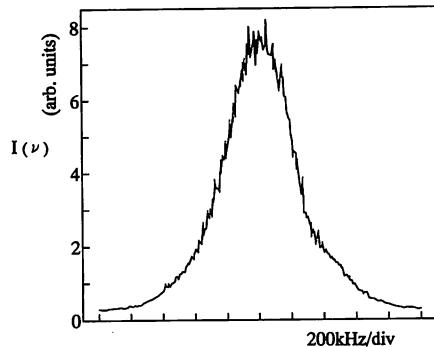


Fig. 7. The profile of the laser field spectrum measured by a delayed self-homodyne technique using a 2-km-long optical fiber.

#### THE FIRST STEP

Initial adjustments.

#### THE SECOND STEP

Increasing the injection current by monitoring the linear absorption spectral lineshapes.

#### THE THIRD STEP

Adjustments of the PZT-C and PZT- $\phi$  voltages for optical feedback.

#### THE FOURTH STEP

Locking the resonant frequency of the external cavity to the laser frequency.

#### THE FIFTH STEP

Decreasing the external cavity length by monitoring the saturated absorption spectral lineshapes.

Closing the feedback loop of the external cavity for frequency locking to the  $j$  component.

(a)

fiber. One of the measured spectral profiles is shown in Fig. 7. By averaging the 100 measured spectral profiles, the full linewidth at half maximum was estimated to be 170 kHz.

#### 4. Computer-controlled Automatic Frequency Locking

Figure 8(a) shows the procedure of how to lock automatically the laser frequency to the  $j$  component of  $^{87}\text{Rb}$  by using the digital signal processing system of Fig. 1(b). The first step of this procedure is the initial adjustments of the heat sink temperature and injection current of the laser, voltages of the PZT-C and PZT- $\phi$ . The heat sink temperature is fixed to the value at which the laser frequency is nearly tuned to the resonant frequency of the  $j$  component. The injection current is adjusted to the value by which the laser frequency is fixed to the lower frequency side of the linear absorption spectral lineshapes of  $^{87}\text{Rb}$ , i.e., at point (1) of Fig. 8(b). The voltages applied to the PZT-C and PZT- $\phi$  are fixed to arbitrary nonzero values.

The second step is to sweep the laser frequency toward the higher frequency side of the first derivative of the four spectral lineshapes of Fig. 8(b) by sweeping the injection current. The two peaks ( $P_{L1}$  and  $P_{L3}$ ) and a dip ( $P_{L2}$ ) in the first derivative curve are used as frequency monitors to determine where the laser frequency is in the process of this sweep. After the laser frequency passes through  $P_{L3}$ , it is tuned to point (2).

The third step is to adjust the applied voltages of the

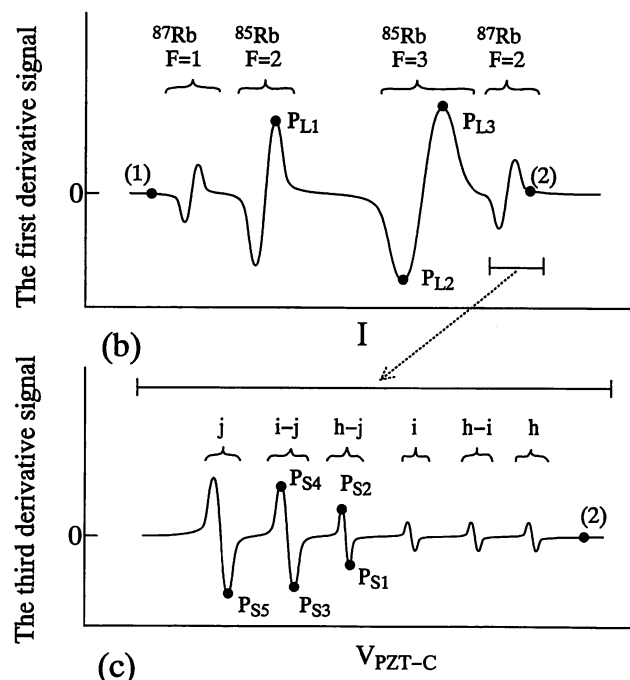


Fig. 8. (a) Flow chart of the procedure to lock automatically the laser frequency to the  $j$  component of  $^{87}\text{Rb}$ . (b) The first derivative of the linear absorption spectral lineshapes in  $^{87}\text{Rb}$  and  $^{85}\text{Rb}$ . The horizontal axis is the injection current of the laser. The laser frequency is tuned from point (1) to point (2) by monitoring the two peaks ( $P_{L1}$  and  $P_{L3}$ ) and the dip ( $P_{L2}$ ) on this curve. (c) The third derivative of the saturated absorption spectral lineshapes in  $^{87}\text{Rb}$ . The horizontal axis represents the voltage applied to the PZT-C. These spectral lineshapes are located in the area represented by a horizontal bar around point (2) of Fig. 8(b). They are identified as  $h$ ,  $h-i$ ,  $i$ ,  $h-j$ ,  $i-j$ , and  $j$  components. The peaks and dips  $P_{S1}$ – $P_{S5}$  on this curve are used to monitor these hyperfine components.

PZT-C and PZT- $\phi$  to realize the optical feedback from the external cavity. Although the laser frequency was slightly shifted from point (2) of Fig. 8(b) by closing the optical feedback loop, this shift is compensated by the next step.

The fourth step is further adjustment of the PZT-C voltage so as to fix the resonance frequency of the external cavity to the laser frequency. The PZT- $\phi$  voltage is simultaneously adjusted to realize a symmetric cavity resonance spectral lineshape. By these adjustments, the laser frequency can be maintained at the center of the locking range of the optical feedback, by which a stable fine frequency tuning is realized in the next step. After the PZT-C voltage is adjusted to obtain the maximum transmitted light power detected by photodetector #1 of Fig. 1, the feedback loop for controlling the PZT- $\phi$  voltage is closed. By this procedure, the injection current of the laser is locked to the center of the locking range of the optical feedback, and thus, the frequency difference between the free-running laser and the optically fed-back laser is kept sufficiently small.

The fifth step is to decrease the external cavity length while monitoring the third derivatives of the saturated absorption spectral lineshapes. The components of saturated absorption lines can be identified by measuring the values of the PZT-C voltages at which the peaks and dips  $P_{S1}$ - $P_{S5}$  of Fig. 8(c) appear. When the second derivative of the  $j$  component takes the maximum after detecting the dip  $P_{S5}$ , the feedback loop is closed in order to lock the optically fed-back laser to the center frequency of the  $j$  component. Stable frequency locking is confirmed by monitoring that the second derivative signal is maintained at the maximum value.

It took about eight minutes to complete all the steps of the procedure for automatic frequency locking. Furthermore, reproducible frequency locking to the  $j$  com-

ponent was realized without inducing mis-locking to other spectral components. In the experiments of the present study, evaluations of the frequency stabilities, presented in the previous sections, have been made under the condition of this automatic frequency locking.

## 5. Conclusions

A frequency-stabilized and highly coherent light source was developed by using an AlGaAs laser at 780 nm wavelength. The main results of the present study are:

(1) The square root of the Allan variance, representing the frequency stability, was  $1.9 \times 10^{-11}$  at the integration time  $\tau$  of 1 s, which was obtained by using the saturated absorption spectral line in Rb vapor as a frequency reference. The minimum was  $2.1 \times 10^{-12}$  at  $\tau = 300$  s.

(2) The field spectral linewidth of laser oscillation was reduced by the optical feedback from the external Fabry-Perot cavity. The full linewidth at the half maximum, estimated from the beat signal between the two independent lasers, was 1.36 MHz at the measurement time of 75 s. The value estimated by the delayed self-homodyne method was narrower than 170 kHz.

(3) Unmodulated output power and frequency were obtained.

(4) A computer-controlled automatic frequency locking procedure was developed and its stable operation was confirmed.

- 1) M. Ohtsu: *Highly Coherent Semiconductor Lasers* (Artech House, Boston, 1992).
- 2) M. Ohtsu, K. Nakagawa, M. Kourōgi and W. Wang: *J. Appl. Phys.* **73** (1993) R1.
- 3) H. Furuta and M. Ohtsu: *Appl. Opt.* **28** (1989) 3737.
- 4) B. Dahmani, L. Holberg and R. Drullinger: *Opt. Lett.* **12** (1987) 876.



## Iodine Absorption-Line-Stabilized Frequency-Tunable Green Light Using Sum-Frequency Generation of Diode Lasers

Weizhi WANG<sup>1</sup> and Motoichi OHTSU<sup>1,2</sup>

<sup>1</sup>Interdisciplinary Graduate School of Science and Engineering, Tokyo Institute of Technology, 4259 Nagatsuta-cho, Midori-ku, Yokohama 227

<sup>2</sup>Kanagawa Academy of Science and Technology, KSP East, Rm. 408, 3-2-1 Sakado, Takatsu-ku, Kawasaki 213

(Received August 18, 1993; accepted for publication December 18, 1993)

A precision frequency-tunable green light source, which involves a frequency reference using a molecular iodine absorption resonance and a tuner, has been demonstrated. The green coherent light was obtained by sum-frequency generation using a 0.82  $\mu\text{m}$  AlGaAs laser and a 1.54  $\mu\text{m}$  distributed-feedback (DFB) laser in a KTP crystal. The reference frequency was locked to an  $\text{I}_2$  absorption resonance and the residual frequency fluctuation was estimated to be within  $\pm 0.5$  MHz. A frequency-tunable range of  $\sim 5$  THz was obtained. Heterodyne beat signals were obtained to measure the frequency difference between the frequency reference and the tunable output. This system was also proposed for measuring the frequency spacings between different resonances of a molecular absorption spectrum.

**KEYWORDS:** sum frequency, tunable source, diode laser, frequency stabilization, iodine spectrum, KTP

### 1. Introduction

Highly precise frequency-tunable light sources are essential tools for spectroscopy and quantum optics. Diode lasers have been used for these purposes because of their high efficiency, convenience in frequency modulation and frequency tunability. In order to extend the tunable range of diode lasers, nonlinear frequency conversion is widely employed. We have proposed a diode-laser-based wideband coherent optical frequency sweep generator (OFSG) to cover the frequencies from ultraviolet to infrared, whose outputs contain direct lasing of multiple diode lasers and their frequency conversion using nonlinear optics effects.<sup>1,2</sup> On the other hand, in the conventional tunable light source system, frequency stabilization is performed by using resonance of an optical resonator whose frequency is vulnerable to acoustic disturbances and thermal fluctuation of the cavity. To solve this problem, atomic/molecular transitions are chosen as frequency references in our system so as to improve long-term stability while short-term stability is easily realized by using optical feedback which is an effective method for diode lasers. However, when the frequencies of fundamental lasers or the generated light frequency in the system is stabilized, the optical frequency inside the system can only serve as a frequency reference; therefore, a tuner whose frequency is tunable and a bridge which links the tunable frequency to the fixed reference must be added to the system.

In this paper, we demonstrate the operation of a frequency-tunable light source using the sum-frequency generation of diode lasers in KTP crystals. A molecular iodine ( $\text{I}_2$ ) absorption line was used as the frequency reference. The measurement of the frequency difference between the reference and the tunable output was carried out by heterodyning these two components.

### 2. Experimental

To obtain frequency-tunable output in a frequency range which cannot be obtained directly by diode lasers, frequency up-conversion was employed. This arrange-

ment offers a compact frequency-tunable system in the green region. The experimental setup, as is shown in Fig. 1, is composed of two parts: the reference part and the tuner part.

In the reference part, the sum-frequency was generated by a single-mode AlGaAs laser (Spectra Diode Labs, SDL5311) at 0.82  $\mu\text{m}$  (LD1, frequency:  $\nu_1$ ) with a maximum output power of 100 mW and an InGaAsP mul-

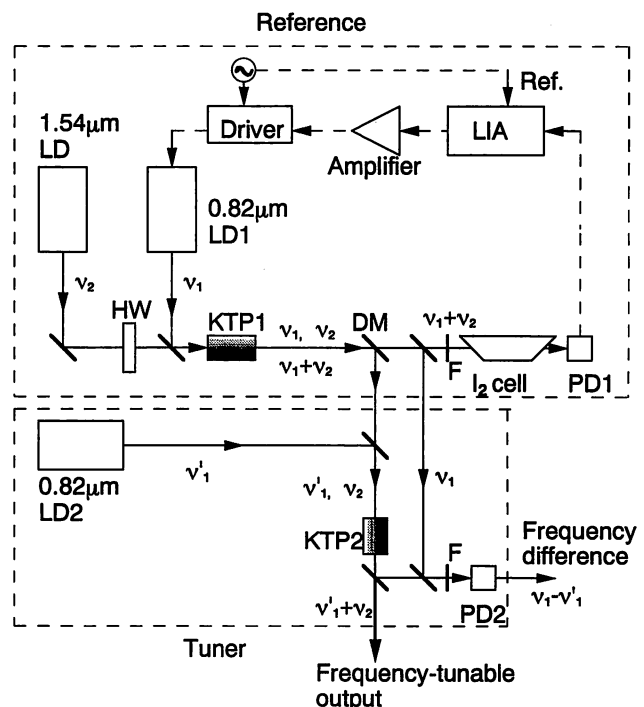


Fig. 1. Experimental setup for a frequency-tunable light source system. LD, 1.54  $\mu\text{m}$  DFB laser; LD1 and 2, 0.82  $\mu\text{m}$  single-mode diode lasers; KTP1 and 2, potassium titanyl phosphate crystals with lengths of 10 mm and 5 mm; DM, dichroic mirror; F, filter with high transmission only for green light; LIA, lock-in amplifier; PD1, Si-photodiode; PD2, avalanche photodiode; HW, half-wave plate at 1.54  $\mu\text{m}$  for rotating the polarization to satisfy the type II phase matching condition.

tielectrode distributed-feedback (DFB) laser at  $1.54 \mu\text{m}$  (LD, frequency:  $\nu_2$ ) with a maximum output power of  $45 \text{ mW}$ .<sup>3)</sup> The nonlinear optical crystal was a 10-mm-long KTP (KTP 1), in which type II angle phase matching was employed at room temperature. The phase-matching orientation of the KTP was  $\phi = 0^\circ$  and  $\theta = 59^\circ$ .<sup>2)</sup>

The tuner part of the system in Fig. 1 was arranged by using another  $0.82 \mu\text{m}$  diode laser (SDL5311) (LD2, frequency:  $\nu_1'$ ) and a second 5-mm-long KTP crystal (KTP2). A dichroic mirror (DM) with high transmission at  $0.82 \mu\text{m}$  and high reflectivity at  $1.54 \mu\text{m}$  was used to separate the  $1.54 \mu\text{m}$  laser component for the second sum-frequency generation with LD2 in KTP2. When the tuner was in operation, the frequency-tunable green light was obtained by changing the temperature and injection current of LD2. To monitor the frequency difference between the reference and the frequency-tunable output, the heterodyne signal between the two  $0.82 \mu\text{m}$  diode lasers was detected using an avalanche photodiode.

Molecular iodine was chosen as the frequency reference in our experiment because of its plenty of absorption lines covering a very large frequency range in the green region. Also, both saturated and Doppler-broadened absorption resonances of  $\text{I}_2$  offer the possibility of obtaining high stability.<sup>4)</sup> The use of a linear absorption resonance as a frequency reference is convenient since only a very low power is needed. For frequency stabilization, the generated green light in the reference part passed through a 15-cm-long  $\text{I}_2$  cell which contains natural iodine and is sealed with two Brewster windows at both ends. A Si photodetector was used to detect the transmitted power of the green beam. Although there are two fundamental lasers involved in the sum-frequency generation, frequency stabilization of the output radiation by controlling only one fundamental laser is possible,<sup>5)</sup> while the other fundamental laser is in free-running. For this purpose, the locking range should be sufficiently large to compensate the frequency drift of the free-running laser. In addition, the power fluctuation, which results from the phase mismatch in the nonlinear conversion when the frequency of the fundamental laser varies, should be sufficiently low. In our case, all laser sources are temperature-stabilized and the power ratio of fluctuations due to the phase mismatch in the KTP crystal is less than  $10^{-4}$ , so that these preliminary conditions are satisfied.

### 3. Results and Discussion

Figure 2(a) shows the absorption spectrum of  $\text{I}_2$  at  $0.53632 \mu\text{m}$  observed when the  $0.82 \mu\text{m}$  fundamental laser was swept by the injection current with a frequency of  $5 \text{ kHz}$ . The maximum power of the sum-frequency generation was  $0.6 \mu\text{W}$ . The linear absorptions of different resonances were measured to be from 2% to 65%. Figure 2(b) shows an absorption resonance used as the frequency reference for frequency stabilization. The width of the absorption resonance measured with a confocal optical resonator of the  $1.5 \text{ GHz}$  free spectral range was  $1.5 \text{ GHz}$  at  $24^\circ\text{C}$ . When the molecular cell was cooled to  $6^\circ\text{C}$ , the resonance width was measured to be  $1.2 \text{ GHz}$ . The pressure of the iodine vapor was estimated to be  $\sim 100 \text{ mTorr}$ . The shape of the resonance was also compared with both

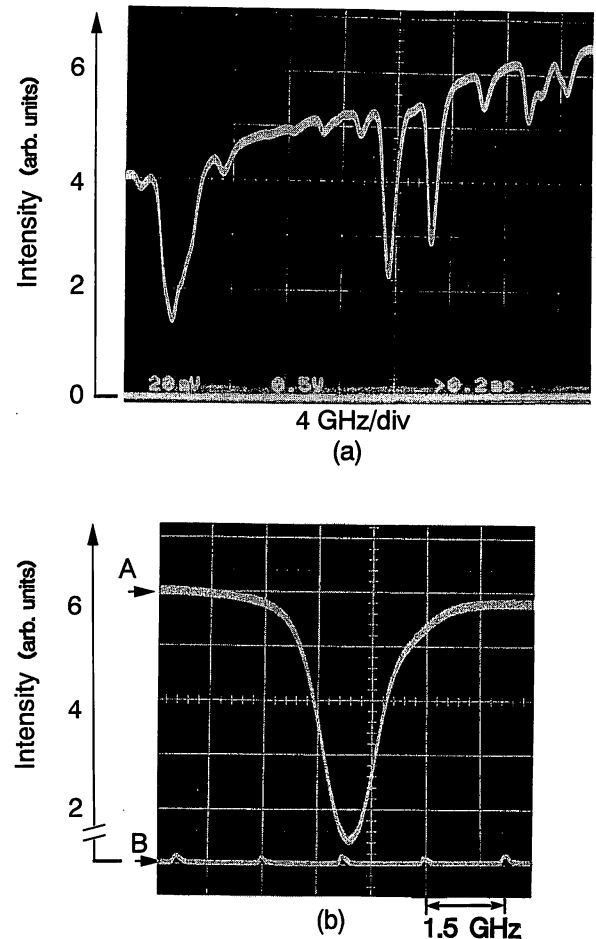


Fig. 2. (a) Molecular iodine absorption spectrum at  $0.53632 \mu\text{m}$  as the injection current of the  $0.82 \mu\text{m}$  fundamental laser was swept with a frequency of  $5 \text{ kHz}$ . The linear absorptions of these lines, with the linewidths of the order of gigahertz, were from 2% to 65%. The slope of the trace was due to the output power variation when the current was swept. (b) Trace A: The absorption resonance used for frequency stabilization at  $6^\circ\text{C}$ . Trace B: The transmission resonances of a confocal optical resonator with a FSR of  $1.5 \text{ GHz}$ , which was used for calibrating the width of the absorption resonance.

Lorentzian and Gaussian profiles at the FWHMs. Better fit with the Gaussian profile implied that the absorption resonance was Doppler-broadened. The observed width was much larger than the temperature-determined Doppler broadening ( $\sim 400 \text{ MHz}$ ) because of the hyperfine splitting.<sup>4)</sup> The total absorption of this resonance was measured to be 55%, and the intensity of the green light was  $15 \mu\text{W}/\text{cm}^2$ .

The conventional phase-sensitive technique was employed to stabilize the  $0.82 \mu\text{m}$  laser while the  $1.54 \mu\text{m}$  laser was in free-running. The temperature of the cell was maintained at  $6^\circ\text{C}$ . The modulation with a frequency of  $5 \text{ kHz}$  was applied to the injection current of the  $0.82 \mu\text{m}$  laser, and the error signal from a lock-in amplifier was fed back to the current source. The output frequency drifts were attributed mainly to the thermal and current fluctuations. Figure 3 shows the first derivative of the absorption resonance shown in Fig. 2(b) and the error signal

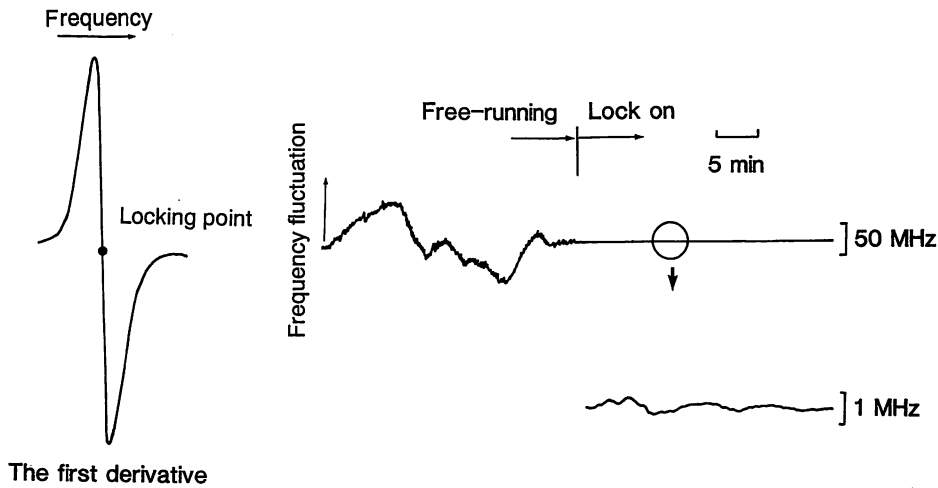


Fig. 3. The first derivative of the absorption resonance in Fig. 2(b) and the error signal from the lock-in amplifier. The residual frequency fluctuation was estimated to be within  $\pm 0.5$  MHz.

from the lock-in amplifier. The residual frequency fluctuation was estimated from the error signal to be within  $\pm 0.5$  MHz, implying a frequency stability better than  $10^{-9}$  at the optical frequency of 560 THz. This result shows that the use of a broad resonance maintains a wide locking range for frequency stabilization, which is preferable in frequency stabilization, by controlling only one fundamental laser in the three-wave frequency mixing.

Figures 4(a) and 4(b) show the measured heterodyne beat signals between two  $0.82 \mu\text{m}$  lasers, and between two green lights, respectively. The scanning time constant was 50 ms. It is obvious that the 50 dB beat signal between  $0.82 \mu\text{m}$  lasers can be used for optical phase locking.

In our experiment, the tunable frequency range of  $\sim 5$  THz was obtained by changing the temperatures of both diode lasers. The use of the  $1.5 \mu\text{m}$  DFB laser ensures the continuous coverage of the output frequency in this wide range, even though another conventional Fabry-Perot-type AlGaAs laser participating in the nonlinear frequency conversion experiences mode hops. The possible continuous frequency tuning range can be as wide as  $\sim 1$  THz by changing only the temperature of the DFB laser. The frequency difference measurement was limited by the responsible bandwidth of the conventional photodetector, which is at most 50–100 GHz. The precision frequency tuning range up to 1 THz can be expected by using an optical frequency comb generated by a microwave-modulated electrooptic modulator.<sup>6)</sup> In this case, the heterodyne beat signal is obtained between LD2 and a sideband of LD1. The experimental result in Fig. 4(b) shows the feasibility of the optical heterodyne phase locking when the signal power is very low; the power in each beam for the obtained beat signal was less than 70 nW.

For truly continuous frequency tuning over the obtained 5 THz frequency range, mode hops in the AlGaAs laser should be prevented. A diode laser with a grating extended cavity, which can provide a continuous tuning range wider than 1 THz at  $0.8 \mu\text{m}$  wavelength and wider

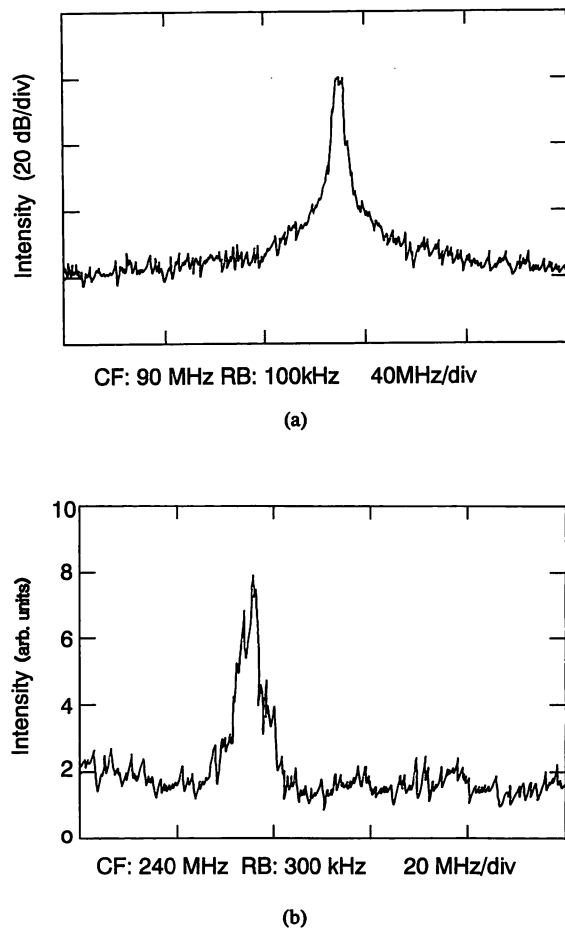


Fig. 4. (a) Heterodyne beat signal between two  $0.82 \mu\text{m}$  fundamental lasers at a scanning time constant of 50 ms. The 3 dB width of this beat signal shows that the linewidth of each diode laser was less than 2 MHz. (b) The heterodyne beat signal between two green lights shows the feasibility of detection in the case of weak power. The scanning time constant was 50 ms. The power of each green light was less than 70 nW. The broadening width of this beat signal compared with (a) was attributed to the linewidth of the  $1.54 \mu\text{m}$  DFB laser which was estimated to be less than 5 MHz. CF: center frequency; RB: resolution bandwidth.

than 10 THz at 1.5  $\mu\text{m}$  wavelength,<sup>7,8)</sup> can be employed.

As an example of the application of our system, we present here the use of the two generated green lights to measure the frequency spacings between different absorption resonances of iodine. Figure 5 shows spectra of iodine when the two green lights passed through the  $\text{I}_2$  cell and were spatially separated. Figures 5(a) and 5(b) are the cases when the two green lights were independently tuned to the same frequency and tuned to different frequencies, respectively, while the injection current of the 1.54  $\mu\text{m}$  laser was swept with a frequency of 5 kHz.

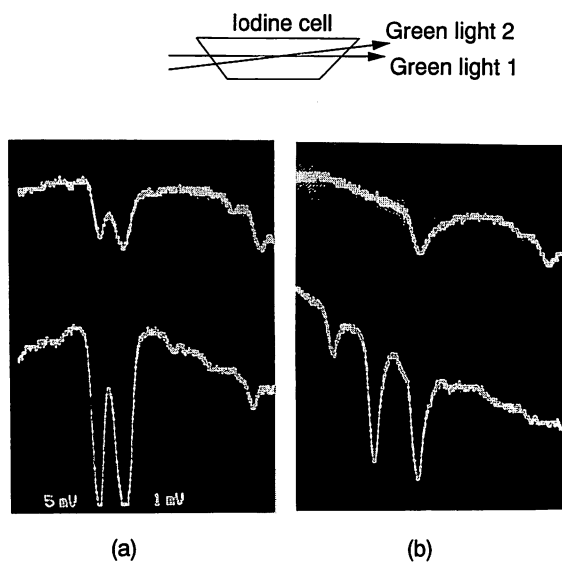


Fig. 5. Two iodine absorption spectra obtained with the two green lights which passed through the same molecular cell and were spatially separated to irradiate different photodetectors. The injection current of the 1.5  $\mu\text{m}$  laser was swept with a frequency of 5 kHz. (a) when the two green lights were independently tuned to the same frequency, and (b) when the two green lights were independently tuned to different frequencies.

#### 4. Conclusions

We have demonstrated operation of a precision frequency-tunable green light source by using the sum-frequency generations of 0.82  $\mu\text{m}$  and 1.54  $\mu\text{m}$  diode lasers in KTP crystals. Molecular iodine absorption resonance at 0.53632  $\mu\text{m}$  was used to stabilize the sum-frequency by controlling only one fundamental laser while the other was in free-running. The residual frequency fluctuation was estimated to be less than  $\pm 0.5$  MHz from the error signal. The heterodyne beat signals were obtained for precisely measuring the frequency interval between the tunable frequency and the frequency reference. A frequency-tunable range of  $\sim 5$  THz was obtained. Precision frequency tuning can be extended to be wider than 1 THz by using an optical frequency comb for frequency difference measurement. This system has been applied for measuring the frequency spacings between different resonances in the  $\text{I}_2$  absorption spectrum. Because our scheme is applicable for other frequency regions, a diode-laser-based wide-band precision frequency-tunable system is feasible in the entire region covered by the nonlinear frequency conversion of diode lasers.

#### Acknowledgement

The authors thank Dr. A. M. Akulshin of P. N. Lebedev Physics Institute, Republic of Russia, for critical comments on the experiment, and Dr. M. Okai of Hitachi Ltd. for helpful discussions on DFB lasers.

- 1) W. Wang and M. Ohtsu: *Opt. Lett.* **18** (1993) 876.
- 2) W. Wang and M. Ohtsu: *Opt. Commun.* **102** (1993) 304.
- 3) M. Okai, T. Tsuchiya, K. Uomi, N. Chinone, and T. Harada: *IEEE Photon. Technol. Lett.* **2** (1990) 529.
- 4) A. Arie, S. Schiller, E. K. Gustafson and R. L. Byer: *Opt. Lett.* **17** (1992) 1204. Also A. Arie and R. L. Byer, manuscript submitted to *Appl. Opt.*
- 5) K. Sugiyama and J. Yoda: *Opt. Commun.* **95** (1993) 77.
- 6) M. Kourogi and M. Ohtsu: IQEC '92 (American Physical Society and European Physical Society, 1992, Vienna) paper TuM5.
- 7) A. T. Schremer and C. L. Tang: *IEEE Photon. Technol. Lett.* **2** (1990) 3.
- 8) F. Favre and D. Le Guen: *Electron. Lett.* **27** (1991) 183.



## Highly sensitive detection of molecular absorption using a high finesse optical cavity

K. Nakagawa<sup>a,b</sup>, T. Katsuda<sup>a</sup>, A.S. Shelkovich<sup>a,1</sup>, M. de Labachellerie<sup>a,2</sup>, M. Ohtsu<sup>a,b</sup>

<sup>a</sup> *Interdisciplinary Graduate School of Science and Engineering, Tokyo Institute of Technology, 4259, Nagatsuta-cho, Midori-ku, Yokohama 227, Japan*

<sup>b</sup> *Kanagawa Academy of Science and Technology, Kanagawa, Japan*

Received 28 September 1993; revised manuscript received 16 November 1993

### Abstract

The highly sensitive detection of molecular absorption in an external optical cavity is demonstrated. An effective absorption length of 5 km is obtained with a high finesse ( $\sim 18000$ ) cavity. A weak absorption ( $\sim 3 \times 10^{-5}$ ) of  $C_2H_2$  at  $1.064 \mu m$  is detected by using this cavity and a diode-laser-pumped Nd:YAG laser.

Laser absorption spectroscopy is a useful technique for sensitive detection of trace gases. Using tunable lead-salt diode lasers in the mid-infrared region, where strong absorption lines of fundamental vibrational bands of molecules are abundant, highly sensitive detections of various molecules have been established [1,2]. In the near-infrared region, there are also many absorption lines of overtone and combination bands of molecules, whereas the absorption of these bands is much weaker than that of the mid-infrared bands. For practical applications, near-infrared molecular absorption lines are attractive because it allows use of diode lasers and diode-laser-pumped solid state lasers operating at room temperature. To get higher sensitivity in absorption spectroscopy, there are mainly two ways. One is to extend the absorption pass length. Using a multiple-pass absorption cell [3], an absorption length of more than

200 m is available. The technique of intracavity laser spectroscopy (ICLAS) also enables to get an effective absorption length on the order of 10 km [4,5]. The other is to get higher signal to noise ratio in absorption signal. Frequency modulation (FM) technique allows to get shot-noise-limited sensitivity [2,6]. In recent years, high quality mirrors with high reflectivity and low loss have been developed and used in ring laser gyroscopes, optical spectrum analyzers, or reference cavities for laser frequency stabilization. Using these mirrors, one can easily get a cavity finesse of higher than 10000 or a cavity photon storage time of  $10 \mu s$ , which corresponds to an optical length of about 3 km. Here we report a highly sensitive detection of weak absorption of molecule using a high finesse optical cavity.

In the case of a Fabry–Pérot cavity with an absorbing medium, the transmitted optical field is given by

$$\frac{a_i}{A_i} = \frac{t_1 t_2 \exp(-i2\pi\nu nL/c) \exp(-\delta/2)}{1 - r_1 r_2 \exp(-i4\pi\nu nL/c) \exp(-\delta)},$$

where  $A_i = A_0 \exp(i2\pi\nu t)$  is the monochromatic optical field incident upon the cavity,  $t_j$  ( $j = 1, 2$ ) are

<sup>1</sup> Permanent address, P.N. Levedev Physics Institute, Moscow, Russian Federation.

<sup>2</sup> Permanent address, Laboratoire de l'Horloge Atomique, CNRS, Orsay, France.

the amplitude transmission coefficients,  $r_j$  ( $j=1, 2$ ) are the amplitude reflection coefficients of two cavity mirrors,  $n$  is the refractive index of the absorbing medium,  $L$  is the cavity length, and  $\delta$  is the one pass absorption loss of the medium. When  $r_j \sim 1$  ( $j=1, 2$ ) and  $\delta < 1 - r_1 r_2$ , the transmitted optical power is given by

$$\frac{P_t}{P_i} = \frac{|A_t|^2}{|A_i|^2} \approx \left(1 - \frac{2\delta}{1 - r_1 r_2}\right) \frac{\kappa^2}{1 + [2(\nu - \nu_0)/\Delta\nu_c]^2}$$

where  $\kappa$  is given by  $t_1 t_2 / (1 - r_1 r_2)$ ,  $\nu_0$  is the cavity resonant frequency given by  $mc / (2nL)$  ( $m=1, 2, \dots$ ),  $\Delta\nu_c$  is the cavity linewidth. At the cavity resonance ( $\nu = \nu_0$ ), the transmitted power  $P_t$  is proportional to  $1 - \delta \times 2 / (1 - r_1 r_2)$ . Thus the effective absorption is enhanced by  $2 / (1 - r_1 r_2)$ . The effective absorption length is given by  $L \times 2 / (1 - r_1 r_2) = L \times 2F / \pi = c / (n\pi\Delta\nu_c)$ , where  $\Delta\nu_c$  is given by  $c / (2nLF)$  and  $F$  is the cavity finesse given by  $\pi\sqrt{r_1 r_2} / (1 - r_1 r_2)$ . If  $r_1^2 = r_2^2 = 0.9999$  ( $F \sim 30000$ ) and  $L = 50$  cm, the effective absorption length is the order of 10 km.

The experimental setup for highly sensitive absorption spectroscopy using a high finesse cavity is shown in Fig. 1. We use a monolithic diode-laser-pumped Nd:YAG laser (Lightwave Model 122-300) as a light source. The spectral linewidth is narrower than 5 kHz in free running. The laser frequency can be slowly tuned over 30 GHz by varying the Nd:YAG crystal temperature. Using a piezoelectric transducer (PZT) bonded to the crystal, fast frequency tuning is achieved with maximum tuning range of about 100 MHz. A high finesse Fabry–Pérot cavity, which is originally used as the reference cavity for frequency stabilization of the Nd:YAG laser [7], is used as an absorption cell. The cavity spacer is made of a Zerodur rod ( $L = 460$  mm) without any tuning element

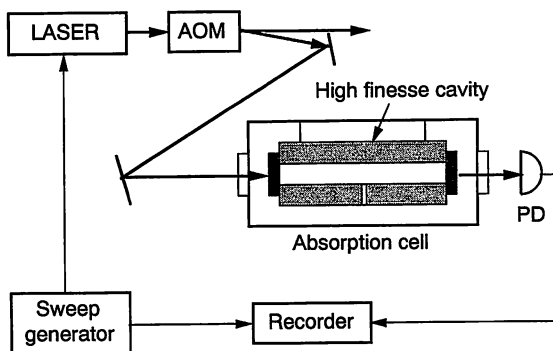


Fig. 1. The schematic diagram of the experiment.

as PZT. Measuring the cavity photon storage time, the cavity linewidth was measured to be about 10 kHz [7]. Thus the cavity finesse and the reflectivity of the cavity mirrors are determined to be about 18000 and 0.99983, respectively. This cavity is mounted in a stainless vacuum chamber.

The  $C_2H_2$  gas is filled in this chamber with a pressure of about 7 Torr. The  $C_2H_2$  absorption line close to the Nd:YAG laser wavelength has been previously observed using an intracavity laser spectrometer (ICLAS) with a resolution of  $0.08 \text{ cm}^{-1}$  and a sensitivity of  $10^{-7}/\text{cm}$  [5]. Only one absorption line assigned as the R(12) transition of the  $(2100^01^1)-(0000^00^0)$  band is within the frequency tuning range of the present Nd:YAG laser, and its center wavenumber was measured to be  $9393.54 \text{ cm}^{-1}$  which corresponds to a vacuum wavelength of  $1.064561 \mu\text{m}$  [5]. Setting the laser temperature to about  $48^\circ\text{C}$ , the laser frequency can be tuned to this wavelength. The laser frequency is scanned around the cavity resonance by the PZT and the cavity transmitted light power is detected by the photodiode. The cavity resonance profiles around the absorption line are shown in Fig. 2. The transmitted power decreases near the absorption line center (Figs. 2b, c). When the  $C_2H_2$  pressure decreases, the decrease of the transmitted power becomes small. There is no other such a decrease within a tuning range of the Nd:YAG laser. Thus the observed decrease of power is due to the absorption of  $C_2H_2$ .

The peak transmitted power is plotted around the absorption line (Fig. 3). The linewidth (fwhm) of the absorption line is about 880 MHz, which is rather wider than the Doppler linewidth of 680 MHz. The absorption at the line center is estimated to be about 34%. It corresponds to a one pass absorption of about  $3 \times 10^{-5}$  or an absorption coefficient of about  $6.5 \times 10^{-7}/\text{cm}$ . The absorption coefficient of this line was not reported in previous measurement using the ICLAS, however, the sensitivity of the ICLAS was reported to be  $10^{-7}/\text{cm}$  which is consistent with the present result [5]. If the minimum detectable variation of transmitted power is assumed to be 0.5%, the sensitivity of the present spectrometer is estimated to be about  $10^{-8}/\text{cm}$ .

The wavelength of the absorption line center is measured to be  $1.064558 \mu\text{m}$  by using a Michelson wavelength meter (ANTITSU MF9630A) with an

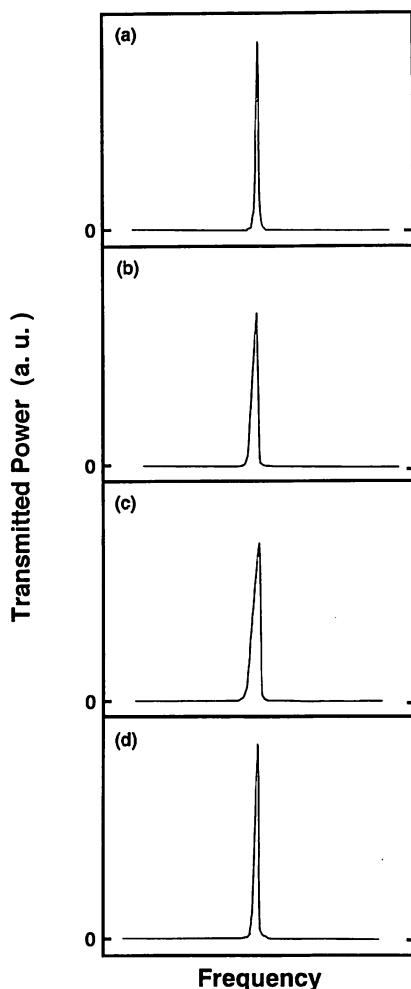


Fig. 2. The cavity transmitted spectrum around the absorption line of  $C_2H_2$ .

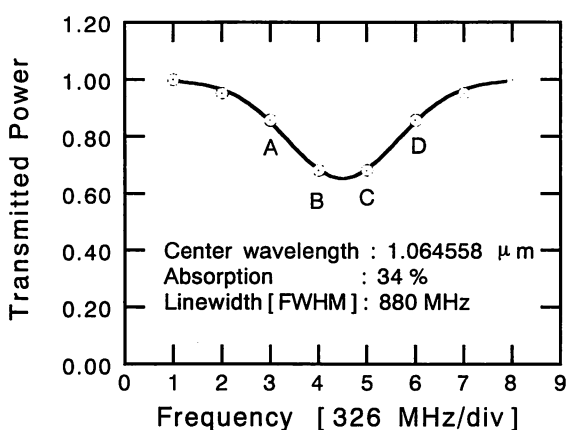


Fig. 3. Doppler broadened absorption profile of  $C_2H_2$  at 1.064558  $\mu\text{m}$ . The dots A, B, C, D correspond the data in Fig. 2a–d, respectively.

accuracy of  $5 \times 10^{-7}$ . This line center frequency is about  $0.03 \text{ cm}^{-1}$  higher than that measured by using the ICLAS [5]. This discrepancy of  $0.03 \text{ cm}^{-1}$  is

mainly due to the low resolution ( $0.08 \text{ cm}^{-1}$ ) of the ICLAS.

The cavity resonant profile near the absorption line center is asymmetric (Figs. 2b, c). In both direction of frequency sweeping, the slope is always lower on the red side compared with the blue side. It is probably due to the heating of molecular gas. When the laser frequency is swept from the low frequency side and below the cavity resonant center, the molecules begin to absorb the laser light and the gas temperature increases. It causes the expansion of gas and a decrease of its refractive index, thus the cavity resonant frequency shifts to be blue side and the resonance slope is therefore reduced. Once the laser frequency is above the resonant center, on the contrary, the gas temperature decreases and the cavity resonant frequency shifts to the red side. Thus it leads to a steep slope on the blue side.

Compared with other sensitive spectrometers, the present method is quite simple and compact. The effective absorption length is inversely proportional to the cavity linewidth. In the present case, the cavity linewidth is 18 kHz and the absorption length is about 5.3 km, which is about two orders longer than that of typical multiple-pass absorption cell with the same length ( $\sim 0.5 \text{ m}$ ). Increasing the cavity finesse to more than 60 000, the cavity linewidth decreases to 5 kHz and the absorption length reaches 20 km. Up to now, a finesse of  $10^6$  has been reported and one can further reduce the cavity linewidth [8]. However, this method requires narrower linewidth of the laser than the cavity linewidth. Diode-laser-pumped solid state lasers show good frequency stability and narrow linewidth, they are preferable for this purpose. If the laser is locked to this high finesse cavity using a FM sideband technique [9], one can easily reduce the laser linewidth below the cavity linewidth. This method is very attractive for diode lasers, whose linewidth is typically more than 1 MHz. Using the FM sideband technique with current modulation, the diode laser linewidth can be reduced to narrower than 100 Hz [10]. It is also helpful to use an optical feedback from an external cavity [11].

To get a higher sensitivity, it is better to detect the dispersion signal rather than the absorption signal using heterodyne techniques [12,13]. One example is to measure the heterodyne beat frequency between two lasers which are locked to different longitudinal

modes of the cavity. One can detect the variation of the beat frequency induced by the dispersion of molecular absorption.

The light field inside a high finesse cavity is largely enhanced and one can also expect nonlinear spectroscopy as saturation [14], double resonance, and two-photon spectroscopy [15]. The saturation spectroscopy of weak molecular absorption lines in the near infrared region can be obtained with a low power diode laser [16]. In the case of the present  $C_2H_2$  transition at  $1.064 \mu m$ , the transition dipole moment is calculated to be  $3 \times 10^{-6}$  Debye from the absorption coefficient. The power density required for saturation is estimated to be about  $5 \text{ MW/cm}^2$ , which corresponds to an input laser power of about  $5 \text{ W}$  even with the high finesse ( $\sim 18000$ ) cavity. Within the Nd:YAG laser frequency tuning range of  $30 \text{ GHz}$ , other available molecular transitions are  $CO_2$  [17] and  $C_2HD$  [18]. The  $C_2HD$  line ( $1.064459 \mu m$ ) seems to be promising for saturation spectroscopy with the Nd:YAG laser because the absorption strength might be stronger than that of the  $C_2H_2$  or  $CO_2$  [19].

In conclusion, we have shown the highly sensitive spectroscopy using a high finesse optical cavity as an absorption cell. The effective absorption length is enhanced by the order of the cavity finesse inside the cavity. We could observe the weak absorption line of  $C_2H_2$  at  $1.064558 \mu m$  by using a cavity with a finesse of  $18000$  and a diode-laser-pumped Nd:YAG laser. The sensitivity of the present spectrometer corresponds to the absorption coefficient of about  $10^{-8}/\text{cm}$ . This method can be widely applied in sensitive detection of various molecules using diode-laser-pumped solid state lasers and diode laser in near infrared region.

This work was supported by the Grant-in-Aid for Scientific Research (No. 04234204) from Ministry of Education, Science, and Culture of Japan.

## References

- [1] D.E. Cooper and C.B. Carlisle, *Optics Lett.* 13 (1988) 719.
- [2] P. Werle, F. Slemr, M. Gehrtz and C. Bräuchle, *Appl. Phys. B* 49 (1989) 99.
- [3] Takahiro Kuga, Tadao Shimizu and Yoshifumi Ueda, *Jpn. J. Appl. Phys.* 24 (1985) L147.
- [4] A. Campargue, F. Stoeckel, M. Chenevier and H. Ben Kraiem, *J. Chem. Phys.* 87 (1987) 5598.
- [5] L.N. Sinitza, *J. Mol. Spectrosc.* 84 (1980) 57.
- [6] W. Lenth and M. Gehrtz, *Appl. Phys. Lett.* 47 (1985) 1263.
- [7] K. Nakagawa, Y. Shimizu, T. Katsuda and M. Ohtsu, *SPIE* 1837 (1992) 40.
- [8] G. Rempe, R.J. Thompson, H.J. Kimble and R. Lalezari, *Optics Lett.* 17 (1992) 363.
- [9] R.W.P. Drever, J.L. Hall, F.V. Kowalski, J. Hough, G.M. Ford, A.J. Munley and H. Ward, *Appl. Phys. B* 31 (1983) 97.
- [10] K. Nakagawa, M. Kourogi and M. Ohtsu, *Optics Lett.* 17 (1992) 934.
- [11] B. Dahmani, L. Hollberg and R. Drullinger, *Optics Lett.* 12 (1987) 876.
- [12] W. Lenth, *Optics Lett.* 8 (1983) 575.
- [13] V.A. Alekseev, M.A. Gubin and E.D. Protsenko, *Laser Physics* 1 (1991) 221.
- [14] Ma Long-Shen and J.L. Hall, *IEEE J. Quantum Electron.* 26 (1990) 2006.
- [15] C. Zimmermann, R. Kallenbach and T.W. Hänsch, *Phys. Rev. Lett.* 65 (1990) 571.
- [16] M. de Labachellerie and K. Nakagawa, under preparation for publication.
- [17] P. Fritschel and R. Weiss, *Appl. Optics* 31 (1992) 1910.
- [18] G. Herzberg, F. Patat and H. Verleger, *Z. Physik.* 102 (1936) 1.
- [19] G. Herzberg, *Molecular spectra and molecular structure* (Van Nostrand Reinhold Company, New York, 1945).



# High Power Diode-Laser-Pumped Twisted-Mode Nd:YAG Laser

Ken'ichi Nakagawa, Yukitaka Shimizu and Motoichi Ohtsu, *Senior Member, IEEE*

**Abstract**—We describe the design and performance of a high power diode-laser-pumped twisted-mode Nd:YAG laser. Using four high power 1 W diode lasers as pumping, nearly single frequency output power of 950 mW was obtained. Stable single frequency operation was realized with the help of injection locking with a master monolithic ring diode-laser-pumped Nd:YAG laser.

## I. INTRODUCTION

**H**IGH POWER single frequency diode-laser-pumped Nd:YAG lasers are required for efficient second harmonics generation [1], space communications [2], and interferometric gravitational wave detectors. Various designs of high power diode-laser-pumped Nd:YAG lasers have been proposed and developed up to now. In general, end-pumped lasers are superior to side-pumped lasers in pumping efficiency and output mode characteristic and suited for both high power and single mode operation. As the maximum output power of one diode laser is limited, multiple laser pumping is required to increase the pump power [3], [4]. Efficient end-pumping was demonstrated with three diode lasers focused into same mode volume [3]. Using a fiber bundle with 38 diode lasers, 7.6 W of multi frequency TEM<sub>00</sub> mode output was obtained at total pump power of 21 W [4]. Using a ring cavity [5], [6] or a twisted-mode cavity [2], [7], high power single frequency operation was realized. Here we describe the design and performance of a twisted-mode Nd:YAG laser pumped by four 1 W diode lasers. We also report the performance of stable single frequency operation using an injection locking technique.

## II. TWISTED-MODE Nd:YAG LASER

To avoid the spatial hole burning for high power single frequency operation, there are two solutions. One is an unidirectional oscillation using a ring cavity [5] [6], and the other is a twisted-mode oscillation using a linear cavity with two quarter wave plates [7]. We first tried the folded ring cavity with discrete four mirrors [6], however, the optical alignment of the cavity is critical to get stable unidirectional and single frequency operation [8]. Another approach is the

Manuscript received November 19, 1993.

The authors are with the Interdisciplinary Graduate School of Science and Engineering, Tokyo Institute of Technology, 4259, Nagatsuta-cho, Midori-ku, Yokohama 227, Japan.

K. Nakagawa and M. Ohtsu are also with the Kanagawa Academy of Science and Technology, 3-2-1 Sakado, Takatsu-ku, Kawasaki 213, Japan.

Y. Shimizu is now with the SHARP Corp., 1-9-2 Nakase, Mihama-ku, Chiba 261, Japan.

IEEE Log Number 9400277.

monolithic ring cavity [5], however, there are some limitations in intracavity elements and output power. For these reasons, we choose the twisted-mode laser pumped by multiple diode lasers [8]. The pumping method is the combination of polarization coupling and astigmatic focusing [3]. Schematic diagram of the pumping optics and the twisted-mode laser cavity is shown in Fig. 1(a). Four pump lasers are broad stripe (200  $\mu\text{m}$ ) high power diode lasers (SONY 304-XT) with maximum output power of 0.9 W. All the pump lasers are mounted as the long dimension of the stripe is vertical. Using half-wave plates (HWP) and polarization beam splitters (PBS), two diode laser outputs are combined at two stages and each combined pump beams are focused into the Nd:YAG crystal with small angle between two beams. Twisted mode cavity consists of one quarter-wave plate (QWP) with high reflection (HR) coating on one facet, a Nd:YAG rod ( $\phi 3 \times 7$  mm), a second quarter-wave plate, a Brewster plate (BP) as a polarizer, and an output coupling (OC) mirror with 97% reflection coating. All interior facet of quarter-wave plates and the Nd:YAG rod are antireflection (AR) coated at 1064 nm. The output mirror is mounted on a piezoelectric transducer (PZT) in order to tune the laser frequency. It is important for realizing high efficiency to match the pump laser beam size to the cavity beam waist size. The pump laser beams are independently focused in horizontal and vertical dimension using one collimating lens and two cylindrical lenses (Fig. 1(b)). The beam waste radii ( $w_h, w_v$ ) in the Nd:YAG crystal are about 230  $\mu\text{m}$  and 150  $\mu\text{m}$  in horizontal and vertical directions, respectively. The cavity length and the output coupling mirror curvature are about 50 mm and 600 mm, respectively. The beam radius near the end facet of the Nd:YAG crystal is calculated to be 240  $\mu\text{m}$ .

Maximum total pump power in front of the cavity end mirror is about 3 W, which is about 20% lower than the sum of pump laser power of 3.6 W (= 0.9 W  $\times$  4). It is mainly due to the loss of the collimating lens with a numerical aperture of 0.5. Input diode laser pump power versus output power of the Nd:YAG laser is shown in Fig. 2. The output power of 950 mW is obtained in twisted-mode operation. For comparison, the output power without an intracavity quarter-wave plate and Brewster plate is also shown in Fig. 2, and its maximum power is 1050 mW. An slope efficiency is 35% for twisted mode operation. This slope efficiency is comparable to that previously reported for the twisted mode laser [2].

The spectrum of the twisted-mode laser is observed with a confocal Fabry-Perot cavity with a free spectral range of 300 MHz and a finesse of 200. At the output power of lower

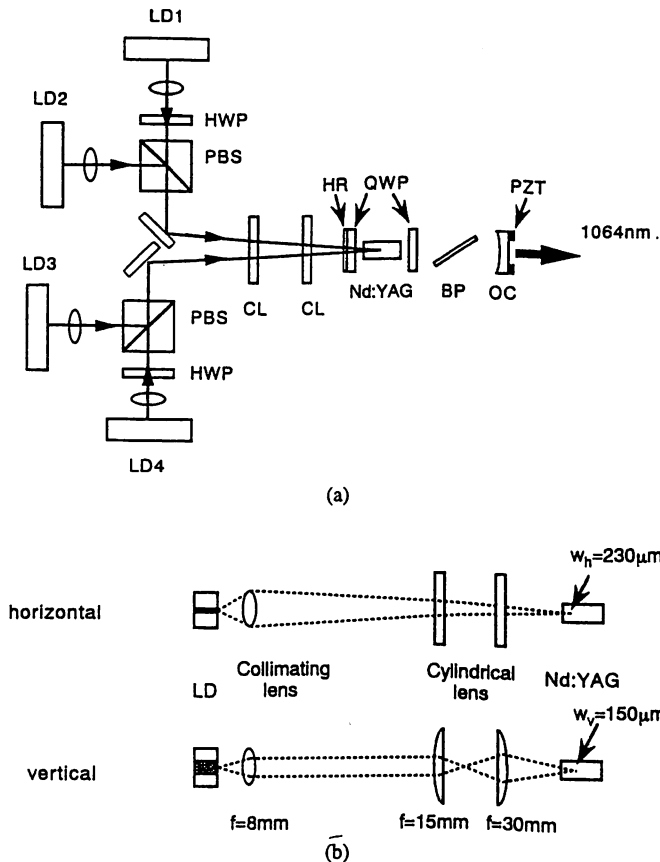


Fig. 1. Schematic diagram of the high power twisted-mode Nd:YAG laser. (a) Pumping optics and the twisted mode laser cavity. LD's, laser diodes; CL, cylindrical lens. (b) Pumping beam geometries in horizontal and vertical directions.

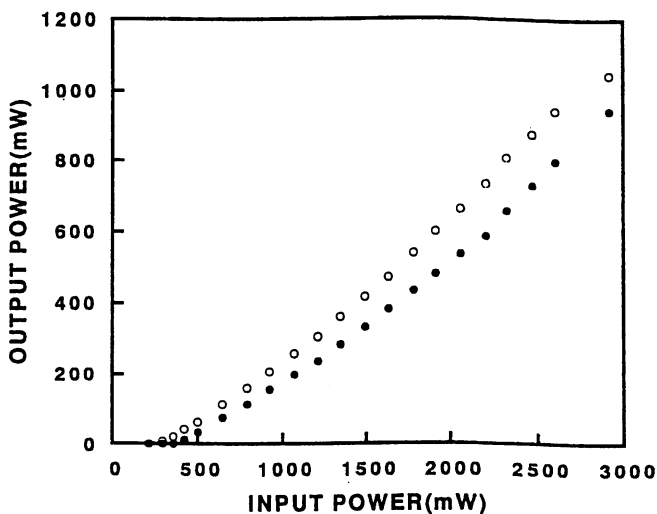


Fig. 2. Output power of the Nd:YAG laser versus input pump power. Open circles, random polarization mode without a Brewster plate (BP) and a quarter-wave plate (QWP); closed circles, twisted mode operation with both elements.

than 700 mW, the laser can oscillate in single mode. It is, to our knowledge, the highest single mode power obtained with the twisted-mode diode-laser-pumped Nd:YAG laser. Both the angle of a quarter-wave plate and the crystal temperature should be adjusted to get stable single mode operation. The

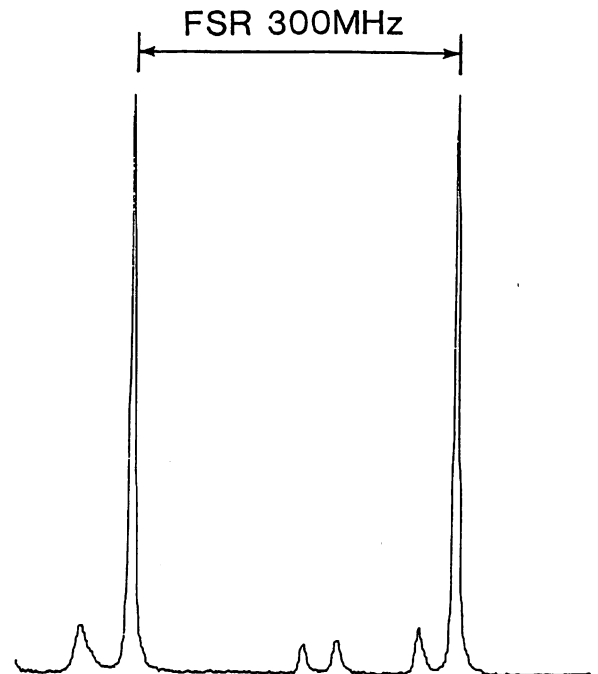


Fig. 3. Spectral analysis of the twisted-mode Nd:YAG laser at maximum output power of 0.95 W. The free spectral range of the Fabry-Perot cavity spectrum analyzer is 300 MHz.

crystal temperature is therefore stabilized by using a Peltier element with a temperature stability of less than  $0.01^\circ\text{C}$ . As increasing the pump power, the tolerances of the quarter-wave plate angle and the crystal temperature become crucial. At the maximum output power of nearly 1 W, the laser oscillates in nearly single mode (Fig. 3). Residual side modes are about 10 dB smaller than main mode and total side mode power is less than 15%. These side modes are probably due to the lack of the loss difference between two polarization modes with one Brewster plate. Another reason is the change of beam size of the laser mode induced by the thermal lens effect of the Nd:YAG crystal. By introducing an additional Brewster plate and by optimizing the pump beam size, a stable single mode operation can be realized with an output power of up to 1 W.

### III. INJECTION LOCKING

Injection locking was employed to get high power single mode operation with high frequency stability with using a stable single frequency master laser. We used a monolithic ring Nd:YAG laser (Lightwave Model 122-300) with output power of 300 mW as a master laser. The laser linewidth is about 5 kHz under free running. To maintain stable injection locking, we stabilized the slave laser cavity length with a PZT-mounted output mirror by using the FM sideband technique [9]. The sideband frequency is 24.25 MHz and the modulation index is about 0.5. A part of the modulated master laser light is introduced into the slave twisted-mode Nd:YAG laser. An optical isolator with an isolation ratio of 60 dB was used to protect the master laser from the output of the slave laser.

Fig. 4 show the spectrum of the injection locked slave laser. The injected master laser power and the slave laser output power are about 50 mW and 750 mW, respectively. The

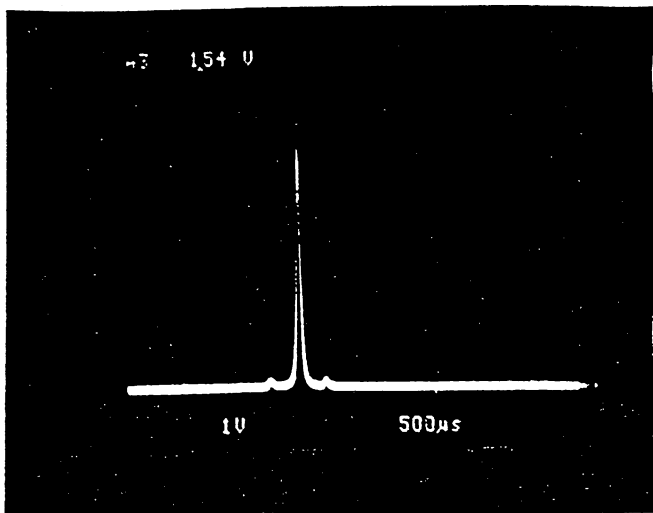


Fig. 4. Photograph of the output spectrum of the twisted-mode laser under injection locking. Two sidebands are due to the phase modulation sidebands of the master laser. The modulation frequency is 24.25 MHz.

locking range is roughly estimated to be 9 MHz by measuring the width of the error signal of the slave laser stabilization [10]. The locking range  $\Delta\nu_L$  is given by  $\Delta\nu_L = \Delta\nu_c \sqrt{P_m/P_s}$ , where  $\Delta\nu_c$  is the slave laser cavity linewidth,  $P_m$  and  $P_s$  are the master and slave laser power, respectively. For the present conditions ( $\Delta\nu_c = 24$  MHz,  $P_m = 50$  mW,  $P_s = 750$  mW),  $\Delta\nu_L$  is calculated to be about 6 MHz, which is agree with the experimental result.

We evaluate the residual phase noise between the injection locked slave laser and the master laser from the feedback error signal. The feedback bandwidth is the order of 1 kHz, which is mainly limited by the mechanical resonance of the PZT or the mirror mount. Using carefully designed PZT and mirror mount, this bandwidth can be extended to more than 10 kHz. Even with rather low feedback bandwidth, injection locking was stable enough. The residual phase noise between the master and slave is less than  $10^{-4}$  rad/ $\sqrt{\text{Hz}}$  at frequency less than 100 Hz, and the phase error variance is smaller than  $10^{-3}$  rad<sup>2</sup>. Thus the slave laser linewidth is estimated to be comparable to that of the free running master laser of about 5 kHz. Further experiment is needed to investigate the frequency noise of injection locked slave laser. In near future, we plan to evaluate the frequency noise of this injection locked slave laser using the frequency stabilized master laser. Recently we have achieved a linewidth of 30 Hz by stabilizing the monolithic ring Nd:YAG laser to a high finesse cavity [11]. Thus we can realize a high power and narrow linewidth Nd:YAG laser.

Straightforward way to increase the pump power in present method is to replace the present 1 W pump diode lasers to higher output power lasers. Using four 2 W lasers, which have

same aperture size ( $200 \mu\text{m} \times 1 \mu\text{m}$ ) as 1 W lasers, one can simply increase the pump power twice and the output power of more than 2 W can be realized. An alternative way is to increase the number of pump diode lasers. Pumping from three directions [3], one can increase the pump power to about 10 W. However, for the pump power of higher than 10 W, the effects of thermal lens and birefringence become crucial and one cannot easily obtain linearly polarized single frequency output [4]. Recently, using a side pumping, maximum single frequency output power of 15 W was obtained with the help of injection locking [12], however, it requires the pump power of 200 W and water flow cooling of the Nd:YAG rod. Up to the pump power of 10 W, the present pumping method is more efficient than other ways as using of fiber bundles [4] or side pumping.

#### IV. SUMMARY

In summary, we have demonstrated the high power twisted-mode Nd:YAG laser pumped by multiple diode lasers. Maximum output power was 950 mW in nearly single mode and about 700 mW in single mode. Stable single mode operation was realized by employing an injection locking with a monolithic ring diode-laser-pumped Nd:YAG laser as a master laser.

#### ACKNOWLEDGMENT

The authors thank N. Kitabayashi of Japan Radio Company Ltd. for the loan of the laser beam measurement instrument. This work was supported by the Grant-in-Aid for Scientific Research (No. 04234204) from Ministry of Education, Science, and Culture of Japan.

#### REFERENCES

- [1] D. C. Gerstenberger, G. E. Tye and R. W. Wallace. *Opt. Lett.*, vol. 16, p. 992, 1991.
- [2] U. Johann and W. Seelert. *SPIE*, vol. 1522, p. 158, 1991.
- [3] T. Y. Fan, A. Sanchez and W. E. DeFeo. *Opt. Lett.*, vol. 14, p. 1057, 1989.
- [4] Y. Kaneda, M. Oka, H. Masuda and S. Kubota. *Opt. Lett.*, vol. 17, p. 1003, 1992.
- [5] T. J. Kane and R. L. Byer. *Opt. Lett.*, vol. 10, p. 65, 1985.
- [6] R. Scheps and J. Myers. *IEEE J. Quantum Electron.*, vol. 26, p. 413, 1990.
- [7] K. Wallmeroth and P. Peuser. *Electron. Lett.*, vol. 24, p. 1086, 1988.
- [8] K. Nakagawa, Y. Shimizu, T. Katsuda and M. Ohtsu. *SPIE*, vol. 1837, p. 40, 1992.
- [9] R. W. P. Drever, J. L. Hall, F. V. Kowalski, J. Hough, G. M. Ford, A. J. Munley and H. Ward. *Appl. Phys. B*, vol. 31, p. 97, 1983.
- [10] C. D. Nabors, A. D. Farinas, T. Day, S. T. Yang, E. K. Gustafson and R. L. Byer. *Opt. Lett.*, vol. 14, p. 1189, 1989.
- [11] K. Nakagawa, A. S. Shelkovnikov, T. Katsuda and M. Ohtsu. *Appl. Opt.*, to be published.
- [12] D. Golla, I. Freitag, H. Zellmer, W. Schone, I. Kropke and H. Welling. *Opt. Commun.*, vol. 98, p. 86, 1993.

# Ultranarrow $^{13}\text{C}_2\text{H}_2$ saturated-absorption lines at $1.5 \mu\text{m}$

M. de Labachellerie,\* K. Nakagawa, and M. Ohtsu

Graduate School at Nagatsuta, Tokyo Institute of Technology, 4259 Nagatsuta-cho, Midori-ku, Yokohama 227, Japan

Received December 14, 1993

The saturation spectroscopy of molecular transitions at  $1.5 \mu\text{m}$  is reported. We show that it is possible, with a low-power laser diode, to obtain 2-MHz-wide acetylene saturated-absorption lines, and we give what is to our knowledge the first experimental estimation of  $^{13}\text{C}_2\text{H}_2$  saturation intensity. To our knowledge, these lines are the narrowest reported  $1.5\text{-}\mu\text{m}$  frequency references and should be suitable for high-quality  $1.5\text{-}\mu\text{m}$  laser frequency standards.

In recent years there have been many studies devoted to the absolute frequency stabilization of  $1.5\text{-}\mu\text{m}$  laser diodes.<sup>1,2</sup> Such frequency stabilizations require absolute frequency references, which until now were obtained mainly by (i) atomic absorption lines from excited states that require preliminary pumping by an electric discharge<sup>2</sup> or another<sup>3,4</sup> laser or (ii) direct absorption of molecular gases from the ground state.<sup>1,5,6</sup> The  $10^{-10}$  frequency stability<sup>4,5</sup> obtained with Doppler-limited lines may be enough for several applications, such as wavelength dense multiplexing in optical fiber communications; however, even in that case a much better calibration standard is required.<sup>7</sup> Such a standard would also be useful for metrological applications in a wavelength region where no high-quality frequency reference is available. Although an important breakthrough was made recently with the detection of Doppler-free lines in electrically<sup>2</sup> or optically<sup>3,4</sup> pumped atomic lines, we now report, for the first time to our knowledge, laser-diode saturation spectroscopy of  $1.5\text{-}\mu\text{m}$  molecular lines that are expected to provide a narrower linewidth, a better signal-to-noise ratio, and a much larger number of reference lines.

Since  $1.5\text{-}\mu\text{m}$  molecular transitions usually involve overtone vibrational levels, their weak transition dipole moment  $d$  leads to a high saturation intensity, which is barely reached by the usual  $1.5\text{-}\mu\text{m}$  laser diodes. We first considered  $\text{C}_2\text{H}_2$ , which is an interesting candidate for frequency stabilizations near  $1.54 \mu\text{m}$ . From the spectroscopic point of view,  $1.5\text{-}\mu\text{m}$   $\text{C}_2\text{H}_2$  lines are similar to methane lines at  $3.39 \mu\text{m}$  (Ref. 8) (both are nonpolar light molecules with similar polarizability). Unlike atomic transitions, collisional relaxation processes should be dominant at low pressures, which leads to a potential linewidth well below 1 MHz. Since we study a low-pressure range for which the mean time between collisions is nearly equal to the interaction time, we can reasonably consider only two levels, whose effective lifetimes depend only on transit time and collisions.<sup>8</sup> The saturation intensity  $I_s$  for such a simple system is given by the basic expression<sup>9</sup>

$$I_s = \frac{\epsilon_0 c \hbar^2}{2d^2 T \tau}, \quad (1)$$

where  $T$  and  $\tau$  are the population and coherence lifetimes, respectively,  $\hbar$  is Planck constant,  $c$  is the speed of light, and  $\epsilon_0$  is the vacuum dielectric constant. For the  $P(12)$  line of the  $^{13}\text{C}_2\text{H}_2$  ( $\nu_1 + \nu_3$ ) vibrational band, the dipole moment  $d$  was estimated with previous linear absorption data: an absorption coefficient  $\kappa = 3 \times 10^{-3} \text{ cm}^{-1} \text{ Torr}^{-1}$  was measured for that level, which should contain 7.5% of the total population. The lifetimes are generally complicated functions of pressure  $p$  and transit time  $T_{tr}$ .<sup>8</sup> As only the pressure-broadening value  $C_p \approx 10 \text{ MHz/Torr}$  has been measured for such transitions, we assume<sup>9</sup> a linear dependence on pressure,  $(2\pi T)^{-1} \approx (2\pi\tau)^{-1} = C_0 + C_p p$ , where  $C_0$  has a weak dependence on pressure and may be assumed constant in our pressure range. Using our estimated values, we obtain numerically

$$I_s \text{ (W/m}^2\text{)} = 22 \times 10^6 [C_0 + 10p \text{ (Torr)}]^2. \quad (2)$$

In the case of a purely collisional regime (large beam diameter,  $C_0 = 0$ ), we find a saturation power of  $\sim 330 \text{ mW}$  for a  $440\text{-}\mu\text{m}$  beam diameter. It is thus necessary to achieve simultaneously a high-power beam, with a narrow linewidth, interacting with a low-pressure gas. Such conditions can be obtained with a buildup cavity, as shown below.

Our experimental scheme is presented in Fig. 1. We used a simple  $L = 20\text{-cm}$ -long confocal piezoelectric-tunable Fabry-Perot (FP) cavity. The cavity mode diameter is therefore equal to  $2W_0 = 440 \mu\text{m}$ , which was used in the above estimation. Both mirrors' reflectivity was  $R = 98\%$ , and their losses were estimated to be  $A = 0.5\%$ . The laser was a three-section multiple-quantum-well distributed-feedback (DFB)  $1.54\text{-}\mu\text{m}$  laser with a free-running submegahertz linewidth.<sup>10</sup> The laser output was coupled through an optical isolator to the FP cavity and frequency locked to the FP resonance by the FM sideband technique<sup>11</sup>: small FM sidebands at 5 MHz were added to the laser frequency through current modulation, and their detection in the FP reflected beam provided an error signal that was used to feed back the DFB laser current. A 500-kHz feedback bandwidth allowed us to reduce the error signal fluctuations to a quasi-white-noise spectrum, corresponding to a

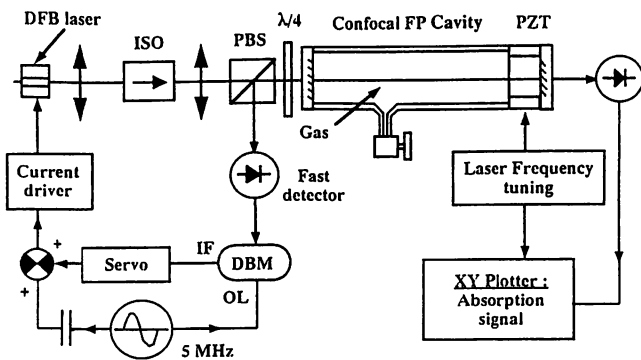


Fig. 1. Experimental setup: ISO, 60-dB isolator; PBS, polarizing beam splitter; PZT, piezoelectric transducer; DBM, double-balanced mixer; IF, intermediate frequency; OL, local oscillator.

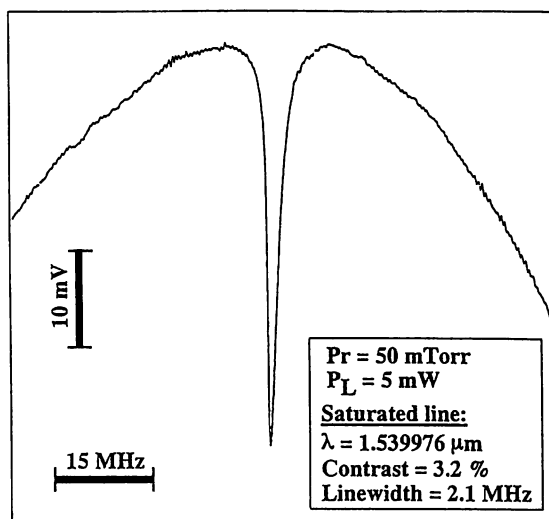


Fig. 2. Recorded saturated-absorption peak under medium conditions.

50-kHz laser frequency fluctuation relative to the FP resonant frequency. Therefore we can reasonably expect the laser linewidth to contribute to our spectral resolution for less than a few hundred kilohertz. The FP cavity was filled with  $^{13}\text{C}_2\text{H}_2$ , whose  $P(12)$  line at  $\lambda = 1.539976 \mu\text{m}$  was studied mainly for comparative measurements. From the measurement of the reflected FP spectral line, we estimated the laser power coupling coefficient into the FP cavity to  $\beta = 75\%$  and its finesse to be  $F \approx 120$ . Provided that the single-pass gas absorption  $\epsilon_a$  is low enough ( $p < 100$  mTorr), the finesse remains larger than 100, which leads to a 12-fold power enhancement inside the cavity. Therefore, with 8.5 mW of maximum available laser-diode power at the FP input,  $\sim 100$  mW of power can be obtained inside the FP cavity, which is enough to saturate the gas absorption efficiently. Another important feature of this setup is the detection sensitivity enhancement: owing to the FP finesse, the equivalent absorption length is  $\sim 100$  times longer than the FP cavity length, which significantly enhances the small absorption signal expected at such low gas pressures.

When locked to the FP resonant frequency, the laser frequency can be tuned only by the FP cav-

ity piezoelectric transducer. While sweeping the frequency, we directly recorded the FP transmitted power, using a standard InGaAs photodiode with a 5-k $\Omega$  load resistor and an XY plotter without any additional filtering. Even small variations of the intracavity absorption led to rather large variations of the transmitted power, which allowed us to record the Doppler profile even for very small pressures. On the top of the Doppler profile, a high-contrast  $\approx 2$ -MHz-wide saturated-absorption peak was obtained for low-enough gas pressures. An example is shown in Fig. 2, which shows what is to our knowledge the narrowest absolute reference line obtained at  $1.5 \mu\text{m}$ . It should also be noted that the signal-to-noise ratio seems to be quite good, even for a direct detection in a  $\approx 10$ -Hz bandwidth. We have successfully saturated several transitions of acetylene in our laser's tuning range (1538–1542 nm), which gave similar results. Then we measured the dependence of the  $P(12)$  line features on gas pressure and laser power. The observed 2-MHz saturation linewidth was almost independent of pressure and power conditions, which suggests that the linewidth is limited by another broadening mechanism, in which the contribution of transit time broadening  $[(2\pi T_{tr})^{-1} \approx 1 \text{ MHz}]$  may be the largest. The line contrast versus laser power and gas pressure is shown in Fig. 3; with the maximum theoretical value being 13.3%, it seems that this maximum was actually reached experimentally.

A long but straightforward calculation of the intensity  $I_t$  transmitted by the FP cavity at resonance shows that it depends on the single-pass gas absorption  $\epsilon_a = \kappa(p, \omega)L$ , with the amplification inversely proportional to the total cavity losses including  $\epsilon_a$ . When the laser frequency is tuned across the line, its variation is  $\Delta I(\kappa) = I_t(0) - I_t(\kappa)$ . The absorption change  $\delta\kappa$  that is due to saturation leads to a variation  $\delta I(\delta\kappa) = I_t(\kappa + \delta\kappa) - I_t(\kappa)$  of the transmitted intensity, and the line contrast  $C(p) = \delta I(\delta\kappa)/\Delta I(\kappa)$  is then given by

$$C(p) = \frac{\delta\kappa}{\kappa} \frac{2}{[1 + \rho_a(p)][2 + \rho_a(p)]}, \quad (3)$$

which is quite precise for  $\rho_a = \epsilon_a/(1 - R) \leq 1$ .

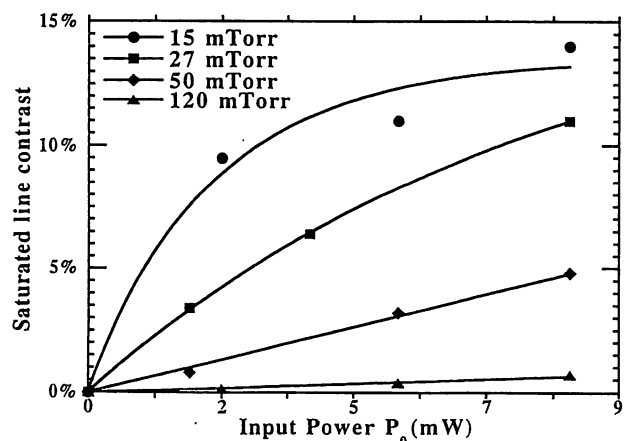


Fig. 3. Dependence of the line contrast on gas pressure and laser input power.

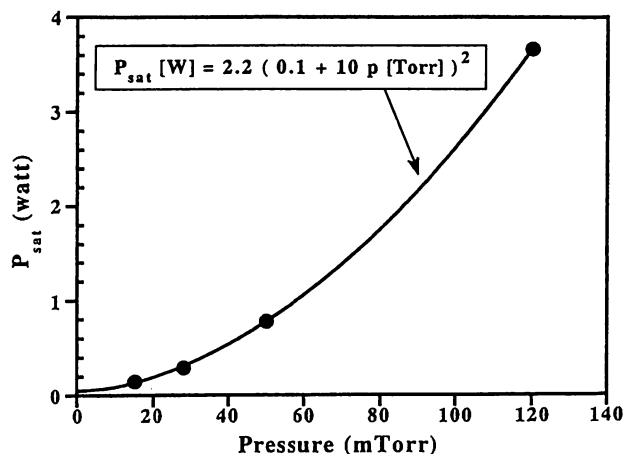


Fig. 4. Estimation of saturation power as a function of gas pressure.

The intracavity power  $P_{in}$  also depends on absorption losses and is given as a function of incident power  $P_0$  by

$$P_{in} = \beta T [F(p)/\pi]^2 P_0. \quad (4)$$

The cavity finesse was measured as a function of gas pressure, and the data were corrected with Eqs. (3) and (4). In case of small saturation, the value obtained for  $\delta\kappa/\kappa$  should be equal<sup>12</sup> to  $P_0/(2P_{sat})$ , which leads to the values of  $P_{sat}$  plotted in Fig. 4. The expression  $P_{sat} = 2.2(0.1 + 10p)^2$  was found to fit these values accurately. Assuming an average beam area of  $\pi W_0^2$ , the saturation intensity was estimated as

$$I_s (W/m^2) = 15 \times 10^6 [0.1 + 10p (\text{Torr})]^2, \quad (5)$$

which agrees quite well with the theoretical estimation obtained in Eq. (1). Although it remains approximate because it comes from a somewhat indirect measurement, Eq. (5) gives a useful practical expression for future designs.

Our experimental study provides what is to our knowledge the first saturated-absorption spectrum of acetylene at  $1.5 \mu\text{m}$  that was fully obtained with a laser diode, and the estimation of  $^{13}\text{C}_2\text{H}_2$  saturation intensity was found to agree quite well with a simple theoretical model. Such a method is suitable for high-resolution spectroscopic studies of  $1.5\text{-}\mu\text{m}$

molecular lines. The 2-MHz-wide lines obtained are to our knowledge the narrowest reported so far at  $1.5 \mu\text{m}$ . Although the influence of various effects affecting the line central frequency (pressure shifts, Stark shifts, etc.) should be studied now, we expect from the great similarity of  $\text{C}_2\text{H}_2$  and methane that these shifts can be reduced to very low levels<sup>8</sup> by a suitable design. Therefore our experiment opens the way to new possible optical frequency standards through a large improvement of present  $1.5\text{-}\mu\text{m}$  molecular frequency standards.

The authors thank H. Sasada for helpful discussions.

\*Permanent address, Laboratoire de l'Horloge Atomique, Centre National de la Recherche Scientifique, Bâtiment 221, Université Paris-Sud, 91405 Orsay, France.

## References

1. S. Sudo, Y. Sakai, H. Yasaka, and T. Ikegami, *IEEE Photon. Technol. Lett.* **10**, 281 (1989).
2. A. J. Lucero, Y. C. Chung, S. Reilly, and R. W. Tkach, *Opt. Lett.* **16**, 849 (1991).
3. M. Breton, P. Tremblay, N. Cyr, C. Julien, and M. Têtu, *Proc. Soc. Photo-Opt. Instrum. Eng.* **1837**, 134 (1992).
4. S. L. Gilbert, *Proc. Soc. Photo-Opt. Instrum. Eng.* **1837**, 146 (1992).
5. M. Labachellerie, C. Latrasse, K. Diomandé, P. Kemssu, and P. Cerez, *IEEE Trans. Instrum. Meas.* **40**, 185 (1991).
6. P. Bertinotto, *Proc. Soc. Photo-Opt. Instrum. Eng.* **1837**, 154 (1992).
7. D. J. E. Knight, P. S. Hansell, H. C. Leeson, G. Duxbury, J. Meldau, and M. Lawrence, *Proc. Soc. Photo-Opt. Instrum. Eng.* **1837**, 106 (1992).
8. V. A. Alekseev, M. A. Gubin, and E. D. Protsenko, *Laser Phys.* **1**, 221 (1991).
9. K. Shimoda, in *High-Resolution Laser Spectroscopy*, Springer Series in Applied Physics (Springer-Verlag, Berlin, 1976), pp. 1-49.
10. M. Okai, T. Tsushiya, K. Uomi, N. Chinone, and T. Harada, *IEEE Photon. Technol. Lett.* **3**, 427 (1991).
11. K. Nakagawa, M. Kourogi, and M. Ohtsu, *Opt. Lett.* **17**, 934 (1992).
12. V. S. Letokhov, in *High-Resolution Laser Spectroscopy*, Springer Series in Applied Physics (Springer-Verlag, Berlin, 1976), pp. 95-199.

TOWARD THE REALIZATION OF  
A PETA-HERTZ OPTICAL FREQUENCY SWEEP GENERATOR

M. Ohtsu<sup>1,2)</sup>, K. Nakagawa<sup>1,2)</sup>, M. Kourogi<sup>1,2)</sup>, and W. Wang<sup>1)</sup>

1) Graduate School, Tokyo Institute of Technology  
4259 Nagatsuta, Midori-ku, Yokohama 227, JAPAN

2) Kanagawa Academy of Science and Technology  
KSP West 614, Sakado, Takatsu-ku, Kawasaki 213, JAPAN

ABSTRACT

This paper reviews the authors' experimental works on realizing a Peta-Hz tunable range ( from UV to IR ) highly coherent optical frequency sweep generator by using semiconductor lasers, nonlinear optical crystals, and the technique of optical phase locking. Experiments on generations of second harmonics, sum/difference-frequencies, proposal and experiments on a highly accurate optical frequency chain, and the performance of a wide-span optical frequency comb generator are described. Especially for the optical frequency comb generator, a 4 Tera-Hz frequency span of the modulation sidebands is realized.

1. INTRODUCTION

Semiconductor lasers can be used as promising candidates of light sources for practical optical frequency conversion systems because of their inherent compatibility with electrical and optical feedback control[1]. Wideband frequency sweep can be realized by combining semiconductor lasers and nonlinear optical crystals because, as is shown by Fig.1, variety of semiconductor lasers, covering wide wavelength ranges, have been developed. Thus, it is expected that the range of frequency sweep, from near infrared to near ultraviolet (, i.e., approximately one Peta-Hz ) can be realized.

Although the method of Fig.1 does not represent that the frequency is swept continuously, a continuous frequency sweep can be expected if fine frequency tuning by heterodyne optical phase locking is auxiliarily employed to fill the gap of the frequency region in which the coarse sweep is not possible. This paper reviews authors' experiments on frequency conversion of semiconductor lasers by using nonlinear optical crystals, novel and accurate optical frequency chain and a wide span optical frequency comb generator, which are used to realize a Peta-Hz class coherent optical frequency sweep generator.

2. NONLINEAR FREQUENCY CONVERSIONS FOR WIDEBAND FREQUENCY SWEEP

Second harmonic, sum-frequency, and difference-frequency generations (, SHG, SFG, and DFG, respectively, ) play essential roles for wideband frequency sweep. Figure 2 shows that a  $\text{KNbO}_3$  crystal is installed in a built-up cavity for fundamental wave to increase the SHG efficiency. The FM noise of the fundamental wave is reduced by the optical feedback by the reflection from the front facet of the crystal[2]. The optical path length between the laser and the built-up cavity is controlled by negative electrical feedback to stabilize SHG power. The SHG power of 6.6 mW was obtained for the 100 mW

fundamental wave power from 0.86  $\mu\text{m}$ -wavelength AlGaAs laser.

As another example of nonlinear frequency conversion, SHG of a strained quantum well InGaAs/AlGaAs laser of 0.98  $\mu\text{m}$ -wavelength has been generated by using a  $\text{KNbO}_3$  crystal installed in a built-up cavity. The SHG power was 2 mW for the incident fundamental power of 70 mW. A white light beam can be obtained if this blue SH light is optically aligned with the green SH light beam from a semiconductor laser-pumped YAG laser and red beam from an InGaAlP laser. The conventional He-Cd white-color lasers can be replaced by this semiconductor laser-based white light source.

The SH wave of a 1.5  $\mu\text{m}$ -wavelength InGaAsP laser can be tuned to a  $\text{Rb}^{87}$  atomic resonance frequency, which can be used as an accurate frequency reference for AlGaAs lasers[3]. Thus, frequency accuracy and stability of the InGaAsP laser can be improved by locking its SH frequency to the  $\text{Rb}^{87}$ . The SH wave has been generated from a KTP crystal installed in a built-up cavity while the FM noise of a fundamental wave is further reduced by the optical feedback from the built-up cavity[4].

To extend the range of frequency sweep, SFG by using an InGaAsP laser and a 0.83  $\mu\text{m}$ -wavelength AlGaAs laser has been carried out with a KTP crystal to obtain the SF power of 230 nW[4], which is the first example of generating a green light by using semiconductor lasers. Although the green lights have been generated by nonlinear optical frequency conversions of solid-state lasers, their frequency cannot be swept for a wide range. On the other hand, the range of frequency sweep of the SF shown above can be as wide as about 30 THz (, i.e., the wavelength range of 0.53  $\mu\text{m}$  - 0.56  $\mu\text{m}$  ) because the oscillation wavelength of AlGaAs laser devices can cover the range from 810 to 890 nm.

DFG has also been carried out for a 1.5  $\mu\text{m}$ -wavelength InGaAsP laser and 0.77  $\mu\text{m}$ -wavelength  $\text{Ti:Al}_2\text{O}_3$  laser by using a KTP crystal. Under the phase-matching condition by adjusting the crystal angle, the 1.6  $\mu\text{m}$ -wavelength DF output power of about 2  $\mu\text{W}$  was obtained when the incident powers of the two lasers were 5 mW and 200 mW, respectively. Since the  $\text{Ti:Al}_2\text{O}_3$  laser can be replaced by an AlGaAs laser, the frequency sweep range of 42 THz, i.e., the wavelength range from 1.5 to 1.9  $\mu\text{m}$ , can be expected.

### 3. NOVEL OPTICAL FREQUENCY CHAIN

Figure 3 shows a novel and accurate optical frequency chain proposed by the authors in order to measure the resonant frequency of Ca spectral line ( $^3\text{P}_1 - ^1\text{S}_0$  at 657.459 nm-wavelength), which falls within the oscillation frequency range of InGaAlP lasers. It has been proposed that this spectral line can be used as a highly accurate frequency standard in the visible region because of its narrow natural linewidth, i.e., 400 Hz[5]. For the measurement of Ca resonant frequency, the frequency of an InGaAlP laser ( the laser #2 in this figure ) is locked to the Ca resonance frequency, and heterodyne-type optical phase locking is provided to the other commercially available InGaAsP lasers, AlGaAs lasers, and the outputs from the nonlinear optical crystals for frequency conversions. The frequency  $\nu_2$  of the laser #2, and thus, the resonant frequency of Ca, can be known accurately by using the following formula by measuring the output microwave frequencies  $f_k$  of the photo-diodes  $\text{PD}_k$  (  $k = 1 - 9$  ):

$$\nu_2 = 256mf_m - f_1 - 2f_2 + 4f_3 + 8f_4 + 16f_5 + 32f_6 + 64f_7 + 128f_8 - 256f_9, \quad (1)$$



where  $f_m$  and  $M$  represent the modulation frequency and the order of sideband in the optical frequency comb generator ( see next section ) which can be used as a local oscillator for measuring the 1.8 THz-frequency difference between the laser #3 ( 876 nm-wavelength ) and the laser #9 ( 872 nm-wavelength ). If a stable Rb atomic clock is used as a driver for the optical frequency comb generator, the order of sideband  $M$  has to be as high as 262 since the value of  $f_m$  is 6.8 GHz. However, this order of sideband can be generated and detected as will be described in the next section. Since all the frequencies of lasers in Fig.3 can be calibrated based on the Ca resonance frequency, this system realizes a highly accurate, multi-color coherent light source.

For realization of this system, several nonlinear frequency conversions have been already demonstrated. They are:

- (1) SHG of the 1.3  $\mu\text{m}$ -wavelength light by a KTP.
- (2) SFG of the two 0.8  $\mu\text{m}$ -wavelength lights by a  $\text{KNbO}_3$ .
- (3) SFG of the 1.3  $\mu\text{m}$ -and 0.74  $\mu\text{m}$ -wavelengths lights by a  $\text{KNbO}_3$ .

#### 4. OPTICAL FREQUENCY COMB GENERATOR

When the heterodyne frequency is as high as several THz, an additional optical local oscillator is required for the frequency measurement. This can be realized by an optical frequency comb ( OFC ) generator shown by Fig. 4. The OFC generator is a system for generating modulation sidebands, i.e., an optical frequency comb, by transmitting a laser beam through a phase modulator which is composed of an electro-optical crystal driven by a microwave with the stable frequency of  $f_m$ .

The main component of the highly efficient phase modulator in Fig. 4 is a  $\text{LiNbO}_3$  crystal which is installed in a Fabry-Perot cavity to realize a high modulation efficiency. This crystal is also enclosed by a microwave waveguide to build up a microwave power for modulation, where the waveguide is designed to realize a spatial overlap between the lightwave and microwave fields and to match the optical group velocity and microwave phase velocity in the crystal. By this configuration, modulation efficiency  $\theta$  as high as 0.2 radian has been achieved at the modulation frequency  $f_m$  of 5.8 GHz even by using a bulky  $\text{LiNbO}_3$  crystal. The value of  $f_m$  was fixed to  $3 \cdot \text{FSR}$ , where FSR is the free spectral range of the Fabry-Perot cavity. The finesse of this crystal-installed Fabry-Perot cavity was 200.

The OFC was generated by inputting a 10 kHz-linewidth DFB laser beam ( 1.5  $\mu\text{m}$ -wavelength ) to the cavity, and the heterodyne signal between one of the modulation sideband in the OFC and another 10 kHz-linewidth reference laser was detected. The signal-to-noise ratio  $S/N$  of this detection was high, i.e., only 5 dB lower than that of the shot noise-limited theoretical value, which is expressed as  $S/N$  ( in the unit of dB ) =  $75 - 0.11 \cdot |M|$ , where  $M$  is the order of sideband in the OFC. The maximum of the shot noise-limited value of  $M$ , corresponding to  $S/N = 0$  dB, is estimated to be 682, which gives the  $M f_m = 4$  THz. Figure 5 shows the obtained experimental results to confirm this estimation. This figure represents the profile of the envelope of the OFC, i.e., a series of modulation sidebands, observed by an optical spectrum analyzer. It was confirmed by this profile that the modulation sidebands were generated within the frequency range of  $\pm 2$  THz around the carrier component, and the profile of the envelope agreed with the theoretical calculation. The width of the profile, i.e., 4 THz, corresponds to the wavelength span as large as 32 nm, which is larger than the tunable wavelength range of existing DFB lasers. The

width of the envelope can be increased to 10 THz if the modulation index is increased to  $\pi/2$  radian by increasing the microwave power.

Experiments on heterodyne optical phase locking were carried out between the 84th sideband of the OFC generator and the reference laser[6]. Although the heterodyne frequency was 200 MHz, the separation between the carrier frequency of the modulated light and reference laser frequency was as large as 487 GHz, i.e., the carrier signal was optically phase-locked to the reference signal with such a large frequency separation. The control bandwidth of this phase locked loop was 250 kHz, and the phase error variance was estimated to be 0.01 radian<sup>2</sup>. The 3 dB-linewidth of the heterodyne signal spectral shape was 30 Hz, being limited by the resolution of the microwave spectrum analyzer, by which a high performances of the phase locking was confirmed.

The OFC generator described can be realized at a variety of wavelength regions by changing the high-reflection or anti-reflection films coated on the surfaces of the relevant optical elements as long as the phase modulator crystal is transparent. If a series of the OFC generators with different wavelength regions are prepared and the sidebands of the adjacent OFC generators are phase-locked with each other, a very wide span OFC is expected, which can be as wide as over 100 THz.

## 5. SUMMARY

This paper reviewed the authors' experimental works on realizing a Peta-Hz tunable range ( from UV to IR ) highly coherent optical frequency sweep generator by using semiconductor lasers, nonlinear optical crystals, and the technique of optical phase locking. Experiments on generations of second harmonics, sum/difference frequencies, proposal and experiments on a highly accurate optical frequency chain, and the performance of a wide-span optical comb generator, were described. By minor improvements of the system developed so far, realization of a Peta-Hz coherent optical sweep generator is expected in the near future.

## REFERENCES

- [1] M. Ohtsu, *Highly Coherent Semiconductor Lasers*, Artech House, Boston, 1992
- [2] T. Senoh, Y. Fujino, Y. Tanabe, M. Hirano, M. Ohtsu, and K. Nakagawa, "Direct modulation of blue radiation from frequency-doubled AlGaAs laser diode using the electro-optic effect in a KNbO<sub>3</sub> nonlinear crystal", *Appl. Phys. Lett.*, Vol.60, pp.1172-1174 (1992)
- [3] H. Furuta and M. Ohtsu, "Evaluations of frequency shift and stability in rubidium vapor stabilized semiconductor lasers", *Appl. Opt.*, Vol.28, pp.3737-3743 (1989)
- [4] W. Wang, K. Nakagawa, Y. Toda, and M. Ohtsu, "1.5 um diode laser-based nonlinear frequency conversions by using potassium titanyl phosphate", *Appl. Phys. Lett.*, Vol.61, pp.1886-1888 (1992)
- [5] J. Helmcke, A. Morinaga, J. Ishikawa, F. Riehle, *IEEE Trans. Instrum. and Meas.*, Vol.IM-38, pp.524 (1989)
- [6] M. Kourogi, K. Nakagawa, and M. Ohtsu, "Wide-Span Optical Frequency Comb Generator for Accurate Optical Frequency Measurement", *IEEE J. Quantum Electron.*, accepted for publication.

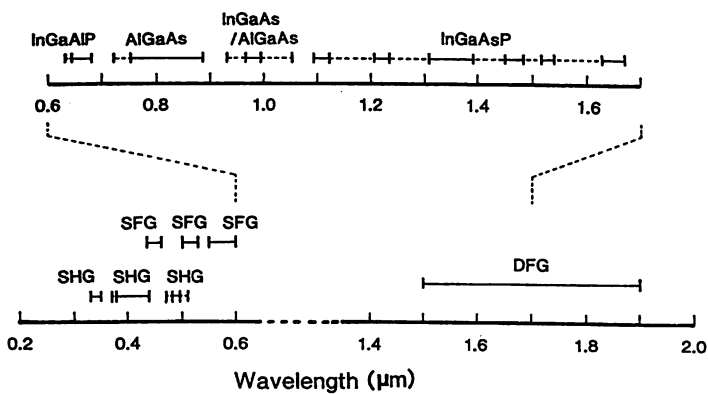


Fig.1  
Possible wavelength ranges of semiconductor lasers.

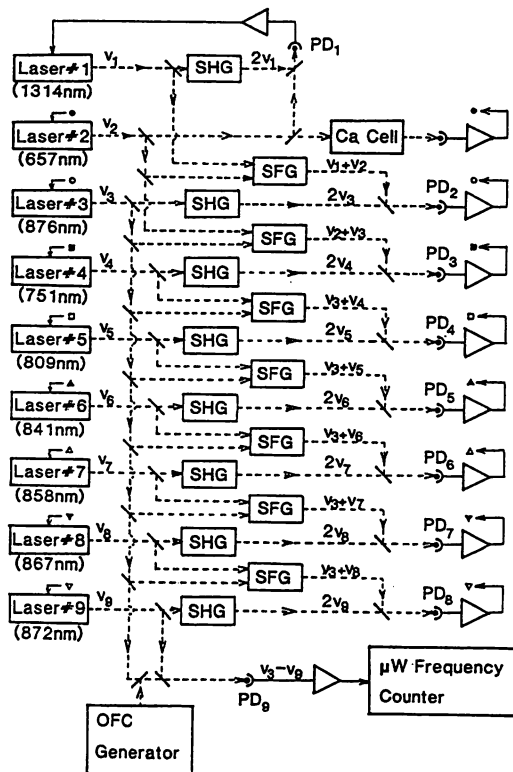


Fig.3  
Proposed system for measuring the resonant frequency of a Ca spectral line at 657 nm-wavelength.

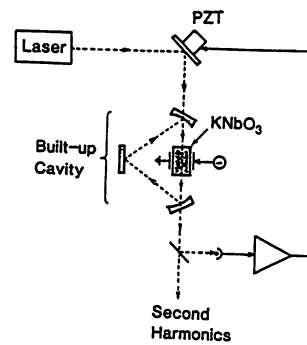


Fig.2  
Experimental setup of SHG of an AlGaAs laser by using a  $\text{KNbO}_3$  crystal which is installed in a build-up cavity.

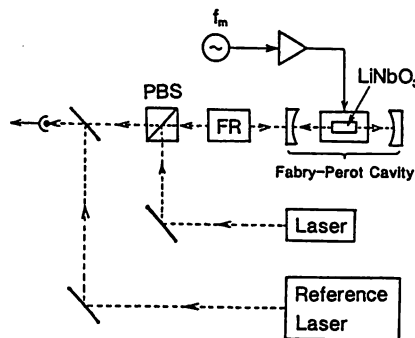


Fig.4  
Schematic explanation of an optical frequency comb generator.

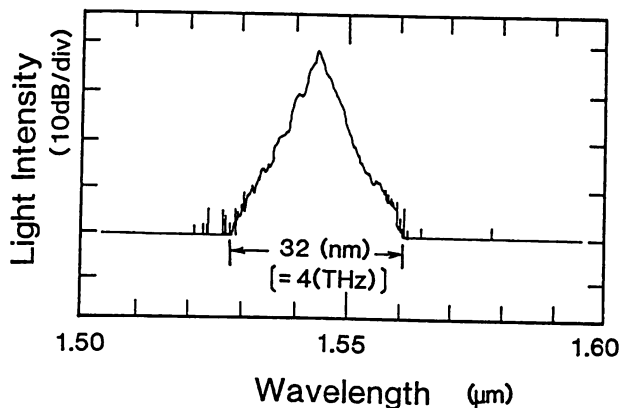


Fig.5  
The profile of the envelope of the modulation sidebands of the OFC generator.

## METROLOGICAL LASERS AROUND 1.5 $\mu\text{m}$ .

M.de Labachellerie, C.Latrasse

Laboratoire de l'Horloge Atomique/CNRS, Bat. 221, Université Paris-Sud, 91405 Orsay-Cedex, FRANCE

K.Nakagawa, M.Ohtsu

The graduate school at Nagatsuta, Tokyo Institute of Technology, Midori-ku, Yokohama 227, JAPAN

**Abstract :** Semiconductor laser are well suited to make optical frequency standards in the 1.3-1.5 $\mu\text{m}$  fiber optics communication band. We summarize the state of the art concerning this topic and demonstrate a new approach which consists in using saturated molecular absorption lines. This approach could lead to a lot of ultra stable frequency standards in the 1.5 $\mu\text{m}$  region.

### INTRODUCTION:

It has been reported in a recent review<sup>1</sup> that better than  $10^{-9}$  accuracy optical frequency standards are strongly needed in the 1.3-1.5 $\mu\text{m}$  optical communication bands for wavelength division multiplexed systems, the most urgently needed being 1.5 $\mu\text{m}$  standards. Moreover, the nice semiconductor laser sources which exist in this wavelength region are well suited to make precise optical frequency standards which are missing between 0.8 $\mu\text{m}$  possible Rubidium<sup>2</sup> or Cesium<sup>3</sup> standards, and the 3.39 $\mu\text{m}$  HeNe standard.

The main features that are required from frequency standards are: low laser linewidth, good frequency stability and good reproducibility. For practical use of a standard, it also very important to obtain a long-term reliable operation. Therefore, among all possible methods, only rugged and simple ones may lead to a real applicable standard.

Optical standards rely on absolute frequency references which are generally provided by resonant optical absorption lines in gases. Though plenty of absorption lines are available, the main problem is to find the simplest way to detect them with a high frequency discrimination, a high S/N ratio and a low sensitivity to external perturbations. The gas absorption is probed by a laser source whose intrinsic qualities are also important: its frequency should be tunable to the transition and, furthermore should be intrinsically stable enough to remain near the line without jumps on all its lifetime.

After a review of suitable 1.5 $\mu\text{m}$  lasers for frequency standards and the past work concerning their frequency stabilization, we will demonstrate that it is actually possible to get very narrow molecular lines in this wavelength region using a rather simple technique. This technique could lead to a new variety of ultra-stable lasers in the 1.2-1.6 $\mu\text{m}$  band.

### A - LASER SOURCES FOR 1.5 $\mu\text{m}$ FREQUENCY STANDARDS:

A 1.52 $\mu\text{m}$  laser light can be obtained from an HeNe laser, however, despite the recent detection of its Lamb dip<sup>4</sup>, a very narrow reference line has not been found in its oscillating bandwidth. Therefore, we can restrict our analysis to InGaAsP semiconductor lasers which are the most promising candidates because they can be tuned to almost any absorption line in the 1.2-1.6 $\mu\text{m}$  wavelength band. However, such lasers are generally multimode unless a spectrally selective element is used to select a single frequency. The spectral selection can be provided by an external grating<sup>5</sup> in the case of extended-cavity structures, or by a built-in grating in the case of DFB or DBR lasers. In the latter case, it is also necessary to reduce the large laser linewidth which may limit the detection of narrow spectral lines. We can thus retain only two candidates which are extended-cavity lasers and linewidth-narrowed DFB lasers.

Extended-cavity lasers: These lasers which have already demonstrated very large tuning capabilities (>100 nm) and low linewidth ( $\approx 50$  kHz) are thus well-suited to detect narrow absorption lines with a high resolution. We have been promoting them for a long time because of their great flexibility, however as they are quite sensitive to misalignments, it was not granted that their frequency could remain in the desired range without mode hops for

all their lifetime. A proper design<sup>6</sup> allowed us to make a laser source which could be tuned to the desired absorption line at construction, with all adjustments secured by glue, except for a grating rotation which provided the wavelength control. A key point was to design a PZT actuated 3Å tuning *without mode hops*<sup>7</sup> for this last movable part, in order to ensure a low probability of accidental frequency jumps. We verified experimentally that no jumps occurred, at least for several months: after initial setting, only the PZT actuated rotation was required to obtain the absorption frequency. This feature is of primary importance to enable actual stabilized lasers applications. The 1~2mW emitted power could also be increased using an injection locking technique: we have recently built a 40 mW low linewidth source with a 8 GHz tuning range without mode hops using a high power 1.5μm laser driven by an extended-cavity laser.

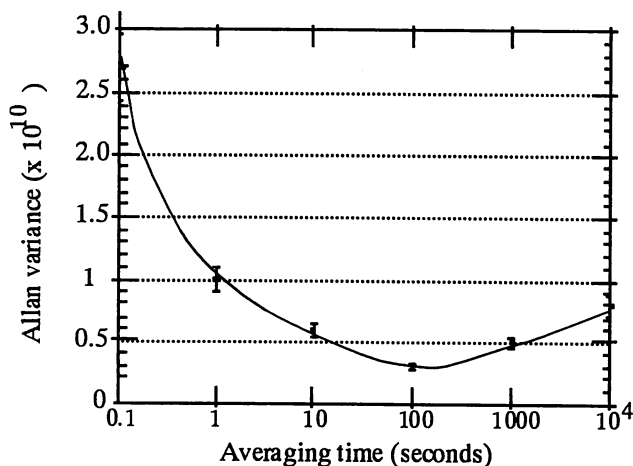
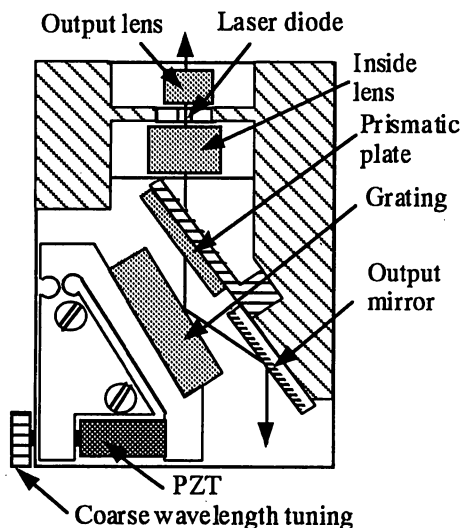


Fig. 1: Extended-cavity laser structure for a stabilization purpose and stability when locked to an  $\text{NH}_3$  line.

Linewidth narrowed DFB lasers: Unlike extended-cavity lasers, these sources are expected to have a very long-term modal stability because of their intrinsically stable built-in grating. Their much lower tuning range (a few nm) is quite inconvenient for laboratory use, but is not an obstacle for industrial development since the wavelength can be selected by the manufacturer. Their main drawback was a large linewidth, however, recent structural improvements<sup>8</sup> have led to sub-Megahertz linewidths which can easily be further narrowed by an electric correction using a Fabry-Perot cavity as the frequency discriminator. A 25 Hz linewidth<sup>9</sup> relative to the Fabry-Perot resonant mode has already been obtained (the laser linewidth is thus mainly determined by the cavity frequency fluctuations).

As a conclusion, well designed extended-cavity lasers are actually good candidates for laboratory frequency standards especially if DFB lasers are not available at the desired wavelength, however low linewidth DFB lasers are definitely the right choice for any practical application.

## **B - FREQUENCY STABILIZATION ON DOPPLER BROADENED LINES:**

Several attempts have been made in order to stabilize laser diodes frequencies to available molecular absorption lines such as  $\text{NH}_3$ <sup>6</sup>,  $\text{C}_2\text{H}_2$ <sup>10</sup>, or  $\text{HCN}$ <sup>11</sup>. The main advantage is that many regularly spaced isolated lines are available, however, these weak transitions does not allow to make very compact cells. Moreover, as only broad ( $\approx 500$  MHz) Doppler limited lines have been used, it is not possible to reach the  $10^{-12}$  order stability that is expected from high quality standards. Nevertheless, we have tested such a simple configuration which provided simultaneously a low linewidth and a  $\approx 10^{-10}$  stability<sup>6</sup> which was enough for an optical communication application. On the other hand, absorptions from excited atomic states pumped by an electric discharge such as Ar or Kr<sup>12</sup> can lead to very compact devices, however the electrical pumping noise may limit stability to even slightly lower values.

Nevertheless, depending on the desired wavelength, both solutions are expected to be industrially developed for medium stability applications which are the most widespread. However, a calibration standard at least two orders of magnitude better can only be provided by much narrower Doppler free lines.

### **C - DOPPLER FREE ATOMIC LINES:**

Doppler free lines are expected to be at least one order of magnitude narrower which could lead to the same improvement on a locked laser frequency stability. Moreover, the laser frequency modulation needed for line detection can be much smaller: it becomes therefore practically useless to spend so many efforts to minimize the residual laser modulation<sup>11</sup> which is actually cumbersome for many applications.

A recent major breakthrough was the detection of Doppler free lines in atomic gases using pumped excited states. Such lines have been obtained in Rubidium cell using a double resonance scheme<sup>13</sup>: a single atomic velocity class is pumped by a 780 nm laser, and only these atoms will absorb at 1.53 $\mu$ m which gives a Doppler free line whose center frequency depends on 780nm laser frequency. If the latter is locked to a 780nm saturated absorption line, the resulting  $\approx$  50MHz line becomes a 1.53 $\mu$ m narrow reference linked to the 780 nm line. Though rather complicated for a standard, this way can provide a link to other frequencies for calibration purposes. Another way of linking consists in locking the 1.5 $\mu$ m second harmonic to some strong atomic line in the 0.7-0.8 $\mu$ m band<sup>14</sup>.

The direct detection of saturated absorption lines in gases excited by electric discharge<sup>15</sup> is more interesting because of its simplicity: narrow  $\approx$  20MHz lines have been demonstrated, however, the effect of discharge pumping on the 1.5 $\mu$ m laser reference frequency can lead to a rather big noise and frequency shifts that are not very well studied up to now.

### **D- SATURATED ABSORPTION MOLECULAR LINES:**

We have demonstrated for the first time a quite simple way to detect molecular saturated absorption lines which can be easily used for a high quality frequency standard. The major problem was that the rather big power which was required to saturate such transitions could not be directly provided by usual laser diodes. We estimated that a 200 mW laser power with a 300 kHz linewidth was enough to obtain the <sup>13</sup>C<sub>2</sub>H<sub>2</sub> saturation intensity using a 200 $\mu$ m diameter beam (the <sup>13</sup>C isotope was chosen because our available laser diode could only be tuned to that isotope's stronger absorption lines). Among many possible solutions to increase optical power, we have decided to use a build-up Fabry Perot cavity in which the gas was inserted.

**Experiments:** A moderate finesse ( $F \approx 100$ ), 20 cm long confocal Fabry Perot cavity, tunable using a PZT element, was filled with a low pressure ( $\approx 50$  mTorr) <sup>13</sup>C<sub>2</sub>H<sub>2</sub> gas. Then, we locked the frequency of a sub-Megahertz linewidth DFB laser to the cavity resonance using a classical Pound-Dever<sup>9</sup> technique: the laser current was slightly modulated in order to add 5 MHz side bands to the laser frequency, and the beam reflected from the cavity was detected with a fast PIN photodiode and demodulated to provide the error signal. The locking bandwidth was large enough to obtain a laser linewidth reduction up to about 50 kHz (relative to FP resonance frequency). The laser frequency was thus following the cavity resonance frequency, which could be tuned using the PZT. The whole setup was compact enough to be mounted on a 400mmx300mm base plate.

**Results:** The absorption of the 1.539976 $\mu$ m line was detected by an ordinary PIN photodiode on the Fabry Perot transmitted beam without any other filtering than the XY recorder response time. With rather standard conditions (Pressure  $P_r = 50$  mTorr, Laser power  $P_L = 5$  mW at FP input), we observed a narrow ( $\approx 2$  MHz wide) saturated absorption line (fig.), with a contrast of several percent with respect to linear absorption and a good signal to noise ratio. In the best cases ( $P_r = 15$  mTorr,  $P_L = 8$  mW), the saturated absorption line contrast was as high as 14% with a 140 mV voltage depth and approximately the same 2 MHz linewidth.

**Discussion:** This good quality saturated absorption line is the narrowest reported so far at 1.5 $\mu$ m, however, as the natural linewidth of such transitions is expected to be much smaller, we are now investigating further narrowing. However, the method is simple and rugged enough in the present state to enable the development of an optical standard with a  $10^{-12}$  frequency stability. The reproducibility of such a standard will

depend on possible frequency shifts which should also be studied by comparing two identical stabilized lasers. The same method should be applicable to other  $C_2H_2$  lines and other molecules such as HCN, allowing to make many high quality frequency standards covering the 1.3 - 1.6  $\mu m$  range. The absolute frequency of such standards could be calibrated against other reference wavelengths, such as HeNe standards using recently proposed frequency chains<sup>16</sup>.

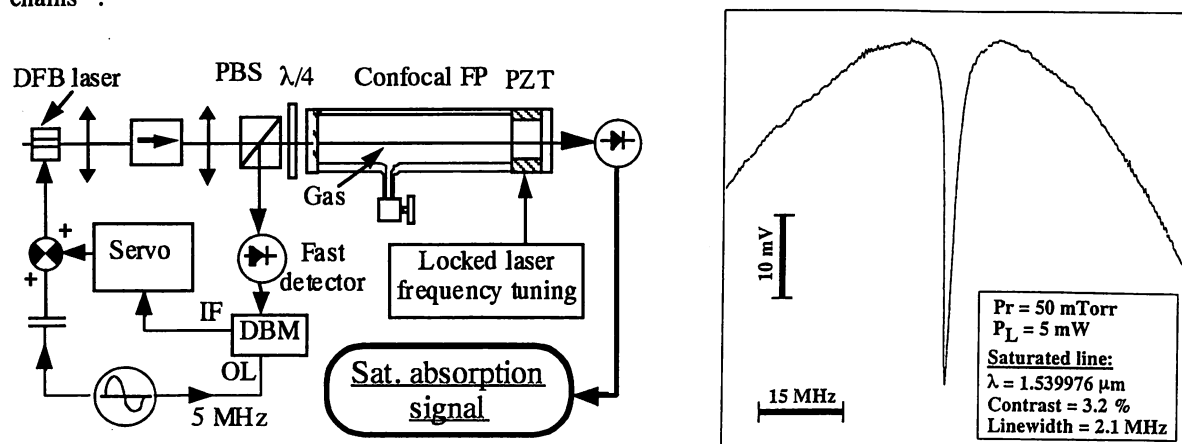


Fig. 2: Saturated absorption detection setup and detected line at  $\lambda = 1.539976 \mu m$ .

## CONCLUSION:

We have shown that most of the devices required to make high quality frequency standards at 1.5  $\mu m$  are now ready for a real development. DFB lasers will be mostly used, however extended-cavity lasers will prove their usefulness for particular wavelengths. Medium stability rugged standards will use molecular Doppler lines or discharge pumped atomic lines, and we hope that our recent detection of 2 MHz wide molecular saturated absorption lines will provide a convenient way to make high quality calibration standards around 1.3 or 1.5  $\mu m$ .

## References:

1. DJE Knight et Al., "A review of user requirements for, and practical possibilities for, frequency standards for the optical fibre communication bands", SPIE Proc. Vol. 1837, Boston, Nov.1992, pp. 106-114 ;
2. G.P. Barwood, P. Gill, W.R.C. Rowley, "Laser diode frequency stabilization to doppler-free rubidium spectra", Electronics Letters, Vol 24(13), June 1988, pp. 769-770 ;
3. M.de Labachellerie, P.Cerez, "Frequency locking of a 850 nm external-cavity semiconductor laser on a Doppler-Free Cs-D<sub>2</sub> line", SPIE Proc. Vol. 701, ECOOSA 86, Florence, Sept.1986, pp. 182-184 ;
4. H.Sasada, O.Kubota, "Lamb-dip stabilized 1.52  $\mu m$  He-Ne lasers", Appl.Phys. B55(2), August 1992, pp. 186-188 ;
5. M.W.Fleming, A.Mooradian, "Spectral characteristics of external-cavity controlled SC lasers", IEEE Journ. of Quantum Electron., Vol. 17, (1981), p.44 ;
6. M. Labachellerie, C. Latrasse, K. Diomandé, P. Kemssu, P. Cerez, "A 1,5 mm absolutely stabilized extended-cavity semiconductor laser", IEEE Trans. on Instr. and Meas., vol 40, n<sup>o</sup>2, Apr. 1991, pp. 185-190 ;
7. Olle Nilsson, E. Gobar, K. Vilhelmson, "Continuously Tunable External-cavity laser", Proc. ECOC 90, 16-20 Sept. 1990, Amsterdam, pp. 373-376 ;
8. K.Nakagawa, M.Kouroggi, M.Ohtsu, "Frequency noise reduction of a diode laser by using the FM sideband technique", Opt. Lett., Vol.17(13), July 1992, pp. 934-936 ;
9. S. Sudo, Y. Sakai, H. Yasaka, T. Ikegami, "Frequency stabilized DFB laser module using 1,53159  $\mu m$  absorption line of  $C_2H_2$ ", IEEE Photonics Technology Letters, Vol 1, n<sup>o</sup>10, Oct. 1989, pp. 281-284 ;
10. Satoshi Yoshitake, Koji Akiyama, Miyako Iritani, Hidekazu Murayama, "1.55  $\mu m$  Band Practical Frequency Stabilized Semiconductor Lasers Using  $C_2H_2$  or HCN Absorption lines", SPIE Proc. 1837, Boston, 1992, pp. 124-133 ;
11. Y.C.Chung, R.M.Derosier, H.M.Presby, C.A.Burrus, Y.Akai, N.Masuda, "A 1.5  $\mu m$  Laser Package Frequency-Locked with a Novel Miniature Discharge Lamp", IEEE Photonics Technology Letters, Vol 3, n<sup>o</sup>9, Sept. 1991, pp. 841-844 ;
12. M.Breton, P.Tremblay, N.Cyr, C.Julien, M.Têtu, "Observation and characterization of <sup>87</sup>Rb resonances for frequency locking purpose of a 1.53  $\mu m$  DFB laser", SPIE Proc. Vol. 1837, Boston, Nov.1992, pp. 134-143 ;
13. M. Ohtsu, E. Ikegami, "Frequency stabilization of 1,5  $\mu m$  DFB laser using internal second harmonic generation and atomic 87 Rb line", Electronics Letters, Vol 25 n<sup>o</sup>1, Jan. 1989, pp. 22-23 ;
14. A.J.Lucero, Y.C.Chung, S.Reilly, R.W.Tkach, "Saturation measurements of excited-state transitions in noble gases using the optogalvanic effect", Opt. Lett., Vol.16(11), June 1991, pp. 849-851 ;
15. M.Kouroggi, K.Nakagawa, C.H.Shin, M.Teshima, M.Ohtsu, "Accurate frequency measurement system for 1.55  $\mu m$  wavelength laser diode", Conf. of Laser and Electro Optics (CLEO91), Baltimore, (1991), Paper nbr. CThR57.

## Iodine absorption line stabilized frequency-tunable green light by sum-frequency generations of diode lasers

W. Wang<sup>1</sup> and M. Ohtsu<sup>1,2</sup>

<sup>1</sup>The Graduate School at Nagatsuta, Tokyo Institute of Technology,  
4259 Nagatsuta, Midori-ku, Yokohama 227, Japan.

<sup>2</sup>Kanagawa Academy of Science and Technology, KSP East, Rm 408, 3-2-1  
Sakado, Takatsu-ku, Kawasaki, 213, Japan.

To realize our intended diode-laser-based wideband coherent optical frequency sweep generator[1], various nonlinear frequency conversions have been carried out by using diode lasers in KTP crystal[2][3]. In addition to extending the tunable frequency output span through these frequency conversions, a continuous tuning scheme which utilizes the heterodyne optical phase locking and an optical frequency comb generator was also proposed[3]. In this paper, we demonstrate, for the first time, the systematic operation of a precision frequency-tunable light source which contains a molecular absorption line stabilized frequency reference and a tunable output in the green light region by using the sum-frequency generations of diode lasers in KTP crystals.

The coherent green lights in the region of  $0.52\sim 0.54\mu\text{m}$  were generated by using AlGaAs single-mode lasers at  $0.78\mu\text{m}$  and  $0.82\mu\text{m}$  and an InGaAsP multi-electrode DFB laser at  $1.54\mu\text{m}$ . Type-II, angle phase-matching for the sum-frequency generation was employed at room temperature. The measured maximum output power was  $0.32\mu\text{W}$  when the two fundamental powers from AlGaAs and InGaAsP lasers were 50 and 40 mW, respectively. Since the molecular iodine ( $\text{I}_2$ ) has a plenty of absorption lines in this region[4], a 15-cm long  $\text{I}_2$  cell was used for observation of the absorption spectra and frequency stabilization. After observing the absorption spectra at both  $0.52$  and  $0.54\mu\text{m}$ , the following experiment was carried out by using  $0.82\mu\text{m}$  and  $1.54\mu\text{m}$  lasers. Although two fundamental lasers are involved in the sum-frequency generation, the frequency stabilization of the generated light by controlling only one laser is still possible[5]. The linear absorption resonance was used for locking the frequency of the green light. The used resonance had a width of 1.5 GHz at  $24^\circ\text{C}$  and 1.2 GHz at  $6^\circ\text{C}$ , implying that the collision broadening due to buffer gases inside the cell was the main limit to reduce the profile width. Such a broad resonance, in other sense, ensures a wide locking range in stabilization of the sum-frequency by controlling only one fundamental laser. By using the conventional phase-sensitive detection technique, the error signal from a lock-in amplifier was feedback to the injection current source of the AlGaAs laser to lock the frequency at the top of the resonance, while the  $1.5\mu\text{m}$  laser was in free-running that offered a freedom for other frequency link[6]. The residual frequency



fluctuation was estimated to be  $\pm 0.5$  MHz from the error signal.

To obtain a precision frequency-tunable output, a second  $0.82\mu\text{m}$  AlGaAs laser was used to be mixed with the  $1.54\mu\text{m}$  laser beam for the first sum-frequency generation, and the green light with an independent output frequency was obtained through a second KTP crystal. This second green light was tunable and the frequency interval between its frequency and the reference frequency (the first green light) was precisely measured by the heterodyne beat signal between the two green lights or the two  $0.82\mu\text{m}$  lasers. It is clear, if these two  $0.82\mu\text{m}$  lasers are linked by an optical frequency comb generator whose span of the sidebands can be as wide as terahertz[7], the precision frequency-tunable range which is limited only by the span of the comb's sidebands, is thus expected to be several terahertz. Because such a scheme is also feasible for other frequency region, a diode-laser-based wide-band precision frequency-tunable system is reasonable in the whole region covered by the nonlinear frequency conversion of diode lasers.

As an application of our system, the two green lights, which passed through the  $\text{I}_2$  cell and were spatially separated, were tuned to different absorption resonances to show this method provides a possibility of precise measurement of the resonance spacings especially for molecular lines which exist in a large frequency range.

## References

- [1] M. Ohtsu, K. Nakagawa, C-H Shin, H. Kusuzawa, M. Kourogi, H. Suzuki, *CLEO'90 (Optical Society of America, Washington, DC, 1990)* paper CME5.
- [2] Weizhi Wang, Kenichi Nakagawa, Yasunori Toda, and Motoichi Ohtsu, *Appl. Phys. Lett.* 61, 1886(1992).
- [3] Weizhi Wang and Motoichi Ohtsu, *Opt. Lett.* 18, 876(1993).
- [4] A. Arie, S. Schiller, E. K. Gustafson and R. L. Byer, *Opt. Lett.* 17, 1204(1992).
- [5] K. Sugiyama and J. Yoda, *Opt. Commun.* 95, 77(1993).
- [6] W. Wang, A. M. Akul'shin, and M. Ohtsu, to be submitted to *Opt. Lett.*
- [7] M. Kourogi and M. Ohtsu, *IQEC'92 (American Physical Society and European Physical Society, June 1992, Vienna, Austria)*paper TuM5.

## Frequency Stabilization of a $1.5\mu\text{m}$ LD by using a Nonlinear Optical Frequency Conversion in an Organic Fiber

Yasunori Toda<sup>1)</sup>, Takashi Enami<sup>1)</sup> and Motoichi Otsu<sup>1)2)</sup>

1)Interdisciplinary Graduate School of Science and Engineering, Tokyo Institute of Technology, 4259 Nagatsuda, Midori-ku, Yokohama, Kanagawa 227, Japan.

2)Kanagawa Academy of Science and Technology, KSP East Rm 408, 3-2-1 Sakado, Takatsu-ku, Kawasaki, 213, Japan.

There has been much interest in frequency doubling devices by using organic materials. In the case of second harmonic(SH) generation by using a waveguide, Cerenkov radiation type of phase matching (CRPM) has advantage of its intrinsic phase matching capability and wide pass band width of fundamental frequency . A 3,5 - dimethyl - 1 - (4 - nitrophenyl) - pyrazole (DMNP) crystal is one of the developed materials and is suitable for CRPM device[1].

On the other hand,  $1.5\mu\text{m}$  diode lasers are widely used as the light sources for the coherent optical communication systems, and the frequency stabilization of these lasers is an important technique to be developed. By using the SH generation, the  $1.5\mu\text{m}$  diode laser frequency can be stabilized to be locked the center of the Rb spectral line which can be used as a stable and accurate frequency reference at  $0.78\mu\text{m}$  wavelength region[2]. In this paper, we demonstrate, for the first time, the SH generation of  $1.5\mu\text{m}$  diode lasers in CRPM - DMNP crystal cored fiber, and stabilization of the fundamental frequency by locking it to the Rb spectral line .

The experimental setup for stabilizing laser frequency is shown in Fig.1(a). In order to obtain higher power for the frequency conversion, injection locking was used for fundamental light source. Under injection locking, the output power is 15mW with a side-mode suppression ratio of 35dB and a locking-range of 8GHz. The schematic explanation of SH generation is shown in Fig.1(b). The DMNP fiber is a single mode fiber with a cladding of super fritt glass(SF15 ). The core diameter and the length were  $1.25\mu\text{m}$  and 5mm, respectively. Under the CRPM condition, the cross sectional profile of SH beam power is conical , which can be collimated by an axicon lens to get high efficiency of focusing. After this collimation, the SH wave was passed through a compact glass cell of Rb atomic vapor, and detected by a Si photodiode. The maximum power of the generated SH wave was 53nW. The SH generation in CRPM organic materials by using  $1.5\mu\text{m}$  diode laser is reported, to our knowledge, for the first time.

Figure.2(a) shows the first derivative signal of the Rb-D2 spectral line, monitored by SH wave. The frequency of the SH wave was locked to the transition spectral line from the  $F=3$  to the excited states of the Rb85 by closing the feedback loop of Fig.1(a). Figure.2(b) shows temporal variation of the error signal from the lock-in amplifier which represents the fluctuation of the laser frequency. When the feedback loop was closed, the fluctuation reduced to less than 0.3MHz over 1 hour. This confirms that the SH generation in CRPM organic cored fiber is one of the promising method for the stabilization of the diode laser frequency at  $1.5\mu\text{m}$ .

### Acknowledgments

The authors would like to thank K.Kamiyama, N.Nozaki and K.Kubo for their useful discussions and comments on the organic cored fiber.

### References

- [1]A. Harada, Y. Okazaki, K. Kamiyama, and S. Umegaki, Appl. Phys. Lett. 59, 1535 (1991)
- [2]M.Ohtsu and E. Ikegami, Electron. Lett. 25, 22 (1989)

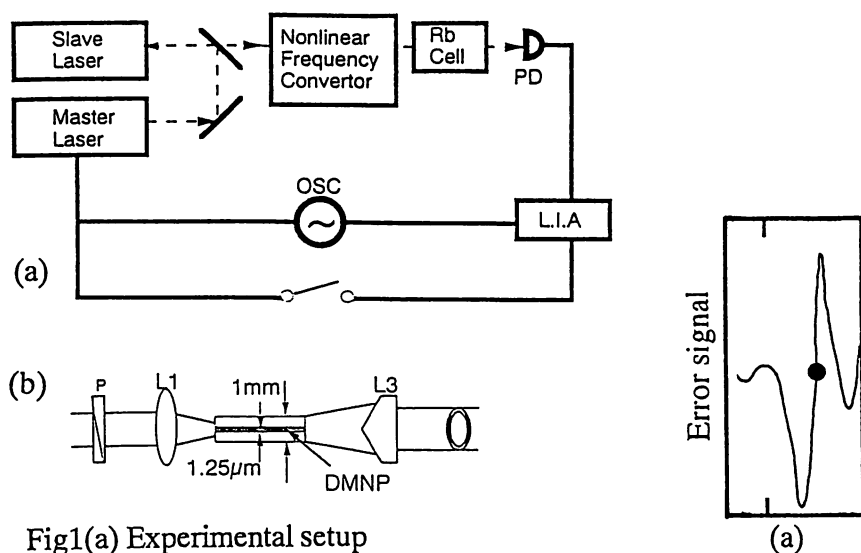


Fig1(a) Experimental setup for stabilizing laser frequency.  
(b) The schematic explanation of SH generation.

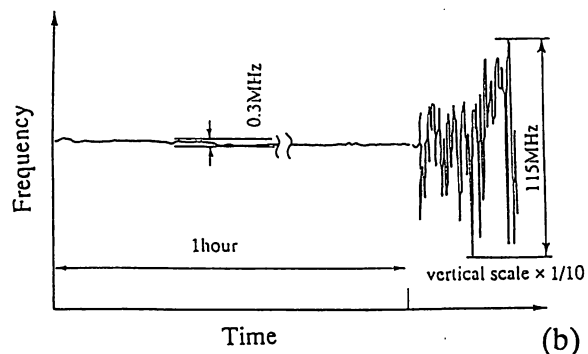


Fig2(a)The First derivative signal of the Rb-D2 spectral line.Filled circle is lock point.  
(b)Fluctuation of the laser frequency.

COMPUTER-CONTROLLED NARROW-LINEWIDTH AND FREQUENCY-STABILIZED  
AlGaAs LASER SYSTEM WITH UNMODULATED OUTPUT

J. KAWAKAMI<sup>1</sup>, M. KOUROGI<sup>2,3</sup>, and M. OHTSU<sup>2,3</sup>

- 1) Main Research Laboratory, NIKON Corporation  
1-6-3 Nishi-Ohi, Sinagawa, Tokyo 140, Japan
- 2) Interdisciplinary Graduate School of Science and  
Technology, Tokyo Institute of Technology,  
4259 Nagatsuta, Midori-ku, Yokohama 227, Japan
- 3) Kanagawa Academy of Science and Technology,  
KSP East, Rm408, 3-2-1 Sakado, Takatsu-ku, Kawasaki 213,  
Japan

A narrow-linewidth semiconductor laser system at 780nm wavelength was developed whose frequency was locked to a saturation absorption resonance frequency of rubidium ( $^{87}\text{Rb}$ ) without modulating the output power and frequency. Optical feedback from an external Fabry-Perot cavity was employed to reduce the linewidth of the laser. The cavity length was varied to tune the optically feedback laser frequency to the  $^{87}\text{Rb}$  saturation absorption resonance. The third derivative of the saturated absorption spectral profile in  $^{87}\text{Rb}$  was used as a frequency demodulator for frequency locking, for which the Zeeman modulation was employed to keep the output power and frequency unmodulated. Figure 1 shows the square root of the Allan variance, representing the magnitude of residual frequency fluctuations. This was measured by heterodyning two independently stabilized lasers. Its minimum was  $2.1 \times 10^{-12}$  at the integration time of 300 s. The full linewidth at the half maximum of the field spectrum was measured to be narrower than 170 kHz by using a delayed self-homodyne method. Computer-control program was developed for automatic optical feedback by an external cavity and frequency locking to the  $^{87}\text{Rb}$  line. It took about eight minutes to complete all the steps of the procedure for computer-controlled automatic frequency

locking. Furthermore, the reproducible frequency locking to the  $j$  component of the Rb saturated absorption lines was realized without inducing mis-locking to other spectral components.

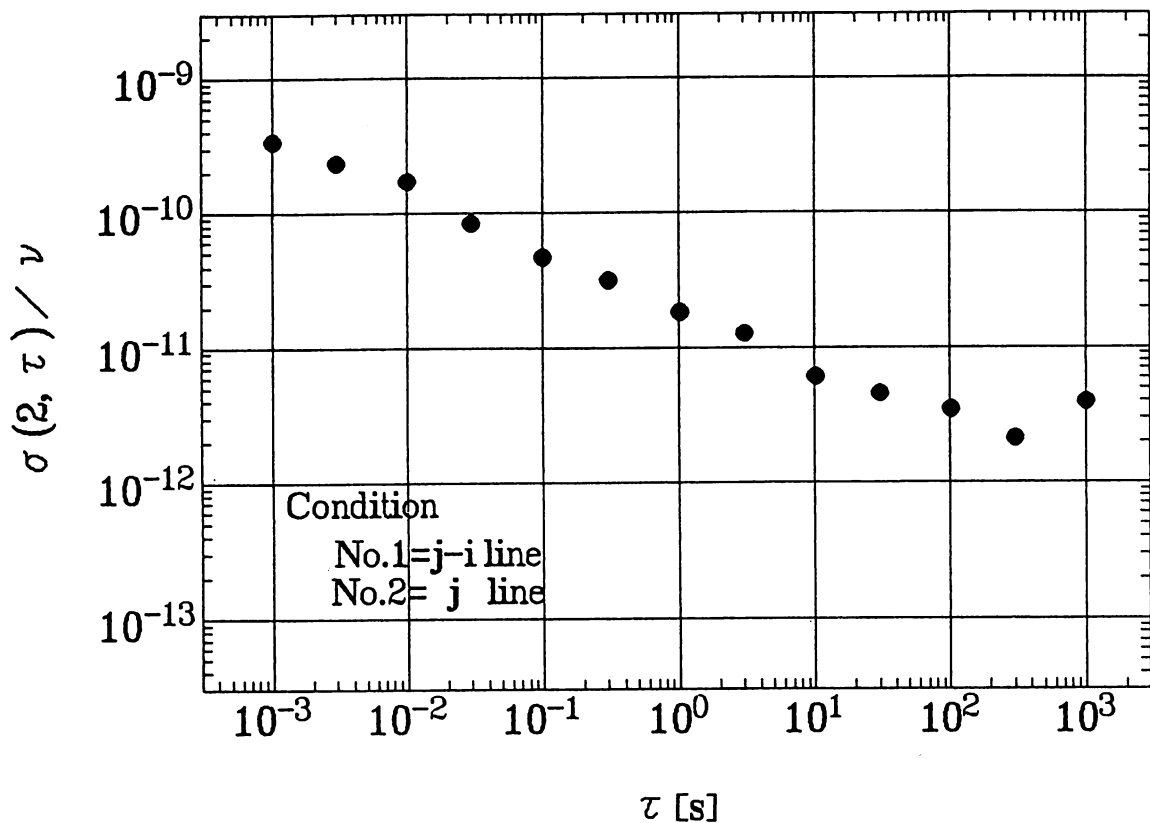


Fig. 1. The square root of the Allan variance.

## Frequency stabilized diode-pumped Nd:YAG lasers and its applications

K. Nakagawa<sup>1,2</sup>, A. S. Shelkownikov<sup>1</sup>, T. Katsuda<sup>1</sup>, and M. Ohtsu<sup>1,2</sup>

<sup>1</sup>Interdisciplinary Graduate School of Science and Engineering,  
Tokyo Institute of Technology, Yokohama, Japan

<sup>2</sup>Kanagawa Academy of Science and Technology, Kanagawa, Japan

Frequency stabilized lasers are required in many fields as, high resolution spectroscopy, optical frequency standards, and gravitational wave detection. Gravitational wave detectors based on a laser interferometer require ultra low frequency noise ( $\sim 10^{-6} Hz/\sqrt{Hz}$ ) of the laser. Recently low frequency and amplitude noise diode-pumped Nd:YAG lasers have been developed, and narrow linewidth and low frequency noise were demonstrated using an active frequency stabilization<sup>1,2,3</sup>. The real frequency stability of these lasers has not been well examined yet. Here we report the performance of frequency stabilization of diode-pumped Nd:YAG lasers. In our previous experiment<sup>4</sup>, using a high finesse ( $\sim 20000$ ) optical cavity as a frequency reference, we stabilized the diode-pumped monolithic Nd:YAG laser (Lightwave Model 122-300) and obtained low frequency noise ( $1.5 \times 10^{-3} Hz/\sqrt{Hz}$ ) estimated from the servo error signal<sup>4</sup>. The feedback bandwidth was limited to be about 30 kHz due to the mechanical resonance of the piezoelectric transducer (PZT) bonded to the Nd:YAG crystal. To extend the feedback bandwidth, we employed the external electro-optic (E/O) phase modulator (LiNbO<sub>3</sub>,  $2 \times 2 \times 20$ mm) for the fast phase correction<sup>5</sup>. Figure 1 shows the frequency noise spectrum estimated from the error signal with (upper trace) and without (lower trace) this fast phase correction. The frequency noise is reduced to less than  $10^{-4} Hz/\sqrt{Hz}$  at the frequency lower than 10 kHz. The residual frequency noise was mainly determined by the thermal noise of the preamplifier. The shot noise limited frequency noise level was estimated to be about  $3 \times 10^{-4} Hz/\sqrt{Hz}$ .

To estimate the real frequency noise, we measured the beat signal between two lasers locked on two independent cavities<sup>6</sup>. Both cavities are suspended in the vacuum chambers by five wires. Figure 2 shows the typical beat spectrum. The linewidth is estimated to be less than 30 Hz which is an instrument resolution bandwidth. More narrower linewidth cannot be easily detected due to the drift of the beat frequency ( $\sim 50 Hz/s$ ). The frequency noise at the Fourier frequency 1 kHz is estimated to be less than  $0.5 Hz/\sqrt{Hz}$ .

We also measured the Allan variance of this beat frequency. The minimum square root of the variance is about 16 Hz or  $\sigma_y(\tau) = 6 \times 10^{-14}$  at  $\tau = 0.01s$ . At  $\tau > 0.1s$ , this variance increases mainly due to the thermal drift of the cavity length. To improve the long term stability, we plan to use a molecular absorption line at  $1.064\mu m$  as an absolute frequency reference. Available molecules are CO<sub>2</sub><sup>7</sup>, C<sub>2</sub>H<sub>2</sub>, H<sub>2</sub>O, so on. It is possible to detect these relatively weak absorption lines using an external high finesse cavity.

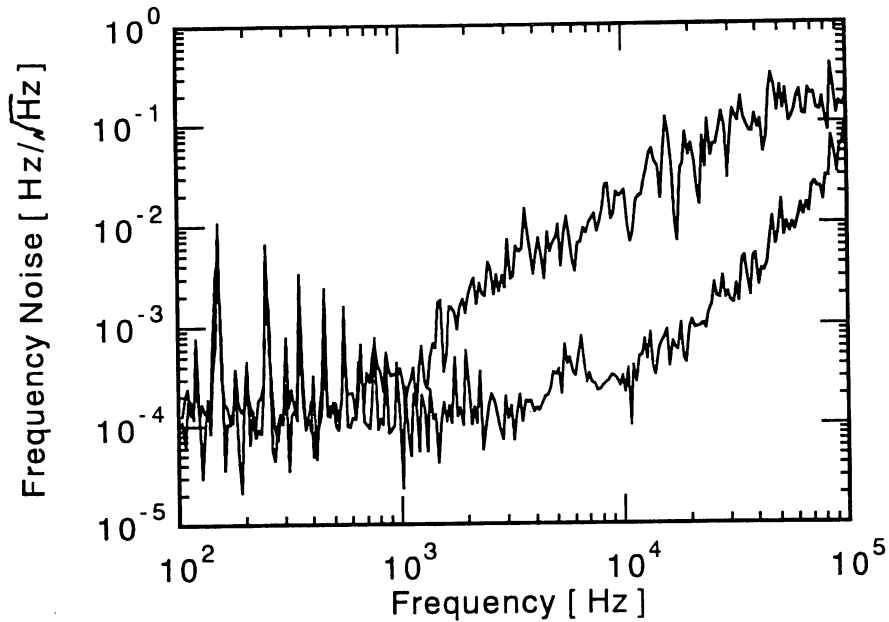


Fig.1 Frequency noise spectrum.

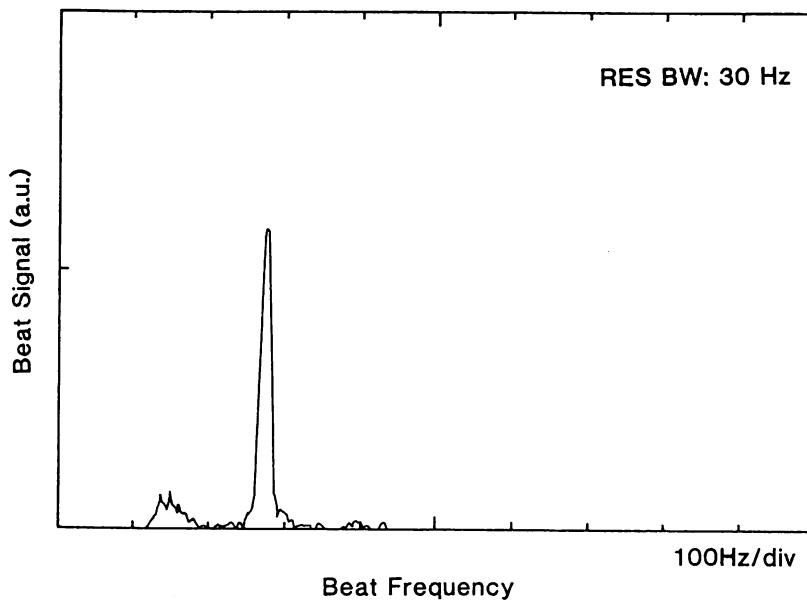


Fig.2 Beat signal between two stabilized lasers.

## References

- 1) D. Shoemaker, A. Brillet, C. N. Man, O. Cregut, and G. Kerr, *Opt. Lett.* **14**, 609(1989).
- 2) T. Day, E. K. Gustafson, and R. L. Byer, *IEEE J. Quantum Electron.* **28**, 1106(1992).
- 3) N. Uehara, K. Ueda, *Opt. Lett.* **18**, 505(1993).
- 4) K. Nakagawa, Y. Shimizu, T. Katsuda, M. Ohtsu, *SPIE Vol.* **1837**, 40(1992).
- 5) J. L. Hall, T. W. Hänsch, *Opt. Lett.* **9**, 502(1984).
- 6) N. M. Sampas, R. Liu, E. K. Gustafson, and R. L. Byer, *SPIE Vol.* **1837**, 278(1992).
- 7) P. Fritschel and R. Weiss, *Appl. Opt.* **31**, 1910(1992).

## Monolithic Optical Frequency Comb Generator for Optical Frequency Difference Measurement

M. KOUROGI<sup>(1)(2)</sup>, T.ENAMI<sup>(1)</sup> and M. OHTSU<sup>(1)(2)</sup>

(1)Interdisciplinary Graduate School of Science and Engineering of Tokyo Institute of Technology, 4259 Nagatuta, Midori-ku, Yokohama, Kanagawa 227 Japan. Phone: +81-45-922-1111 ex.2526,Fax+81-45-921-1156

(2)Kanagawa Academy of Science & Technology, KSP East Building, Room 408, 3-2-1 Sakado, Takatsu-ku, Kawasaki, Kanagawa 213 Japan. Phone: +81-044-819-2071,Fax+81-044-819-2072

Highly accurate laser frequency measurement which directly measures the absolute optical frequency is an essential technique for industrial applications such as coherent optical communication systems and for precision physical measurements such as standard of length and Rydberg constant measurements. These systems require frequency difference measurements to determine the arbitrary frequencies of lasers which are spaced in a span as wide as several THz. However it is difficult to measure such a high frequency difference. In order to overcome this difficulty, we have recently proposed a highly accurate, and wide span optical frequency difference measurement system [1] using an optical frequency comb (OFC) generator. We have also reported experimental results [2][3] of the proposed frequency difference measurement system using an electro optic (EO) phase modulator installed in an Fabry-Perot cavity [4] as an OFC generator, and have confirmed the OFC generation with the span of 4 THz. Furthermore, we have shown that a 4 THz frequency difference can be measured, and have demonstrated a heterodyne optical phase locking with a heterodyne frequency of 0.5THz.

In this presentation, we report the experimental results of a monolithic OFC generator which was developed by using an improved bulk type EO phase modulator with high reflection coatings (99%) on the both ends of the EO crystal ( $\text{LiNbO}_3$ ,  $1.25 \times 1.0 \times 23.4 \text{ mm}^3$ ), i.e., the EO phase modulator constructed a Fabry-Perot cavity at the same time. The modulation frequency and the modulation index of the OFC generator as a EO phase modulator were 5.870GHz and  $0.22\pi$ radian, respectively. The finesse and the efficiency of the OFC generator as a Fabry-Perot cavity were 250 and  $\cong 50\%$ , respectively. The advantages of the monolithic OFC generator are given in the followings. (1)The OFC generator become compact. (2)The OFC can be generated with wider span. The reason why the advantage of (2) is expected is that the optical loss in the Fabry-Perot cavity is reduced. Figure shows the envelope of the OFC spectrum generated by the monolithic OFC generator. In this figure, the center wavelength is fixed to the value of the wavelength of the



laser which was used for the optical frequency comb generation. It is seen from this figure that the envelope extended to a width as wide as 48nm (or 6.1THz). This value is 1.5 times as wide as the value reported in Ref.[2][3]. To our knowledge, this value is the widest span of an OFC generated by EO modulation. The number of the sidebands corresponding to the width is larger than 1000. Because the measurement of the optical beat signal, which is used for the proposed frequency difference measurement, is more sensitive than the measurement using an optical spectrum analyzer, it is possible to detect higher order sidebands which have not been observed with the optical spectrum analyzer.

We also report here about the monolithic OFC generator using a waveguide type EO phase modulator.

[References]

- [1]M.Kouroggi, K.Nakagawa, C.H.Shin, M.Teshima, and M.Ohtsu, in Proc. Conf. on Lasers and Electro-Opt., Baltimore, May 1991, paper number CThR57.
- [2]M.Kouroggi and M.Ohtsu, in Proc. SPIE's OE/Technology, Boston, November 1992, paper number 1837-27.
- [3]M.Kouroggi, K.Nakagawa, and M.Ohtsu, "Wide-Span Optical Frequency Comb Generator for Accurate Optical Frequency Difference Measurement", IEEE J. Quantum Electron., (1993) October issue.
- [4] T.Kobayashi, T.Sueta, Y.Cho and Y.Matsuo, Appl. Phys. Lett., vol. 21 pp.341-343, 1972.

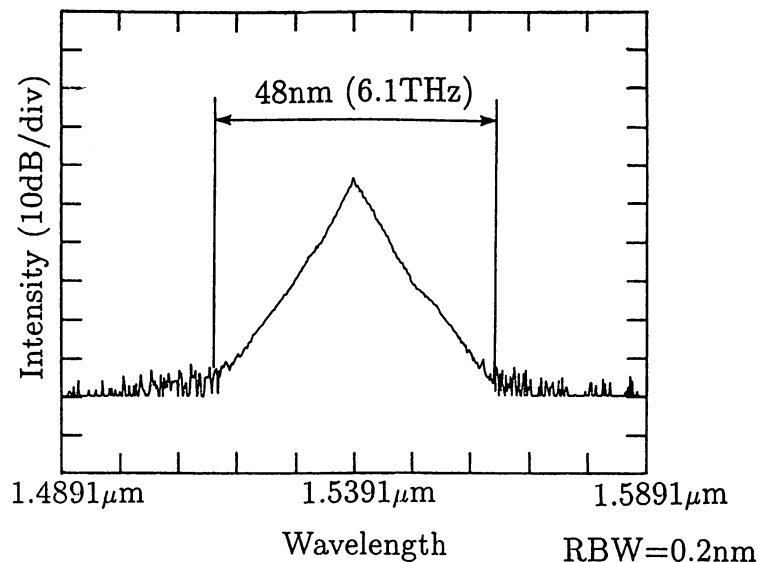


Fig.1 Experimental results of the spectral envelope of the OFC. This envelope was observed by an optical spectrum analyzer.

## Development of LD Sources for Studies of Sr Ions Confined in R.f.trap

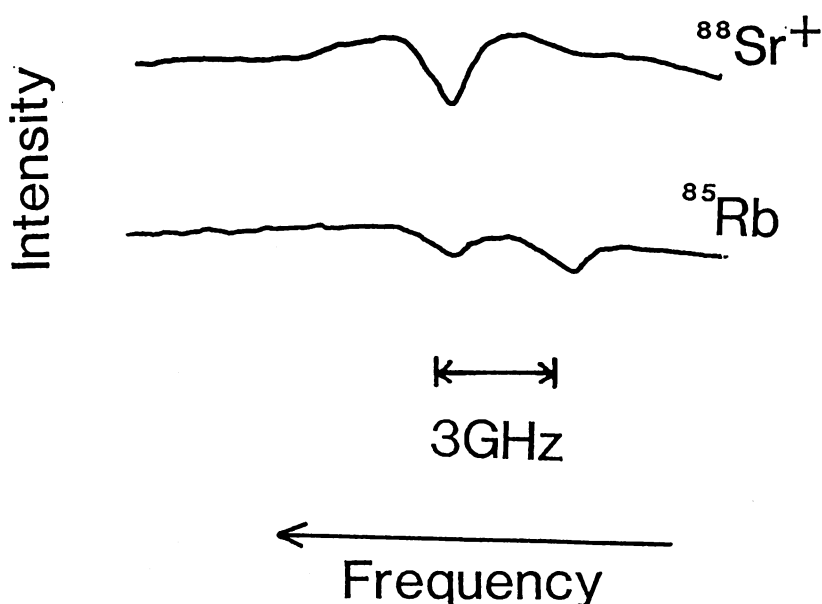
Mitsuru Musha<sup>1</sup>, Andrei Zvyagin<sup>1</sup>, Kenichi Nakagawa<sup>1,2</sup>, Motoichi Ohtsu<sup>1,2</sup>

1. Interdisciplinary Graduate school of Science and Engineering, Tokyo Institute of Technology  
4259 Nagatsuta, Midori-ku, Yokohama, Kanagawa 227, Japan
2. Kanagawa Academy of Science and Technology,  
KSP East Room 408, 3-2-1 Sakado, Takatsu-ku, Kawasaki 213, Japan

One of the application of the ion trapping and cooling technique is fundamental studies, such as investigation of energy relaxation processes in a 1-dimensional chain by using ions confined in a linear r.f. trap. As a first step of realizing this purpose, we are going to present at this symposium the results about the development of two semiconductor lasers based optical sources for detection and cooling experiments of trapped Sr ions. Although cooling of Sr ions has already been carried out with a fiber laser and LD [1] [2], we are going to do this experiment by means of semiconductor lasers only.

For cooling ions, the coherent light with the wavelength of 422nm is required which is resonant to the transition of  $6S_{1/2} - 6P_{1/2}$ . This light was obtained by single-pass frequency doubling of 843nm LD light from a KNbO<sub>3</sub> crystal. 20 $\mu$ W power at 422nm was generated with the 100mW of incident pump power. In order to control the longitudinal mode of this LD a thin glass plate mounted on a PZT was placed just in front of the LD facet. The absorption of Sr ion was observed by passing this 422nm light through the Sr hollow cathode lamp. The upper trace in Fig.1 shows a linear absorption spectrum of Sr ions which was obtained by sweeping the injection current of the LD. We also detected the linear absorption of <sup>85</sup>Rb atoms in a cell. It is represented as the lower trace in Fig.1, and it is shown that the resonance frequency corresponding to the transition  $6S_{1/2} - 6P_{1/2}$  of Sr ion coincides with the frequency corresponding to the transition  $5S_{1/2}(F=3) - 6P_{1/2}$  of <sup>85</sup>Rb within 1 GHz.

Sr ion in  $6P_{1/2}$  state can also decay into  $6D_{3/2}$  metastable state at branching ratio of 1/13 and once an ion decays to this state, it hardly returns back to the cooling cycle. In order to avoid decreasing the effect of cooling, another coherent light is required with wavelength of 1092nm corresponding to the transition of  $6D_{3/2}-6S_{1/2}$ . An InGaAsP multimode semiconductor laser was used to generate 1092nm light for depopulation of the metastable state. Grating feedback was applied to realize the single mode oscillation. 0.2mW of single mode oscillation at 1092nm was achieved with side mode suppression ratio of 20 dB, and with the tuning range of 1GHz. Those lasers is found to be available for cooling Sr ion.



The Upper trace shows the absorption spectrum of  $6S_{1/2}-6P_{1/2}$  in  $^{88}\text{Sr}$ , while the lower trace shows the absorption spectrum of  $5S_{1/2}(F=3) - 6P_{1/2}$  in  $^{85}\text{Rb}$

#### Reference

1. A.A.Madej, W.E.Berger, G.R.Hanes Optics Comm. 73 (1989) 147
2. G.P.Barwood, C.S. Edwards, P.Gill, H.A.Klein, W.R.C.Rowley Optics Let. 18 (1993) 732

## A Laser Cooled Cesium Fountain Raman Clock: A Proposal.

V. Barychev, M. Ohtsu<sup>1,2</sup>.

Institute of Metrology for Time and Space (VNIIFTRI)  
Mendeleevo, Moscow, 141570 Russia.

1) The Graduate School at Nagatsuta, Tokyo Inst. of  
Technology 4259 Nagatsuta-cho, Midori -ku, Yokohama 227,  
Japan.

2) Kanagawa Academy of Science and Technology, KSP East, Rm  
408, 3-2-1 Sakado, Takatsu-ku, Kawasaki 213 Japan.

A scheme of fountain type cesium clock utilizing Raman induced transitions is proposed (Fig.1). The scheme combines the idea of stimulated-resonance Raman interactions in an atomic beam [1] with the idea of atomic fountain continuously operating under low launch temperatures [2]. The proposed scheme can noticeably simplify the construction of a clock since it doesn't need to insert the microwave set-up into the vacuum chamber. The end-to-end cavity phase shift and the distributed-cavity phase shift are eliminated in proposed clock design as well as Ramsey pulling [3].

The most serious source of frequency uncertainty introduced by optical interrogation techniques is that of near resonant light shift [4]. It implies that a cesium clock based on this Raman Ramsey interrogation technique requires a good estimation of the systematic light shift and a good frequency stability and frequency correlation of both of two lasers as well as their power stabilization. Fortunately, it is possible to take advantage of the behavior of clock signal line asymmetry due to the inhomogeneity of the light shift near the point where this shift is zero in order to lock the frequencies of the lasers [1,5,6]. A condition for zero light shift also means the maximum of the signal.

In order to set the lasers to the desirable frequency separation for the purpose of Raman interrogation, a scheme of the optically stabilized laser with simultaneous locking to another laser via Raman induced transition is proposed (Fig.2). The scheme exploits the idea of self-quenching of the fundamental semiconductor laser frequency fluctuations to a level that is orders of magnitude below the Schawlow-Townes limit for a solitary laser [7]. Linewidth reduction by a factor more than  $10^3$  could also be obtained by using a narrow Doppler-free Faraday Raman optical feed back signal in Cs vapor.

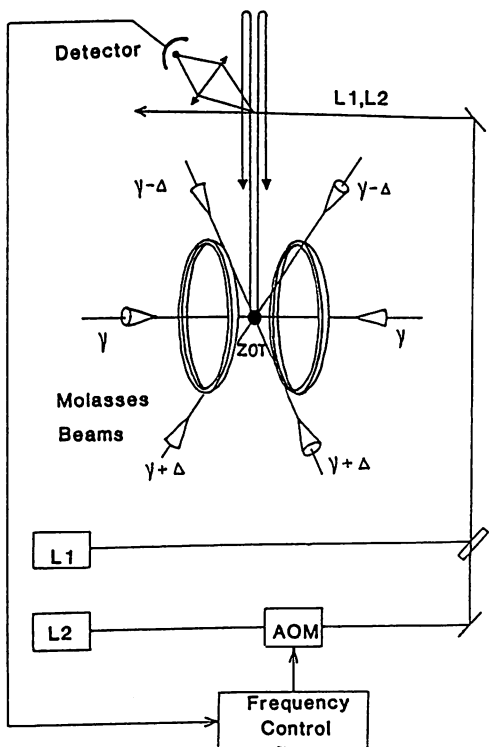


FIG.1 . A proposed scheme of fountain type cesium clock utilizing Raman induced transition.

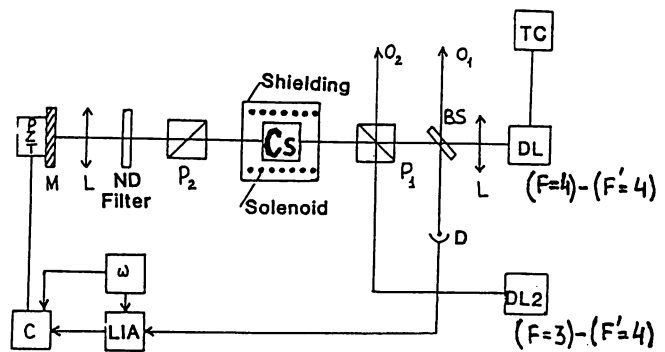


FIG.2. Block diagram of the optically stabilized laser with simultaneous locking to another laser via Raman induced transition.

### References:

- 1) P.Hemmer et al., J. Opt. Soc. Am. B, v.3, 1986, 219-230.
- 2) K. Gibble and S.Chu, Metrologia, v.29, 1992, 201-212.
- 3) L.Cutler et al., J. Appl Phys., v.69, 1991, 2780-2792.
- 4) E. De Clercq and P.Gerez, Opt. Comm., v.45, 1983, 91-94.
- 5) N.Cyr et al., Proceedings SPIE, November 1992, Boston, v.1837, 314-321.
- 6) M.Hashimoto and M.Ohtsu, IEEE Trans. Instr. Meas., v.IM-39, 1990, 458-462.
- 7) Y.Shevy et al., Opt Lett., v.17, 1992, 661-663.

## A1-5 Invited

A1: Electromagnetic Metrology

One Peta Hertz Coherent Optical Frequency Sweep Generator  
and Accurate Optical Frequency Counting

M. Ohtsu, K. Kakagawa, M. Kourogi, W. Wang, Y. Awaji, and Y. Toda  
Interdisciplinary Graduate School of Science and Engineering,  
Tokyo Institute of Technology,  
4259 Magatsuta, Midori-ku, Yokohama 227, JAPAN  
(Phone: +81-45-922-1111 (ext.2526), Fax: +81-45-921-1156)

### Introduction

A highly coherent and wideband tunable light source and an accurate frequency counter are essential systems for electromagnetic metrology in the optical region. They are also important for optical communication, optical sensing, and optical frequency standards. This paper reviews recent progress of our works toward realizing such systems[1].

### One Peta Hertz Coherent Optical Frequency Sweep Generator

Preliminary experiments of realizing a coherent light source with a wide tuning range ( from near IR to near UV, corresponding to one Peta Hz frequency tuning range ) have been carried out by using semiconductor lasers as primary light sources. Techniques of wideband negative electrical feedback and optical phase locking were employed to improve the coherence and to realize frequency/phase link, respectively. Furthermore, techniques of nonlinear optical frequency conversions were used for wideband frequency tuning. They are: Second harmonics, sum-, and difference-frequency generations by using inorganic oxide nonlinear optical crystals. Converted wavelength ranged from 422- to 1.67-um. It was confirmed that the converted powers, being several micro-watts, were sufficiently high for optical phase locking. Higher powers can be expected by installing the crystals in a built-up cavity for fundamental wave.

### Accurate Optical Frequency Counting System

We have proposed optical frequency counting system with the accuracy of about  $2 \times 10^{-10}$ . For frequency measurement in 1.5-um wavelength region, two frequency-stabilized He-Ne lasers ( 0.63- and 3.39-um wavelengths ) are used as primary optical frequency references. A LD-pumped YAG laser is used as a local oscillator and an InGaAsP laser is used as a secondary frequency reference, for which the sum- and difference-frequency of these lasers are phase-locked to the 0.63- and 3.39-um He-Ne lasers, respectively. For accurate optical heterodyne frequency measurement between the secondary standard and the laser with unknown frequency in 1.5-um wavelength region, a wide-span optical frequency comb generator is used as a local oscillator, for which an E/O modulator installed in microwave and optical cavities are used to generate modulated sidebands. The span of the modulated sidebands, as wide as 4 THz was achieved.

### Summary

It can be expected that wideband ( one Peta-Hz ) and continuous tunable coherent light sources and accurate optical frequency counting are realized in the near future by extending our techniques.

### References

- [1] See, for example, M. Ohtsu, Highly Coherent Semiconductor Lasers, Artech House, Inc., Boston, 1991

CThA4

9:00 am

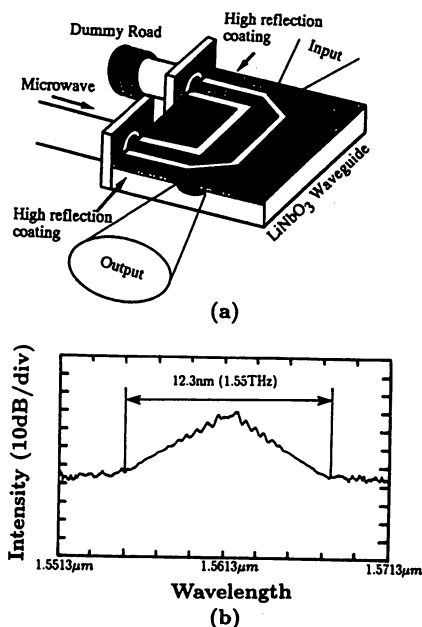
#### Monolithic optical frequency comb generators at 1.5- $\mu\text{m}$ wavelength region

M. Kourogi, T. Saito,\* T. Enami, M. Ohtsu, *Interdisciplinary Graduate School of Science and Engineering of Tokyo Institute of Technology, 4259 Nagatuta, Midori-ku, Yokohama, Kanagawa 227 Japan*

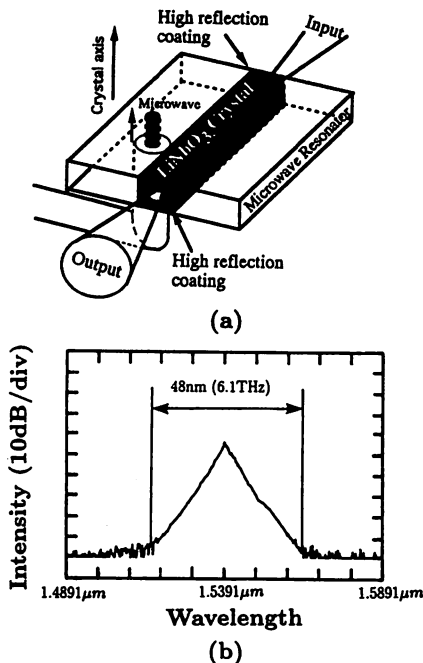
Measurement of frequency difference between two independent lasers which are spaced in a span as wide as several THz is required for industrial applications such as optical frequency division multiplexing in optical communication systems and for precision physical measurements such as highly accurate absolute laser frequency measurement using a frequency-multiplication chain. However it has been difficult to measure such a high frequency difference because of the lack of reliable ultra-high speed optical heterodyne receiver. In order to overcome this difficulty, we have proposed a highly accurate and wide span optical frequency difference measurement method<sup>1</sup> using an optical frequency comb (OFC) generator which generates a precisely spaced comb of frequencies through large-index phase modulation. We have al-

ready demonstrated the OFC generation with a span of 4 THz and heterodyne optical phase locking with a heterodyne frequency of 0.5 THz<sup>2</sup> by using an OFC generator which is composed of an electro-optic phase modulator installed within a Fabry-Perot cavity so that the modulation efficiency is increased by multiple passes of light through the modulator.

In this presentation, we report two types of novel monolithic OFC generators. One is a bulk-type monolithic OFC generator shown in Fig. 1(a), which was fabricated by coating high-reflection films on the facets of a bulky LiNbO<sub>3</sub> crystal used for the electro-optic phase modulator, i.e., the electro-optic modulator became an optical cavity. This OFC generator was compact, and the span of an OFC could be extended because the optical round-trip loss in this optical cavity was reduced. Figure 1(b) shows the envelope of the generated OFC spectrum observed by using an optical spectrum analyzer. It is confirmed from this figure that the envelope extended to a width as wide as 48 nm (6.1 THz). This value is 1.5 times wider than the value reported in ref. 2. To our knowledge, this value is the widest span of an OFC among the previously reported values. Because the measurement of the optical beat signal, which is used for the proposed frequency difference measurement, is more sensitive than the measurement using an optical spectrum analyzer, it is possible to detect higher order sidebands which have not been observed with the optical spectrum analyzer.



**CThA4** Fig. 1. (a) Schematic illustration of the bulk-type monolithic OFC generator. (b) Spectrum of the generated OFC envelope observed by an optical spectrum analyzer. The resolution of the optical spectrum analyzer was 0.2 nm. The wavelength and the linewidth of the laser which was used for the optical frequency comb generation was 1.539  $\mu\text{m}$  and 1 MHz, respectively. The modulation frequency, the modulation index and the finesse of the OFC generator were 5.87 GHz, 0.22  $\pi$ radian and 250, respectively.



**CTh44** Fig. 2. (a) Schematic illustration of the waveguide type monolithic OFC generator. (b) Spectrum of the OFC envelope observed by an optical spectrum analyzer. The resolution of the optical spectrum analyzer was 0.2 nm. The wavelength of the laser which was used for the optical frequency comb generation was 1.5613  $\mu\text{m}$ . The modulation frequency, the modulation index and the finesse of the OFC generator were 10.3 GHz,  $2\pi$  radian and 6, respectively.

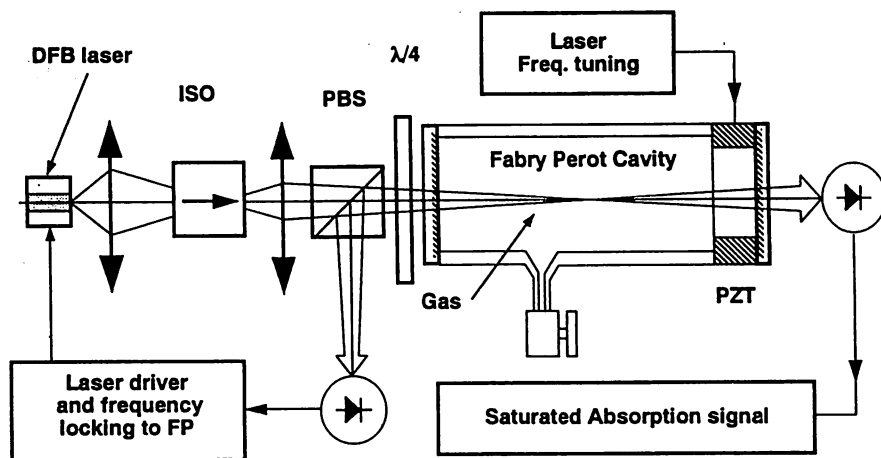
If the laser linewidth is reduced to a value narrower than 10 kHz, the maximum measurable frequency difference using the present OFC generator can reach to 6.1 THz. The details of this estimation are shown in section three of ref. 2.

Another version of the monolithic OFC generator is the waveguide-type monolithic OFC generator shown by Fig. 2(a), which was fabricated by coating high-reflection films on the facets of a waveguide-type  $\text{LiNbO}_3$  electro-optic phase modulator, i.e., the waveguide-type electro-optic modulator became an optical cavity. The waveguide-type monolithic OFC generator was compact, and suitable for the optical fiber system. Figure 2(b) shows the envelope of the generated OFC spectrum observed by using an optical spectrum analyzer. It is seen from this figure that the envelope extended to a width as wide as 12.3 nm (1.55 THz). This value was limited by the propagation loss of the waveguide.

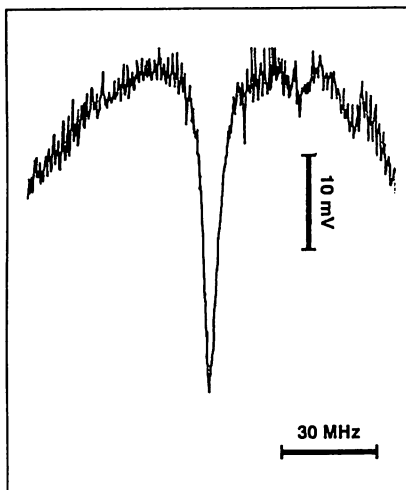
\* Kanagawa Academy of Science & Technology, KSP East Building, Room 408, 3-2-1 Sakado, Takatsu-ku, Kawasaki, Kanagawa 213 Japan

1. M. Kourogi, N. Nakagawa, C. H. Shin, M. Teshima, M. Ohtsu, in *Conference on Lasers and Electro-Optics*, 1991 OSA Technical Digest Series (Optical Society of America, Washington, DC, 1991), paper CThR57.
2. M. Kourogi, K. Nakagawa, M. Ohtsu, *IEEE J. Quantum Electron.* (October 1993).





QTuL3 Fig. 1. Experimental setup including: 60 dB Isolator, PBS (polarizing beam splitter), and Quarter Wave Plate. The DFB laser frequency is locked to FP resonance using a FM sideband technique in which error signal is provided by the FP reflected beam. The laser is then tuned using the FP piezoelectric element (PZT) and FP transmission provides saturated line signal.



QTuL3 Fig. 2. Saturated absorption peak of an HCN line ( $2\nu_1$  vibrational band) at  $1.54 \mu\text{m}$  recorded with a 8 mW laser power. The observed FWHM of the line is about 5 MHz.

bilized  $1.5\text{-}\mu\text{m}$  laser diode. As shown in Fig. 1, a 20-cm-long confocal Fabry-Perot cavity filled with the absorbing gas at low pressure was used as a frequency reference. With a cavity finesse of about 100, a 8 mW DFB laser was enough to obtain the saturated absorption. However, several practical applications of such frequency stabilized lasers are linked to optical communications which may require a  $1.56\text{-}\mu\text{m}$  wavelength in order to be compatible with optical fibers minimum absorption wavelength. Therefore, we show here that this technique is also applicable without modifications to HCN gas, which has several strong absorption lines at  $1.56 \mu\text{m}$ . However, as no  $1.56\text{-}\mu\text{m}$  lasers were available, we demonstrated this possibility with a very similar  $1.54\text{-}\mu\text{m}$  HCN line: in Fig. 2, we show a 5-MHz-wide HCN saturated absorption line which has been obtained with the same experimental apparatus. Another

important topic that we have investigated for practical purpose is the use of high finesse cavities which allow, either to increase the detection sensitivity by several orders of magnitude, or to decrease the size of the device. In this framework, we also demonstrated a compact version of such frequency references: a 25-mm long high finesse ( $\mathcal{F} > 10,000$ ) reference cell filled with  $\text{C}_2\text{H}_2$  provided a 2.8 MHz wide absorption line with a large 140-mV signal corresponding to 4% of total transmitted power, and a very good S/N. The obtained line, shown in Fig. 3, is almost perfectly fitted by a Lorentzian lineshape and the observed linewidth is probably limited by power broadening. It must be noticed that the linewidth of these frequency references are mainly instrumentally limited and could be well improved by further design improvements. The frequency stabilization of laser diodes using this technique is underway and should lead to a 2 orders of magnitude improvement of current  $1.5\text{-}\mu\text{m}$  laser diode frequency standards. These achievements open the way to new absolute laser frequency standards in the  $1.5\text{-}\mu\text{m}$  wavelength region: for that purpose, we are now considering the absolute measurement of such narrow molecular lines using an existing laser reference frequency.

\*On leave from LHA/CNRS, Bat. 221, Université Paris-Sud, 91405 Orsay Cedex, France

\*\*Department of Physics, Faculty of Science and Technology, Keio University, Hiyoshi, Yokohama 223, Japan

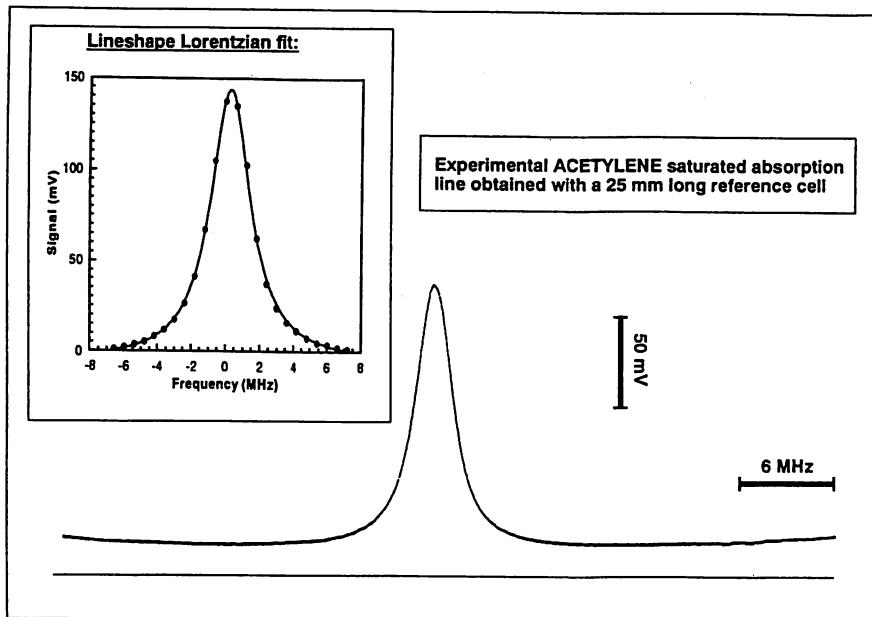
1. S. Sudo, Y. Sakai, H. Yasaka, T. Ikegami, IEEE Photon. Technol. Lett. 10, 281 (1989).
2. M. Labachellerie, C. Latrasse, K. Diomandé, P. Kemssu, P. Cerez, IEEE Trans. on Instr. and Meas. 40, 185 (1991).
3. F. Bertinetto, P. Gambini, R. Lano, M. Puelo, SPIE Conference on Frequency Stabilized Lasers and their Applications, Boston, Massachusetts, Nov. 16-18, 1992, SPIE Proc. 1837, 154.

QTuL3 3:00 pm

#### Compact narrow linewidth $1.5\text{-}\mu\text{m}$ frequency references for laser diode frequency stabilization

M. de Labachellerie,\* K. Nakagawa, M. Ohtsu, H. Sasada,\*\* Graduate School at Nagatsuta, Tokyo Institute of Technology, 4259 Nagatsuta-cho, Midori-ku, Yokohama 227, Japan

In several previous works about  $1.5\text{-}\mu\text{m}$  laser diode frequency stabilization, the best laser frequency stabilities were limited to  $\delta\nu/\nu \approx 10^{-10}$  by the lack of narrow linewidth  $1.5 \mu\text{m}$  frequency references.<sup>1-3</sup> Although numerous molecular absorption lines are found in this wavelength region, their  $\approx 500\text{-MHz}$ -wide Doppler limited absorptions were too large to obtain a laser diode frequency reference with a high stability. We addressed this issue recently and obtained the first 2-MHz-wide  $1.54\text{-}\mu\text{m}$  saturated absorption line in acetylene using a simple buildup cavity method<sup>4</sup> which is well suited to the practical construction of a frequency sta-



QTul3 Fig. 3. Saturated absorption peak of  $C_2H_2$  using the compact 25 mm long high finesse cavity. The quasi-perfect Lorentzian fit of this line indicates a 2.8 MHz FWHM.

4. M. Labachellerie, C. Latrasse, K. Nakagawa, M. N. Ohtsu, Int'l. Symposium on Atomic Frequency Standards and Coherent Quantum Electronics, Nara, Japan, Aug. 18-20, 1993, paper I-4.

## ULTRA-WIDE BAND OPTICAL FREQUENCY GRIDS GENERATION

Motoichi OHTSU

Interdisciplinary Graduate School of Science and Engineering,  
Tokyo Institute of Technology,  
4259 Nagatsuta Midori-ku, Yokohama 227, Japan  
Phone:+81-45-924-5455, Fax:+81-45-921-1204,  
E-mail: ohtsu@ae.titech.ac.jp

### Abstract

We have carried out nonlinear optical frequency conversions to realize a diode-laser-based wideband coherent optical frequency sweep generator. We can conclude that the present frequency grids provide with the frequency stability of  $10^{-9}$  -  $10^{-10}$  and the frequency-tunable range of 600 THz.

### 1. Introduction

Continuous-wave highly coherent frequency-tunable light sources have become more important in ultra-high speed and ultra-parallel optoelectronics. Semiconductor lasers were paid attention for their intrinsic tunable characteristics. Frequency tuning and frequency/intensity modulation of diode lasers can be easily carried out and extremely low amplitude noise compared to most other laser sources is an inherent advantage in the above-mentioned applications. Furthermore, in recent years the remarkable results in improvement of coherence, tunability and diode

laser based optical phase locking have been achieved, and these developments make it possible to develop a diode-laser-based wideband coherent optical frequency sweep generator (OFSG) which could offer highly coherent light (spectrally and spatially) with tunability capable of covering 1 PHz frequency span, and its realization is in progress [1,2]. We will review in this paper the recent progress of our study in realizing the OFSG.

### 2. Principle of Wideband Optical Frequency Sweep Generator

Figure 1 is a block diagram to show the systematic configuration of the OFSG which is capable of carrying out simultaneously absolute frequency stabilization, continuous frequency tuning and precision measurements of frequency difference. In contrast to the tuning mechanisms of the conventional tunable lasers, this system contains multiple highly coherent diode lasers with their own tunability. Furthermore, absolute frequency stabilization is introduced to the system. Coherent light generation for providing frequency reference grids in a wide frequency span can be realized by using diode lasers and their frequency conversions with the help of atomic or molecular transitions. KTP is found to have a wide phase matchable range whose upper limit is 680 THz ( $0.45 \mu\text{m}$ ) by sum-frequency generation, while the difference-frequency generation can provide infrared light from 300 THz ( $1 \mu\text{m}$ ) to the frequency as low as 100 THz ( $3 \mu\text{m}$ ). Furthermore, generation of the light in the above-mentioned entire frequency span can be possible by using only type II angle tuning at room temperature. Because the presently available diode laser do not satisfy such a continuous lasing spectrum, a multi-reference scheme is necessary for the OFSG. For measuring precisely the frequency difference between the tunable output and the frequency reference, the tunable output is heterodyne phase-locked to one of the frequency reference grids in the corresponding region. The frequency sweeping accuracy can be sufficiently high with the help of the optical phase locking.

### 3. Generation of Frequency-Tunable Light in a Wide Frequency Span

Because the available wavelengths of the present diode lasers exist incontinuously in the region from 0.6 to 1.5  $\mu\text{m}$  with some gaps, we should use frequency conversions to extend coverage of frequency to the region where direct diode laser spectra are not available. Second-harmonic generation[3], sum-frequency generation and difference-frequency generation or parametric amplification[4,5], have been experimentally performed by using AlGaAs (0.78/0.8  $\mu\text{m}$ ) and Ingram (1.5  $\mu\text{m}$ ) DFB lasers. Use of the DFB laser in frequency conversions offers a continuous frequency tuning range wider than 1 THz and ensures the continuous frequency coverage of the entire frequency-tunable span determined by the two lasers. Multi-electrodes corrugation-pitch-modulated MQW-DFB lasers[6] at 1.5  $\mu\text{m}$  with a maximum output power of 50 mW and a MHz-linewidth, single-mode AlGaAs lasers at 0.8  $\mu\text{m}$  and at 0.78  $\mu\text{m}$  were employed as the fundamental laser sources for both sum- and difference-frequency generations. The linewidths of AlGaAs lasers in experiment were narrowed to less than 100 kHz by using optical feedback from an external confocal FP cavity[7].

In sum-frequency generation, the maximum green light power of 0.68  $\mu\text{m}$  was obtained and the linear dependence of the output power at sum-frequency on either of the fundamental powers was confirmed. The measured frequency tuning bandwidths tuned by the 1.5  $\mu\text{m}$  laser were 100 GHz in cases when another fundamental laser was at 0.78  $\mu\text{m}$  and 0.8  $\mu\text{m}$ . The calculated values are 85 and 90 GHz for a 1-cm KTP, respectively. The calculation also gives a frequency tuning bandwidth of 350 GHz, for a 1-cm KTP when the 0.78/0.8  $\mu\text{m}$  laser is tuned. By using combination of these diode lasers, highly coherent frequency-tunable green light has been obtained from 0.51 to 0.56  $\mu\text{m}$  (50 THz) with a continuous tuning range of 1 THz.

In difference-frequency generation, 0.3  $\mu\text{m}$  output power was obtained when two fundamental lasers were at 1.5 and 0.78  $\mu\text{m}$ . The difference-frequency was round 1.6  $\mu\text{m}$ . The tuning range was larger than 5 THz (1.58 - 1.62  $\mu\text{m}$ ) which corresponded to the wavelength range of the AlGaAs laser from 0.78 to 0.79  $\mu\text{m}$  by controlling the operation temperatures and currents of the lasers. Both experiment and calculation show that the frequency tuning bandwidth was 200 GHz for a 1-cm KTP by tuning the 1.5  $\mu\text{m}$  DFB laser. The obtained tunable range was from 1.38 to 1.67  $\mu\text{m}$  (38 THz) which corresponded to the pump wavelength from 0.73 to 0.80  $\mu\text{m}$ . The maximum available tuning range can be as wide as 600 nm (65 THz) around 1.54  $\mu\text{m}$  which is limited only by the present crystal size.

#### 4. Atomic/Molecular Resonance Stabilized Frequency Reference Grids

In order to provide the reference frequency grids in a wide frequency span in the OFSG, absolute frequency stabilization of these frequencies have to be also performed, in which atomic/molecular absorption resonances are used as frequency references. Two schemes are used for generating the coarse frequency grids. The fine frequency grids are generated by the frequency comb generators, which has been published elsewhere[8].

##### 4.1. Frequency Reference and Linking Using Optical Double Resonance in Potassium

Potassium ( $^{41}\text{K}$ ) was chosen for this scheme by which the coarse frequency reference grids can be obtained at 0.77, 1.54, and 0.51  $\mu\text{m}$  simultaneously[9]. The pump-probe spectroscopy scheme is shown by Fig.3. The second-harmonic wave of 1.54  $\mu\text{m}$  DFB laser was used as a probe. The fundamental power was 40 mW and the detected power after the spectroscopic system was measured to be 20 nW. A saturation-spectroscopy scheme was arranged for locking the laser frequency to the saturated absorption resonance. The atomic cell containing  $^{41}\text{K}$  (2 cm long) was installed inside an oven to maintain the temperature close to 60°C.

Frequency stabilization of the pump laser was carried out by locking the laser frequency to the saturated cross-over absorption

peak of the  $^{41}\text{K-D}_1$  line by using the phase-sensitive detection technique. The residual frequency fluctuations were estimated to be less than 50 kHz from the error signal, implying a frequency stability as high as  $10^{-10}$ .

For the pump-probe spectroscopy, the second-harmonic wave was arranged as a probe co- and counter-propagating to the pump beam as shown in Fig.2. A high contrast (>60%) of the nonlinear absorption with a resonance width of 10 MHz was obtained in the co-propagating scheme, which was preferable for frequency stabilization.

#### 4.2. Frequency References Using Molecular Iodine Absorption Resonances

In order to extend further the tunable frequency span, different kinds of AlGaAs laser, e.g., in the 0.8  $\mu\text{m}$  region, are mixed with the InGaAsP laser. A second scheme, shown by Fig.3, for providing frequency references is considered, which does not limit another laser frequency but needs a frequency reference in the generated frequency region. Molecular iodine ( $\text{I}_2$ ) was chosen for the frequency reference for our experiment because of its plenty of absorption lines covering a very large frequency range in the green region[10].

For frequency stabilization, the generated green light passed through a 15cm-long  $\text{I}_2$  cell which contains natural iodine. A resonance with an absorption of 55% and a width of 1.2 GHz was used as the reference at 536.32nm (560THz). The phase-sensitive detection technique was employed to stabilize the 0.82  $\mu\text{m}$  laser while the 1.54  $\mu\text{m}$  laser was in free-running. The residual frequency fluctuations were estimated to be within 0.5<sup>-9</sup> MHz, implying a normalized frequency stability better than  $10^{-9}$  at the optical frequency of 560 THz.

The combination of the above two schemes, generation of frequency reference grids can be realized at 0.51, 0.77, 0.83, 1.54, 1.7  $\mu\text{m}$  through sum- and difference-frequency generations.

#### 5. Summary

From the results of the nonlinear frequency conversions using diode lasers and generation of frequency reference grids, we can conclude that the present<sup>9</sup> frequency reference grids with the frequency stability of  $10^{-9}$  -  $10^{-10}$ , as well as the frequency-tunable output, can be extended from the present 600 THz (0.5  $\mu\text{m}$ ) to 900 THz (0.3  $\mu\text{m}$ ) by adding InGaAlP visible diode lasers and InGaAsP lasers at 1.3  $\mu\text{m}$  region to the present system.

#### References

- [1] M. Ohtsu, Highly Coherent Semiconductor Lasers, Artech House, Inc., Norwood, (1992) Chapters 2 - 5
- [2] M. Ohtsu, et.al., J. Appl. Phys., Vol.73 (1993) R1-R17
- [3] W. Wang, et.al., Appl. Phys. Lett., Vol.61 (1992) 1886-1888
- [4] W. Wang and M. Ohtsu, Opt. Commun., Vol.102 (1993) 304-308
- [5] W. Wang and M. Ohtsu, Opt. Lett., Vol.18 (1993) 876-878
- [6] M. Okai, et.al., IEEE Photon. Technol. Lett., Vol.2 (1990) 529-530
- [7] B. Dahmani, et.al., Opt. Lett., Vol.12, (1987) 876-878
- [8] M. Kourogi, et.al., IEEE J. Quantum Electron., QE-29 (1993) 2693-2701
- [9] W. Wang, et.al., IEEE Photon. Technol. Lett., Vol.6 (1994) 95-97
- [10] W. Wang and M. Ohtsu, Jpn. J. Appl. Phys., Vol.33 (1994) 1648-1651

